

Enclosure C

Holtec Licensing Report for Beaver Valley Unit 2 Rerack

(Non-proprietary Version)



Holtec Center, 555 Lincoln Drive West, Marlton, NJ 08053

Telephone (856) 797- 0900

Fax (856) 797 - 0909

LICENSING REPORT FOR BEAVER VALLEY UNIT 2 RERACK

FOR

FIRST ENERGY

Holtec Report No: HI-2084175

Holtec Project No: 1702

Sponsoring Holtec Division: NPD

Report Class : SAFETY RELATED

COMPANY PRIVATE

This document is the property of Holtec International and its Client. It is to be used only in connection with the performance of work by Holtec International or its designated subcontractors. Reproduction, publication or representation, in whole or in part, for any other purpose by any party other than the Client is expressly forbidden.

HOLTEC INTERNATIONAL

DOCUMENT ISSUANCE AND REVISION STATUS¹

DOCUMENT NAME:	LICENSING REPORT FOR BEAVER VALLEY UNIT 2 RERACK		
DOCUMENT NO.:	HI-2084175	CATEGORY:	<input type="checkbox"/> GENERIC
PROJECT NO.:	1702		<input checked="" type="checkbox"/> PROJECT SPECIFIC
Rev. No. ²	Date Approved	Author's Initials	VIR #
3	3/16/2009	M.McGinley	689507

DOCUMENT CATEGORIZATION

In accordance with the Holtec Quality Assurance Manual and associated Holtec Quality Procedures (HQP's), this document is categorized as a:

- Calculation Package³ (Per HQP 3.2) Technical Report (Per HQP 3.2)
(Such as a Licensing Report)
- Design Criterion Document (Per HQP 3.4) Design Specification (Per HQP 3.4)
- Other (Specify):

DOCUMENT FORMATTING

The formatting of the contents of this document is in accordance with the instructions of HQP 3.2 or 3.4 except as noted below:

DECLARATION OF PROPRIETARY STATUS

- Nonproprietary Holtec Proprietary Privileged Intellectual Property (PIP)

This document contains extremely valuable intellectual property of Holtec International. Holtec's rights to the ideas, methods, models, and precepts described in this document are protected against unauthorized use, in whole or in part, by any other party under the U.S. and international intellectual property laws. Unauthorized dissemination of any part of this document by the recipient will be deemed to constitute a willful breach of contract governing this project. The recipient of this document bears sole responsibility to honor Holtec's unabridged ownership rights of this document, to observe its confidentiality, and to limit use to the purpose for which it was delivered to the recipient. Portions of this document may be subject to copyright protection against unauthorized reproduction by a third party.

Notes

1. This document has been subjected to review, verification and approval process set forth in the Holtec Quality Assurance Procedures Manual. Password controlled signatures of Holtec personnel who participated in the preparation, review, and QA validation of this document are saved on the company's network. The Validation Identifier Record (VIR) number is a random number that is generated by the computer after the specific revision of this document has undergone the required review and approval process, and the appropriate Holtec personnel have recorded their password-controlled electronic concurrence to the document.
2. A revision to this document will be ordered by the Project Manager and carried out if any of its contents is materially affected during evolution of this project. The determination as to the need for revision will be made by the Project Manager with input from others, as deemed necessary by him.
3. Revisions to this document may be made by adding supplements to the document and replacing the "Table of Contents", this page and the "Revision Log".

SUMMARY OF REVISIONS

Revision 0 – Original Revision.

Revision 1 – Incorporated Client comments in Chapters 4 and 6.

Revision 2 – Incorporated additional client comments throughout.

Revision 3 – Incorporated additional client comments in Chapters 1, 4, 5, 6, 8 and 9.

TABLE OF CONTENTS

<u>Section</u>	<u>Description</u>	<u>Page</u>
1.0	INTRODUCTION	1-1
1.1	References.....	1-4
2.0	FUEL STORAGE RACKS.....	2-1
2.1	Introduction.....	2-1
2.2	Summary of Principal Design Criteria.....	2-2
2.3	Applicable Codes and Standards	2-3
2.4	Quality Assurance Program	2-9
2.5	Mechanical Design	2-9
2.6	Rack Fabrication.....	2-10
3.0	MATERIAL CONSIDERATIONS.....	3-1
3.1	Introduction.....	3-1
3.2	Structural Materials.....	3-1
3.3	Neutron Absorbing Material.....	3-1
3.4	In-Service Surveillance of the Neutron Absorber.....	3-4
3.5	References.....	3-7
4.0	CRITICALITY SAFETY ANALYSIS.....	4-1
4.1	Introduction and Summary	4-1
4.2	Methodology.....	4-3
4.3	Acceptance Criteria.....	4-7
4.4	Assumptions.....	4-9
4.5	Input Data	4-11
4.6	Computer Codes.....	4-14
4.7	Analysis	4-15
4.8	References.....	4-30
	Appendix A	
5.0	STRUCTURAL/SEISMIC CONSIDERATIONS.....	5-1
5.1	Introduction.....	5-1
5.2	Acceptance Criteria.....	5-1
5.3	Loads and Load Combinations	5-2
5.4	Analysis Methods	5-3
5.5	Structural Evaluation of Racks	5-15
5.6	Mechanical Evaluation of Racks	5-22
5.7	Cask Pit Rack Platform Analysis.....	5-32
5.8	Bearing Pad Analysis.....	5-32
5.9	Interface Loads on Spent Fuel Pool Structure	5-34
5.10	References.....	5-36

TABLE OF CONTENTS (continued)

<u>Section</u>	<u>Description</u>	<u>Page</u>
6.0	THERMAL-HYDRAULIC EVALUATION	6-1
6.1	Introduction.....	6-1
6.2	Acceptance Criteria.....	6-2
6.3	Assumptions and Design Data	6-3
6.4	Fuel Rod Cladding Temperatures	6-6
6.5	Description of Spent Fuel Pool Cooling System	6-8
6.6	Heat Loads and Bulk Pool Temperatures	6-8
6.7	Local Water and Fuel Cladding Temperatures	6-12
6.8	References.....	6-14
7.0	MECHANICAL ACCIDENTS CONSIDERATIONS.....	7-1
7.1	Introduction.....	7-1
7.2	Description of Mechanical Accidents.....	7-1
7.3	Incident Impact Velocity	7-3
7.4	Mathematical Model	7-5
7.5	Results.....	7-5
7.6	Conclusion	7-8
7.7	References.....	7-9
8.0	RADIOLOGICAL EVALUATION	8-1
8.1	Introduction.....	8-1
8.2	Acceptance Criteria.....	8-1
8.3	Assumptions.....	8-1
8.4	Dose Rate at the Surface of the Pool	8-2
8.5	Fuel Handling Accident	8-3
8.6	Person-Rem Exposure.....	8-3
8.7	Conclusion	8-3
9.0	INSTALLATION	9-1
9.1	Introduction.....	9-1
9.2	Rack Arrangement	9-4
9.3	Installation Sequence	9-4

LIST OF TABLES

<u>Table</u>	<u>Description</u>	<u>Page</u>
2.1.1	GEOMETRIC AND PHYSICAL DATA FOR THE NEW FUEL RACKS	2-13
2.5.1	MODULE DATA FOR NON-FLUX TRAP FUEL RACKS.....	2-14
3.4.1	SAMPLE COUPON MEASUREMENT SCHEDULE	3-9
4.5.1	FUEL ASSEMBLY SPECIFICATION AND DESIGN BASIS FUEL ASSEMBLY SELECTION	4-31
4.5.2	SPECIFICATION OF THE DESIGN BASIS FUEL ASSEMBLY	4-32
4.5.3	CORE OPERATING PARAMETER FOR CASMO DEPLETION ANALYSES ..	4-33
4.5.4	CALCULATION OF SOLUBLE BORON FOR CASMO-4.....	4-34
4.5.5	CALCULATION OF AXIAL BURNUP DISTRIBUTION	4-35
4.5.6	BOUNDING AXIAL BURNUP PROFILE SUMMARY	4-37
4.5.7	IFBA ROD SPECIFICATION	4-38
4.5.8	WATER DISPLACER ROD SPECIFICATION	4-39
4.5.9	WABA SPECIFICATION.....	4-40
4.5.10	STORAGE CELL SPECIFICATION.....	4-41
4.5.11	SPECIFICATION OF THE FUEL ROD STORAGE BASKET	4-42
4.5.12	SPECIFICATION FOR THE BORON DILUTION ANALYSIS.....	4-43
4.7.1	SUMMARY OF THE REGION 2 INITIAL ENRICHMENT AND BURNUP COMBINATIONS	4-44
4.7.2	SUMMARY OF THE REGION 3 INITIAL ENRICHMENT AND BURNUP COMBINATIONS	4-45
4.7.3	SUMMARY OF THE MTZR SOLUBLE BORON REQUIREMENTS FOR NORMAL CONDITIONS	4-46
4.7.4	SUMMARY OF ACCIDENT CASES	4-47
4.7.5	CASMO-4 CALCULATION OF THE EFFECT OF SPACER GRIDS AND BORON CONCENTRATION ON REACTIVITY	4-48
4.7.6	CALCULATION OF THE INITIAL ENRICHMENT AND BURNUP COMBINATIONS FOR REGION 2	4-49
4.7.7	CALCULATION OF THE INITIAL ENRICHMENT AND BURNUP COMBINATIONS FOR REGION 3	4-50
4.7.8	RESULTS OF THE CASMO-4 CALCULATIONS OF THE IFBA BIAS	4-51
4.7.9	RESULTS OF THE CASMO-4 CALCULATIONS OF WDR REACTIVITY DEPENDENCE ON NUMBER OF WDR RODS AND FUEL ENRICHMNET	4-52
4.7.10	RESULTS OF THE CASMO-4 CALCULATIONS OF A FUEL ASSEMBLY WITH BOTH IFBA AND WDR BIAS DEPENDENCE ON THE NUMBER OF WDR RODS AND FUEL ENRICHMNET.....	4-53
4.7.11	RESULTS OF THE CASMO-4 CALCULATIONS OF WABA BIAS DEPENDENCE ON NUMBER OF WABA RODS AND FUEL ENRICHMNET	4-54

LIST OF TABLES (continued)

<u>Table</u>	<u>Description</u>	<u>Page</u>
4.7.12	RESULTS FOR THE CALCULATION OF THE ECCENTRIC FUEL POSITIONING REACTIVITY EFFECT.....	4-55
4.7.13	REGION 2 CASMO CALCULATIONS FOR FUEL TOLERANCE UNCERTAINTIES	4-56
4.7.14	CASMO CALCULATIONS FOR MANUFACTURING TOLERANCE UNCERTAINTIES FOR FUEL STORAGE CELL.....	4-57
4.7.15	CASMO CALCULATIONS FOR POOL TEMPERATURE REACTIVITY EFFECT	4-58
4.7.16	VERIFICATION OF THE INITIAL ENRICHMENT AND BURNUP COMBINATIONS AND CALCULATIONS OF SOLUBLE BORON REQUIREMENTS.....	4-59
4.7.17	CALCULATION OF THE MISLOADED FRESH FUEL ASSEMBLE ACCIDENT	4-62
4.7.18	CALCULATION OF THE MISLOCATED FRESH FUEL ASSEMBLE ACCIDENT	4-63
4.7.19	RESULTS OF THE SENSITIVITY STUDY OF THE EFFECT OF SOLUBLE BORON ON THE CALCULATION OF FUEL AND STORAGE RACK MANUFACTURING TOLERANCES	4-64
4.7.20	MCNP4a CALCULATION FOR THE FUEL ROD STORAGE BASKET	4-65
4.7.21	BEAVER VALLEY POWER STATION UNIT NO. 2 SPENT FUEL POOL BORON DILUTION ACCIDENT ANALYSIS	4-66
5.4.1	PARTIAL LISTING OF FUEL RACK APPLICATIONS USING DYNARACK	5-38
5.4.2	DEGREES-OF-FREEDOM.....	5-41
5.4.3	RACK MATERIAL DATA (200°F)	5-42
6.1.1	PARTIAL LISTING OF RERACK APPLICATIONS USING SIMILAR METHODS OF THERMAL-HYDRAULIC ANALYSIS	6-15
6.3.1	SUMMARY OF INPUTS FOR BULK TEMPERATURE ANALYSIS	6-17
6.3.2	SUMMARY OF INPUTS FOR LOCAL TEMPERATURE ANALYSIS.....	6-18
6.6.1	SUMMARY OF BULK POOL TEMPERATURE RESULTS	6-19
6.6.2	SUMMARY OF TIME-TO-BOIL RESULTS	6-20
6.7.1	SUMMARY OF LOCAL TEMPERATURE RESULTS	6-21
7.4.1	IMPACT EVENT DATA	7-10
7.4.2	MATERIAL DEFINITION	7-11
8.3.1	PARAMETER VALUES UTILIZED IN THE RADIOLOGICAL EVALUATIONS	8-4
8.6.1	PERSON-REM EXPOSURE FROM RE-REACKING ONE PLANT	8-4

LIST OF FIGURES

<u>Figure</u>	<u>Description</u>	<u>Page</u>
1.1	PROPOSED NEW RACK LAYOUT FOR BEAVER VALLEY POWER STATION (BVPS) UNIT No. 2	1-5
2.1.1	ISOMETRIC VIEW OF GENERIC NON-FLUX TRAP RACK	2-15
2.6.1	ISOMETRIC VIEW OF COMPOSITE BOX ASSEMBLY	2-16
2.6.2	PLAN VIEW OF GENERIC NON-FLUX TRAP RACK ARRAY	2-17
2.6.3	ADJUSTABLE PEDESTAL DESIGN	2-18
2.6.4	NON-FLUX-TRAP RACK CELLS ELEVATION VIEW	2-19
4.5.1	128 IFBA PIN LOADING PATTERN FOR 17x17 FUEL ASSEMBLIES	4-67
4.5.2	A TWO DIMENSIONAL REPRESENTATION OF THE MZTR MCNP4a MODEL	4-68
4.5.3	MZTR 9 X 12 RACK PERMISSIBLE LOADING CONFIGURATION	4-69
4.5.4	MZTR 9 X 13 RACK PERMISSIBLE LOADING CONFIGURATION	4-70
4.5.5	200 IFBA PIN LOADING PATTERN FOR 17x17 FUEL ASSEMBLY	4-71
4.5.6	A TWO DIMENSIONAL REPRESENTATION OF THE MCNP4a FRSB MODEL	4-72
4.7.1	REGION 2 INITIAL ENRICHMENT AND BURNUP COMBINATIONS	4-73
4.7.2	REGION 3 INITIAL ENRICHMENT AND BURNUP COMBINATIONS	4-74
4.7.3	A TWO DIMENSIONAL REPRESENTATION OF THE MCNP4a MISLOCATED FUEL ASSEMBLY ACCIDENT MODEL	4-75
4.7.4	REPRESENTATION OF MISLOADING ACCIDENT MCNP MODEL WITH REFLECTIVE BOUNDARY CONDITIONS	4-76
5.1	SINGLE RACK DYNAMIC MODEL	5-43
5.2	FUEL-TO-RACK IMPACT SPRINGS	5-44
5.3	2-D SCHEMATIC ELEVATION OF THE STORAGE RACK MODEL	5-45
5.4	RACK DEGREES OF FREEDOM AND MODELING TECHNIQUE	5-46
5.5	2-D INTER-RACK IMPACT SPRINGS	5-47
6.6.1	SIMPLIFIED HEAT EXCHANGER ALIGNMENT	6-22
6.6.2	SFP BULK TEMPERATURE, NET SFP HEAT AND PASSIVE HEAT LOSS PROFILES – NORMAL FULL CORE	6-23
6.6.3	SFP BULK TEMPERATURE, NET SFP HEAT AND PASSIVE HEAT LOSS PROFILES – ABNORMAL FULL CORE	6-24
6.7.1	CONTOURS OF STATIC TEMPERATURE IN A VERTICLE PLANE THROUGH THE CENER OF THE SFP	6-25
7.2.1	SCHEMATICS OF THE STRAIGHT SHALLOW DROP ON A RACK CELL.	7-12
7.2.2	SCHEMATICS OF THE “DEEP” DROP (SCENARIO 1) ON A CENTER CELL LOCATION	7-13
7.2.3	SCHEMATICS OF THE “DEEP” DROP (SCENARIO 2) ON A SUPPORT LEG LOCATION	7-14
7.2.4	SCHEMATIC OF RACK DROP SCENARIO	7-15
7.5.1	SHALLOW DROP-RACK CELL DEFORMATION	7-16

LIST OF FIGURES (continued)

7.5.2	PEAK BASEPLATE VERTICLE DEFLECTION - DEEP DROP SCENARIO 1	7-17
7.5.3	SFP FLOOR LINER MAXIMUM PLASTIC STAIN – RACK DROP	7-18
7.5.4	SFP FLOOR CONCRETE SAB MAXIMUM COMPRESSIVE STRESS – RACK DROP	7-19
7.5.5	DEFORMED SHAPE OF FUEL RODS (RACK CELL NOT SHOWN) – FUEL-TO-FUEL IMPACT	7-20

1.0 INTRODUCTION

The Beaver Valley Power Station (BVPS) Unit No. 2 is a pressurized water reactor (PWR), designed by Westinghouse, with a reactor core sized for 157 Westinghouse 17x17 fuel assemblies. The station is owned and operated by FirstEnergy Nuclear Operating Company (FENOC). The station's reactor has a thermal output of 2900 MWt (megawatts thermal). FENOC has determined that continued operation of the station will require additional storage space to accommodate the accumulating spent nuclear fuel. This report provides a description of a proposed modification to the Spent Fuel Pool (SFP) rack configuration and a summary of the evaluations performed to support this change.

The station's SFP currently contains 1088 storage cells in seventeen spent fuel storage racks. All existing racks are of the flux trap¹ style. The seventeen existing racks in the SFP will be removed and replaced by fifteen new freestanding racks of the following sizes:

Rack Array Size	Number of Racks (and Rack IDs)	Usable Storage Locations
9 by 8	1 (A3)	1 x 72 = 72
9 by 12	1 (A1)	1 x 96 = 96
9 by 12	5 (A2, B2, C2, B3 & C3)	5 x 108 = 540
9 by 13	1 (B1)	1 x 111 = 111
9 by 13	1 (C1)	1 x 117 = 117
9 by 14	2 (B4 & C4)	2 x 126 = 252
10 by 12	2 (D2 & D3)	2 x 120 = 240
10 by 13	1 (D1)	1 x 122 = 122
10 by 14	1 (D4)	1 x 140 = 140
		1690

All of the new racks are non-flux-trap racks and are designated in a mixed-zone three-region (MZTR) array, where loading patterns are used to control criticality. The resulting fuel storage rack array proposed for the station contains 1690 storage cells and is shown in the plan view

¹ Flux trap style racks contain a water-filled gap with neutron absorber on both sides, called a flux trap, between adjacent fuel storage locations.

provided in Figure 1.1. The total fuel assembly storage capacity of the racks, however, depends on the storage patterns used for low-burned fuel. Figures 4.5.3 and 4.5.4 show some allowable loading patterns.

All SFP storage racks are freestanding and self-supporting. The principal construction materials for the racks are SA240 Types 304 or 304L stainless steel sheet and plate stock, and SA564-630 (precipitation hardened) stainless steel for the adjustable support pedestals. The only non-stainless material utilized in the rack is the neutron absorber material, which is a boron carbide and aluminum metal matrix composite available under the patented product name Metamic™.

The racks are designed to the stress limits of, and analyzed in accordance with, Section III, Division 1, Subsection NF of the ASME Boiler and Pressure Vessel (B&PV) Code [1-1]. The material procurement, analysis, and fabrication of the rack modules conform to USNRC 10CFR50 Appendix B requirements.

The rack design and analysis methodologies employed are a direct evolution of previous license applications. This report documents the design and analyses performed to demonstrate that the racks meet all governing requirements of the applicable codes and standards; in particular the "OT Position for Review and Acceptance of Spent Fuel Storage and Handling Applications," USNRC (1978) and 1979 Addendum thereto [1-2].

This report provides the design basis for the replacement of fuel storage racks at BVPS Unit No. 2 and is prepared to support the license amendment process for the station. This report provides discussions of the new rack design, analysis methodology, and results. Holtec prepared the design and performed the engineering evaluations, and will also fabricate and install the racks.

Sections 2 and 3 of this report provide an abstract of the design and material information on the racks.

The criticality safety analysis sets the requirements on the Metamic™ panel length and the amount of B10 per unit area (i.e., loading density) of the Metamic™ panels for the SFP racks.

being added. The criticality safety analysis requires that the neutron multiplication factor for the stored fuel array be bounded by the USNRC k_{eff} limit of 0.95 under assumptions of 95% probability and 95% confidence.

Rack module structural analysis requires that primary stresses in the rack module structure remain below the ASME B&PV Code (Subsection NF) [1-1] allowable stresses. Demonstrations of seismic and structural adequacy are presented in Section 5.

Thermal-hydraulic consideration requires that fuel cladding will not fail due to excessive thermal stress, and that the steady state pool bulk temperature will remain within the limits prescribed for the spent fuel pool to satisfy the pool structural strength, operational, and regulatory requirements. The thermal-hydraulic analyses carried out in support of this storage expansion effort are described in Section 6.

Mechanical accident qualification requires that the subcriticality of the stored fuel will be maintained under all postulated accident scenarios. The structural consequences of these postulated accidents are evaluated and presented in Section 7 of this report.

Section 8 discusses the results of the radiological evaluation performed to support the rerack. Section 9 addresses the most important considerations in the installation of the racks.

All computer programs utilized to perform the analyses documented in this report are benchmarked and verified. These programs have been utilized in numerous license applications over the past decade.

The analyses presented herein clearly demonstrate that the rack module arrays possess wide margins of safety in respect to all considerations of safety specified in the USNRC OT Position Paper [1-2], namely, nuclear subcriticality, thermal-hydraulic safety, seismic and structural adequacy, radiological compliance, and mechanical integrity.

1.1 References

- [1-1] American Society of Mechanical Engineers (ASME), Boiler & Pressure Vessel Code, Section III, Subsection NF, latest Edition.
- [1-2] USNRC, "OT Position for Review and Acceptance of Spent Fuel Storage and Handling Applications," April 14, 1978, and Addendum dated January 18, 1979.

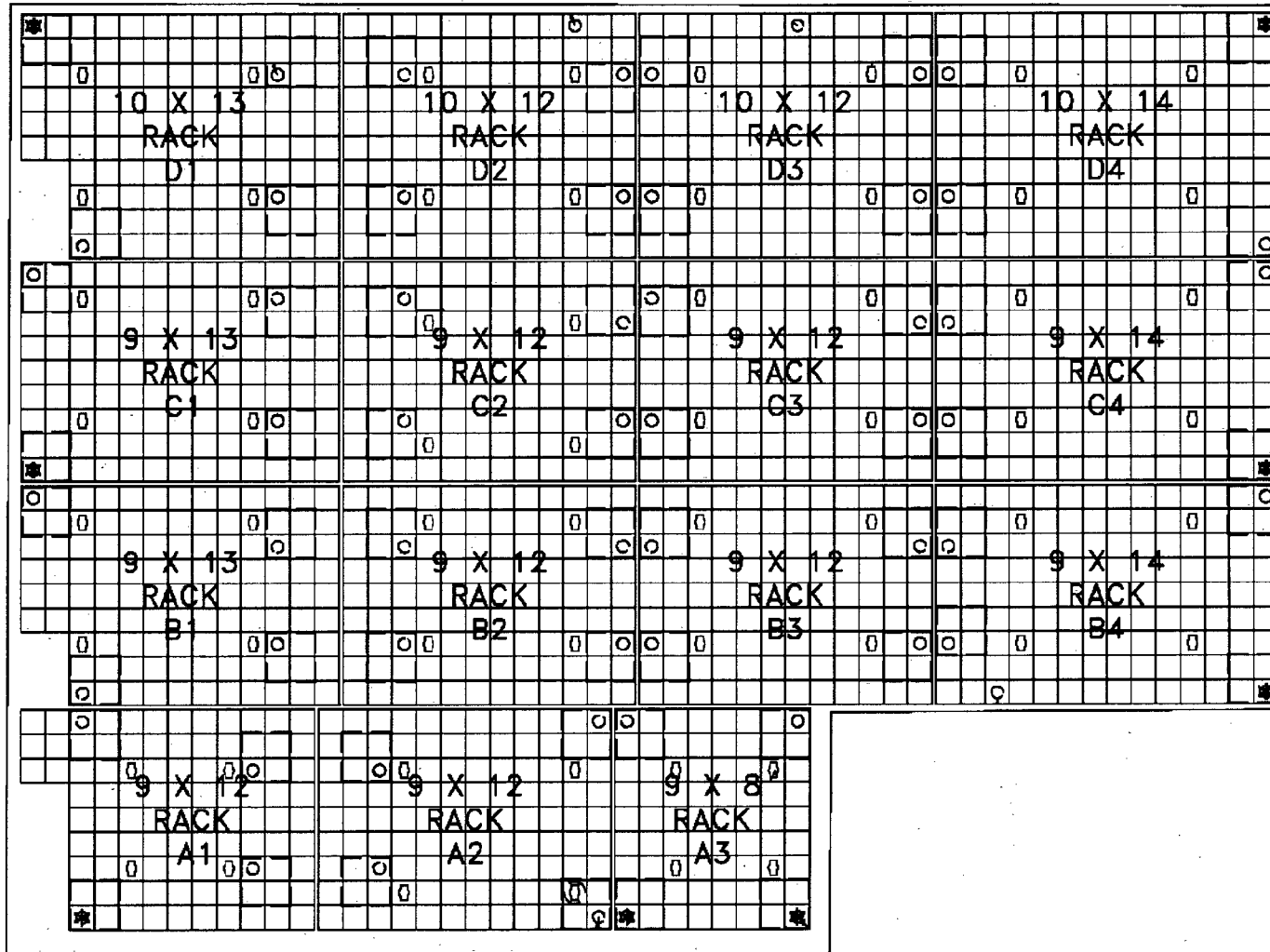


FIGURE 1.1 – PROPOSED NEW RACK LAYOUT FOR BEAVER VALLEY POWER STATION (BVPS) UNIT No. 2

2.0 FUEL STORAGE RACKS

2.1 Introduction

In its fully implemented configuration, the Spent Fuel Pool will contain 15 fuel racks with a maximum storage capacity of 1690 assemblies. All fuel storage rack arrays being added will consist of freestanding modules, made primarily from austenitic stainless steel containing honeycomb storage cells interconnected through longitudinal welds. A panel of Metamic metal matrix composite containing a high areal loading of the Boron-10 (B-10) isotope provides appropriate neutron attenuation between adjacent storage cells. Figure 2.1.1 provides an isometric schematic of a typical non-flux trap design storage rack module. Data on the cross sectional dimensions, weight and cell count for each rack module is presented in Table 2.1.1.

The baseplates on all spent fuel rack modules extend out beyond the rack module periphery wall such that the plate protrusions act to set a required minimum separation between the facing cells in adjacent rack modules. Each spent fuel rack module is supported by four or five pedestals, which are remotely adjustable. The rack module support pedestals length adjustment is primarily provided to accommodate minor level variations in the pool floor flatness. Thus, the racks can be installed in a vertical position and the top of the racks can easily be made co-planar with each other. Some pedestals will be supported by the existing sub-base beams. Between the rack module pedestals and the pool floor liner is a bearing pad, which serves to diffuse the dead load of the loaded racks into the reinforced concrete structure of the pool slab. The bearing pads are part of the new rack installation.

The overall design of the rack modules is similar to those presently in service in the spent fuel pools at many other nuclear plants. Altogether, Holtec has provided over 50 thousand storage cells of this design to various nuclear plants around the world.

2.2 Summary of Principal Design Criteria

The key design criteria for the new spent fuel racks are set forth in the USNRC memorandum entitled "OT Position for Review and Acceptance of Spent Fuel Storage and Handling Applications," dated 14 April 1978 as modified by amendment dated 18 January 1979. The individual sections of this report expound on the specific design bases derived from the above-mentioned "OT Position Paper". A brief summary of the design bases for the racks is presented in the following:

- a. Disposition: All new rack modules are required to be freestanding.
- b. Kinematic Stability: All freestanding modules must be kinematically stable (against tipping or overturning) if a seismic event is imposed on any module.
- c. Structural Compliance: All primary stresses in the rack modules must satisfy the limits postulated in Section III Subsection NF of the ASME B&PV Code.
- d. Thermal-Hydraulic Compliance: The spatial average bulk pool temperature is required to remain below allowable levels subsequent to an offload, with due consideration of a worst-case single active cooling system failure.
- e. Criticality Compliance: The fuel storage racks must be able to store Zircaloy clad fuel of 5.0 weight percent (w/o) maximum enrichment while maintaining the reactivity (K_{eff}) less than 1.0 without soluble boron and 0.95 with soluble boron.
- f. Bearing Pads: The bearing pad size and thickness must ensure that the pressure on the concrete continues to satisfy the American Concrete Institute (ACI) limits during and after a seismic event.
- g. Accident Events: In the event of postulated drop events (uncontrolled lowering of a fuel assembly, for instance), it is necessary to demonstrate that the subcritical geometry of the rack structure is not compromised.

The foregoing design bases are further articulated in Sections 4 through 7 of this licensing report.

2.3 Applicable Codes and Standards

The following codes, standards and practices are used as applicable for the design, construction, and assembly of the fuel storage racks. Additional specific references related to detailed analyses are given in each section.

a. Design Codes

- (1) AISC Manual of Steel Construction, 1969 or 1978 edition or latest Edition.
- (2) ANSI N210-1976, "Design Requirements for Light Water Reactor Spent Fuel Storage Facilities at Nuclear Power Stations" (contains guidelines for fuel rack design).
- (3) American Society of Mechanical Engineers (ASME), Boiler and Pressure Vessel Code Section III, Subsection NF 1998 Edition.; Section VIII ; and Section XI, all latest Edition.
- (4) ASNT-TC-1A June 1980 American Society for Nondestructive Testing (Recommended Practice for Personnel Qualifications), latest Edition.
- (5) American Concrete Institute Building Code Requirements for Reinforced Concrete (ACI318-63) and (ACI318-71).
- (6) Code Requirements for Nuclear Safety Related Concrete Structures, ACI349-85/ACI349R-85, and ACI349.1R-80.
- (7) ASME NQA-1, Quality Assurance Program Requirements for Nuclear Facilities
- (8) ASME NQA-2-1989, Quality Assurance Requirements for Nuclear Facility Applications.
- (9) ANSI Y14.5M, Dimensioning and Tolerancing for Engineering Drawings and Related Documentation Practices
- (10) ACI -315, Manual of standard practice for detailing reinforced concrete structures, 1965 or 1974 edition or latest edition.

b. Material Codes - Standards of ASTM

- (1) E165 - Standard Methods for Liquid Penetrant Inspection.

- (2) A240 - Standard Specification for Heat-Resisting Chromium and Chromium-Nickel Stainless Steel Plate, Sheet and Strip for Fusion-Welded Unfired Pressure Vessels.
 - (3) A262 - Detecting Susceptibility to Intergranular Attack in Austenitic Stainless Steel.
 - (4) A276 - Standard Specification for Stainless and Heat-Resisting Steel Bars and Shapes.
 - (5) A479 - Steel Bars for Boilers & Pressure Vessels.
 - (6) A564, Standard Specification for Hot-Rolled and Cold-Finished Age-Hardening Stainless and Heat-Resisting Steel Bars and Shapes.
 - (7) C750 - Standard Specification for Nuclear-Grade Boron Carbide Powder.
 - (8) A380 - Recommended Practice for Descaling, Cleaning and Marking Stainless Steel Parts and Equipment.
 - (9) C992 - Standard Specification for Boron-Based Neutron Absorbing Material Systems for Use in Nuclear Spent Fuel Storage Racks.
 - (10) E3, Preparation of Metallographic Specimens
 - (11) E190, Guided Bend Test for Ductility of Welds
 - (12) American Society of Mechanical Engineers (ASME), Boiler and Pressure Vessel Code, Section II-Parts A and C, 1998 Edition.
 - (13) NCA3800 - Metallic Material Manufacturer's and Material Supplier's Quality System Program.
- c. Welding Codes: ASME Boiler and Pressure Vessel Code, Section IX - Welding and Brazing Qualifications, latest Edition.
- d. Quality Assurance, Cleanliness, Packaging, Shipping, Receiving, Storage, and Handling Requirements
- (1) ANSI 45.2.1 - Cleaning of Fluid Systems and Associated Components during Construction Phase of Nuclear Power Plants.
 - (2) ANSI N45.2.2 - Packaging, Shipping, Receiving, Storage and Handling of Items for Nuclear Power Plants (During the Construction Phase).

- (3) ANSI - N45.2.6 - Qualifications of Inspection, Examination, and Testing Personnel for Nuclear Power Plants (Regulatory Guide 1.58).
- (4) ANSI-N45.2.8, Supplementary Quality Assurance Requirements for Installation, Inspection and Testing of Mechanical Equipment and Systems for the Construction Phase of Nuclear Plants.
- (5) ANSI - N45.2.11, Quality Assurance Requirements for the Design of Nuclear Power Plants.
- (6) ANSI-N45.2.12, Requirements for Auditing of Quality Assurance Programs for Nuclear Power Plants.
- (7) ANSI N45.2.13 - Quality Assurance Requirements for Control of Procurement of Equipment Materials and Services for Nuclear Power Plants (Regulatory Guide 1.123).
- (8) ANSI N45.2.15-18 - Hoisting, Rigging, and Transporting of Items For Nuclear Power Plants.
- (9) ANSI N45.2.23 - Qualification of Quality Assurance Program Audit Personnel for Nuclear Power Plants (Regulatory Guide 1.146).
- (10) ASME Boiler and Pressure Vessel, Section V, Nondestructive Examination, latest Edition.
- (11) ANSI - N16.9-75 Validation of Calculation Methods for Nuclear Criticality Safety.
- (12) ASME Boiler and Pressure Vessel Code NCA3550 Requirements for Design Documents, latest Edition.
- (13) ASME Boiler and Pressure Vessel Code NCA4000 - Quality Assurance, latest Edition.
- (14) ASME NQA-1, Requirements for the establishment and execution of quality assurance programs for the siting, design, construction, operation, and decommissioning of nuclear facilities, 1994 Edition.

e. Governing NRC Design Documents

- (1) NUREG-0800, Radiological Consequences of Fuel Handling Accidents.
- (2) "OT Position for Review and Acceptance of Spent Fuel Storage and Handling Applications," dated April 14, 1978, and the modifications to this document of January 18, 1979.

- (3) NUREG-0612, "Control of Heavy Loads at Nuclear Power Plants", USNRC, Washington, D.C., July 1980.

f. Other ANSI Standards (not listed in the preceding)

- (1) ANSI/ANS 8.1 (N16.1) - Nuclear Criticality Safety in Operations with Fissionable Materials Outside Reactors
- (2) ANSI/ANS 8.17, Criticality Safety Criteria for the Handling, Storage, and Transportation of LWR Fuel Outside Reactors
- (3) ANSI N45.2 - Quality Assurance Program Requirements for Nuclear Facilities - 1971
- (4) ANSI N45.2.9 - Requirements for Collection, Storage and Maintenance of Quality Assurance Records for Nuclear Power Plants - 1974
- (5) ANSI N45.2.10 - Quality Assurance Terms and Definitions -1973
- (6) ANSI/ANS 57.2 - Design Requirements for Light Water Reactor Spent Fuel Storage Facilities at Nuclear Power Plants - 1983.
- (7) ANSI N14.6 - American National Standard for Special Lifting Devices for Shipping Containers Weighing 10,000 pounds (4500 kg) or more for Nuclear Materials-1992
- (8) ANSI/ASME N626-3, Qualification and Duties of Personnel Engaged in ASME Boiler and Pressure Vessel Code Section III, Div. 1, Certifying Activities

g. Code of Federal Regulations

- (1) 10CFR20 - Standards for Protection Against Radiation
- (2) 10CFR21 - Reporting of Defects and Non-compliance
- (3) 10CFR50 - Appendix A - General Design Criteria for Nuclear Power Plants
- (4) 10CFR50 - Appendix B - Quality Assurance Criteria for Nuclear Power Plants and Fuel Reprocessing Plants
- (5) 10CFR61 - Licensing Requirements for Land Disposal of Radioactive Material
- (6) 10CFR71 - Packaging and Transportation of Radioactive Material

h. Regulatory Guides (RG)

- (1) RG 1.13 - Spent Fuel Storage Facility Design Basis (Revision 2 Proposed)
- (2) RG 1.25 - Assumptions Used for Evaluating the Potential Radiological Consequences of a Fuel Handling Accident in the Fuel Handling and Storage Facility of Boiling and Pressurized Water Reactors
- (3) RG 1.28 - (ANSI N45.2) - Quality Assurance Program Requirements
- (4) RG 1.29 - Seismic Design Classification (Rev. 3)
- (5) RG 1.31 - Control of Ferrite Content in Stainless Steel Weld Material
- (6) RG 1.38 - (ANSI N45.2.2) Quality Assurance Requirements for Packaging, Shipping, Receiving, Storage and Handling of Items for Water-Cooled Nuclear Power Plants
- (7) RG 1.44 - Control of the Use of Sensitized Stainless Steel
- (8) RG 1.58 - (ANSI N45.2.6) Qualification of Nuclear Power Plant Inspection, Examination, and Testing Personnel
- (9) RG 1.61 - Damping Values for Seismic Design of Nuclear Power Plants, Rev. 0, 1973
- (10) RG 1.64 - (ANSI N45.2.11) Quality Assurance Requirements for the Design of Nuclear Power Plants
- (11) RG 1.71 - Welder Qualifications for Areas of Limited Accessibility
- (12) RG 1.74 - (ANSI N45.2.10) Quality Assurance Terms and Definitions
- (13) RG 1.85 - Materials Code Case Acceptability - ASME Section 3, Div. 1
- (14) RG 1.88 - (ANSI N45.2.9) Collection, Storage and Maintenance of Nuclear Power Plant Quality Assurance Records
- (15) RG 1.92 - Combining Modal Responses and Spatial Components in Seismic Response Analysis
- (16) RG 1.122 - Development of Floor Design Response Spectra for Seismic Design of Floor-Supported Equipment or Components
- (17) RG 1.123 - (ANSI N45.2.13) Quality Assurance Requirements for Control of Procurement of Items and Services for Nuclear Power Plants

- (18) RG 1.124 - Service Limits and Loading Combinations for Class 1 Linear-Type Component Supports, Revision 1, 1978
- (19) RG 3.4 - Nuclear Criticality Safety in Operations with Fissionable Materials at Fuels and Materials Facilities
- (20) RG 3.41 - Validation of Calculational Methods for Nuclear Criticality Safety, Revision 1, 1977
- (21) RG 8.8 - Information Relative to Ensuring that Occupational Radiation Exposure at Nuclear Power Plants will be as Low as Reasonably Achievable (ALARA)
- (22) DG-8006, "Control of Access to High and Very High Radiation Areas in Nuclear Power Plants"
- (23) IE Information Notice 83-29 - Fuel Binding Caused by Fuel Rack Deformation
- (24) RG 8.38 - Control of Access to High and Very High Radiation Areas in Nuclear Power Plants, June, 1993

i. Branch Technical Position

- (1) CPB 9.1-1 - Criticality in Fuel Storage Facilities

j. Standard Review Plan

- (1) SRP 3.2.1 - Seismic Classification
- (2) SRP 3.2.2 - System Quality Group Classification
- (3) SRP 3.7.1 - Seismic Design Parameters
- (4) SRP 3.7.2 - Seismic System Analysis
- (5) SRP 3.7.3 - Seismic Subsystem Analysis
- (6) SRP 3.8.4 - Other Seismic Category I Structures (including Appendix D), Technical Position on Spent Fuel Rack
- (7) SRP 3.8.5 - Foundations for Seismic Category I Structures, Revision 1, 1981
- (8) SRP 9.1.2 - Spent Fuel Storage, Revision 3, 1981
- (9) SRP 9.1.3 - Spent Fuel Pool Cooling and Cleanup System

- (10) SRP 9.1.4 - Light Load Handling System
- (11) SRP 9.1.5 - Heavy Load Handling System
- (12) SRP 15.7.4 - Radiological Consequences of Fuel Handling Accidents

k. AWS Standards

- (1) AWS D1.1 - Structural Welding Code, Steel
 - (2) AWS D1.3 - Structure Welding Code - Sheet Steel
 - (3) AWS D9.1 - Welding of Sheet Metal
 - (4) AWS A2.4 - Standard Symbols for Welding, Brazing and Nondestructive Examination
 - (5) AWS A3.0 - Standard Welding Terms and Definitions
 - (6) AWS A5.12 - Tungsten Arc-welding Electrodes
 - (7) AWS QC1 - Standards and Guide for Qualification and Certification of Welding Inspectors
- l. EPRI: "A Methodology for Assessment of Nuclear Power Plant Seismic Margin (Rev. 1), EPRI NP-60415L.

2.4 Quality Assurance Program

The governing quality assurance requirements for design and fabrication of the spent fuel racks are stated in 10CFR50 Appendix B. Holtec's Nuclear Quality Assurance program complies with this regulation and is designed to provide a flexible but highly controlled system for the design, analysis and licensing of customized components in accordance with various codes, specifications, and regulatory requirements.

2.5 Mechanical Design

The rack modules are designed as cellular structures such that each fuel assembly has a square opening with conforming lateral support and a flat horizontal-bearing surface. All of the storage locations are constructed with multiple cooling flow holes to ensure that redundant flow paths

for the coolant are available. The basic characteristics of the spent fuel racks are summarized in Table 2.5.1.

A central objective in the design of the new rack modules is to maximize structural strength while minimizing inertial mass and dynamic response. Accordingly, the rack modules have been designed to simulate multi-flange beam structures resulting in excellent de-tuning characteristics with respect to the applicable seismic events. The next subsection presents an item-by-item description of the rack modules in the context of the fabrication methodology.

2.6 Rack Fabrication

The object of this section is to provide a brief description of the rack module construction activities, which enable an independent appraisal of the adequacy of design. The pertinent methods used in manufacturing the spent fuel storage racks may be stated as follows:

1. The rack modules are fabricated in such a manner that the storage cell surfaces, which would come in contact with the fuel assembly, will be free of harmful chemicals and projections (e.g., weld splatter).
2. The component connection sequence and welding processes are selected to reduce fabrication distortions.
3. The fabrication process involves operational sequences that permit immediate accessibility for verification by the inspection staff.
4. The racks are fabricated per the Holtec Appendix B Quality Assurance program, which ensures, and documents, that the fabricated rack modules meet all of the requirements of the design and fabrication documents.

2.6.1 Non-Flux-Trap Rack Module Description

This section describes the constituent elements of the non-flux-trap rack module in the fabrication sequence. Figure 2.1.1 provides a schematic view of a typical non-flux-trap rack.

The rack module manufacturing begins with fabrication of the “box”. The boxes are fabricated from two precision formed channels by seam welding in a machine equipped with copper chill bars and pneumatic clamps to minimize distortion due to welding heat input. Figure 2.6.1 shows the box. The minimum weld seam penetration is 80% of the box metal gage, which is 0.075 inch (14 gauge).

Each box constitutes a storage location. Each external box side is equipped with a stainless steel sheathing, which holds one integral Metamic sheet (neutron absorber material). The design objective calls for attaching Metamic tightly on the box surface. This is accomplished by die forming the internal and external box sheathings, as shown in Figure 2.6.1. The flanges of the sheathing are attached to the box using skip welds and spot welds. The sheathings serve to locate and position the neutron absorber sheet accurately, and to preclude its movement under seismic conditions.

Having fabricated the required number of composite box assemblies, they are arranged in a checkerboard array to form an assemblage of storage cell locations (Figure 2.6.2). Filler panels and corner angles are welded to the edges of boxes at the outside boundary of the rack to make the peripheral formed cells. The inter-box welding and pitch adjustment are accomplished by small longitudinal connectors. This assemblage of box assemblies is welded edge-to-edge as shown in Figure 2.6.2, resulting in a honeycomb structure with axial, flexural and torsional rigidity depending on the extent of inter-cell welding provided. It can be seen from Figure 2.6.2 that two edges of each interior box are connected to the contiguous boxes resulting in a well-defined path for “shear flow”, and essentially makes the box assemblage into a multi-flanged beam-type structure.

The “baseplate” provides a continuous horizontal surface for supporting the fuel assemblies. The baseplate is attached to the bottom edge of the boxes. The baseplate is a 3/4-inch thick austenitic stainless steel plate stock that has 5-inch diameter holes (except at lift locations that have

irregular shaped cut-outs of similar area) cut out in a pitch identical to the box pitch. The baseplate is attached to the cell assemblage by fillet welding the box edge to the plate.

In the final step, adjustable leg supports (shown in Figure 2.6.3) are welded to the underside of the baseplate. The bottom part is made of A564 Gr. 630 17-4 Ph series stainless steel to avoid galling problems. The adjustable legs provide a +1/4-inch, -1/2-inch vertical height adjustment at each leg location.

Appropriate NDE (nondestructive examination) occurs on all welds including visual examination of sheathing welds, box longitudinal seam welds, box-to-baseplate welds, and box-to-box connection welds, as well as liquid penetrant examination of support leg welds, in accordance with the design drawings.

An elevation view of three contiguous rack cells is shown in Figure 2.6.4.

TABLE 2.1.1: GEOMETRIC AND PHYSICAL DATA FOR THE NEW FUEL RACKS

RACK I.D.	RACK TYPE	NO. OF CELLS		MODULE ENVELOPE SIZE (Nom.)		WEIGHT (Lbs) (approx)	NO. OF CELLS PER RACK
		N-S Direction	E-W Direction	N-S	E-W		
A1	Non-Flux-Trap	9	12	81.565	108.655	16,200	96
A2	Non-Flux-Trap	9	12	81.565	108.655	17,800	108
A3	Non-Flux-Trap	9	8	81.565	72.535	11,700	72
B1	Non-Flux-Trap	9	13	81.565	117.685	18,500	111
B2	Non-Flux-Trap	9	12	81.565	108.655	17,800	108
B3	Non-Flux-Trap	9	12	81.565	108.655	17,800	108
B4	Non-Flux-Trap	9	14	81.565	126.715	19,500	126
C1	Non-Flux-Trap	9	13	81.565	117.685	18,800	117
C2	Non-Flux-Trap	9	12	81.565	108.655	17,800	108
C3	Non-Flux-Trap	9	12	81.565	108.655	17,800	108
C4	Non-Flux-Trap	9	14	81.565	126.715	20,100	126
D1	Non-Flux-Trap	10	13	90.595	117.685	19,600	122
D2	Non-Flux-Trap	10	12	90.595	108.655	19,000	120
D3	Non-Flux-Trap	10	12	90.595	108.655	19,000	120
D4	Non-Flux-Trap	10	14	90.595	126.715	21,400	140

Table 2.5.1 MODULE DATA FOR NON-FLUX TRAP FUEL RACKS ¹	
Storage Cell Inside Dimension	8.8 in.
Cell Pitch	9.03 in.
Storage Cell Height (above baseplate)	168-5/8 in.
Baseplate Hole Size (except for lift locations)	5 in.
Baseplate Thickness	3/4 in.
Support Pedestal Height (including bearing pad)	11-3/8 in.
Support Pedestal Type	Remotely adjustable pedestals
Number Of Support Pedestals Per Rack	4 or 5
Number Of Cell Walls Containing Auxiliary Flow Holes At Base Of Cell Wall	4
Remote Lifting And Handling Provisions	Yes
Neutron Absorber Material	Metamic
Neutron Absorber Length	146 in.
Neutron Absorber Width	7-1/2 in.

¹ All dimensions indicate nominal values.

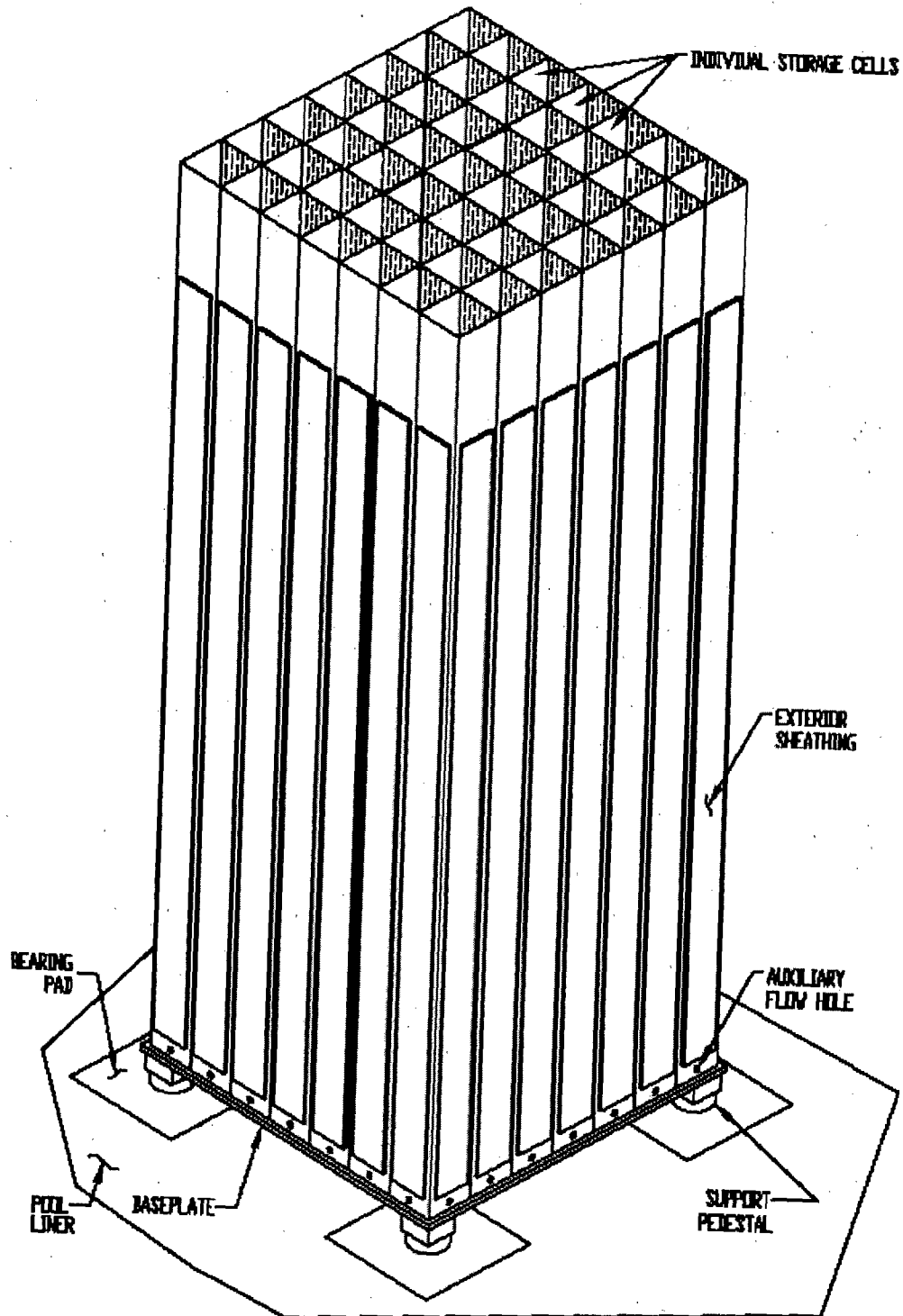


FIGURE 2.1.1 – ISOMETRIC VIEW OF GENERIC NON-FLUX TRAP RACK

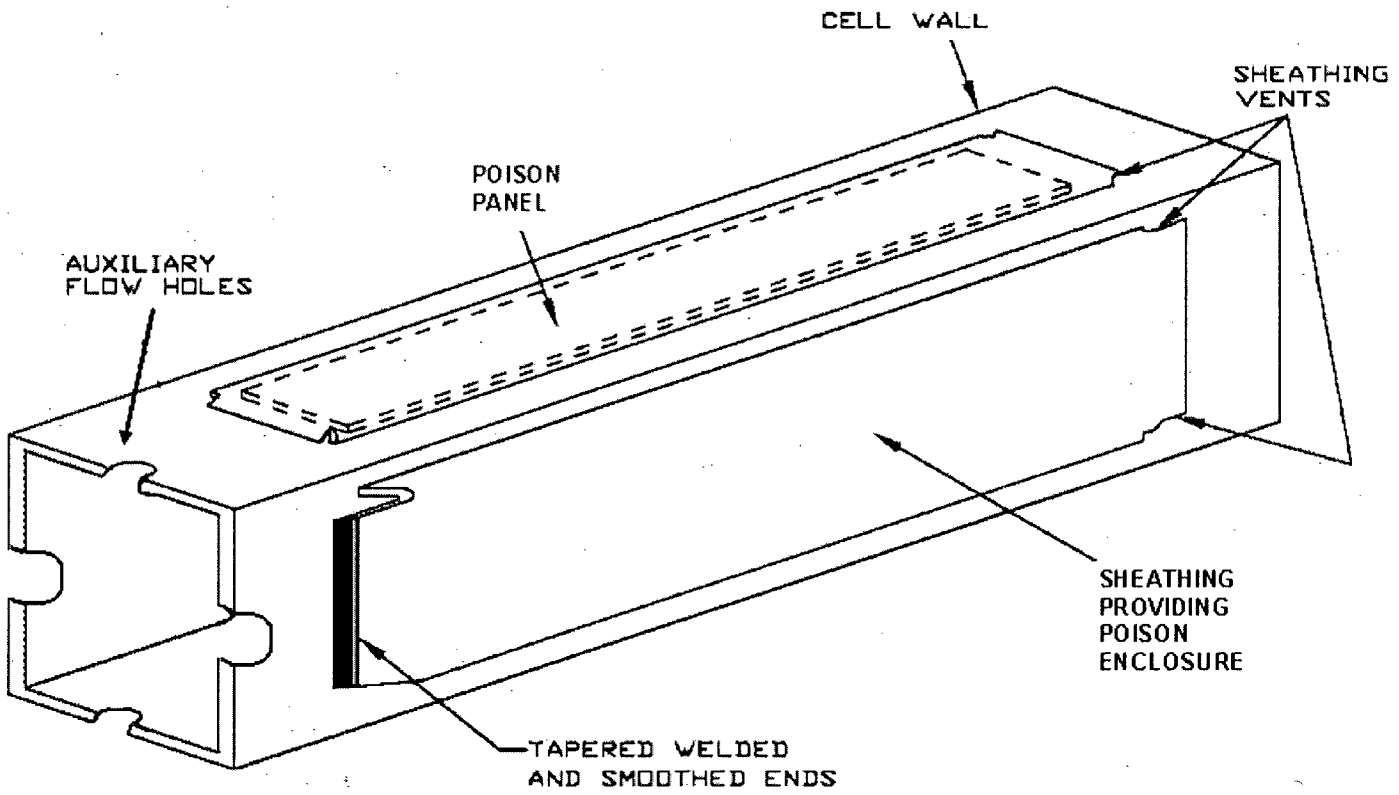


FIGURE 2.6.1 - ISOMETRIC VIEW OF COMPOSITE BOX ASSEMBLY
(Flared Top End for Flux Trap Boxes Not Shown)

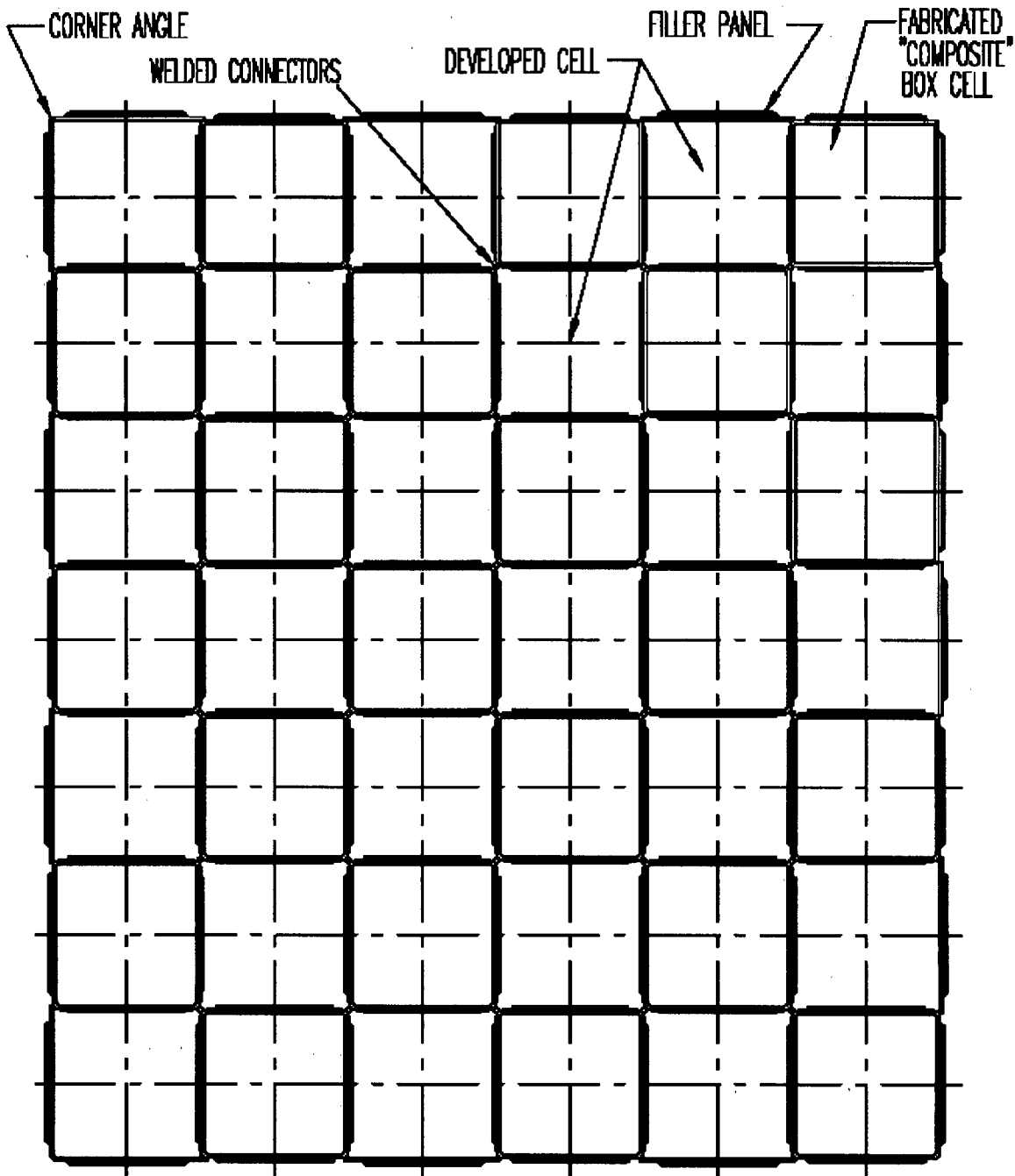
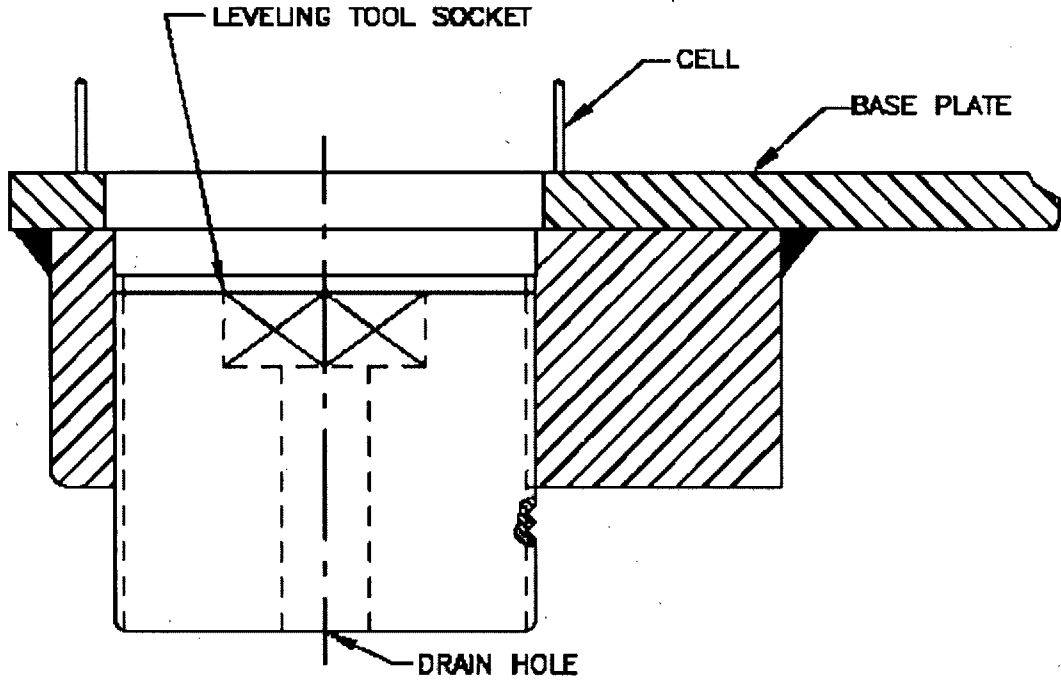
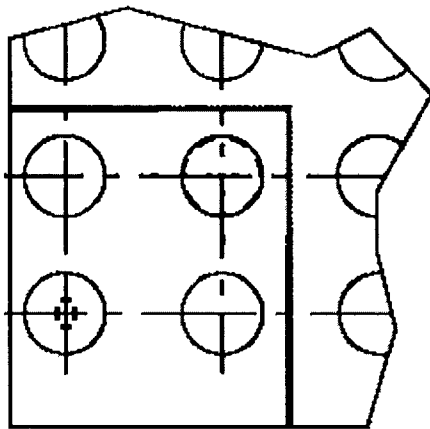


FIGURE 2.6.2 – PLAN VIEW OF GENERIC NON-FLUX TRAP RACK ARRAY



TYPICAL ELEVATION VIEW



TYPICAL PLAN VIEWS OF RACK BASEPLATE CORNER

FIGURE 2.6.3 – ADJUSTABLE PEDESTAL DESIGN

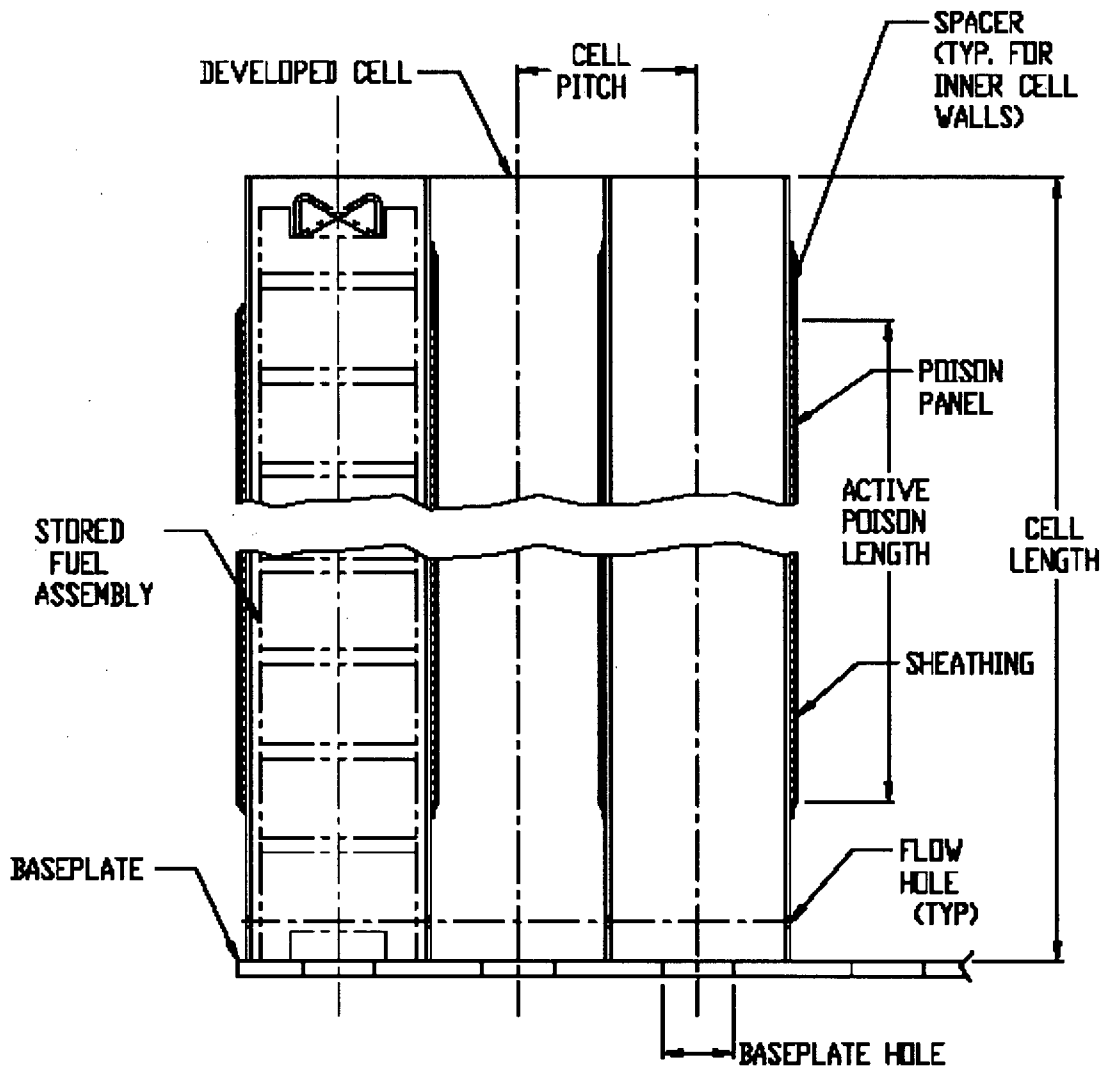


FIGURE 2.6.4 – NON-FLUX-TRAP RACK CELLS ELEVATION VIEW

3.0 MATERIAL CONSIDERATIONS

3.1 Introduction

Safe storage of nuclear fuel in the pool requires that the materials utilized in the rack fabrication be of proven durability and compatible with the pool water environment. This section provides a synopsis of the considerations with regard to long-term service life.

3.2 Structural Materials

The following structural materials are utilized in the fabrication of the fuel racks:

- a. ASTM A240 Types 304 or 304L for all sheet metal stock and baseplate
- b. Internally threaded support pedestals: ASTM A240 Type 304
- c. Externally threaded support pedestals: ASTM A564-630 precipitation hardened stainless steel (heat treated to 1100°F)
- d. Weld material - ASTM Types 308 or 308L

3.3 Neutron Absorbing Material

The Metamic™ neutron absorber material, proposed for use in the new racks, is manufactured by the Holtec Nanotec Materials Division in Lakeland, Florida. As discussed below, Metamic™ has been subjected to rigorous tests by various organizations including Holtec International, and has been approved by the USNRC in recent dry (Dockets 71-9261 and 72-1014) as well as recent wet storage applications for Arkansas Nuclear One Units 1 and 2 (Dockets 50-313 and 50-368), Clinton (Docket 50-461), Diablo Canyon Units 1 and 2 (Dockets 50-275 and 50-323), St. Lucie Unit 2 (Docket 50-389), Turkey Point Unit 3 (Docket 50-250) and Cooper Nuclear Station (Docket 50-298).

Metamic™ was developed in the mid-1990s by the Reynolds Metals Company [3.2.9] with the technical support of the Electric Power Research Institute (EPRI) for spent fuel reactivity control in dry and wet storage applications with the explicit objective to eliminate the performance frailties of aluminum cermet type of absorbers reported in the industry. Metallurgically,

Metamic™ is a metal matrix composite (MMC) consisting of a matrix of aluminum reinforced with Type 1 ASTM C-750 boron carbide. Metamic™ is characterized by extremely fine aluminum (325 mesh or smaller) and boron carbide (B₄C) powder. Typically, the average B₄C particle size is between 10 and 40 microns. The high performance and reliability of Metamic™ derives from the fineness of the B₄C particle size and uniformity of its distribution, which is solidified into a metal matrix composite structure by the powder metallurgy process. This yields excellent homogeneity and a porosity-free material.

In Metamic™'s manufacturing process, the aluminum and boron carbide powders are carefully blended without binders or other additives that could potentially adversely influence Metamic™'s performance. The blend of powders is isostatically compacted into a green billet under high pressure and vacuum sintered to near theoretical density. The billet is extruded and subjected to multiple rolling operations to produce sheet stock of the required thickness and a tight thickness tolerance. An array of U.S. patents discloses the unique technologies that underlie the Metamic™ neutron absorber [3.2.1-3.2.4].

In recognition of the central role of the neutron absorber in maintaining the subcriticality, Holtec International utilizes appropriately rigorous technical and quality assurance criteria and acceptance protocols to ensure satisfactory neutron absorber performance over the service life of the fuel racks. Holtec International's Quality Assurance Program ensures that Metamic™ will be manufactured under the control and surveillance of a Quality Assurance/Quality Control Program that conforms to the requirements of 10CFR50 Appendix B, "Quality Assurance Criteria for Nuclear Power Plants." Consistent with its role in reactivity control, all neutron absorbing material procured for use in the Holtec racks is categorized as Safety Related (SR). SR manufactured items, as required by Holtec's NRC-approved Quality Assurance program, must be produced to essentially preclude, to the extent possible, the potential of an error in the procurement of constituent materials and the manufacturing processes.

Accordingly, material and manufacturing control processes must be established to eliminate the incidence of errors, and inspection steps are implemented to serve as an independent set of

barriers to ensure that all critical characteristics defined for the material by Holtec's design team are met in the manufactured product.

3.3.1 Characteristics of Metamic™

Because Metamic™ is a porosity-free material, unlike Boral, there is no capillary path through which spent fuel pool water can penetrate Metamic™ panels and chemically react with aluminum in the interior of the material to generate hydrogen. Thus, the potential of swelling and generation of significant quantities of hydrogen is eliminated.

To determine its physical stability and performance characteristics, Metamic™ was subjected to an extensive array of tests sponsored by EPRI that evaluated the functional performance of the material at elevated temperatures (up to 900°F) and radiation levels (1E+11 rads gamma). The results of the tests documented in an EPRI report [3.2.5] indicate that Metamic™ maintains its physical and neutron absorption properties with little variation in its properties from the unirradiated state. The main conclusions provided in the above-referenced EPRI report, which endorsed Metamic™ for dry and wet storage applications on a generic basis, are summarized below:

- The metal matrix configuration produced by the powder metallurgy process with almost a complete absence of open porosity in Metamic™ ensures that its density is essentially equal to the theoretical density.
- The physical and neutronic properties of Metamic™ are essentially unaltered under exposure to elevated temperatures (750° F - 900° F).
- No detectable change in the neutron attenuation characteristics under accelerated corrosion test conditions has been observed.

Additional technical information on Metamic™ in the literature includes independent measurements of boron carbide particle distribution in Metamic™ panels, which showed extremely small particle-to-particle distance [3.2.6]. The USNRC has previously approved Metamic™ for use in both wet storage [3.2.7] and dry storage [3.2.8] applications.

Metamic™ has also been subjected to independent performance assessment tests by Holtec International in the company's Florida laboratories since 2001 [3.2.9, 3.2.10]. The three-year long experimental study simulated limiting environmental conditions in wet and dry storage. No anomalous material behavior was observed in any of the tests. These independent Holtec tests essentially confirmed earlier EPRI and other industry reports cited in the foregoing with regard to Metamic™'s suitability as a neutron absorber in fuel storage applications.

3.4 In-Service Surveillance of the Neutron Absorber

3.4.1 Purpose

Metamic™, the neutron absorbing material incorporated in the spent fuel storage rack design to assist in controlling system reactivity, consists of finely divided particles of boron carbide (B₄C) uniformly distributed in type 6061 aluminum powder. Tests simulating the radiation, thermal and chemical (i.e., boric acid solutions) environment of the spent fuel pool have demonstrated the stability and chemical inertness of Metamic.

Based upon the accelerated test programs, Metamic is considered a satisfactory material for reactivity control in spent fuel storage racks and is fully expected to fulfill its design function over the lifetime of the racks. Nevertheless, as a defense-in-depth measure, a Metamic surveillance program has been developed and will be implemented for the SFP in order to monitor the integrity and performance of Metamic.

The purpose of the surveillance program is to characterize certain properties of the Metamic with the objective of providing data necessary to assess the capability of the Metamic panels in the racks to continue to perform their intended function. The surveillance program is also capable of detecting the onset of any significant degradation with ample time to take such corrective action as may be necessary.

The Metamic surveillance program depends primarily on representative coupon samples to monitor performance of the absorber material without disrupting the integrity of the storage

system. The principal parameters to be measured are the thickness (to monitor for swelling) and B-10 loading (to monitor for the continued presence of boron in the Metamic).

3.4.2 Coupon Surveillance Program

3.4.2.1 Coupon Description

The coupon measurement program includes coupons suspended on a mounting (called a "tree"), placed in a designated cell, and surrounded by spent fuel. Coupons may be removed from the array on a prescribed schedule and certain physical and chemical properties measured from which the stability and integrity of the Metamic in the storage cells may be inferred.

The coupon surveillance program uses a tree with a total of 8 to 10 test coupons. In mounting the coupons on the tree, the coupons are positioned axially within the central eight feet (approximate) of the active fuel zone where the gamma flux is expected to be reasonably uniform.

The coupons are taken from the same lot as that used for construction of the racks. Each coupon is carefully precharacterized prior to insertion in the pool to provide reference initial values for comparison with measurements made after irradiation. As a minimum, the surveillance coupons are precharacterized for weight, dimensions (especially thickness) and B-10 loading.

3.4.2.2 Surveillance Coupon Testing Schedule

To assure that the coupons will have experienced a slightly higher radiation dose than the Metamic in the racks, one of the following strategies shall be implemented:

1. The coupon tree is surrounded by freshly-discharged fuel assemblies after each of the first four refueling outages. At the time of the first fuel offload following installation of the coupon tree, the four storage cells surrounding the tree shall be loaded with discharged fuel assemblies which are not scheduled to be returned to the core.

2. At least one (1) location adjacent to the coupon tree is loaded with freshly-discharged fuel assemblies after each refueling outage for the life of the racks. At the time of the first fuel offload following installation of the coupon tree, one of the four storage cells surrounding the tree shall be loaded with a discharged fuel assembly which is not scheduled to be returned to the core.

At the scheduled test date, the coupon tree is removed and a coupon removed for evaluation. A sample coupon measurement schedule is shown in Table 3.4.1.

Evaluation of the coupons removed will provide information of the effects of the radiation, thermal and chemical environment of the pool and by inference, comparable information on the Metamic panels in the racks. Over the duration of the coupon testing program, the coupons will have accumulated more radiation dose than the expected lifetime dose for normal storage cells. Coupons that have not been destructively analyzed by wet-chemical processes may optionally be returned to the storage pool and remounted on the tree. They will then be available for subsequent investigation of defects, should any be found.

3.4.2.3 Measurement Program

The coupon measurement program is intended to monitor changes in physical properties of the Metamic absorber material by performing the following measurements on the preplanned schedule:

- Visual Observation and Photography
- Neutron Attenuation
- Dimensional Measurements (length, width and thickness)
- Weight and Specific Gravity

3.4.2.4 Surveillance Coupon Acceptance Criteria

Of the measurements to be performed on the Metamic surveillance coupons, the most important are (1) the neutron attenuation¹ measurements (to verify the continued presence of the boron) and (2) the thickness measurement (as a monitor of potential swelling). Acceptance criteria for these measurements are as follows:

- A decrease of no more than 5% in Boron-10 (B-10) content, as determined by neutron attenuation, is acceptable. (This is equivalent to a requirement for no loss in boron within the accuracy of the measurement.)
- An increase in thickness at any point should not exceed 10% of the initial thickness at that point.

Changes in excess of either of these two criteria requires investigation and engineering evaluation which may include early retrieval and measurement of one or more of the remaining coupons to provide corroborative evidence that the indicated change(s) is real. If the deviation is determined to be real, an engineering evaluation shall be performed to identify further testing or any corrective action that may be necessary.

The remaining measurement parameters serve a supporting role and should be examined for early indications of the potential onset of Metamic degradation that would suggest a need for further attention and possibly a change in measurement schedule. These include (1) visual or photographic evidence of unusual surface pitting, blistering, corrosion or edge deterioration, or (2) unaccountable weight loss in excess of the measurement accuracy.

3.5 References

- [3.2.1] U.S. Patent # 6,332,906 entitled "Aluminum-Silicon Alloy formed by Powder", Thomas G. Haynes III and Dr. Kevin Anderson, issued December 25, 2001.

¹ Neutron attenuation measurements are a precise instrumental method of chemical analysis for Boron-10 content using a nondestructive technique in which the percentage of thermal neutrons transmitted through the panel is measured and compared with predetermined calibration data. Boron-10 is the nuclide of principal interest since it is the isotope responsible for neutron absorption in the Metamic panel.

- [3.2.2] U.S. Patent # 5,965,829 entitled “Radiation Absorbing Refractory Composition and Method of Manufacture”, Dr. Kevin Anderson, Thomas G. Haynes III, and Edward Oschmann, issued October 12, 1999.
- [3.2.3] U.S. Patent # 6,042,779 entitled “Extrusion Fabrication Process for Discontinuous Carbide Particulate Metal and Super Hypereutectic Al/Si Alloys”, Thomas G. Haynes III and Edward Oschmann, issued March 28, 2000.
- [3.2.4] U.S. Patent Application 09/433773 entitled “High Surface Area Metal Matrix Composite Radiation Absorbing Product”, Thomas G. Haynes III and Goldie Oliver, filed May 1, 2002.
- [3.2.5] “Qualification of METAMIC® for Spent Fuel Storage Application,” EPRI, 1003137, Final Report, October 2001.
- [3.2.6] “METAMIC Neutron Shielding”, by K. Anderson, T. Haynes, and R. Kazmier, EPRI Boraflex Conference, November 19-20 (1998).
- [3.2.7] “Safety Evaluation by the Office of Nuclear Reactor Regulation Related to Holtec International Report HI-2022871 Regarding Use of Metamic in Fuel Pool Applications,” Facility Operating License Nos. DPR-51 and NPF-6, Entergy Operations, Inc., Docket No. 50-313 and 50-368, USNRC, June 2003.
- [3.2.8] USNRC Docket No. 72-1004, NRC’s Safety Evaluation Report on NUHOMS 61BT (2002).
- [3.2.9] “Use of METAMIC® in Fuel Pool Applications,” Holtec Information Report No. HI-2022871, Revision 1 (2002).
- [3.2.10] “Sourcebook for Metamic™ Performance Assessment” by Dr. Stanley Turner, Holtec Report No. HI-2043215, Revision 2 (2006).

Table 3.4.1 SAMPLE COUPON MEASUREMENT SCHEDULE	
Coupon	Years ¹
1	2
2	4
3	6
4	8
5	10
6	15
7	20
8	25
9	30
10	40

¹ The years pertain to those after the installation of new racks.

4.0 CRITICALITY SAFETY ANALYSIS

4.1 Introduction and Summary

This chapter documents the criticality safety evaluation for the storage of fresh and spent fuel assemblies with an nominal initial enrichment of up to 5.0 wt% ^{235}U in a Mixed-Zone Three Region (MZTR) storage arrangement (a loading pattern that includes a region of fresh fuel and two regions of spent fuel together in each storage rack) in Holtec high-density spent fuel storage racks (SFSRs) at the Beaver Valley Power Station (BVPS) Unit No. 2 operated by FirstEnergy Nuclear Operating Company (FENOC). This is a new criticality safety evaluation to support the installation of new racks to increase the storage capacity of the spent fuel pool.

The objective of this chapter is to demonstrate that the effective neutron multiplication factor (k_{eff}) is less than 1.0 with the storage racks fully loaded with fuel of the highest anticipated reactivity and the pool flooded with unborated water at a temperature corresponding to the highest reactivity. In addition, it is demonstrated that k_{eff} is less than or equal to 0.95 with the storage racks fully loaded with fuel of the highest anticipated reactivity and the pool flooded with borated water at a temperature corresponding to the highest reactivity. The maximum calculated reactivity includes a margin for uncertainty in reactivity calculations including manufacturing tolerances and is shown to be less than 0.95 with a 95% probability at a 95% confidence level. Reactivity effects of abnormal and accident conditions have also been evaluated to assure that under all credible abnormal and accident conditions, the reactivity will not exceed the regulatory limit of 0.95.

The new storage racks to be installed at BVPS Unit No. 2 spent fuel pool have storage cells that are regionalized for loading purposes into three distinct regions, with independent criteria defining each region (see also Figure 4.5.3 and Figure 4.5.4):

- Region 1 is designed to accommodate fresh fuel with a maximum initial enrichment up to 5.0 wt% ^{235}U . Region 1 storage cells are located on the periphery of each rack (outer row only) and are therefore separated from other Region 1 cells in adjacent racks by the gap between the racks. Region 1 cells are additionally separated from other Region 1 cells within the same rack by Region 2 cells (including a Region 2 cell in the diagonal

direction, see Figure 4.5.3). Since Region 1 cells are qualified for the storage of fresh fuel, any fuel assembly (fresh or burned) meeting the maximum enrichment requirement may be stored in a Region 1 location.

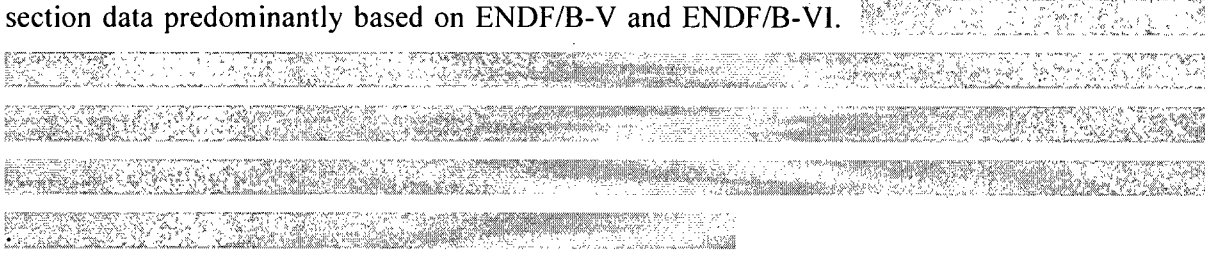
- Region 2 is designed to accommodate fuel with a maximum initial enrichment of up to 5.0 wt% ^{235}U and a high burnup defined according to the calculated Region 2 initial enrichment and burnup combination in Table 4.7.1 (see Section 4.7). Region 2 cells are located on the rack periphery (outer row) interspaced with (separating) Region 1 cells and are also located in the second row of cells (from the outside of the rack) separating the Region 1 cells from the Region 3 cells.
- Region 3 is designed to accommodate fuel with a maximum initial enrichment of up to 5.0 wt% ^{235}U and a moderate burnup defined according to the calculated Region 3 initial enrichment and burnup combination in Table 4.7.2 (see Section 4.7). Region 3 cells are located on the interior of the rack (at least three rows in from the rack periphery) and are prohibited from being located in the outer two rows of the rack.

Additionally, reactivity effects of abnormal and accident conditions have also been evaluated. A summary of the types of accidents analyzed and the soluble boron required ensuring that the maximum k_{eff} remains below 0.95 are shown in Table 4.7.4. The most limiting accident is a misloaded fresh fuel assembly in the outer row of the rack in a Region 2 location. A minimum soluble boron requirement must be maintained in the spent fuel pool to ensure that the maximum k_{eff} is less than 0.95 under accident conditions.

4.2 Methodology

4.2.1 Criticality Analysis

The principal method for the criticality analysis of the high-density storage racks is the use of the three-dimensional Monte Carlo code MCNP4a [4.2]. MCNP4a is a continuous energy three-dimensional Monte Carlo code developed at the Los Alamos National Laboratory. MCNP4a was selected because it has been used previously and verified for criticality analyses and has all of the necessary features for this analysis. MCNP4a calculations used continuous energy cross-section data predominantly based on ENDF/B-V and ENDF/B-VI.



Benchmark calculations, presented in Appendix A, indicate a bias of 0.0009 with an uncertainty of ± 0.0011 for MCNP4a, evaluated with a 95% probability at the 95% confidence level [4.1]. The calculations for this analysis utilize the same computer platform and cross-section libraries used for the benchmark calculations discussed in Appendix A.

The convergence of a Monte Carlo criticality problem is sensitive to the following parameters: (1) number of histories per cycle, (2) the number of cycles skipped before averaging, (3) the total number of cycles and (4) the initial source distribution. The MCNP4a criticality output contains a great deal of useful information that may be used to determine the acceptability of the problem convergence. This information has been used in parametric studies to develop appropriate values for the aforementioned criticality parameters to be used in storage rack criticality calculations. Based on these studies, a minimum of 10,000 histories were simulated per cycle, a minimum of 50 cycles were skipped before averaging, a minimum of 100 cycles were accumulated, and the initial source was specified as uniform over the fueled regions (assemblies). Further, the output was reviewed to ensure that each calculation achieved

acceptable convergence. These parameters represent an acceptable compromise between calculational precision and computational time.

CASMO-4 is used in this application to determine reactivity differences for temperature variation, manufacturing tolerances, depletion uncertainty and to calculate the isotopic inventory of the spent fuel for use in MCNP4a. References [4.5] and [4.6] are Studsvik proprietary documents related to the appropriateness of CASMO-4 for calculating the multiplication factor, k_{eff} . These references were previously provided to the NRC in support of staff approval of EMF-2158 as documented in letter "Document Control Desk ATTN: Chief, Planning, Program and Management Support Branch, Subject: Transmittal of Copies of CASMO-4 Benchmark Reports Relevant to EMF-2158(P) Revision 0 "Siemens Power Corporation Methodology for Boiling Water Reactors: Evaluation and Validation of CASMO-4/MICROBURN-B2," from J.A. Umbarger, dated April 30, 1999.

Holtec International has been using the CASMO-4 code since approximately mid-1999 for calculating the reactivity effects of manufacturing tolerances, moderator temperature and depletion effects. CASMO-4 has been previously used and approved by the USNRC over the past 10 years on multiple licensing efforts by Holtec International for spent fuel storage racks. Specifically, CASMO-4 has been reviewed and approved for use on the following PWR spent fuel pool analyses for calculating the reactivity effect of moderator manufacturing tolerances, moderator temperature and depletion effects: Crystal River 3, Arkansas Nuclear 1 & 2, Harris, St. Lucie, Diablo Canyon, Turkey Point, V.C. Summer, Three Mile Island, Comanche Peak, Davis-Besse, Robinson, and Sequoyah. From the above list of plants, the following specific subset of NRC issued SERs and amendment approval references are identified where CASMO-4 and MCNP4a have been used by Holtec International for spent fuel pool criticality analyses:

- F.E. Saba (NRC) to J.S. Forbes (Entergy) dated January 26, 2007, "ARKANSAS NUCLEAR ONE, UNIT NO.1 – ISSUANCE OF AMMENDMENT FOR USE OF METAMIC® POISON INSERT ASSEMBLIES IN THE SPENT FUEL POOL (TAC NO. MD2674)"

- K.N. Jabbour (NRC) to C. M. Crane (Amerigen) dated October 31, 2005, “CLINTON POWER STATION, UNIT 1 – ISSUANCE OF AN AMENDMENT –RE: ONSITE SPENT FUEL STORAGE EXPANSION (TAC NO. MC4202)”
- S.N. Baily (NRC) to D. E. Young (Crystal River) dated October 25, 2007, “CRYSTAL RIVER, UNIT 3 – ISSUANCE OF AMENDMENT REGARDING FUEL STORAGE PATTERNS IN THE SPENT FUEL POOL (TAC NO. MD3308)”

The BVPS Unit No. 2 spent fuel pool racks are similar in material and geometric configuration as those spent fuel racks used at other PWRs identified above. The use of CASMO-4 by Holtec International for spent fuel pool licensing activities on these PWR plants, and NRC approval of that use, provides the justification for using CASMO-4 for relative reactivity calculations for the BVPS Unit No. 2 spent fuel pool analysis.

As previously stated fuel depletion analyses during core operation were performed with CASMO-4 (using the 70-group cross-section library), a two-dimensional multigroup transport theory code based on the Method of Characteristics [4.4]-[4.6]. Detailed neutron energy spectra for each rod type are obtained in collision probability micro-group calculations for use in the condensation of the cross sections. CASMO-4 is used to determine the isotopic composition of the spent fuel. In addition, the CASMO-4 calculations are restarted in the storage rack geometry, yielding the two-dimensional infinite multiplication factor (k_{inf}) for the storage rack to determine the reactivity effect of fuel and rack tolerances, temperature variation, and to perform various studies. For all calculations in the spent fuel pool racks, the Xe-135 concentration in the fuel is conservatively set to zero.

The maximum k_{eff} is determined from the MCNP4a calculated k_{eff} , the calculational bias, the temperature bias, and the applicable uncertainties and tolerances (bias uncertainty, calculational uncertainty, rack tolerances, fuel tolerances, depletion uncertainty) using the following formula:

$$\text{Max } k_{eff} = \text{Calculated } k_{eff} + \text{biases} + [\sum_i (\text{Uncertainty})^2]^{1/2}$$

In the geometric models used for the calculations, each fuel rod and its cladding were described explicitly, and when applicable reflecting boundary conditions were used in the radial direction which has the effect of creating an infinite radial array of storage cells.

4.2.2 Boron Dilution Analysis

The methodology related to the Boron Dilution accident follows the general equation for boron dilution which is,

$$C_t = C_o e^{(-1)\frac{F}{V}t},$$

where

- C_t = boron concentration at time t,
- C_o = initial boron concentration,
- V = credited volume of water in the pool, and
- F = flow rate of unborated water into the pool

This equation conservatively assumes the unborated water flowing into the pool mixes instantaneously with the water in the pool. The conservatism is with respect to the calculation of the time of dilution since any mixing rate factor is neglected. The volume of water in the SFP is conservatively set as the volume above the storage racks only. With respect to the reactivity in the spent fuel pool, pockets of unmixed unborated water may exist briefly during a dilution event and expose the fuel to an increased reactivity situation. However, the criticality calculations in Section 4.7 demonstrate that the spent fuel racks remain subcritical even with total loss of soluble boron.

For convenience, the above equation may be re-arranged to permit calculating the time required to dilute the soluble boron from its initial concentration to a specified minimum concentration, which is given below.

$$t = \frac{V}{F} \ln(C_o / C_i)$$

If V is expressed in gallons and F in gallons per minute (gpm), the time, t, will be in minutes.

4.3 Acceptance Criteria

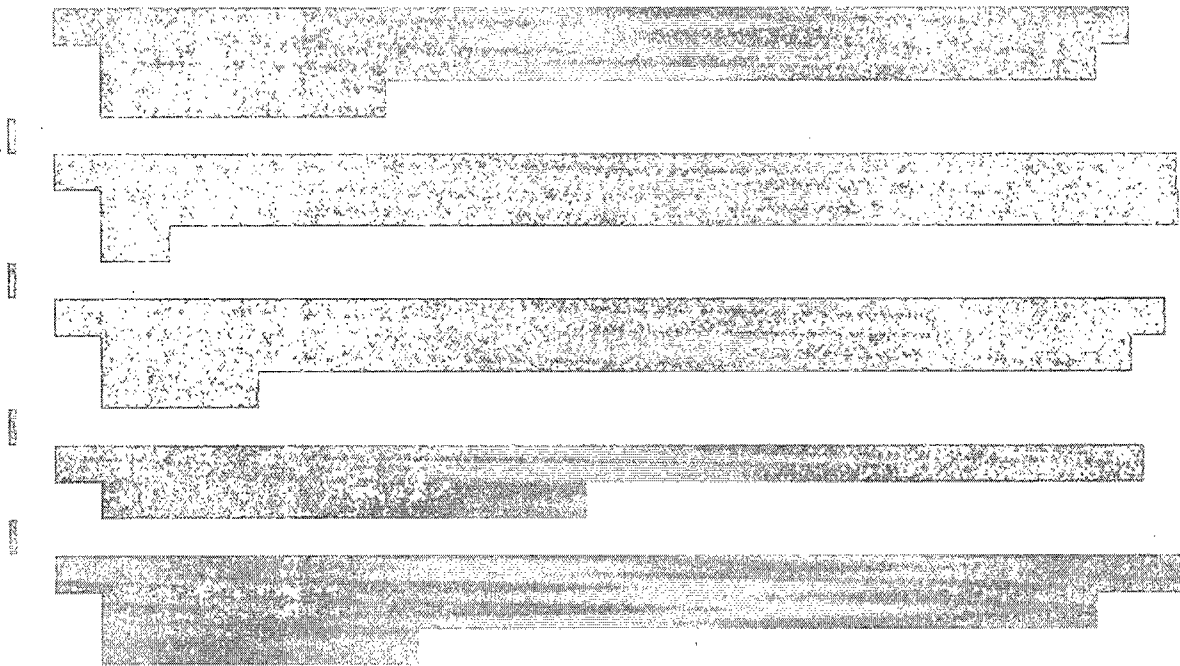
The high-density spent fuel PWR storage racks for BVPS Unit No. 2 are designed in accordance with the applicable codes and standards listed below. The objective of this evaluation is to show that the effective neutron multiplication factor, k_{eff} , is less than 1.0 with the storage racks fully loaded with fuel of the highest anticipated reactivity and the pool flooded with unborated water at a temperature corresponding to the highest reactivity. In addition, it is demonstrated that k_{eff} is less than or equal to 0.95 with the storage racks fully loaded with fuel of the highest anticipated reactivity and the pool flooded with borated water at a temperature corresponding to the highest reactivity. The maximum calculated reactivity includes a margin for uncertainty in reactivity calculations including manufacturing tolerances and is shown to be less than 0.95 with a 95% probability at a 95% confidence level [4.1]. Reactivity effects of abnormal and accident conditions have also been evaluated to assure that under all credible abnormal and accident conditions, the reactivity will not exceed the regulatory limit of 0.95 under borated conditions.

Applicable codes, standard, and regulations or pertinent sections thereof, include the following:

- Code of Federal Regulations, Title 10, Part 50, Appendix A, General Design Criterion 62, "Prevention of Criticality in Fuel Storage and Handling."
- USNRC Standard Review Plan, NUREG-0800, Section 9.1.1, Criticality Safety of Fresh and Spent Fuel Storage and Handling, Rev. 3 – March 2007.
- USNRC letter of April 14, 1978, to all Power Reactor Licensees - OT Position for Review and Acceptance of Spent Fuel Storage and Handling Applications (GL-78-011), including modification letter dated January 18, 1979 (GL-79-004).

- L. Kopp, "Guidance on the Regulatory Requirements for Criticality Analysis of Fuel Storage at Light-Water Reactor Power Plants," NRC Memorandum from L. Kopp to T. Collins, August 19, 1998.
- USNRC Regulatory Guide 1.13, Spent Fuel Storage Facility Design Basis, Rev. 2, March 2007.
- ANSI ANS-8.17-1984, Criticality Safety Criteria for the Handling, Storage and Transportation of LWR Fuel Outside Reactors.
- Code of Federal Regulations, Title 10, Part 50, Section 68, "Criticality Accident Requirements."

Additionally, the following NUREG's were reviewed and the criticality calculations presented here are consistent with the recommendations provided within:



Since credit is taken for soluble boron in the spent fuel pool (SFP), a boron dilution analysis is performed to ensure that sufficient time is available to detect and suppress the worst dilution

event that can occur to reduce the SFP boron concentration from the operating concentration to the minimum required concentration as determined by this analysis. The boron dilution analysis considers all possible dilution events, sources and flow rates, as well as instrumentation and administrative procedures. The analysis justifies the surveillance interval for verifying the Technical Specification requirement concentration.

4.4 Assumptions

Various assumptions used in this criticality analysis are conservative to provide an additional margin of criticality safety and to assure that the true reactivity will always be less than the calculated reactivity. The following conservative design criteria and assumptions were employed:

- 1) The SFP moderator is water at a temperature in the operating range that results in the highest reactivity, as determined by the analysis (see Section 4.7.8).
- 2) Neutron absorption in minor structural members is neglected; spacer grids are replaced by water (see Section 4.7.1) because they have a negligible effect on reactivity.
- 3) The effective multiplication factor of an infinite radial array of fuel assemblies was used in the analyses, except for the assessment of certain abnormal/accident conditions and conditions where leakage is inherent.
- 4) The spent fuel rack neutron absorber length is modeled to be the same length as the active region of the fuel instead of the actual height of 146 inches.
- 5) A conservative cooling time of 0 hours is used along with setting the xenon concentration to zero for all CASMO-4 calculations in the rack models (see Section 4.7.4). No credit is taken for the significant cooling time of older fuel assemblies.

- 7) A maximum fuel pellet density (97% theoretical) is conservatively considered in the analysis over the entire fuel rod length and therefore no tolerance is needed for fuel pellet density (see Table 4.5.2). Fuel pellet dishing, champhering or pellets with an annulus are conservatively modeled as solid fuel pellet cylinders with the maximum density.
- 8) The guide tube dimensions used in the design basis assembly were conservatively set to the combination of diameters that provided the minimum thickness. Additionally, a tolerance is statistically considered (see Section 4.7.7).
- 9) The presence of burnable absorbers in fresh fuel is neglected for the design basis assembly. This is conservative as burnable absorbers would reduce the reactivity of the fresh fuel assembly. To account for the possible positive reactivity effect of spent fuel in the storage rack with burnable absorbers, a conservative bias is applied to all final reactivity calculations (see Section 4.5.4).
- 10) In the depletion calculations with burnable absorbers, the burnable absorber was modeled over the entire active fuel length.
- 11) A very conservative segmented axial burnup profile was used (see Section 4.5.3).
- 12) The BVPS Unit No. 2 Cycle 14 uprated core operating parameters were conservatively applied to all the CASMO-4 depletion calculations. These parameters are bounding and conservative because higher temperatures (maximum fuel and moderator) and boron concentrations (bounding average) hardens the neutron spectrum in the core which leads to greater Pu production and therefore greater reactivity in the spent fuel pool.

- 13) The targeted reactivity (not including tolerances and applicable bias) by the initial enrichment and burnup combinations is conservatively set to 0.995 (minus relevant uncertainties and biases) for the pure water calculations (instead of the limit of 1.0) and 0.945 (minus relevant uncertainties and biases) for the borated water calculations (instead of the limit of 0.95).
- 14) For the boron dilution analysis low flow rate dilution accident a flow rate of 2 gpm is assumed. This flow rate is assumed to be typical of undetectable leakage around seals and pumps.
- 15) The fuel rod pellet to cladding gap is conservatively modeled as being filled with pure water in the MCNP4a reactivity calculations.
- 16) The fuel assemblies and fuel storage racks are assumed to have no non-integral reactivity control devices. The inclusion of such devices in the SFP reduces reactivity. Additionally, the storage of non-fissile material is not included in the reactivity calculations because they do not have a positive impact on reactivity. Although these non-fuel devices may exist and be stored in the SFP, they do not impact reactivity and therefore it is unnecessary to include them in the criticality calculations.

4.5 Input Data

4.5.1 Design Basis Fuel Assembly Specification

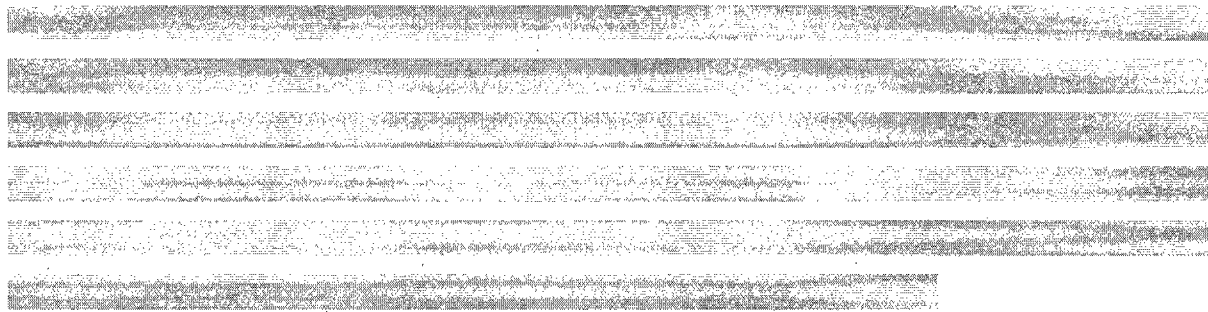
The spent fuel storage racks are designed to accommodate various Westinghouse designed 17x17 fuel assemblies used at BVPS Unit No. 2. Data provided by FENOC encompasses various regions of 17x17 fuel assemblies (STD, V5H, RFA, RFA-2). The design specifications for these fuel assemblies were compared (see Table 4.5.1 and Table 4.5.2) to select a design basis assembly that is conservatively bounding for the purposes of this analysis.

4.5.2 Core Operating Parameters

Core operating parameters are necessary for fuel depletion calculations performed with CASMO-4. The core parameters used for the depletion calculations are presented in Table 4.5.3. The soluble boron concentration used bounds the average for BVPS Unit No. 2 Cycle 14 (see Table 4.5.4). The moderator and fuel temperatures are the maximum (most conservative) over the core for BVPS Unit No. 2 for Cycle 14. The neutron spectrum is hardened by each of these parameters, leading to a greater production of plutonium during depletion, which results in conservative reactivity results in the spent fuel pool.

4.5.3 Axial Burnup Distribution

An axial relative burnup profile was determined using data provided by FENOC for Cycles 1-14 and is specified for 24 equally-spaced axial nodes (see Table 4.5.5 and Table 4.5.6).



4.5.4 Integral and Non-integral Fuel Assembly Reactivity Control Devices

The BVPS Unit No. 2 fuel had multiple regions that made use of integral fuel burnable absorbers (IFBAs). The design specifications for the IFBA rods are given in Table 4.5.7, Figure 4.5.1 and Figure 4.5.5. Generic studies [10] have investigated the effect that IFBA has on the reactivity of spent fuel assemblies. These studies have concluded that there is a small positive reactivity effect associated with the presence of IFBA rods. Two separate IFBA rod loading patterns were analyzed to cover current and future fuel designs: 128 and 200 IFBA pins.

The BVPS Unit No. 2 fuel also had two fuel regions that made use of water displacement rods (WDR) that were used with and without IFBA rods. The WDR design specification is given in Table 4.5.8.

The BVPS Unit No. 2 fuel also had two fuel regions that made use of wet annular burnable absorber (WABA) rods. The WABA rod specification is given in Table 4.5.9. Both WABA's and WDRs are present in the fuel assembly guide tubes.

4.5.5 Storage Rack Specification

The storage cell characteristics that were used in the criticality evaluations are summarized in Table 4.5.10. The spent fuel pool racks storage cells are composed of stainless steel boxes with a single fixed Metamic neutron absorber panel (attached by stainless steel sheathing), centered on each side. The stainless steel boxes are arranged in an alternating pattern such that the connection of the box corners forms the storage cells. Neutron absorber panels are installed on all exterior walls facing other racks.



4.5.6 Rack Interfaces and Cask Loading Pit

The storage cell racks are separated by a 1.5 inch gap that is determined by the rack baseplate extensions. This gap represents the minimum possible separation and is used in the design basis models and therefore no further rack interface calculations are necessary. Additionally, one of the storage rack modules may be placed in the cask pit loading area during fuel movement operations. The results presented in this chapter are also applicable to this interim configuration.

4.5.7 Fuel Rod Storage Basket

The BVPS Unit No. 2 SFP has a Fuel Rod Storage Basket (FRSB) with the dimensions shown in Table 4.5.11 and presented in Figure 4.5.6. The FRSB is a basket that contains fuel rods is currently stored in a fuel storage rack cell in the SFP. For the purposes of this analysis the FRSB was modeled as shown in Figure 4.5.6, fully loaded with fresh fuel pins at 5.0 wt% ^{235}U . The model contains fuel rods only, conservatively neglecting the steel box walls.

4.5.8 Boron Dilution Accident Evaluation

The BVPS Unit No. 2 SFP has a Technical Specification Limiting Condition for Operation that requires a soluble boron concentration of 2000 ppm during normal operating conditions. The SFP volume is shown in Table 4.5.12 and conservatively considers only the volume of water above the storage racks. Under certain postulated abnormal conditions, introduction of unborated water into the spent fuel pool could reduce the spent fuel pool boron concentration below the Technical Specification requirement of 2000 ppm. The boron dilution accident evaluation considers two scenarios; the worst case high flow rate accident and an undetected low flow rate accident.

For the purposes of the boron dilution analysis it was determined that the source of water with the highest potential flow rate (worst case dilution event) was from the Service Water System. This system is capable of providing the highest sustainable flow rate of unborated water to the SFP (of all possible sources) at 3000 gpm.

4.6 Computer Codes

The following computer codes were used during this analysis.

- MCNP4a [2] is a three-dimensional continuous energy Monte Carlo code developed at Los Alamos National Laboratory. This code offers the capability of performing full three-

dimensional calculations for the loaded storage racks. MCNP4a was run on the PCs at Holtec.

- CASMO-4, Version 2.05.14 [[4.4]-[4.6]] is a two-dimensional multigroup transport theory code developed by Studsvik of Sweden. CASMO-4 performs cell criticality calculations and burnup. CASMO-4 has the capability of analytically restarting burned fuel assemblies in the rack configuration. This code was used to determine the reactivity effects of tolerances and fuel depletion. As proof of its acceptability in this application, CASMO-4 has been benchmarked [4.5, 4.6] against Monte Carlo calculations and critical experiments similar to spent fuel storage rack geometries. References 4.5 and 4.6 were previously provided to the NRC in support of staff approval of EMF-2158 for Siemens BWR methodology (see Section 4.2.1).

4.7 Analysis

This section describes the calculations that were used to determine the acceptable storage criteria for the MZTR. In addition, this section discusses the possible abnormal and accident conditions.

Unless otherwise stated, all calculations assumed nominal characteristics for the fuel and the fuel storage cells. The effect of the manufacturing tolerances is accounted for within the uncertainty analysis as discussed below.

As discussed in Section 4.2, MCNP4a was the primary code used. CASMO-4 was used to determine the reactivity effect of tolerances, temperature variation and for depletion calculations. MCNP4a was used for reference cases and to determine the maximum reactivity of the spent fuel racks, eccentric fuel positioning, axial burnup distributions, and fuel misloading).

Additionally, complex 3-D geometries were modeled using MCNP4a, e.g. Figure 4.5.2 shows the  basic model that was used in MCNP4a and includes fuel assemblies from all three Regions. This picture was created with the two-dimensional plotter and clearly indicates the

explicit modeling of fuel rods in each fuel assembly. In CASMO-4, a single cell is modeled, and since CASMO-4 is a two-dimensional code, the fuel assembly hardware above and below the active fuel length is not represented. The three-dimensional MCNP4a models that included axial leakage assumed approximately 30 cm of water above and below the active fuel length. Additional models were generated with MCNP4a to investigate the effect of abnormal and normal conditions. These models are discussed in the appropriate section.

4.7.1 Identification of Design Basis Fuel Assembly

All of the fuel assembly data provided by FENOC was analyzed as shown in Table 4.5.1 to determine which parameters would be bounding for use as the design basis fuel assembly. Many of the fuel assembly parameters were equivalent. The guide tube thickness varied between fuel assembly types and therefore a minimum thickness was conservatively chosen (see Table 4.5.2).

For all assemblies, the presence of burnable absorbers in the fuel assembly (WABA, IFBA) was neglected for determination of the design basis fuel assembly (see Section 4.7.2 for a discussion of the effect of burnable poison).

The fuel assembly was conservatively modeled without spacer grids. However, calculations were performed to determine the reactivity effect of spacer grids in borated water. Specifically, the calculations were performed to determine if the spacer grids displace enough boron to cause a significant positive reactivity effect. [REDACTED]

[REDACTED] This model is very conservative because it is axially infinite whereas the spacer grids are axially localized and therefore the results overestimate the reactivity effect.

The results of the calculations are shown in Table 4.7.5. For burnups under approximately 40 GWD/MTU, the spacer grid model shows a decrease in reactivity from the reference case. For burnups over approximately 40 GWD/MTU, the spacer grid model begins to show a small

positive reactivity effect (approximately $0.0050 \Delta k_{\text{eff}}$) that is magnified by increasing the soluble boron concentration.

This reactivity increase is due to a slight hardening of the neutron spectrum. As the fuel to moderator ratio increases, the number of fissions in the Pu increases and the number of fissions in the ^{235}U decreases due to the spectral shift. In fuel with a high burnup this increases the reactivity of the fuel assembly because of the greater Pu concentrations. However, since the spacer grids are in reality a localized moderator displacer, the effect shown in Table 4.7.5 is further reduced. Therefore, it is conservative to neglect the fuel assembly spacer grids for the MZTR racks because they will be primarily dominated by the high reactivity fresh fuel, where the absence of modeling the grid spacers results in a conservatism of approximately $0.01 \Delta k$.

4.7.2 Reactivity Effect of Fuel Assembly Reactivity Control Devices

The BVPS Unit No. 2 fuel may include the use of IFBA, IFBA with WDRs, WABA or only WDRs. The reactivity effect of these fuel assembly reactivity control devices was investigated in order to determine a bias to be applied to the final calculated reactivity. Bounding cases were selected and the maximum reactivity effect over all cases was applied to the final calculated k_{eff} as a reactivity control bias (see Table 4.7.6 and Table 4.7.7).

Depletion calculations were performed with CASMO-4 for selected configurations of IFBA, WDR and WABA rods based on the specifications in Table 4.5.7, Table 4.5.8 and Table 4.5.9. For the IFBA and WABA cases, using the maximum IFBA loading and maximum number of IFBA pins or WABA rods per assembly is conservative because the reactivity effect increases with the maximum number of IFBA pins or WABA rods and decreasing enrichment. This is because the burnable absorber hardens the spectrum and increases Pu production, making it more reactive than a fuel assembly with no burnable absorber at an equivalent exposure. Therefore, the cases presented bound all possible configurations at BVPS Unit No. 2.

The WABA and WDR rod cases were modeled in the fuel assembly for 17 and 14 GWD/MTU respectively, then removed and not included for any of the rack calculations. The WDR rods

were analyzed for multiple cases with and without IFBA pins. The results of these calculations are shown in Table 4.7.8 through Table 4.7.11.

4.7.3 Reactivity Effect of Axial Burnup Distribution

Initially, fuel loaded into the reactor will burn with a slightly skewed cosine power distribution. As burnup progresses, the burnup distribution will tend to flatten, becoming more highly burned in the central regions than in the upper and lower ends. At high burnup, the more reactive fuel near the ends of the fuel assembly (less than average burnup) occurs in regions of lower reactivity worth due to neutron leakage. Consequently, it would be expected that over most of the burnup history, distributed burnup fuel assemblies would exhibit a slightly lower reactivity than that calculated for the average burnup. As burnup progresses, the distribution, to some extent, tends to be self-regulating as controlled by the axial power distribution, precluding the existence of large regions of significantly reduced burnup.

Generic analytic results of the axial burnup effect for assemblies without axial blankets have been provided by Turner [4.9] based upon calculated and measured axial burnup distributions. These analyses confirm the minor and generally negative reactivity effect of the axially distributed burnup compared to a flat distribution, becoming positive at burnups greater than about 30 GWD/MTU. The trends observed in [[4.9]] suggest the possibility of a small positive reactivity effect above 30 GWD/MTU, increasing to slightly over 1% Δk at 40 GWD/MTU. The required burnup for the maximum enrichment is higher than 30 GWD/MTU. Therefore, a positive reactivity effect of the axially distributed burnup is possible. Calculations are performed with the axial burnup distribution shown in Table 4.5.6 (see Section 4.5.3) and with an axially constant burnup, and the higher reactivity is used in the analyses.

4.7.4 Isotopic Compositions

To perform the criticality evaluation for spent fuel in MCNP4a, the isotopic composition of the fuel is calculated with the depletion code CASMO-4 and then specified as input data into MCNP4a. The CASMO-4 calculations to obtain the isotopic compositions for MCNP4a were

performed generically, with one calculation for each enrichment, and burnups in increments of 2.5 GWD/MTU or less. The isotopic composition for any given burnup is then determined by linear interpolation. For conservatism, the isotopic concentrations are determined at zero cooling time, without xenon, and [REDACTED].

4.7.5 Uncertainty in Depletion Calculations

To address uncertainties associated with the calculated depletion of fuel assemblies to obtain burnup credit in the fuel storage rack geometry, a burnup-dependent uncertainty in reactivity for burnup calculations of 5% of the reactivity decrement is used, as discussed in [4.7]. This 5% uncertainty is intended to encompass the following calculational uncertainties:

- Lack of critical experiment data of spent fuel storage rack geometries containing both actinides and fission products.
- Uncertainty in actual versus calculated isotopics.
- Changes in fuel geometry (clad creep, pellet densification, etc.) during irradiation.

A separate calculation is done for both Region 2 and Region 3. For each enrichment case in Table 4.7.6 and Table 4.7.7, MCNP4a calculates the reactivity of the system with each Region being considered as fresh fuel. The calculated reactivity with spent fuel is then subtracted from the reactivity with fresh fuel and the 5% allowance is statistically combined with the other reactivity allowances in the determination of the maximum k_{eff} for normal conditions where assembly burnup is credited.

4.7.6 Eccentric Fuel Assembly Positioning

The fuel assembly is assumed to be normally located in the center of the storage rack cell. To investigate the potential reactivity effect of eccentric positioning of assemblies in the cells, MCNP4a calculations were performed with two separate cases. Case 1 models all the fuel assemblies eccentrically positioned toward the center of the rack model. Case 2 models all the fuel assemblies in four-assembly clusters repeated throughout the rack. The results of these

calculations are presented in Table 4.7.12 and indicate that eccentric fuel positioning results in a slight increase in reactivity. Therefore, the maximum reactivity increase associated with eccentric positioning is statistically combined with the other uncertainties in the final calculated reactivity as shown in Table 4.7.6 and Table 4.7.7.

4.7.7 Uncertainties Due to Manufacturing Tolerances

In the calculation of the final k_{eff} , the effect of manufacturing tolerances on reactivity is included as discussed in Section 4.2. CASMO-4 was used to perform these calculations. As allowed in [4.7], the methodology employed to calculate the tolerance effects combine both the worst-case bounding value and sensitivity study approaches. The evaluations include tolerances of the rack dimensions (see Table 4.7.14) and tolerances of the fuel dimensions (see Table 4.7.13).

The calculations are performed for different enrichments (2.0 to 5.0 wt% ^{235}U) at various burnups and with a soluble boron concentration of 0 ppm (the effect of soluble boron on these calculations was examined and as can be seen in Table 4.7.19 the effect of soluble boron is negligible. The tolerance used at each enrichment case is the maximum over all burnups for conservatism. To determine the Δk associated with a specific manufacturing tolerance, the k_{inf} calculated for the reference condition is compared to the k_{inf} from a calculation with the tolerance included. Note that for the individual parameters associated with a tolerance, no statistical approach is utilized. Instead, the full tolerance value is utilized to determine the maximum reactivity effect. All of the Δk values from the various tolerances are statistically combined (square root of the sum of the squares) to determine the final reactivity allowance for fuel assembly and storage rack manufacturing tolerances. Only the Δk values in the positive direction (increasing reactivity) were used in the statistical combination. The fuel and rack tolerances included in this analysis are given in Table 4.5.2 and Table 4.5.10. The results of the manufacturing tolerances are shown in Table 4.7.13 and Table 4.7.14. The tolerance used in the final reactivity determination is shown in Table 4.7.6 and Table 4.7.7.

4.7.8 Temperature and Water Density Effects

Pool water temperature effects on reactivity in the MZTR racks have been calculated with CASMO-4 for various enrichments with a maximum value of up to 5.0 wt% ²³⁵U and the results are presented in Table 4.7.15. The results show that the spent fuel pool temperature coefficient of reactivity is negative, i.e., a higher temperature results in a lower reactivity. Consequently, all CASMO-4 calculations are evaluated at 32 °F.

In MCNP4a, the Doppler treatment and cross-sections may only be valid at 300K (80.33 °F). Therefore, a Δk is determined in CASMO-4 from 32 °F to 80.33 °F, and is included in the final k_{eff} calculation as a bias (see Table 4.7.6, Table 4.7.7, and Table 4.7.15).

4.7.9 Calculation of Maximum k_{eff}

Using the calculational model shown in Figure 4.5.2 and the design basis fuel assembly specified in Table 4.5.1, the k_{eff} in the MZTR storage racks has been calculated with MCNP4a. The determination of the maximum k_{eff} values, based on the formula in Section 4.4.2, was calculated for initial enrichments between 2.0 wt% ²³⁵U and 5.0 wt% ²³⁵U. The results show that the maximum k_{eff} of the MZTR rack loaded with the maximum number of fresh fuel assemblies is less than 1.0 at a 95% probability and at a 95% confidence level without credit for soluble boron and less than or equal to 0.95 at a 95% probability and at a 95% confidence level with credit for soluble boron (see Table 4.7.3).





Additionally, to account for the uncertainty in the method used to measure or calculate burnup at BVPS Unit No. 2, a 5% burnup factor is added to the initial enrichment and burnup combinations as presented in Table 4.7.6 and Table 4.7.7. These new values were then plotted and a polynomial was applied to the curve. Since the initial polynomial curve did not bound all the calculated points, the polynomial's coefficients were adjusted so that each point on the curve was greater than the burnup with the 5% uncertainty (See Table 4.7.1 and Table 4.7.2). These final polynomials were then plotted in Figure 4.7.1 and Figure 4.7.2.

4.7.10 Interfaces Within and Between Racks

The design basis model is a  array of cells representing all three Regions of the MZTR and also includes the interface of 4 MZTR rack modules at the minimum separation between racks. The design basis model also considered the Region 1 cells from the adjacent racks to be directly across from each other, thereby considering the worst case. Therefore, no additional calculations involving interfaces within or between racks are required.

4.7.11 Verification of the Initial Burnup and Enrichment Combinations

The methodology utilized for the determination of the Region 2 and Region 3 initial enrichment and burnup combinations was verified by calculating the reactivity of the system with MCNP4a at the combinations of Region 2 and Region 3 calculated initial enrichment and burnup combinations results shown in Table 4.7.6 and Table 4.7.7 (without including the 5% burnup uncertainty and polynomial fit adjustment). The results of these verification calculations are provided in Table 4.7.16 and show that the calculations are generally acceptable and within the statistical uncertainty of the calculations (within 2σ) to the maximum reactivity from Region 2 and Region 3 and therefore validate the calculated initial enrichment and burnup combinations. Two cases at the 2.5 wt% ^{235}U case were greater than the statistical uncertainty of the code. This difference is relatively small and part of a general trend in the results from Table 4.7.16 that show a smaller delta reactivity for the lower enrichment cases than the higher ones. When these more reactive combinations of lower enrichment low burnup requirement fuel assemblies (and not the 5.0 wt% high burnup fuel assemblies assumed in the methodology) are combined, the results show a small positive reactivity effect. However, since the reactivity effect is small and the verification cases were all run at the lower calculated burnup and not the final burnup requirement shown in Table 4.7.6 and Table 4.7.7, burnup versus enrichment curves are conservative.

4.7.12 Soluble Boron Concentration Calculation

The SFP storage racks require some amount of soluble boron to meet the acceptance criteria of k_{eff} less than or equal to 0.95 (see Section 4.3). In order to calculate the maximum soluble boron requirement required, the MCNP4a cases used for Section 4.7.11 above, i.e. the curve verification cases, were rerun with 800 ppm soluble boron. The reactivity of the 800 ppm case was then used to interpolate the required soluble boron concentration required to obtain a reactivity of 0.945 minus the maximum total corrections for the given burnup and enrichment case from Table 4.7.6 and Table 4.7.7. These soluble boron concentrations are conservative since they are determined for the calculated burnups and do not include the 5% burnup uncertainty or the polynomial fit adjustment. The result is shown in Table 4.7.3.

4.7.13 Abnormal and Accident Conditions

The effects on reactivity of credible abnormal and accident conditions are examined in this section. This section identifies which of the credible abnormal or accident conditions will result in exceeding the limiting reactivity ($k_{\text{eff}} \leq 0.95$). For those accident or abnormal conditions that result in exceeding the limiting reactivity, a minimum soluble boron concentration is determined to ensure that $k_{\text{eff}} \leq 0.95$. The double contingency principle of ANS-8.1/N16.1-1975 [[4.8]] (and the USNRC letter of April 1978) specifies that it shall require at least two unlikely, independent and concurrent events to produce a criticality accident. This principle precludes the necessity of considering the simultaneous occurrence of multiple accident conditions. For those cases where the reactivity of the accident is greater than the limit of $k_{\text{eff}} \leq 0.95$, the calculation was re-performed with soluble boron and the concentration required to meet the limit was interpolated.

4.7.13.1 Abnormal Temperature

All calculations for the MZTR are performed at a pool temperature of 32 °F. As shown in Section 4.7.8 above, the temperature coefficient of reactivity is negative; therefore no additional calculations are required, because a further increase in temperature reduces the reactivity.

4.7.13.2 Dropped Assembly – Horizontal

For the case in which a fuel assembly is assumed to be dropped on top of a rack, the fuel assembly will come to rest horizontally on top of the rack with a minimum separation distance from the active fuel region of more than 22 inches, which is sufficient to preclude neutron coupling (i.e., an effectively infinite separation). Consequently, the horizontal fuel assembly drop accident will not result in a significant increase in reactivity. Furthermore, the soluble boron in the spent fuel pool water assures that the true reactivity is always less than the limiting value for this dropped fuel accident.

4.7.13.3 Dropped Assembly - Vertical

It is also possible to vertically drop an assembly into a location that might be occupied by another assembly or that might be empty. Such a vertical impact has previously been shown to cause no damage to either fuel assembly but may result in a small deformation of the baseplate

for an empty cell. These deformations could potentially increase reactivity. However, the reactivity increase would be small compared to the reactivity increase created by the misloading of a fresh assembly discussed in the following section. The vertical drop is therefore bounded by this misloading accident and no separate calculation is performed for the drop accident.

4.7.13.4 Abnormal Location of a Fuel Assembly

4.7.13.4.1 Misloaded Fresh Fuel Assembly

The misloading of a fresh unburned fuel assembly could, in the absence of soluble poison, result in exceeding the regulatory limit (k_{eff} of 0.95). This could possibly occur if a fresh fuel assembly of the highest permissible enrichment (5.0 wt% ^{235}U) were to be inadvertently misloaded into a storage cell intended to be used for spent fuel. However, administrative controls make this highly unlikely. For example, on site reactor engineering determines the fuel assembly storage location based on initial enrichment and fuel assembly burnups and uses refueling procedures for handling of fuel assemblies per Technical Specification requirements. These procedures are controlled by the 10CFR50.59 process. The reactivity consequence of this situation was investigated for various combinations of the Region 2 and Region 3 initial burnup and enrichment combinations determined above. The misloaded fuel assembly model conservatively used reflective boundary conditions, thereby simulating an infinite array of storage racks with misloaded fuel assemblies (see Figure 4.7.4). These results are summarized in Table 4.7.17 for the two relevant Regions of the MZTR. As expected, a fuel assembly placed in a Region 2 cell on the periphery of the rack between two Region 1 (fresh fuel) storage cells is the worst case. The results of the analysis are summarized in Table 4.7.4, including the soluble boron level calculated to be sufficient to ensure that the maximum k_{eff} value for this condition remains less than or equal to 0.95.

4.7.13.4.2 Mislocated Fresh Fuel Assembly

The mislocation of a fresh unburned fuel assembly could, in the absence of soluble poison, result in exceeding the regulatory limit (k_{eff} of 0.95). This could possibly occur if a fresh fuel assembly of the

highest permissible enrichment (5.0 wt% ^{235}U) were to be accidentally mislocated outside of a storage rack adjacent to other fuel assemblies. The pool layout was examined to determine a credible worst case location for this accident, and it was determined to be a junction of two racks that form an empty corner in the SFP.

The MCNP4a model consists of a cut away corner section of a storage rack (the gap between racks is not modeled for conservatism) as shown in Figure 4.7.3 with periodic boundary conditions. A 5.0 wt% ^{235}U unburned assembly is modeled adjacent to two poisoned faces of the rack that are both Region 1 cells to maximize the reactivity effect. The poison thickness along the outer rack edge adjacent to the mislocated fuel assembly was modeled with half the normal thickness and without steel sheathing for conservatism. This accident case was investigated for various combinations of the Region 2 and Region 3 initial burnup and enrichment combinations determined above. The results of the analysis are listed in Table 4.7.18 and summarized in Table 4.7.4, including the soluble boron level sufficient to ensure that the maximum k_{eff} value for this condition remains less than or equal to 0.95.

4.7.14 Fuel Rod Storage Basket

The FRSB is modeled as described in Section 4.5 and shown in Figure 4.5.6, as bare fuel pins with fresh fuel enriched to 5.0 wt % ^{235}U . The FRSB was fully reflected by water (at least 12 inches surrounding on all sides) and reflective boundary conditions. The reactivity of the FRSB model was compared to the reactivity of three separate fuel assemblies with the parameters described in Table 4.5.1 at each of the three burnup cases determined by the MZTR (not including the 5% burnup uncertainty or the polynomial fit adjustment): a fresh unburned Region 1 5.0 wt% case, a Region 2 5.0 wt% fuel assembly with a burnup of 52.22 GWD/MTU case, and a Region 3 5.0 wt% fuel assembly with a burnup of 44.48 GWD/MTU case. The three cases were modeled in the same manner as the FRSB, fully reflected by water and reflective boundary conditions. The results of these calculations are presented in Table 4.7.20 and show that the reactivity of the FRSB is less than the Region 1, Region 2 and Region 3 cases and therefore may be stored in any location in the MZTR.

4.7.15 Boron Dilution Analysis

The SFP contains a Technical Specification required minimum soluble boron concentration of 2000 ppm. Significant loss or dilution of the soluble boron concentration in the SFP is extremely unlikely, however, the guidance presented in [4.7] requires that the boron dilution analysis should determine that sufficient time is available to detect and suppress the worst dilution event that can occur to reduce the boron concentration to the level needed to maintain k_{eff} less than or equal to 0.95. Since a boron dilution accident is already an abnormal condition, additional accident conditions such as a misloaded fuel assembly do not need to be considered [4.8].

The required minimum soluble boron concentration is 472 ppm under normal conditions (see Table 4.7.3). The volume of water in the pool is given in Table 4.7.21 along with the volume of water needed to dilute the SFP with a soluble boron concentration of 2000 ppm to 472 ppm. The spent fuel pool cannot hold such a volume of water and would overflow. However, in the event that somehow this volume of water were to dilute the SFP to 472 ppm, there would be no criticality consequence since the racks are still qualified for unborated water to a k_{eff} of less than 1.0.

4.7.15.1 High Flow Rate Dilution

The worst case dilution accident would occur during operator actions to align the Service Water System piping with the SFP. The service water system is capable of providing 3000 gpm of unborated water to the SFP. The result of the boron dilution analysis is presented in Table 4.7.21. It can be seen that the SFP volume would increase rapidly and the High Level Alarm Set Point would be reached in 2.62 minutes. At this point, operators would initiate actions to mitigate the accident. The results show that in order to dilute the SFP to 472 ppm soluble boron, the Service Water System piping and pumps would need to remain operating and aligned with the SFP for 85.2 additional minutes. Upon receiving a SFP high/low level alarm, an operator would respond according to the Alarm Response Procedure and take appropriate action.

4.7.15.2 Low Flow Rate Dilution

Small dilution flow around pump seals and valve stems or mis-aligned valves could possibly occur in the normal soluble boron control system or related systems. Such failures might not be immediately detected. These flow rates would be of the order of a 2 gpm maximum and the increased frequency of makeup flow might not be observed. However, an assumed loss flow-rate of 2 gpm dilution flow rate would require approximately 2.73 days in order to reach the high level alarm set point and then an additional 88.7 days to reduce the boron concentration to the minimum required 472 ppm. Since the SFP boron concentration is measured administratively every 7 days, there is ample time to react to both the high level alarm set point and lower soluble boron concentration and take corrective actions.

4.7.16 Lateral Rack Movement

In the event of seismic activity, there is the possibility that the SFP storage racks may move. Since the base plate extensions preclude the racks from moving closer together (see Section 4.5.5.1), the only rack movement which might impact reactivity is lateral rack movement. However, as discussed in Section 5.5, the design basis model is the bounding worst case scenario, with fresh fuel assemblies at their closest proximity to each other across the gap between racks. Therefore, any lateral rack movement effect on reactivity is bounded by the design basis case and no further calculations are required.

4.7.17 Interim Configurations

During installation of the new racks in BVPS Unit No. 2 SFP, there will be times when both the new racks and the existing racks will be present in the SFP and loaded with fuel at the same time. During these interim configurations it is important to maintain continued criticality safety by ensuring that the fuel in the new and existing racks remains neutronically decoupled. This can be assured by maintaining at least two rows of empty storage locations (approximately 20 inches; 12 inches provides effectively an infinite neutron reflector) between the fuel in the new racks and fuel in the existing racks. These two rows may be in either type of rack or split

between the two racks (1 empty row in each rack). This requirement is specified in lieu of performing detailed calculations on interfaces between the new and existing racks. This requirement does not need to be imposed on fuel in racks adjacent to the same type of rack, since this is already addressed in this chapter for the new racks, and the analysis of record for the existing racks.

4.8 References

- [4.1] M.G. Natrella, Experimental Statistics, National Bureau of Standards, Handbook 91, August 1963.
- [4.2] J.F. Briesmeister, Editor, "MCNP - A General Monte Carlo N-Particle Transport Code, Version 4A," LA-12625, Los Alamos National Laboratory (1993).
- [4.3] "Lumped Fission Product and Pm148m Cross Sections for MCNP," Holtec Report HI-2033031, Rev 0, September 2003.
- [4.4] M. Edenius, K. Ekberg, B.H. Forssén, and D. Knott, "CASMO-4 A Fuel Assembly Burnup Program User's Manual," Studsvik/SOA-95/1, Studsvik of America, Inc. and Studsvik Core Analysis AB (proprietary).
- [4.5] D. Knott, "CASMO-4 Benchmark Against Critical Experiments", SOA-94/13, Studsvik of America, Inc., (proprietary).
- [4.6] D. Knott, "CASMO-4 Benchmark Against MCNP," SOA-94/12, Studsvik of America, Inc., (proprietary).
- [4.7] L.I. Kopp, "Guidance on the Regulatory Requirements for Criticality Analysis of Fuel Storage at Light-Water Reactor Power Plants," NRC Memorandum from L. Kopp to T. Collins, August 19, 1998.
- [4.8] ANS-8.1/N16.1-1975, "American National Standard for Nuclear Criticality Safety in Operations with Fissionable Materials Outside Reactors," April 14, 1975.
- [4.9] S.E. Turner, "Uncertainty Analysis - Burnup Distributions", presented at the DOE/SANDIA Technical Meeting on Fuel Burnup Credit, Special Session, ANS/ENS Conference, Washington, D.C., November 2, 1988.
- [4.10] Study of the Effect of Integral Burnable Absorbers for PWR Burnup Credit," NUREG/CR-6760, ORNL/TM-2000-321, March 2002.
- [4.11] ASME Boiler & Pressure Vessel code, Section III, Subsection NB, American Society of Mechanical Engineers, 1995 with Addenda through 1997.

Table 4.5.1
Fuel Assembly Specification and Design Basis Fuel Assembly Selection

Parameter	Value											
Fuel Region	1	2	2A	3	4A	4B	5A	5B	5C	6A	6B	7A
Number of fuel rods	264	264	264	264	264	264	264	264	264	264	264	264
Fuel rod pitch, in.	0.496	0.496	0.496	0.496	0.496	0.496	0.496	0.496	0.496	0.496	0.496	0.496
Active Fuel Length, in.	144	144	144	144	144	144	144	144	144	144	144	144
Pellet diameter, in.	0.3225	0.3225	0.3225	0.3225	0.3225	0.3225	0.3225	0.3225	0.3225	0.3225	0.3225	0.3225
Cladding ID, in.	0.329	0.329	0.329	0.329	0.329	0.329	0.329	0.329	0.329	0.329	0.329	0.329
Cladding OD, in.	0.374	0.374	0.374	0.374	0.374	0.374	0.374	0.374	0.374	0.374	0.374	0.374
GT/IT ID, in.	0.448	0.448	0.448	0.448	0.448	0.448	0.448	0.448	0.448	0.442	0.442	0.442
GT/IT OD, in.	0.484	0.484	0.484	0.484	0.484	0.484	0.484	0.484	0.484	0.474	0.474	0.474
Parameter	Value											
Fuel Region	7B	8A	8B	9A	9B	10A	10B	11A	11B	12A	12B	13A
Number of fuel rods	264	264	264	264	264	264	264	264	264	264	264	264
Fuel rod pitch, in.	0.496	0.496	0.496	0.496	0.496	0.496	0.496	0.496	0.496	0.496	0.496	0.496
Active Fuel Length, in.	144	144	144	144	144	144	144	144	144	144	144	144
Pellet diameter, in.	0.3225	0.3225	0.3225	0.3225	0.3225	0.3225	0.3225	0.3225	0.3225	0.3225	0.3225	0.3225
Cladding ID, in.	0.329	0.329	0.329	0.329	0.329	0.329	0.329	0.329	0.329	0.329	0.329	0.329
Cladding OD, in.	0.374	0.374	0.374	0.374	0.374	0.374	0.374	0.374	0.374	0.374	0.374	0.374
GT/IT ID, in.	0.442	0.442	0.442	0.442	0.442	0.442	0.442	0.442	0.442	0.442	0.442	0.442
GT/IT OD, in.	0.474	0.474	0.474	0.474	0.474	0.474	0.474	0.474	0.474	0.482	0.482	0.482
Parameter	Value					Note: The guide tube parameters were selected to maximize reactivity.	Parameter		Design Basis FA			
Fuel Region	13B	14A	14B	15A	15B		Min	Max				
Number of fuel rods	264	264	264	264	264		264	264	264			
Fuel rod pitch, in.	0.496	0.496	0.496	0.496	0.496		0.496	0.496	0.496			
Active Fuel Length, in.	144	144	144	144	144		144	144	144			
Pellet diameter, in.	0.3225	0.3225	0.3225	0.3225	0.3225		0.3225	0.3225	0.3225			
Cladding ID, in.	0.329	0.329	0.329	0.329	0.329		0.329	0.329	0.329			
Cladding OD, in.	0.374	0.374	0.374	0.374	0.374		0.374	0.374	0.374			
GT/IT ID, in.	0.442	0.442	0.442	0.442	0.442		0.442	0.448	0.448			
GT/IT OD, in.	0.482	0.482	0.482	0.482	0.482		0.474	0.484	0.474			

Table 4.5.2
Specification of the Design Basis Fuel Assembly

Parameter	Design Basis Fuel Assembly	Tolerance
Number of fuel rods	264	n/a
Fuel rod pitch, in.†	0.496	+0.00044,-0.0075
Active Fuel Length, in.	144	n/a
Fuel Pellet diameter, in.	0.3225	+/-0.0005
Cladding ID, in.	0.329	+/-0.0015
Cladding OD, in.	0.374	+/-0.0015
Fuel pellet density, g/cc (max)	10.6312	n/a
GT/IT ID, in.	0.448	+/-0.002
GT/IT OD, in.	0.474	+/-0.002
Enrichment, wt% ²³⁵ U (max)	5.00	+0.05

†The positive tolerance was calculated by dividing the maximum pitch tolerance of 0.0075 by 17.

Table 4.5.3
Core Operating Parameter for CASMO Depletion Analyses

Parameter	Value
Bounding Cycle Average Soluble Boron Concentration, ppm	1050
Bounding Reactor Specific Power, MW/MTU	40.4
Bounding Core Fuel Temp., °F	1516
Bounding Core Average Exit Moderator Temp., °F	620
In-Core Assembly Pitch, Inches	8.466

Table 4.5.4
Calculation of Soluble Boron for CASMO-4

GWD/MTU	Predicted ppm
0	1506
0.15	1498
0.5	1486
1	1485
2	1488
3	1466
4	1424
6	1294
8	1126
10	936
12	735
14	530
16	325
18	125
18.8	46
19.8	-50
20	-70
Average	1031
Bounding	1050

Note: The boron concentrations from the last two steps were neglected.

Table 4.5.6
Bounding Axial Burnup Profile Summary

Node (top to bottom)	Relative Burnup (GWD/MTU)
24	0.2089
23	0.7163
22	0.8480
21	0.9658
20	1.0250
19	1.0405
18	1.0560
17	1.0736
16	1.0853
15	1.0610
14	1.0884
13	1.0911
12	1.0808
11	1.0973
10	1.1020
9	1.1020
8	1.0850
7	1.1112
6	1.1107
5	1.0638
4	1.0639
3	0.9915
2	0.7916
1	0.2217
Note: Node size is 6 inches.	

Table 4.5.7
IFBA Rod Specification

Parameter	Value
Maximum number of IFBA rods	128 or 200
Max. IFBA Loading, mgB-10/inch	2.35
IFBA thickness, cm	0.00243

Table 4.5.8
Water Displacer Rod Specification

Parameter	Value
Fuel Region - Number of WDR rodlets per assembly	4A - 4, 8 4B - 4
WDR Cladding Inner Radius (cm)	0.43688
WDR Cladding Outer Radius (cm)	0.48387
Cladding Material	304 Stainless Steel
Fuel Assembly Axial Layout	
Number of Assemblies	
4A - 100 IFBA Rods - 4 WDRs	12
4A - 128 IFBA Rods - No WDRs	4
4A - 128 IFBA Rods - 8 WDRs	4
4B - 32 IFBA Rods - No WDRs	8
4B - 64 IFBA Rods - No WDRs	8
4B - 100 IFBA Rods - 4 WDRs	8
4B - 128 IFBA Rods - No WDRs	4
4B - 128 IFBA Rods - 4 WDRs	8

Table 4.5.9
WABA Specification

Parameter	Fuel Region	
	2	3
	Value	
WABA rods in FA with 3.099 wt% U-235	n/a	12,16
WABA rods in FA with 2.602 wt% U-235	12,20	n/a
Inner Water Hole Radius (cm)	0.28575	0.28575
Inside Cladding Outer Radius (cm)	0.33909	0.33909
Absorber Inner Radius (cm)	0.35306	0.35306
Absorber Outer Radius (cm)	0.40386	0.40386
Outside Cladding Inner Radius (cm)	0.41783	0.41783
Outside Cladding Outer Radius (cm)	0.48387	0.48387
Cladding Material	Zircaloy-4	Zircaloy-4
Absorber Material (wt%)	B ₄ C - 14% Al ₂ O ₃ - 86%	B ₄ C - 14% Al ₂ O ₃ - 86%
Absorber Density (g/cm ³)	2.47436	2.47436

Table 4.5.10
Storage Cell Specification

Parameter	Value	Tolerance
Cell ID, in.	8.8	
Cell Wall thickness, in.	0.075	
Cell Pitch, in. †	9.03	n/a
Inner Sheathing Thickness, in.	0.035	
Poison Thickness, in.	0.106	
Poison Width, in.	7.5	
Poison Gap, (min) in.	0.112	n/a
Gap Between Racks, in.	1.5	n/a
Metamic B4C Loading, () %		
Metamic Density, g/cc		
Metamic B-10, %		
Metamic B-11, %		
Metamic C, %		
Metamic Al, %		

† In the CASMO-4 Model used the cell pitch tolerance is accounted for in the cell I.D. tolerance.

Table 4.5.11
Specification of the Fuel Rod Storage Basket

Parameter	Value
Number of Cells	52
Cell Pitch	0.937 inches
Array Type	8x8
Basket Wall Thickness †	0.035 inches

† Conservatively neglected in the analysis.

Table 4.5.12
Specification for the Boron Dilution Analysis

Parameter	Value
Credited Volume of SFP	182,472 gal
Service Water System	3000 gpm
Volume to High Level Alarm Set point [†]	7850 gal

[†] Calculated as 1 ft of SFP volume.

Table 4.7.1
Summary of the Region 2 Initial Enrichment and Burnup Combinations

Enrichment (wt% U-235)	Calculated Burnup (GWD/MTU)	Burnup with 5% Uncertainty and Polynomial Fit (GWD/MTU)
2.0	8.10	8.83
2.5	16.13	16.94
3.0	23.45	24.89
3.5	30.82	32.71
4.0	37.93	40.37
4.5	45.29	47.89
5.0	52.22	55.27

$$BU = -0.2916 * E^2 + 17.521 * E - 25.045$$

Table 4.7.2
 Summary of the Region 3 Initial Enrichment and Burnup Combinations:

Enrichment (wt% U-235)	Calculated Burnup (GWD/MTU)	Burnup with 5% Uncertainty and Polynomial Fit (GWD/MTU)
2.0	0.00	0.00
2.5	5.08	6.42
3.0	13.44	14.39
3.5	21.34	23.43
4.0	31.02	32.56
4.5	37.61	40.80
5.0	44.48	47.17

$$BU = -1.3118 \cdot E^3 + 13.957 \cdot E^2 - 30.989 \cdot E + 17.163$$

Table 4.7.3
Summary of the MTZR Soluble Boron Requirements
For Normal Conditions

Parameter	Value
Soluble Boron Requirement, ppm	472

Table 4.7.4
Summary of Accident Cases

Case	Soluble Boron Requirement (ppm)
Mislocated Fresh Fuel Assembly	1179
Misloaded Fresh Fuel Assembly in Region 2 (outer row)	1192
Misloaded Fresh Fuel Assembly in Region 2 (inner row)	1006
Misloaded Fresh Fuel Assembly in Region 3	894

Table 4.7.5
CASMO-4 Calculation of the Effect of Spacer Grids and Boron Concentration on Reactivity

Burnup (GWD/MTU)	Boron (ppm)	Reference Case Reactivity	Spacer Grid Case Reactivity	Delta-k
0	400	1.1459	1.1352	-0.0107
	800	1.1007	1.0924	-0.0083
	1000	1.0797	1.0725	-0.0072
	1200	1.0597	1.0534	-0.0063
	1400	1.0406	1.0352	-0.0054
	1600	1.0223	1.0177	-0.0046
	1800	1.0047	1.0009	-0.0038
	2000	0.9879	0.9849	-0.0031
20	400	1.0035	0.9950	-0.0085
	800	0.9648	0.9586	-0.0062
	1000	0.9469	0.9418	-0.0051
	1200	0.9299	0.9257	-0.0042
	1400	0.9136	0.9103	-0.0033
	1600	0.8980	0.8955	-0.0025
	1800	0.8832	0.8814	-0.0018
	2000	0.8690	0.8679	-0.0011
40	400	0.8896	0.8855	-0.0041
	800	0.8539	0.8521	-0.0017
	1000	0.8374	0.8367	-0.0007
	1200	0.8218	0.8220	0.0002
	1400	0.8070	0.8080	0.0010
	1600	0.7928	0.7946	0.0018
	1800	0.7794	0.7819	0.0025
	2000	0.7665	0.7696	0.0031
60	400	0.7895	0.7914	0.0019
	800	0.7564	0.7605	0.0041
	1000	0.7412	0.7462	0.0050
	1200	0.7269	0.7327	0.0059
	1400	0.7132	0.7199	0.0066
	1600	0.7003	0.7076	0.0073
	1800	0.6880	0.6960	0.0079
	2000	0.6764	0.6848	0.0085

Table 4.7.6
Calculation of the Initial Enrichment and Burnup Combinations for Region 2

Enrichment (wt% ²³⁵ U)	2.0	2.5	3.0	3.5	4.0	4.5	5.0
Burnup (GWD/MTU)	10.0	20.0	25.0	35.0	40.0	50.0	55.0
Reactivity Uniform Profile	0.9698	0.9657	0.9711	0.9654	0.9687	0.9614	0.9626
Reactivity Segmented Profile	0.9702	0.9671	0.9694	0.9676	0.9699	0.9670	0.9693
Max Reactivity	0.9702	0.9671	0.9711	0.9676	0.9699	0.9670	0.9693
Burnup (GWD/MTU)	5.0	15.0	20.0	30.0	35.0	45.0	50.0
Reactivity Uniform Profile	0.9841	0.9773	0.9821	0.9745	0.9750	0.9693	0.9686
Reactivity Segmented Profile	0.9840	0.9756	0.9806	0.9750	0.9780	0.9729	0.9743
Max Reactivity	0.9841	0.9773	0.9821	0.9750	0.9780	0.9729	0.9743
Manufacturing Tolerances Uncertainty [†]	0.0037	0.0037	0.0037	0.0037	0.0037	0.0037	0.0037
Fuel Tolerances Uncertainty [†]	0.0074	0.0074	0.0074	0.0074	0.0074	0.0074	0.0074
Calculation Uncertainty (2σ)	0.0014	0.0014	0.0014	0.0016	0.0014	0.0012	0.0014
Depletion Uncertainty k _{eff}	0.9972	1.0323	1.0600	1.0829	1.1045	1.1235	1.1390
Depletion Uncertainty	0.0014	0.0033	0.0044	0.0058	0.0067	0.0078	0.0085
Eccentric Fuel Positioning	0.0004	0.0004	0.0004	0.0004	0.0004	0.0004	0.0004
MCNP Code Uncertainty	0.0011	0.0011	0.0011	0.0011	0.0011	0.0011	0.0011
Total Uncertainty (statistical combination)	0.0086	0.0091	0.0096	0.0103	0.0108	0.0115	0.0120
Code Bias	0.0009	0.0009	0.0009	0.0009	0.0009	0.0009	0.0009
Temperature Bias ^{††}	0.0038	0.0038	0.0038	0.0038	0.0038	0.0038	0.0038
Reactivity Control Bias	0.0062	0.0062	0.0062	0.0062	0.0062	0.0062	0.0062
Total Corrections	0.0195	0.0200	0.0205	0.0212	0.0218	0.0224	0.0229
Maximum k _{eff}	0.995	0.995	0.995	0.995	0.995	0.995	0.995
Target k _{eff} (0.995-corrections)	0.9755	0.9750	0.9745	0.9738	0.9732	0.9726	0.9721
Calculated Burnup (GWD/MTU)	8.10	16.13	23.45	30.82	37.93	45.29	52.22
Calculated Burnup (GWD/MTU) + 5%	8.50	16.94	24.63	32.36	39.83	47.55	54.83
Adjusted Polynomial Fit ^{†††} (Bu = -0.2916* E ² + 17.521*E - 25.045)	8.83	16.94	24.89	32.71	40.37	47.89	55.27

[†] These tolerance uncertainties are the maximum from all burnups and enrichments.

^{††} The temperature bias is from the 5.0 wt% ²³⁵U fresh calculation.

^{†††} The polynomial was created with the calculated burnup + 5% values, and then adjusted to bound every point.

Table 4.7.7
Calculation of the Initial Enrichment and Burnup Combinations for Region 3

Enrichment (wt% ²³⁵ U)	2.0	2.5	3.0	3.5	4.0	4.5	5.0
Burnup (GWD/MTU)	5.0	10.0	15.0	25.0	35.0	40.0	45.0
Reactivity Uniform Profile	0.9713	0.9727	0.9726	0.9711	0.9687	0.9704	0.9708
Reactivity Segmented Profile	0.9705	0.9717	0.9728	0.9719	0.9722	0.9706	0.9700
Max Reactivity	0.9713	0.9727	0.9728	0.9719	0.9722	0.9706	0.9708
Burnup (GWD/MTU)	0.0	5.0	10.0	20.0	30.0	35.0	40.0
Reactivity Uniform Profile	0.9729	0.9751	0.9765	0.9736	0.9730	0.9714	0.9710
Reactivity Segmented Profile	0.9729	0.9755	0.9789	0.9745	0.9716	0.9734	0.9743
Max Reactivity	0.9729	0.9755	0.9789	0.9745	0.9730	0.9734	0.9743
Manufacturing Tolerances Uncertainty [†]	0.0028	0.0030	0.0032	0.0034	0.0035	0.0036	0.0037
Fuel Tolerances Uncertainty [†]	0.0074	0.0057	0.0046	0.0039	0.0035	0.0032	0.0030
Calculation Uncertainty (2σ)	0.0014	0.0014	0.0014	0.0014	0.0014	0.0014	0.0014
Depletion Uncertainty k_{eff}	0.9734	1.0038	1.0513	1.0879	1.1197	1.1435	1.1655
Depletion Uncertainty	0.0001	0.0016	0.0039	0.0058	0.0074	0.0086	0.0097
Eccentric Fuel Positioning	0.0004	0.0004	0.0004	0.0004	0.0004	0.0004	0.0004
MCNP Code Uncertainty	0.0011	0.0011	0.0011	0.0011	0.0011	0.0011	0.0011
Total Uncertainty (statistical combination)	0.0085	0.0086	0.0094	0.0103	0.0112	0.0121	0.0129
Code Bias	0.0009	0.0009	0.0009	0.0009	0.0009	0.0009	0.0009
Temperature Bias ^{††}	0.0038	0.0038	0.0038	0.0038	0.0038	0.0038	0.0038
Reactivity Control Bias	0.0062	0.0062	0.0062	0.0062	0.0062	0.0062	0.0062
Total Corrections	0.0194	0.0195	0.0203	0.0212	0.0222	0.0231	0.0238
Maximum k_{eff}	0.995	0.995	0.995	0.995	0.995	0.995	0.995
Target k_{eff} (0.995-corrections)	0.9756	0.9755	0.9747	0.9738	0.9728	0.9719	0.9712
Calculated Burnup (GWD/MTU)	0.00	5.08	13.44	21.34	31.02	37.61	44.48
Calculated Burnup (GWD/MTU) + 5%	0.00	5.33	14.11	22.41	32.57	39.49	46.70
Polynomial Fit ^{†††} (Bu = -1.3118*E ³ +13.957*E ² -30.989*E+17.163)	0.00	6.42	14.39	23.43	32.56	40.80	47.17

[†] These tolerance uncertainties are the maximum from all burnups and enrichments.

^{††} The temperature bias is from the 5.0 wt% ²³⁵U fresh calculations.

^{†††} The polynomial was created with the calculated burnup + 5% values, and then adjusted to bound every point.

Table 4.7.8
Results of the CASMO-4 Calculations of the IFBA Bias

IFBA Pins	0	100	n/a	0	128	n/a	0	200	n/a		
Enrichment wt% U-235	2.0			3.8							
Burnup (GWD/MTU)	Ref	k_{inf}	Delta-k	Ref	k_{inf}	Delta-k	k_{inf}	k_{inf}	Delta-k	Max Delta-k	
0.0	0.9656	0.7595	-0.2061	1.1358	0.9182	-0.2176	1.1358	0.8405	-0.2953	-0.2061	
0.1	0.9625	0.7612	-0.2013	1.1336	0.9191	-0.2146	1.1336	0.8423	-0.2913	-0.2013	
2.0	0.9484	0.8240	-0.1244	1.1131	0.9513	-0.1618	1.1131	0.8912	-0.2219	-0.1244	
4.0	0.9330	0.8615	-0.0715	1.0967	0.9774	-0.1193	1.0967	0.9313	-0.1654	-0.0715	
6.0	0.9168	0.8782	-0.0386	1.0799	0.9936	-0.0863	1.0799	0.9589	-0.1211	-0.0386	
8.0	0.9011	0.8819	-0.0192	1.0636	1.0023	-0.0613	1.0636	0.9767	-0.0869	-0.0192	
10.0	0.8861	0.8781	-0.0080	1.0478	1.0053	-0.0426	1.0478	0.9868	-0.0611	-0.0080	
11.0	0.8789	0.8744	-0.0044	1.0402	1.0050	-0.0352	1.0402	0.9895	-0.0508	-0.0044	
12.5	0.8684	0.8676	-0.0008	1.0290	1.0029	-0.0261	1.0290	0.9911	-0.0380	-0.0008	
15.0	0.8517	0.8543	0.0025	1.0111	0.9959	-0.0151	1.0111	0.9888	-0.0223	0.0025	
17.5	0.8359	0.8398	0.0039	0.9936	0.9856	-0.0080	0.9936	0.9816	-0.0120	0.0039	
20.0	0.8210	0.8254	0.0044	0.9767	0.9732	-0.0035	0.9767	0.9714	-0.0053	0.0044	
22.5	0.8069	0.8114	0.0044	0.9602	0.9596	-0.0006	0.9602	0.9592	-0.0010	0.0044	
25.0	0.7938	0.7981	0.0043	0.9441	0.9453	0.0012	0.9441	0.9458	0.0017	0.0043	
27.5	0.7815	0.7856	0.0041	0.9284	0.9307	0.0023	0.9284	0.9317	0.0033	0.0041	
30.0	0.7701	0.7739	0.0039	0.9130	0.9160	0.0030	0.9130	0.9174	0.0044	0.0044	
32.5	0.7595	0.7632	0.0036	0.8980	0.9013	0.0034	0.8980	0.9030	0.0050	0.0050	
35.0	0.7499	0.7532	0.0033	0.8833	0.8869	0.0036	0.8833	0.8887	0.0054	0.0054	
37.5	0.7411	0.7442	0.0031	0.8690	0.8727	0.0037	0.8690	0.8746	0.0056	0.0056	
40.0	0.7330	0.7359	0.0028	0.8551	0.8589	0.0038	0.8551	0.8608	0.0057	0.0057	
42.5				0.8417	0.8454	0.0038	0.8417	0.8474	0.0058	0.0058	
45.0				0.8287	0.8324	0.0038	0.8287	0.8344	0.0057	0.0057	
47.5				0.8162	0.8199	0.0037	0.8162	0.8219	0.0057	0.0057	
50.0		n/a		0.8043	0.8079	0.0037	0.8043	0.8098	0.0056	0.0056	
52.5				0.7929	0.7964	0.0036	0.7929	0.7983	0.0055	0.0055	
55.0				0.7821	0.7855	0.0035	0.7821	0.7873	0.0053	0.0053	

Table 4.7.9
Results of the CASMO-4 Calculations of WDR Reactivity Dependence on Number of WDR
Rods and Fuel Enrichment

WDR Rods	0	4	8	n/a
Enrichment wt% U-235	3.4			
Burnup (GWD/MTU)	Ref	k_{inf}	k_{inf}	Delta-k (max - ref)
0.0	1.1093	1.1093	1.1093	0.0000
0.1	1.1069	1.1069	1.1069	0.0000
2.0	1.0868	1.0868	1.0868	0.0000
4.0	1.0700	1.0699	1.0700	0.0000
6.0	1.0529	1.0529	1.0529	0.0001
8.0	1.0362	1.0362	1.0364	0.0002
10.0	1.0202	1.0203	1.0205	0.0003
11.0	1.0124	1.0125	1.0127	0.0003
12.5	1.0010	1.0011	1.0014	0.0003
15.0	0.9828	0.9828	0.9831	0.0003
17.5	0.9651	0.9653	0.9655	0.0004
20.0	0.9480	0.9481	0.9484	0.0004
22.5	0.9313	0.9314	0.9317	0.0003
25.0	0.9151	0.9152	0.9154	0.0003
27.5	0.8993	0.8994	0.8996	0.0003
30.0	0.8840	0.8840	0.8843	0.0003
32.5	0.8691	0.8692	0.8694	0.0003
35.0	0.8547	0.8548	0.8550	0.0003
37.5	0.8408	0.8409	0.8411	0.0003
40.0	0.8274	0.8275	0.8277	0.0003
42.5	0.8146	0.8147	0.8149	0.0003
45.0	0.8024	0.8025	0.8026	0.0002
47.5	0.7908	0.7908	0.7910	0.0002
50.0	0.7798	0.7798	0.7800	0.0002
52.5	0.7695	0.7695	0.7697	0.0002

Table 4.7.10
Results of the CASMO-4 Calculations of a Fuel Assembly with both IFBA and WDR Bias
Dependence on the Number of WDR Rods and Fuel Enrichment

WDR Rods	0	4	8	n/a
Enrichment wt% U-235	3.4			
Burnup (GWD/MTU)	Ref	k_{inf}	k_{inf}	Delta-k (max - ref)
0.0	1.1093	0.9104	0.9104	-0.1989
0.1	1.1069	0.9111	0.9111	-0.1959
2.0	1.0868	0.9420	0.9421	-0.1448
4.0	1.0700	0.9658	0.9659	-0.1042
6.0	1.0529	0.9795	0.9795	-0.0733
8.0	1.0362	0.9857	0.9858	-0.0504
10.0	1.0202	0.9863	0.9864	-0.0337
11.0	1.0124	0.9850	0.9851	-0.0273
12.5	1.0010	0.9814	0.9816	-0.0195
15.0	0.9828	0.9722	0.9724	-0.0104
17.5	0.9651	0.9605	0.9607	-0.0044
20.0	0.9480	0.9469	0.9472	-0.0008
22.5	0.9313	0.9325	0.9327	0.0013
25.0	0.9151	0.9175	0.9178	0.0027
27.5	0.8993	0.9025	0.9027	0.0034
30.0	0.8840	0.8876	0.8879	0.0039
32.5	0.8691	0.8730	0.8732	0.0041
35.0	0.8547	0.8587	0.8589	0.0042
37.5	0.8408	0.8448	0.8451	0.0043
40.0	0.8274	0.8315	0.8317	0.0043
42.5	0.8146	0.8186	0.8188	0.0042
45.0	0.8024	0.8063	0.8065	0.0041
47.5	0.7908	0.7946	0.7948	0.0040
50.0	0.7798	0.7835	0.7837	0.0039
52.5	0.7695	0.7730	0.7732	0.0037

Table 4.7.11
Results of the CASMO-4 Calculations of WABA Bias Dependence on Number of WABA Rods
and Fuel Enrichment

WABA Rods	0	12	20	n/a	0	12	16	n/a	
Enrichment wt% U-235	2.6				3.0				
Burnup (GWD/MTU)	Ref	k_{inf}	k_{inf}	Delta-k (max - ref)	Ref	k_{inf}	k_{inf}	Delta- k (max - ref)	Max Delta-k
0.0	1.0400	0.9710	0.9316	-0.0690	1.0779	1.0110	0.9922	-0.0669	-0.0669
0.1	1.0373	0.9693	0.9305	-0.0680	1.0754	1.0093	0.9908	-0.0660	-0.0660
2.0	1.0192	0.9686	0.9394	-0.0506	1.0560	1.0051	0.9906	-0.0508	-0.0506
4.0	1.0022	0.9669	0.9461	-0.0354	1.0389	1.0016	0.9907	-0.0373	-0.0354
6.0	0.9849	0.9611	0.9469	-0.0238	1.0215	0.9949	0.9870	-0.0266	-0.0238
8.0	0.9680	0.9524	0.9428	-0.0156	1.0046	0.9861	0.9803	-0.0186	-0.0156
10.0	0.9520	0.9416	0.9351	-0.0103	0.9885	0.9755	0.9714	-0.0130	-0.0103
11.0	0.9442	0.9356	0.9302	-0.0085	0.9806	0.9696	0.9662	-0.0110	-0.0085
12.5	0.9328	0.9264	0.9222	-0.0065	0.9692	0.9606	0.9578	-0.0086	-0.0065
15.0	0.9147	0.9105	0.9077	-0.0042	0.9509	0.9450	0.9430	-0.0059	-0.0042
17.5	0.8972	0.9009	0.9034	0.0062	0.9331	0.9363	0.9373	0.0041	0.0062
20.0	0.8804	0.8840	0.8863	0.0060	0.9160	0.9191	0.9200	0.0041	0.0060
22.5	0.8642	0.8676	0.8698	0.0055	0.8993	0.9023	0.9032	0.0039	0.0055
25.0	0.8488	0.8519	0.8540	0.0052	0.8833	0.8861	0.8869	0.0037	0.0052
27.5	0.8340	0.8370	0.8389	0.0049	0.8677	0.8704	0.8712	0.0035	0.0049
30.0	0.8200	0.8227	0.8246	0.0047	0.8528	0.8554	0.8562	0.0034	0.0047
32.5	0.8066	0.8093	0.8111	0.0044	0.8384	0.8409	0.8417	0.0033	0.0044
35.0	0.7940	0.7965	0.7983	0.0042	0.8247	0.8271	0.8279	0.0032	0.0042
37.5	0.7822	0.7846	0.7862	0.0040	0.8116	0.8139	0.8146	0.0031	0.0040
40.0	0.7712	0.7734	0.7750	0.0038	0.7991	0.8013	0.8021	0.0030	0.0038

Table 4.7.12
Results for the Calculation of the Eccentric Fuel Positioning Reactivity Effect

Region 2 Enrichment, wt% ²³⁵ U	5.0	5.0	5.0	5.0	5.0	5.0	5.0
Region 2 Burnup, GWD/MTU	48	48	48	48	48	48	48
Region 3 Enrichment, wt% ²³⁵ U	2.0	2.5	3.0	3.5	4.0	4.5	5.0
Region 3 Burnup, GWD/MTU	0.00	5.00	12.00	20.00	31.00	37.00	43.00
Reference Case Reactivity	0.9734	0.9755	0.975	0.9745	0.9747	0.9738	0.9735
Reactivity, Eccentric Case 1	0.9734	0.9747	0.9752	0.9749	0.9746	0.9738	0.9738
Delta-k _{eff}	0.0000	-0.0008	0.0002	0.0004	0.0001	0.0000	0.0003
Reactivity, Eccentric Case 2	0.9730	0.9748	0.9734	0.9727	0.9721	0.9733	0.9729
Delta-k _{eff}	-0.0004	-0.0007	-0.0016	-0.0018	0.0026	-0.0005	-0.0006
Maximum Delta-k _{eff}	0.0000	-0.0007	0.0002	0.0004	0.0001	0.0000	0.0003

Table 4.7.13
Region 2 CASMO Calculations for Fuel Tolerance Uncertainties

Burnup (GWD/MTU)	Enr	Ref Case	Rod Pitch +	Rod Pitch -	Clad OD +	Clad OD -	Clad ID +	Clad ID -	Fuel Pellet OD +	Fuel Pellet Enr +	Stat. Combo
0.0 2		0.9656	0.0006	-0.0080	-0.0013	0.0012	0.0002	-0.0003	0.0004	0.0073	0.0074
8.0 2		0.9011	0.0006	-0.0082	-0.0009	0.0009	0.0002	-0.0002	0.0005	0.0062	0.0063
0.0 2.5		1.0293	0.0007	-0.0098	-0.0013	0.0013	0.0002	-0.0002	0.0003	0.0054	0.0057
4.0 2.5		0.9920	0.0007	-0.0098	-0.0012	0.0012	0.0002	-0.0002	0.0003	0.0052	0.0054
15.0 2.5		0.9049	0.0007	-0.0093	-0.0008	0.0008	0.0002	-0.0002	0.0005	0.0049	0.0051
0.0 3.0		1.0779	0.0008	-0.0113	-0.0014	0.0014	0.0002	-0.0002	0.0003	0.0042	0.0045
12.5 3.0		0.9692	0.0008	-0.0108	-0.0011	0.0010	0.0002	-0.0002	0.0003	0.0042	0.0044
22.5 3.0		0.8993	0.0007	-0.0100	-0.0007	0.0007	0.0002	-0.0002	0.0005	0.0042	0.0043
0.0 3.5		1.1163	0.0009	-0.0125	-0.0014	0.0014	0.0002	-0.0002	0.0003	0.0034	0.0038
20.0 3.5		0.9555	0.0008	-0.0113	-0.0009	0.0009	0.0002	-0.0002	0.0004	0.0037	0.0039
30.0 3.5		0.8914	0.0007	-0.0105	-0.0006	0.0006	0.0002	-0.0002	0.0005	0.0037	0.0038
0.0 4.0		1.1476	0.0009	-0.0135	-0.0015	0.0014	0.0002	-0.0002	0.0002	0.0028	0.0033
30.0 4.0		0.9266	0.0008	-0.0114	-0.0008	0.0008	0.0002	-0.0002	0.0004	0.0033	0.0035
37.5	4.0	0.8825	0.0007	-0.0108	-0.0005	0.0005	0.0002	-0.0002	0.0005	0.0033	0.0035
0.0 4.5		1.1737	0.0010	-0.0143	-0.0015	0.0015	0.0002	-0.0002	0.0002	0.0024	0.0030
37.5	4.5	0.9144	0.0008	-0.0117	-0.0007	0.0007	0.0002	-0.0002	0.0004	0.0030	0.0032
45.0	4.5	0.8730	0.0007	-0.0110	-0.0004	0.0004	0.0002	-0.0002	0.0005	0.0030	0.0032
0.0 5.0		1.1958	0.0010	-0.0150	-0.0015	0.0015	0.0002	-0.0002	0.0002	0.0020	0.0027
42.5	5.0	0.9158	0.0008	-0.0120	-0.0007	0.0007	0.0002	-0.0002	0.0004	0.0028	0.0030
50.0	5.0	0.8760	0.0007	-0.0114	-0.0004	0.0004	0.0002	-0.0002	0.0005	0.0028	0.0030

Table 4.7.14
CASMO Calculations for Manufacturing Tolerance Uncertainties for Fuel Storage Cell

Burnup (GWD/MTU)	Enr	Ref Case	Cell ID +	Cell ID -	Poison Width -	Sheathing +	Sheathing -	Box Wall +	Box Wall -	Poison Thick. -	B-10 Loadin g Min	Statistical Combo
0.0	2.0	0.9656	0.0014	0.0012	0.0011	0.0002	-0.0002	0.0001	-0.0001	0.0017	0.0014	0.0028
8.0	2.0	0.9011	0.0010	0.0013	0.0011	0.0002	-0.0002	0.0001	-0.0001	0.0015	0.0013	0.0026
0.0	2.5	1.0293	0.0011	0.0015	0.0012	0.0002	-0.0002	0.0001	-0.0001	0.0018	0.0015	0.0030
4.0	2.5	0.9920	0.0009	0.0015	0.0012	0.0002	-0.0002	0.0001	-0.0001	0.0017	0.0014	0.0029
15.0	2.5	0.9049	0.0008	0.0014	0.0011	0.0002	-0.0002	0.0001	-0.0001	0.0016	0.0013	0.0027
0.0	3.0	1.0779	0.0009	0.0017	0.0013	0.0002	-0.0002	0.0001	-0.0001	0.0018	0.0015	0.0032
12.5	3.0	0.9692	0.0006	0.0015	0.0011	0.0002	-0.0002	0.0001	-0.0001	0.0016	0.0014	0.0029
22.5	3.0	0.8993	0.0006	0.0014	0.0011	0.0001	-0.0002	0.0001	-0.0001	0.0015	0.0013	0.0027
0.0	3.5	1.1163	0.0006	0.0019	0.0013	0.0002	-0.0002	0.0001	-0.0001	0.0019	0.0016	0.0034
20.0	3.5	0.9555	0.0005	0.0016	0.0011	0.0002	-0.0002	0.0001	-0.0001	0.0016	0.0014	0.0029
30.0	3.5	0.8914	0.0005	0.0014	0.0011	0.0001	-0.0002	0.0001	-0.0001	0.0015	0.0013	0.0027
0.0	4.0	1.1476	0.0004	0.0020	0.0013	0.0002	-0.0002	0.0001	-0.0001	0.0019	0.0016	0.0035
30.0	4.0	0.9266	0.0004	0.0015	0.0011	0.0001	-0.0002	0.0001	-0.0001	0.0016	0.0013	0.0028
37.5	4.0	0.8825	0.0004	0.0014	0.0011	0.0001	-0.0002	0.0001	-0.0001	0.0015	0.0013	0.0026
0.0	4.5	1.1737	0.0002	0.0021	0.0014	0.0002	-0.0002	0.0001	-0.0001	0.0020	0.0017	0.0036
37.5	4.5	0.9144	0.0003	0.0015	0.0011	0.0001	-0.0002	0.0001	-0.0001	0.0015	0.0013	0.0027
45.0	4.5	0.8730	0.0003	0.0014	0.0011	0.0001	-0.0002	0.0001	-0.0001	0.0015	0.0012	0.0026
0.0	5.0	1.1958	0.0000	0.0023	0.0014	0.0002	-0.0002	0.0001	-0.0001	0.0020	0.0017	0.0037
42.5	5.0	0.9158	0.0002	0.0015	0.0011	0.0001	-0.0002	0.0001	-0.0001	0.0015	0.0013	0.0028
50.0	5.0	0.8760	0.0003	0.0014	0.0011	0.0001	-0.0002	0.0001	-0.0001	0.0015	0.0013	0.0026

Table 4.7.15
CASMO Calculations for Pool Temperature Reactivity Effect

Burnup (GWD/MTU)	Enr	Ref Case T = 32 F	T = 39.2 F	T = 80.33 F	T = 140 F	T = 255 F, 0% Voids	T = 255 F, 10% Voids
8.0	2.0	0.9011	-0.0005	-0.0040	-0.0102	-0.0245	-0.0440
0.0	2.5	1.0293	-0.0007	-0.0051	-0.0130	-0.0317	-0.0535
4.0	2.5	0.9920	-0.0006	-0.0046	-0.0117	-0.0286	-0.0499
15.0	2.5	0.9049	-0.0004	-0.0034	-0.0090	-0.0224	-0.0429
0.0	3.0	1.0779	-0.0006	-0.0047	-0.0122	-0.0306	-0.0534
12.5	3.0	0.9692	-0.0005	-0.0038	-0.0100	-0.0251	-0.0471
22.5	3.0	0.8993	-0.0003	-0.0030	-0.0082	-0.0209	-0.0420
0.0	3.5	1.1163	-0.0005	-0.0044	-0.0116	-0.0295	-0.0531
20.0	3.5	0.9555	-0.0004	-0.0033	-0.0091	-0.0234	-0.0457
30.0	3.5	0.8914	-0.0003	-0.0027	-0.0076	-0.0198	-0.0412
0.0	4.0	1.1476	-0.0005	-0.0041	-0.0110	-0.0286	-0.0526
30.0	4.0	0.9266	-0.0003	-0.0029	-0.0081	-0.0213	-0.0436
37.5	4.0	0.8825	-0.0003	-0.0025	-0.0071	-0.0190	-0.0405
0.0	4.5	1.1737	-0.0004	-0.0038	-0.0105	-0.0277	-0.0520
37.5	4.5	0.9144	-0.0003	-0.0027	-0.0076	-0.0204	-0.0427
45.0	4.5	0.8730	-0.0002	-0.0023	-0.0067	-0.0182	-0.0398
47.5	4.5	0.8598	-0.0002	-0.0021	-0.0064	-0.0175	-0.0389
0.0	5.0	1.1958	-0.0004	-0.0036	-0.0101	-0.0269	-0.0514
42.5	5.0	0.9158	-0.0003	-0.0026	-0.0075	-0.0202	-0.0428
50.0	5.0	0.8760	-0.0002	-0.0022	-0.0066	-0.0183	-0.0401

Table 4.7.16
Verification of the Initial Enrichment and Burnup Combinations and Calculation of Soluble Boron Requirements

Region 3 Enrichment (wt% U-235)	2.0	2.0	2.0	2.0	2.0	2.0	2.0
Region 3 Burnup (GWD/MTU)	0.00	0.00	0.00	0.00	0.00	0.00	0.00
Region 2 Enrichment (wt% U-235)	2.0	2.5	3.0	3.5	4.0	4.5	5.0
Region 2 Burnup (GWD/MTU)	8.10	16.13	23.45	30.82	37.93	45.29	52.22
Reference Reactivity (Calculated k_{eff}) †	0.9756	0.9756	0.9756	0.9756	0.9756	0.9756	0.9756
Curve Verification Reactivity, 0 ppm	0.9759	0.9747	0.9719	0.9701	0.9681	0.9671	0.9650
Delta Reactivity	0.0003	-0.0009	-0.0037	-0.0055	-0.0075	-0.0085	-0.0106
Calculational Uncertainty (2σ)	0.0014	0.0014	0.0014	0.0016	0.0016	0.0014	0.0014
Soluble Boron Reactivity, 800 ppm	0.8834	0.8857	0.8840	0.8832	0.8853	0.8860	0.8848
Soluble Boron Requirement	436	447	431	426	437	445	437
Region 3 Enrichment (wt% U-235)	2.5	2.5	2.5	2.5	2.5	2.5	2.5
Region 3 Burnup (GWD/MTU)	5.08	5.08	5.08	5.08	5.08	5.08	5.08
Region 2 Enrichment (wt% U-235)	2.0	2.5	3.0	3.5	4.0	4.5	5.0
Region 2 Burnup (GWD/MTU)	8.10	16.13	23.45	30.82	37.93	45.29	52.22
Reference Reactivity (Calculated k_{eff}) †	0.9755	0.9755	0.9755	0.9755	0.9755	0.9755	0.9755
Curve Verification Reactivity, 0 ppm	0.9779	0.9784	0.9756	0.9737	0.9722	0.9696	0.9688
Delta Reactivity	0.0024	0.0029	0.0001	-0.0018	-0.0033	-0.0059	-0.0067
Calculational Uncertainty (2σ)	0.0014	0.0014	0.0014	0.0016	0.0014	0.0014	0.0014
Soluble Boron Reactivity, 800 ppm	0.8832	0.8879	0.8872	0.8862	0.8877	0.8852	0.8860
Soluble Boron Requirement	443	472	462	456	467	452	460
Region 3 Enrichment (wt% U-235)	3	3	3	3	3	3	3
Region 3 Burnup (GWD/MTU)	13.44	13.44	13.44	13.44	13.44	13.44	13.44
Region 2 Enrichment (wt% U-235)	2	2.5	3	3.5	4	4.5	5
Region 2 Burnup (GWD/MTU)	8.0968	16.1313	23.4534	30.8155	37.9321	45.2885	52.2206
Reference Reactivity (Calculated k_{eff}) †	0.9755	0.9750	0.9747	0.9747	0.9747	0.9747	0.9747
Curve Verification Reactivity, 0 ppm	0.9749	0.9743	0.9721	0.9693	0.9670	0.9647	0.9655
Delta Reactivity	-0.0006	-0.0007	-0.0026	-0.0054	-0.0077	-0.0100	-0.0092
Calculational Uncertainty (2σ)	0.0016	0.0016	0.0016	0.0016	0.0016	0.0016	0.0016
Soluble Boron Reactivity, 800 ppm	0.8839	0.8879	0.8866	0.8862	0.8863	0.8855	0.8861
Soluble Boron Requirement	434	457	445	438	438	432	447

† Maximum of Region 2 and Region 3 target k_{eff} .

Table 4.7.16 Continued

Region 3 Enrichment (wt% U-235)	3.5	3.5	3.5	3.5	3.5	3.5	3.5
Region 3 Burnup (GWD/MTU)	21.34	21.34	21.34	21.34	21.34	21.34	21.34
Region 2 Enrichment (wt% U-235)	2.0	2.5	3.0	3.5	4.0	4.5	5.0
Region 2 Burnup (GWD/MTU)	8.10	16.13	23.45	30.82	37.93	45.29	52.22
Reference Reactivity (Calculated k_{eff}) †	0.9755	0.9750	0.9745	0.9738	0.9738	0.9738	0.9738
Curve Verification Reactivity, 0 ppm	0.9747	0.9725	0.9694	0.9688	0.9685	0.9647	0.9644
Delta Reactivity	-0.0008	-	-0.0051	-0.0050	-	-0.0091	-0.0094
		0.0025			0.0053		
Calculational Uncertainty (2σ)	0.0014	0.0014	0.0014	0.0016	0.0014	0.0014	0.0014
Soluble Boron Reactivity, 800 ppm	0.8842	0.8862	0.8851	0.8861	0.8879	0.8856	0.8858
Soluble Boron Requirement	435	440	426	435	453	432	440
Region 3 Enrichment (wt% U-235)	4	4	4	4	4	4	4
Region 3 Burnup (GWD/MTU)	31.02	31.02	31.02	31.02	31.02	31.02	31.02
Region 2 Enrichment (wt% U-235)	2	2.5	3	3.5	4	4.5	5
Region 2 Burnup (GWD/MTU)	8.10	16.13	23.45	30.82	37.93	45.29	52.22
Reference Reactivity (Calculated k_{eff}) †	0.9755	0.9750	0.9745	0.9738	0.9732	0.9728	0.9728
Curve Verification Reactivity, 0 ppm	0.9722	0.9736	0.9690	0.9675	0.9670	0.9664	0.9660
Delta Reactivity	-0.0033	-	-0.0055	-0.0063	-	-0.0064	-0.0068
		0.0014			0.0062		
Calculational Uncertainty (2σ)	0.0014	0.0014	0.0014	0.0016	0.0016	0.0014	0.0014
Soluble Boron Reactivity, 800 ppm	0.8820	0.8859	0.8859	0.8851	0.8865	0.8869	0.8861
Soluble Boron Requirement	414	443	428	424	439	447	449
Region 3 Enrichment (wt% U-235)	4.5	4.5	4.5	4.5	4.5	4.5	4.5
Region 3 Burnup (GWD/MTU)	37.61	37.61	37.61	37.61	37.61	37.61	37.61
Region 2 Enrichment (wt% U-235)	2.0	2.5	3.0	3.5	4.0	4.5	5.0
Region 2 Burnup (GWD/MTU)	8.10	16.13	23.45	30.82	37.93	45.29	52.22
Reference Reactivity (Calculated k_{eff}) †	0.9755	0.9750	0.9745	0.9738	0.9732	0.9726	0.9721
Curve Verification Reactivity, 0 ppm	0.9731	0.9739	0.9698	0.9691	0.9671	0.9655	0.9657
Delta Reactivity	-0.0024	-	-0.0047	-0.0047	-	-0.0071	-0.0064
		0.0011			0.0061		
Calculational Uncertainty (2σ)	0.0016	0.0016	0.0016	0.0016	0.0016	0.0016	0.0016
Soluble Boron Reactivity, 800 ppm	0.8842	0.8874	0.8871	0.8848	0.8867	0.8861	0.8878
Soluble Boron Requirement	428	452	438	430	440	439	457

† Maximum of Region 2 and Region 3 target k_{eff} .

Table 4.7.16 Continued

Region 3 Enrichment (wt% U-235)	5.0	5.0	5.0	5.0	5.0	5.0	5.0
Region 3 Burnup (GWD/MTU)	44.48	44.48	44.48	44.48	44.48	44.48	44.48
Region 2 Enrichment (wt% U-235)	2.0	2.5	3.0	3.5	4.0	4.5	5.0
Region 2 Burnup (GWD/MTU)	8.10	16.13	23.45	30.82	37.93	45.29	52.22
Reference Reactivity (Calculated k_{eff}) †	0.9755	0.9750	0.9745	0.9738	0.9732	0.9726	0.9721
Curve Verification Reactivity, 0 ppm	0.9730	0.9733	0.9700	0.9694	0.9677	0.9649	0.9656
Delta Reactivity	-0.0025	-0.0017	-0.0045	-0.0044	-0.0055	-0.0077	-0.0065
Calculational Uncertainty (2σ)	0.0014	0.0016	0.0014	0.0016	0.0014	0.0014	0.0014
Soluble Boron Reactivity, 800 ppm	0.8818	0.8838	0.8852	0.8860	0.8867	0.8851	0.8883
Soluble Boron Requirement	417	432	429	437	443	431	460

† Maximum of Region 2 and Region 3 target k_{eff} .

Table 4.7.17
Calculation of the Misloaded Fresh Fuel Assembly Accident

Region 2 Enrichment (wt% U-235)	5.0	5.0	5.0
Region 2 Burnup (GWD/MTU)	48	48	48
Region 3 Enrichment (wt% U-235)	2.0	3.5	5.0
Region 3 Burnup (GWD/MTU)	0.00	20.00	42.00
Misloaded Fresh Fuel Assembly in Region 2 (outer row)			
Reactivity, 0 ppm	1.0229	1.0241	1.0222
Reactivity, 2500 ppm	0.8108	0.8101	0.8117
Target k_{eff} (0.945-corrections)†	0.9221	0.9221	0.9221
Soluble Boron Requirement, ppm	1188	1192	1189
Misloaded Fresh Fuel Assembly in Region 2 (inner row)			
Reactivity, 0 ppm	1.0047	1.0073	1.0050
Reactivity, 2500 ppm	0.7923	0.7956	0.7978
Target k_{eff} (0.945-corrections)†	0.9221	0.9221	0.9221
Soluble Boron Requirement, ppm	972	1006	1000
Misloaded Fresh Fuel Assembly in Region 3			
Reactivity, 0 ppm	0.9963	0.9999	0.9930
Reactivity, 2500 ppm	0.7678	0.7823	0.7916
Target k_{eff} (0.945-corrections)†	0.9221	0.9221	0.9221
Soluble Boron Requirement, ppm	812	894	880

† Maximum of total corrections for the Region 2 and Region 3 enrichment and burnup combination.

Table 4.7.18
Calculation of the Mislocated Fresh Fuel Assembly Accident

Region 2 Enrichment (wt% U-235)	5.0	5.0	5.0
Region 2 Burnup (GWD/MTU)	48	48	48
Region 3 Enrichment (wt% U-235)	2.0	3.5	5.0
Region 3 Burnup (GWD/MTU)	0.00	20.00	42.00
Mislocated Case Reactivity, 0 ppm	1.0273	1.0293	1.0287
Mislocated Case Reactivity, 2500 ppm	0.8017	0.8002	0.8026
Target k_{eff} (0.945-corrections)†	0.9221	0.9221	0.9221
Soluble Boron Requirement, ppm	1166	1170	1179

† Maximum of total corrections for the Region 2 and Region 3 enrichment and burnup combination.

Table 4.7.19
Results of the Sensitivity Study of the Effect of Soluble Boron on the Calculation of Fuel and
Storage Rack Manufacturing Tolerances

Parameter	0 ppm Soluble Boron		2000 ppm Soluble Boron	
	k_{inf}	Delta k_{inf}	k_{inf}	Delta k_{inf}
Reference Case	1.1958	n/a	0.9879	n/a
Storage Cell ID Increase	1.1958	0.0000	0.9865	-0.0015
Storage Cell ID Decrease	1.1981	0.0023	0.9908	0.0029
Storage Cell Poison Width Decrease	1.1972	0.0014	0.9888	0.0009
Storage Cell Sheathing Increase	1.1960	0.0002	0.9881	0.0001
Storage Cell Sheathing Decrease	1.1956	-0.0002	0.9878	-0.0001
Storage Cell Box Wall Increase	1.1960	0.0001	0.9881	0.0001
Storage Cell Box Wall Decrease	1.1957	-0.0001	0.9878	-0.0001
Storage Cell Poison Thickness	1.1978	0.0020	0.9895	0.0015
Storage Cell Poison B-10 Loading Minimum	1.1976	0.0017	0.9893	0.0014
Fuel Rod Pitch Increase	1.1969	0.0010	0.9884	0.0005
Fuel Rod Pitch Decrease	1.1809	-0.0150	0.9807	-0.0072
Fuel Rod Clad OD Increase	1.1944	-0.0015	0.9876	-0.0003
Fuel Rod Clad OD Decrease	1.1973	0.0015	0.9882	0.0003
Fuel Rod Clad ID Increase	1.1961	0.0002	0.9882	0.0002
Fuel Rod Clad ID Decrease	1.1956	-0.0002	0.9877	-0.0002
Fuel Pellet OD Increase	1.1960	0.0002	0.9886	0.0006
Fuel Pellet Enrichment Increase	1.1979	0.0020	0.9908	0.0028
Statistical Combination				
		0.0046		0.0047

Table 4.7.20
MCNP4a Calculations for the Fuel Rod Storage Basket

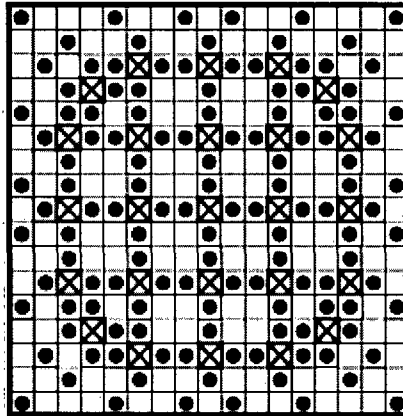
Case	k_{eff}
Fresh Fuel Assembly, 5.0 wt% ^{235}U	0.9474
5.0 wt% ^{235}U at 44.48 GWD/MTU	0.7561
5.0 wt% ^{235}U at 52.22 GWD/MTU	0.7405
FRSB Full with 5.0 wt% ^{235}U Fuel Pins	0.7269

Table 4.7.21
 Beaver Valley Power Station Unit No. 2 Spent Fuel Pool
 Boron Dilution Accident Analysis

Parameters	Value	
Technical Specification Soluble Boron Concentration	2000	ppm
Soluble Boron Concentration to Maintain k_{eff} 0.9500	472	ppm
Credited Volume of 2000 ppm Water in SFP	182,472	gallons
High Flow Rate Accident Evaluation		
High Flow Rate (Service Water System)	3000	gpm
Volume Needed to High Level Alarm Setpoint	7850	gallons
Time to High Level Alarm Setpoint	2.62	minutes
Time Needed to Dilute to 472 ppm	88	minutes
Volume Needed to Dilute to 472 ppm	263,432	gallons
Time to Respond to High Level Alarm Setpoint	85.2	minutes
Low Flow Rate Accident Evaluation		
Low Flow Rate	2	gpm
Volume Needed to High Level Alarm Setpoint	7850	gallons
Time to High Level Alarm Setpoint	2.73	days
Time Needed to Dilute to 472 ppm	91	days
Volume Needed to Dilute to 472 ppm	263,432	gallons
Time to Respond to High Level Alarm Setpoint	88.7	days

Figure 4.5.1

128 IFBA Pin Loading Pattern for 17x17 Fuel Assemblies



LEGEND

- = IFBA ROD
- = NON IFBA ROD
- ⊗ = THIMBLE & INSTRUMENT TUBE LOCATIONS

Figure 4.5.2
A Two Dimensional Representation of the MZTR MCNP4a Model

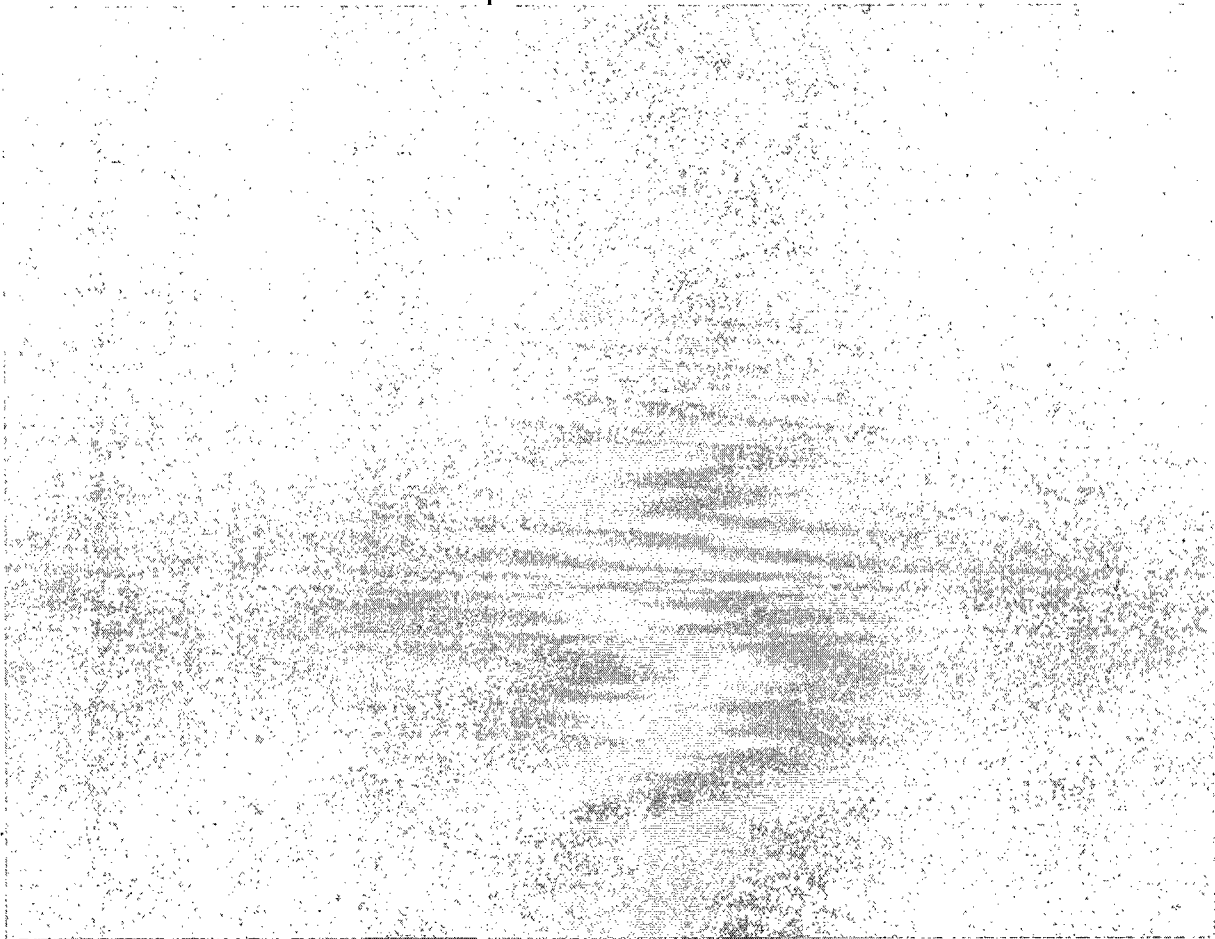


Figure 4.5.3
MZTR 9 X 12 Rack Permissible Loading Configuration

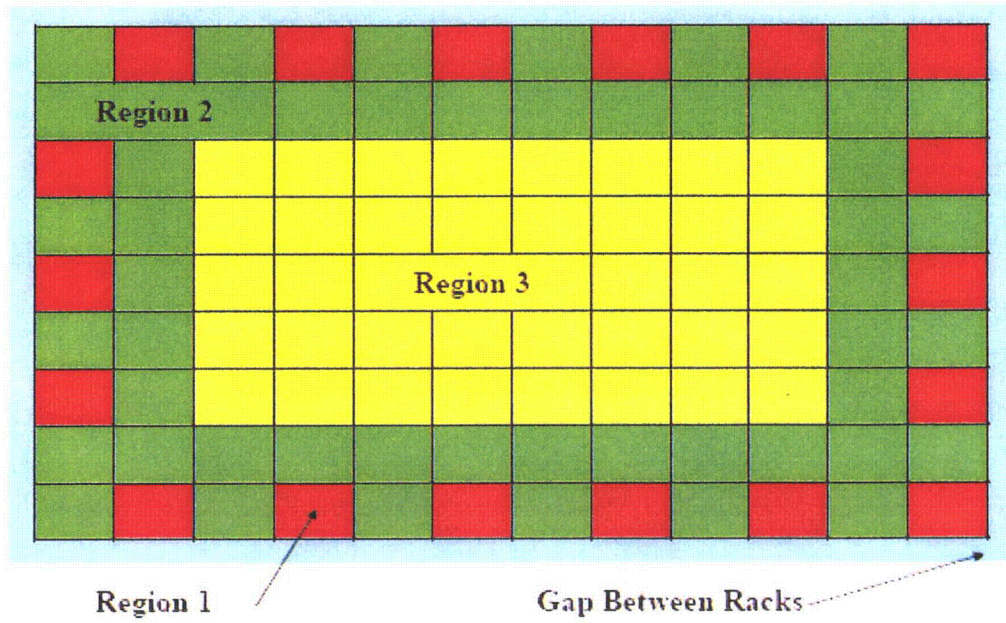


Figure 4.5.4
MZTR 9 X 13 Rack Permissible Loading Configuration

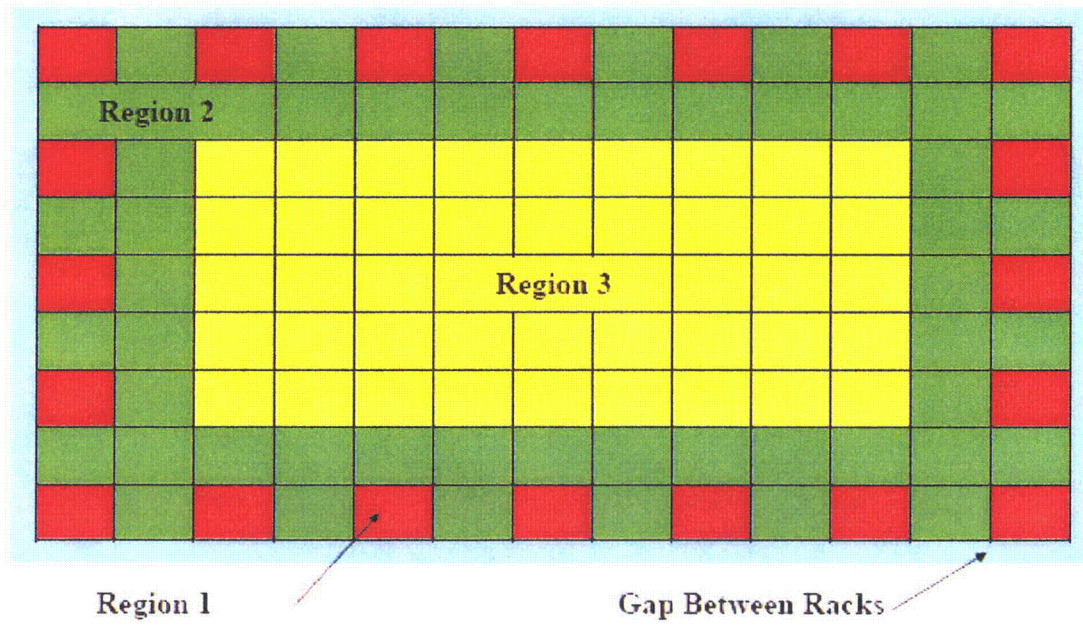
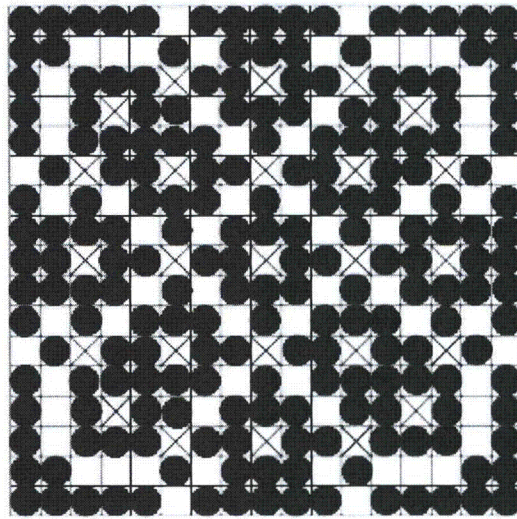


Figure 4.5.5

200 IFBA Pin Loading Pattern for 17x17 Fuel Assembly



LEGEND

- = IFBA ROD
- = NON IFBA ROD
- ⊗ = THIMBLE & INSTRUMENT TUBE LOCATIONS

Figure 4.5.6
A Two Dimensional Representation of the MCNP4a FRSB Model

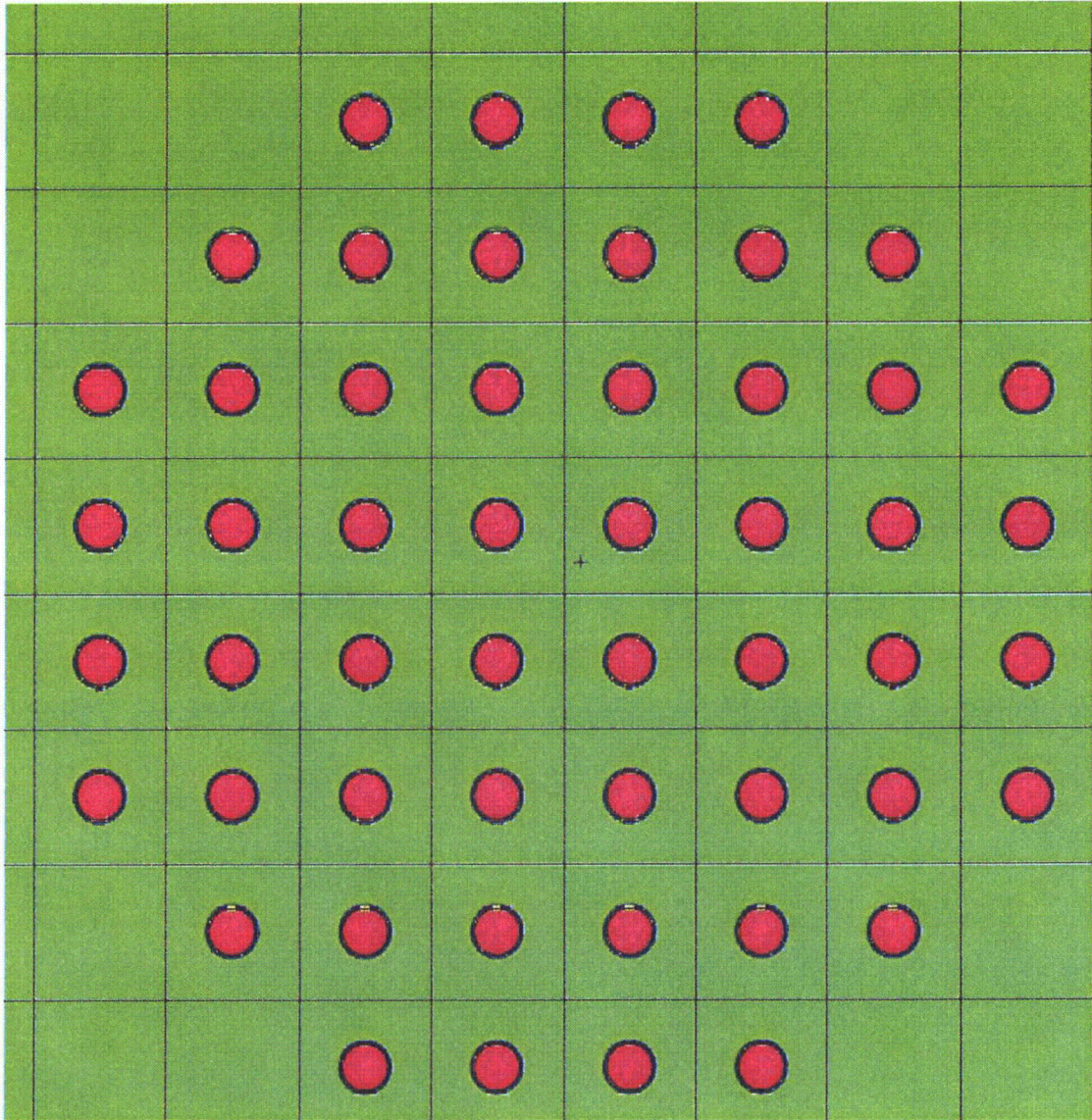


Figure 4.7.1
Region 2 Initial Enrichment and Burnup Combinaitons
(Includes 5% Burnup Uncertainty and Polynomial Fit Adjustment)

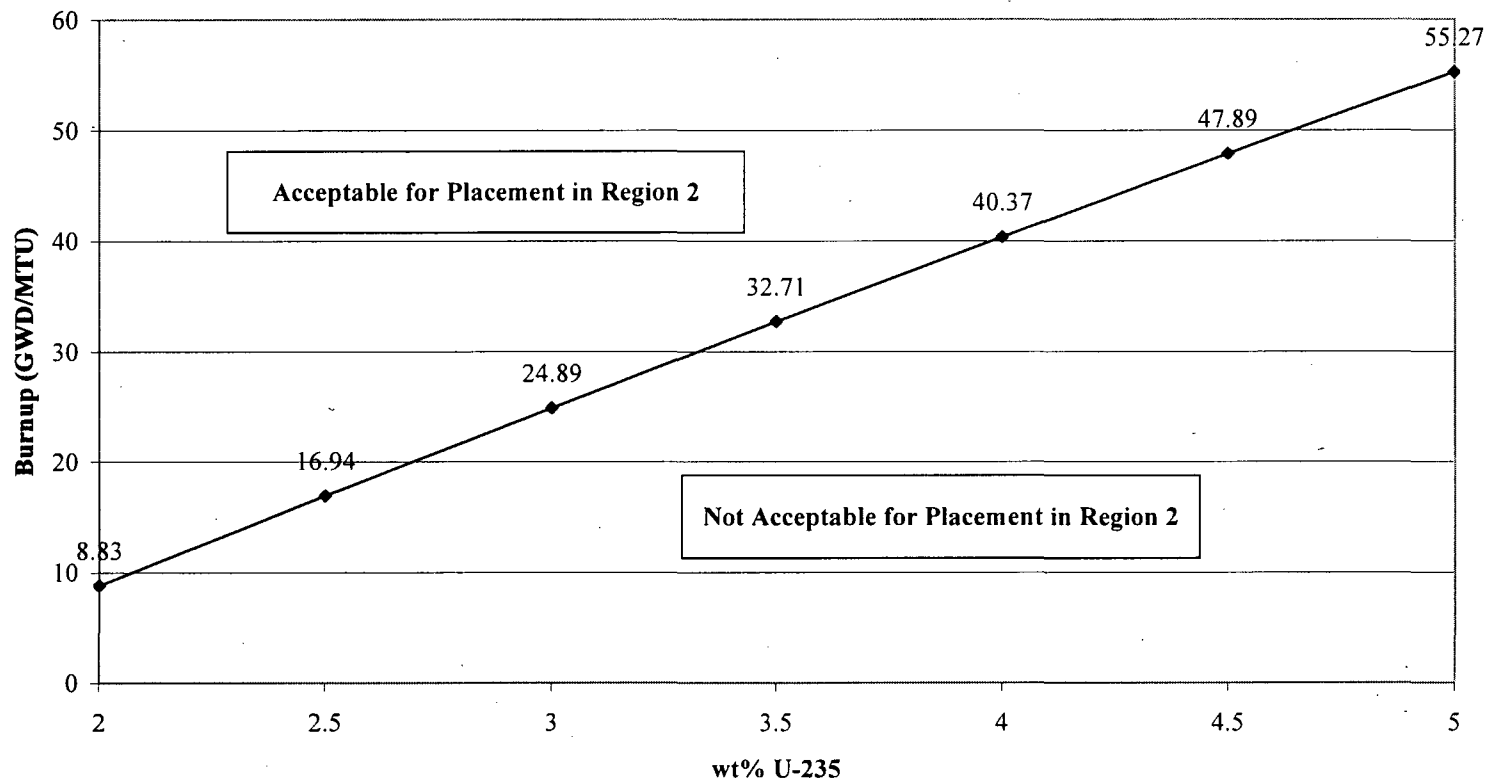


Figure 4.7.2
Region 3 Initial Enrichment and Burnup Combinaitons
(Includes 5% Burnup Uncertainty and Polynomial Fit Adjustment)

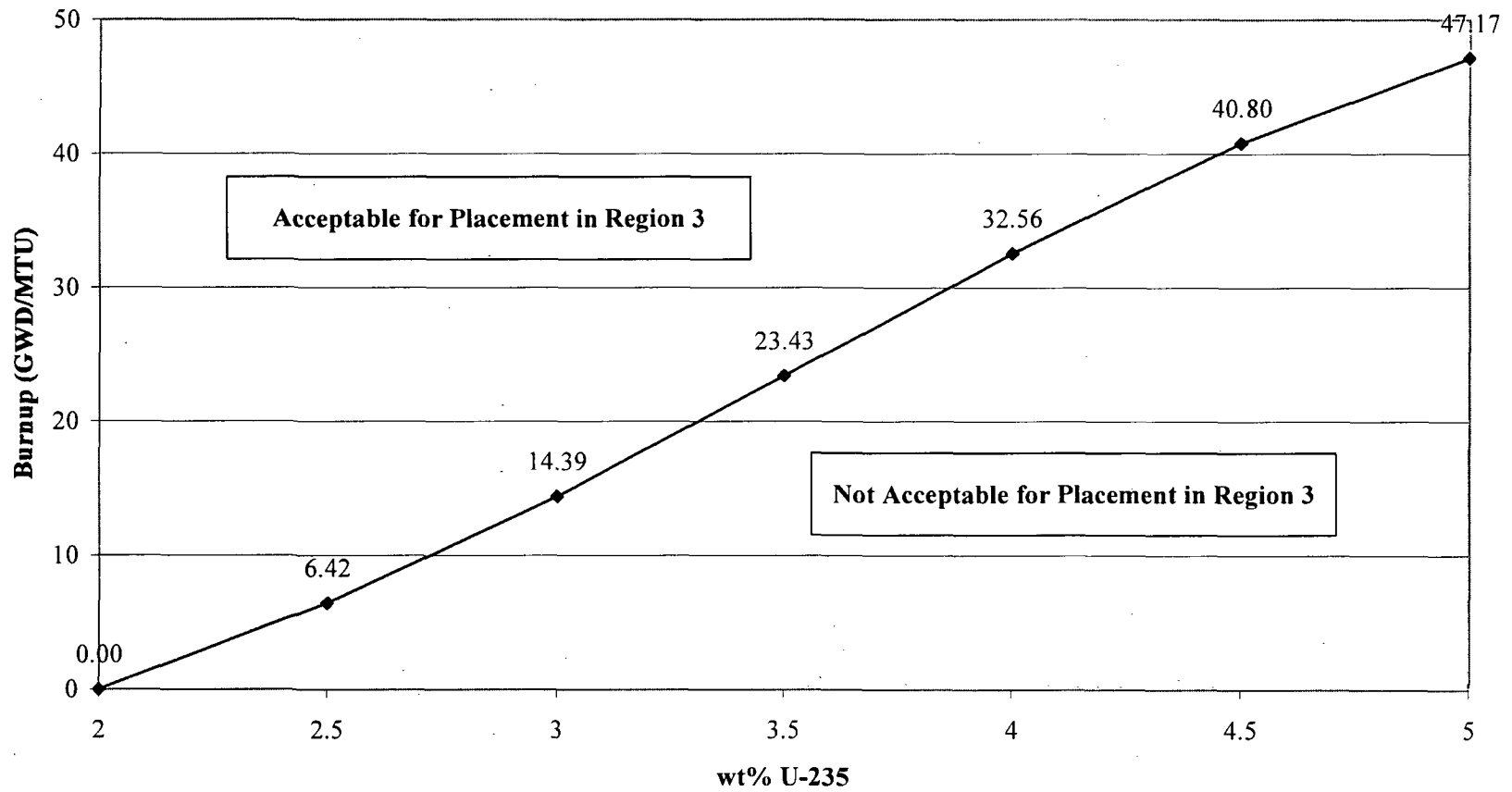


Figure 4.7.3
A Two Dimensional Representation of the MCNP4a Mislocated Fuel Assembly Accident Model

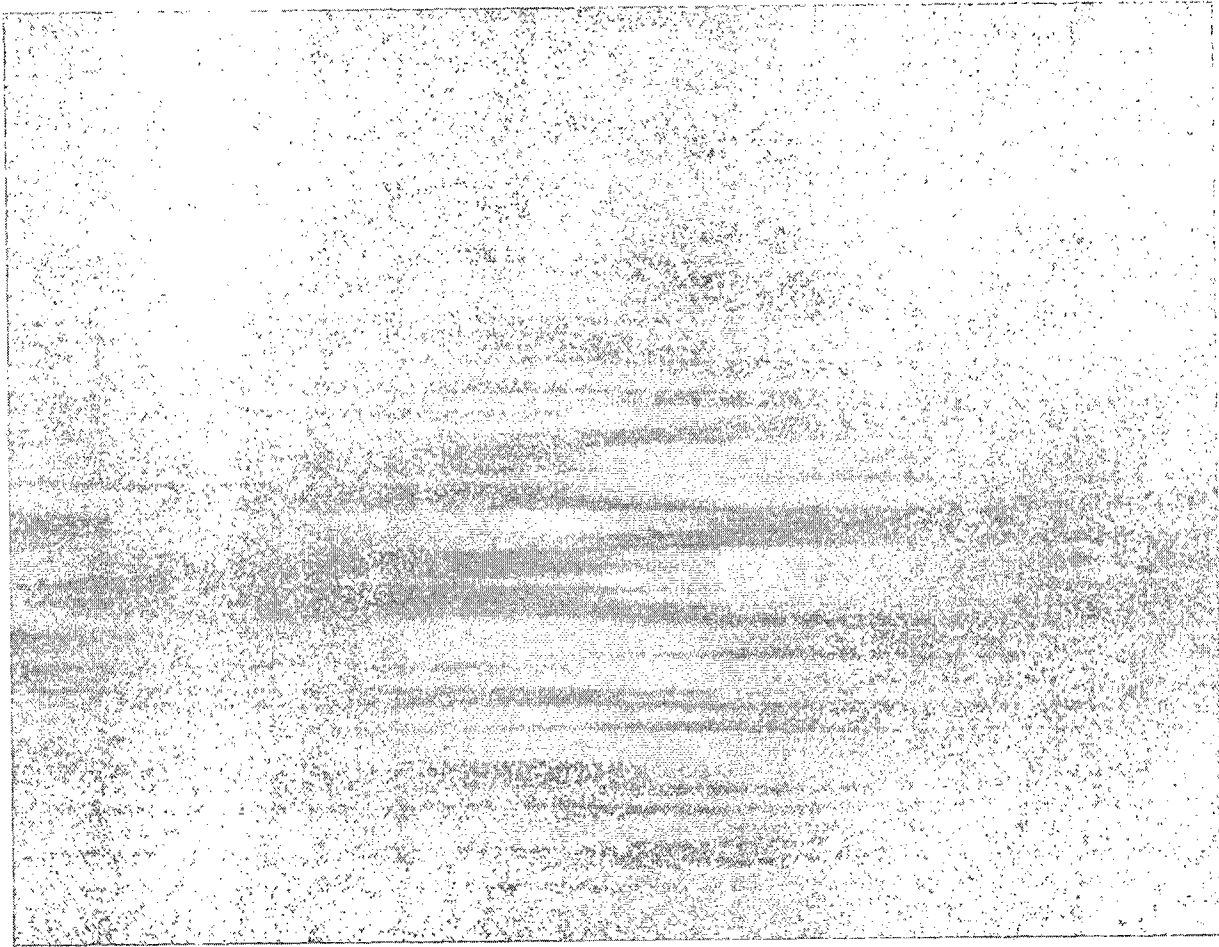


Figure 4.7.4
Representation of Misloading Accident MCNP Model with Reflective Boundary Conditions



Appendix A
Benchmark Calculations

(total number of pages: 26 including this page)

Note: because this appendix was taken from a different report, the next page is labeled
“Appendix 4A, Page 1”.

APPENDIX 4A: BENCHMARK CALCULATIONS

4A.1 INTRODUCTION AND SUMMARY

Benchmark calculations have been made on selected critical experiments, chosen, in so far as possible, to bound the range of variables in the rack designs. Two independent methods of analysis were used, differing in cross section libraries and in the treatment of the cross sections. MCNP4a [4A.1] is a continuous energy Monte Carlo code and KENO5a [4A.2] uses group-dependent cross sections. For the KENO5a analyses reported here, the 238-group library was chosen, processed through the NITAWL-II [4A.2] program to create a working library and to account for resonance self-shielding in uranium-238 (Nordheim integral treatment). The 238 group library was chosen to avoid or minimize the errors[†] (trends) that have been reported (e.g., [4A.3 through 4A.5]) for calculations with collapsed cross section sets.

In rack designs, the three most significant parameters affecting criticality are (1) the fuel enrichment, (2) the ¹⁰B loading in the neutron absorber, and (3) the lattice spacing (or water-gap thickness if a flux-trap design is used). Other parameters, within the normal range of rack and fuel designs, have a smaller effect, but are also included in the analyses.

Table 4A.1 summarizes results of the benchmark calculations for all cases selected and analyzed, as referenced in the table. The effect of the major variables are discussed in subsequent sections below. It is important to note that there is obviously considerable overlap in parameters since it is not possible to vary a single parameter and maintain criticality; some other parameter or parameters must be concurrently varied to maintain criticality.

One possible way of representing the data is through a spectrum index that incorporates all of the variations in parameters. KENO5a computes and prints the "energy of the average lethargy causing fission" (EALF). In MCNP4a, by utilizing the tally option with the identical 238-group energy structure as in KENO5a, the number of fissions in each group may be collected and the EALF determined (post-processing).

[†] Small but observable trends (errors) have been reported for calculations with the 27-group and 44-group collapsed libraries. These errors are probably due to the use of a single collapsing spectrum when the spectrum should be different for the various cases analyzed, as evidenced by the spectrum indices.

Figures 4A.1 and 4A.2 show the calculated k_{eff} for the benchmark critical experiments as a function of the EALF for MCNP4a and KENO5a, respectively (UO₂ fuel only). The scatter in the data (even for comparatively minor variation in critical parameters) represents experimental error[†] in performing the critical experiments within each laboratory, as well as between the various testing laboratories. The B&W critical experiments show a larger experimental error than the PNL criticals. This would be expected since the B&W criticals encompass a greater range of critical parameters than the PNL criticals.

Linear regression analysis of the data in Figures 4A.1 and 4A.2 show that there are no trends, as evidenced by very low values of the correlation coefficient (0.13 for MCNP4a and 0.21 for KENO5a). The total bias (systematic error, or mean of the deviation from a k_{eff} of exactly 1.000) for the two methods of analysis are shown in the table below.

Calculational Bias of MCNP4a and KENO5a	
MCNP4a	0.0009 ± 0.0011
KENO5a	0.0030 ± 0.0012

The bias and standard error of the bias were derived directly from the calculated k_{eff} values in Table 4A.1 using the following equations^{††}, with the standard error multiplied by the one-sided K-factor for 95% probability at the 95% confidence level from NBS Handbook 91 [4A.18] (for the number of cases analyzed, the K-factor is ~2.05 or slightly more than 2).

$$\bar{k} = \frac{1}{n} \sum_i^n k_i \quad (4A.1)$$

† A classical example of experimental error is the corrected enrichment in the PNL experiments, first as an addendum to the initial report and, secondly, by revised values in subsequent reports for the same fuel rods.

†† These equations may be found in any standard text on statistics, for example, reference [4A.6] (or the MCNP4a manual) and is the same methodology used in MCNP4a and in KENO5a.

$$\sigma_k^2 = \frac{\sum_{i=1}^n k_i^2 - (\sum_{i=1}^n k_i)^2 / n}{n(n-1)} \quad (4A.2)$$

$$Bias = (1 - \bar{k}) \pm K \sigma_{\bar{k}} \quad (4A.3)$$

where k_i are the calculated reactivities of n critical experiments; $\sigma_{\bar{k}}$ is the unbiased estimator of the standard deviation of the mean (also called the standard error of the bias (mean)); K is the one-sided multiplier for 95% probability at the 95% confidence level (NBS Handbook 91 [4A.18]).

Formula 4.A.3 is based on the methodology of the National Bureau of Standards (now NIST) and is used to calculate the values presented on page 4.A-2. The first portion of the equation, $(1 - \bar{k})$, is the actual bias which is added to the MCNP4a and KENO5a results. The second term, $K\sigma_{\bar{k}}$, is the uncertainty or standard error associated with the bias. The K values used were obtained from the National Bureau of Standards Handbook 91 and are for one-sided statistical tolerance limits for 95% probability at the 95% confidence level. The actual K values for the 56 critical experiments evaluated with MCNP4a and the 53 critical experiments evaluated with KENO5a are 2.04 and 2.05, respectively.

The bias values are used to evaluate the maximum k_{eff} values for the rack designs. KENO5a has a slightly larger systematic error than MCNP4a, but both result in greater precision than published data [4A.3 through 4A.5] would indicate for collapsed cross section sets in KENO5a (SCALE) calculations.

4A.2 Effect of Enrichment

The benchmark critical experiments include those with enrichments ranging from 2.46 w/o to 5.74 w/o and therefore span the enrichment range for rack designs. Figures 4A.3 and 4A.4 show the calculated k_{eff} values (Table 4A.1) as a function of the fuel enrichment reported for the critical experiments. Linear regression analyses for these data confirms that there are no trends, as indicated by low values of the correlation coefficients (0.03 for MCNP4a and 0.38 for KENO5a). Thus, there are no corrections to the bias for the various enrichments.

As further confirmation of the absence of any trends with enrichment, a typical configuration was calculated with both MCNP4a and KENO5a for various enrichments. The cross-comparison of calculations with codes of comparable sophistication is suggested in Reg. Guide 3.41. Results of this comparison, shown in Table 4A.2 and Figure 4A.5, confirm no significant difference in the calculated values of k_{eff} for the two independent codes as evidenced by the 45° slope of the curve. Since it is very unlikely that two independent methods of analysis would be subject to the same error, this comparison is considered confirmation of the absence of an enrichment effect (trend) in the bias.

4A.3 Effect of ^{10}B Loading

Several laboratories have performed critical experiments with a variety of thin absorber panels similar to the Boral panels in the rack designs. Of these critical experiments, those performed by B&W are the most representative of the rack designs. PNL has also made some measurements with absorber plates, but, with one exception (a flux-trap experiment), the reactivity worth of the absorbers in the PNL tests is very low and any significant errors that might exist in the treatment of strong thin absorbers could not be revealed.

Table 4A.3 lists the subset of experiments using thin neutron absorbers (from Table 4A.1) and shows the reactivity worth (Δk) of the absorber.[†]

No trends with reactivity worth of the absorber are evident, although based on the calculations shown in Table 4A.3, some of the B&W critical experiments seem to have unusually large experimental errors. B&W made an effort to report some of their experimental errors. Other laboratories did not evaluate their experimental errors.

To further confirm the absence of a significant trend with ^{10}B concentration in the absorber, a cross-comparison was made with MCNP4a and KENO5a (as suggested in Reg. Guide 3.41). Results are shown in Figure 4A.6 and Table 4A.4 for a typical geometry. These data substantiate the absence of any error (trend) in either of the two codes for the conditions analyzed (data points fall on a 45° line, within an expected 95% probability limit).

[†] The reactivity worth of the absorber panels was determined by repeating the calculation with the absorber analytically removed and calculating the incremental (Δk) change in reactivity due to the absorber.

4A.4 Miscellaneous and Minor Parameters

4A.4.1 Reflector Material and Spacings

PNL has performed a number of critical experiments with thick steel and lead reflectors.[†] Analysis of these critical experiments are listed in Table 4A.5 (subset of data in Table 4A.1). There appears to be a small tendency toward overprediction of k_{eff} at the lower spacing, although there are an insufficient number of data points in each series to allow a quantitative determination of any trends. The tendency toward overprediction at close spacing means that the rack calculations may be slightly more conservative than otherwise.

4A.4.2 Fuel Pellet Diameter and Lattice Pitch

The critical experiments selected for analysis cover a range of fuel pellet diameters from 0.311 to 0.444 inches, and lattice spacings from 0.476 to 1.00 inches. In the rack designs, the fuel pellet diameters range from 0.303 to 0.3805 inches O.D. (0.496 to 0.580 inch lattice spacing) for PWR fuel and from 0.3224 to 0.494 inches O.D. (0.488 to 0.740 inch lattice spacing) for BWR fuel. Thus, the critical experiments analyzed provide a reasonable representation of power reactor fuel. Based on the data in Table 4A.1, there does not appear to be any observable trend with either fuel pellet diameter or lattice pitch, at least over the range of the critical experiments applicable to rack designs.

4A.4.3 Soluble Boron Concentration Effects

Various soluble boron concentrations were used in the B&W series of critical experiments and in one PNL experiment, with boron concentrations ranging up to 2550 ppm. Results of MCNP4a (and one KENO5a) calculations are shown in Table 4A.6. Analyses of the very high boron concentration experiments (> 1300 ppm) show a tendency to slightly overpredict reactivity for the three experiments exceeding 1300 ppm. In turn, this would suggest that the evaluation of the racks with higher soluble boron concentrations could be slightly conservative.

[†] Parallel experiments with a depleted uranium reflector were also performed but not included in the present analysis since they are not pertinent to the Holtec rack design.

The number of critical experiments with PuO_2 bearing fuel (MOX) is more limited than for UO_2 fuel. However, a number of MOX critical experiments have been analyzed and the results are shown in Table 4A.7. Results of these analyses are generally above a k_{eff} of 1.00, indicating that when Pu is present, both MCNP4a and KENO5a overpredict the reactivity. This may indicate that calculation for MOX fuel will be expected to be conservative, especially with MCNP4a. It may be noted that for the larger lattice spacings, the KENO5a calculated reactivities are below 1.00, suggesting that a small trend may exist with KENO5a. It is also possible that the overprediction in k_{eff} for both codes may be due to a small inadequacy in the determination of the Pu-241 decay and Am-241 growth. This possibility is supported by the consistency in calculated k_{eff} over a wide range of the spectral index (energy of the average lethargy causing fission).

References

- [4A.1] J.F. Briesmeister, Ed., "MCNP4a - A General Monte Carlo N-Particle Transport Code, Version 4A; Los Alamos National Laboratory, LA-12625-M (1993).
- [4A.2] SCALE 4.3, "A Modular Code System for Performing Standardized Computer Analyses for Licensing Evaluation", NUREG-0200 (ORNL-NUREG-CSD-2/U2/R5, Revision 5, Oak Ridge National Laboratory, September 1995.
- [4A.3] M.D. DeHart and S.M. Bowman, "Validation of the SCALE Broad Structure 44-G Group ENDF/B-Y Cross-Section Library for Use in Criticality Safety Analyses", NUREG/CR-6102 (ORNL/TM-12460) Oak Ridge National Laboratory, September 1994.
- [4A.4] W.C. Jordan et al., "Validation of KENO.V.a", CSD/TM-238, Martin Marietta Energy Systems, Inc., Oak Ridge National Laboratory, December 1986.
- [4A.5] O.W. Hermann et al., "Validation of the Scale System for PWR Spent Fuel Isotopic Composition Analysis", ORNL-TM-12667, Oak Ridge National Laboratory, undated.
- [4A.6] R.J. Larsen and M.L. Marx, An Introduction to Mathematical Statistics and its Applications, Prentice-Hall, 1986.
- [4A.7] M.N. Baldwin et al., Critical Experiments Supporting Close Proximity Water Storage of Power Reactor Fuel, BAW-1484-7, Babcock and Wilcox Company, July 1979.
- [4A.8] G.S. Hoovier et al., Critical Experiments Supporting Underwater Storage of Tightly Packed Configurations of Spent Fuel Pins, BAW-1645-4, Babcock & Wilcox Company, November 1991.
- [4A.9] L.W. Newman et al., Urania Gadolinia: Nuclear Model Development and Critical Experiment Benchmark, BAW-1810, Babcock and Wilcox Company, April 1984.

- [4A.10] J.C. Manaranche et al., "Dissolution and Storage Experimental Program with 4.75 w/o Enriched Uranium-Oxide Rods," Trans. Am. Nucl. Soc. 33: 362-364 (1979).
- [4A.11] S.R. Bierman and E.D. Clayton, Criticality Experiments with Subcritical Clusters of 2.35 w/o and 4.31 w/o ^{235}U Enriched UO_2 Rods in Water with Steel Reflecting Walls, PNL-3602, Battelle Pacific Northwest Laboratory, April 1981.
- [4A.12] S.R. Bierman et al., Criticality Experiments with Subcritical Clusters of 2.35 w/o and 4.31 w/o ^{235}U Enriched UO_2 Rods in Water with Uranium or Lead Reflecting Walls, PNL-3926, Battelle Pacific Northwest Laboratory, December, 1981.
- [4A.13] S.R. Bierman et al., Critical Separation Between Subcritical Clusters of 4.31 w/o ^{235}U Enriched UO_2 Rods in Water with Fixed Neutron Poisons, PNL-2615, Battelle Pacific Northwest Laboratory, October 1977.
- [4A.14] S.R. Bierman, Criticality Experiments with Neutron Flux Traps Containing Voids, PNL-7167, Battelle Pacific Northwest Laboratory, April 1990.
- [4A.15] B.M. Durst et al., Critical Experiments with 4.31 wt % ^{235}U Enriched UO_2 Rods in Highly Borated Water Lattices, PNL-4267, Battelle Pacific Northwest Laboratory, August 1982.
- [4A.16] S.R. Bierman, Criticality Experiments with Fast Test Reactor Fuel Pins in Organic Moderator, PNL-5803, Battelle Pacific Northwest Laboratory, December 1981.
- [4A.17] E.G. Taylor et al., Saxton Plutonium Program Critical Experiments for the Saxton Partial Plutonium Core, WCAP-3385-54, Westinghouse Electric Corp., Atomic Power Division, December 1965.
- [4A.18] M.G. Natrella, Experimental Statistics, National Bureau of Standards, Handbook 91, August 1963.

Table 4A.1
Summary of Criticality Benchmark Calculations

Reference	Identification	Enrich.	Calculated k_{eff}		EALF [†] (eV)		
			MCNP4a	KENO5a	MCNP4a	KENO5a	
1	B&W-1484 (4A.7)	Core I	2.46	0.9964 ± 0.0010	0.9898 ± 0.0006	0.1759	0.1753
2	B&W-1484 (4A.7)	Core II	2.46	1.0008 ± 0.0011	1.0015 ± 0.0005	0.2553	0.2446
3	B&W-1484 (4A.7)	Core III	2.46	1.0010 ± 0.0012	1.0005 ± 0.0005	0.1999	0.1939
4	B&W-1484 (4A.7)	Core IX	2.46	0.9956 ± 0.0012	0.9901 ± 0.0006	0.1422	0.1426
5	B&W-1484 (4A.7)	Core X	2.46	0.9980 ± 0.0014	0.9922 ± 0.0006	0.1513	0.1499
6	B&W-1484 (4A.7)	Core XI	2.46	0.9978 ± 0.0012	1.0005 ± 0.0005	0.2031	0.1947
7	B&W-1484 (4A.7)	Core XII	2.46	0.9988 ± 0.0011	0.9978 ± 0.0006	0.1718	0.1662
8	B&W-1484 (4A.7)	Core XIII	2.46	1.0020 ± 0.0010	0.9952 ± 0.0006	0.1988	0.1965
9	B&W-1484 (4A.7)	Core XIV	2.46	0.9953 ± 0.0011	0.9928 ± 0.0006	0.2022	0.1986
10	B&W-1484 (4A.7)	Core XV ^{††}	2.46	0.9910 ± 0.0011	0.9909 ± 0.0006	0.2092	0.2014
11	B&W-1484 (4A.7)	Core XVI ^{††}	2.46	0.9935 ± 0.0010	0.9889 ± 0.0006	0.1757	0.1713
12	B&W-1484 (4A.7)	Core XVII	2.46	0.9962 ± 0.0012	0.9942 ± 0.0005	0.2083	0.2021
13	B&W-1484 (4A.7)	Core XVIII	2.46	1.0036 ± 0.0012	0.9931 ± 0.0006	0.1705	0.1708

Table 4A.1

Summary of Criticality Benchmark Calculations

Reference	Identification	Enrich.	Calculated k_{eff}		EALF [†] (eV)		
			MCNP4a	KENO5a	MCNP4a	KENO5a	
14	B&W-1484 (4A.7)	Core XIX	2.46	0.9961 ± 0.0012	0.9971 ± 0.0005	0.2103	0.2011
15	B&W-1484 (4A.7)	Core XX	2.46	1.0008 ± 0.0011	0.9932 ± 0.0006	0.1724	0.1701
16	B&W-1484 (4A.7)	Core XXI	2.46	0.9994 ± 0.0010	0.9918 ± 0.0006	0.1544	0.1536
17	B&W-1645 (4A.8)	S-type Fuel, w/886 ppm B	2.46	0.9970 ± 0.0010	0.9924 ± 0.0006	1.4475	1.4680
18	B&W-1645 (4A.8)	S-type Fuel, w/746 ppm B	2.46	0.9990 ± 0.0010	0.9913 ± 0.0006	1.5463	1.5660
19	B&W-1645 (4A.8)	SO-type Fuel, w/1156 ppm B	2.46	0.9972 ± 0.0009	0.9949 ± 0.0005	0.4241	0.4331
20	B&W-1810 (4A.9)	Case 1 1337 ppm B	2.46	1.0023 ± 0.0010	NC	0.1531	NC
21	B&W-1810 (4A.9)	Case 12 1899 ppm B	2.46/4.02	1.0060 ± 0.0009	NC	0.4493	NC
22	French (4A.10)	Water Moderator 0 gap	4.75	0.9966 ± 0.0013	NC	0.2172	NC
23	French (4A.10)	Water Moderator 2.5 cm gap	4.75	0.9952 ± 0.0012	NC	0.1778	NC
24	French (4A.10)	Water Moderator 5 cm gap	4.75	0.9943 ± 0.0010	NC	0.1677	NC
25	French (4A.10)	Water Moderator 10 cm gap	4.75	0.9979 ± 0.0010	NC	0.1736	NC
26	PNL-3602 (4A.11)	Steel Reflector, 0 separation	2.35	NC	1.0004 ± 0.0006	NC	0.1018

Table 4A.1
Summary of Criticality Benchmark Calculations

Reference	Identification	Enrich.	Calculated k_{eff}		EALF ¹ (eV)		
			MCNP4a	KENO5a	MCNP4a	KENO5a	
27	PNL-3602 (4A.11)	Steel Reflector, 1.321 cm sepn.	2.35	0.9980 ± 0.0009	0.9992 ± 0.0006	0.1000	0.0909
28	PNL-3602 (4A.11)	Steel Reflector, 2.616 cm sepn	2.35	0.9968 ± 0.0009	0.9964 ± 0.0006	0.0981	0.0975
29	PNL-3602 (4A.11)	Steel Reflector, 3.912 cm sepn.	2.35	0.9974 ± 0.0010	0.9980 ± 0.0006	0.0976	0.0970
30	PNL-3602 (4A.11)	Steel Reflector, infinite sepn.	2.35	0.9962 ± 0.0008	0.9939 ± 0.0006	0.0973	0.0968
31	PNL-3602 (4A.11)	Steel Reflector, 0 cm sepn.	4.306	NC	1.0003 ± 0.0007	NC	0.3282
32	PNL-3602 (4A.11)	Steel Reflector, 1.321 cm sepn.	4.306	0.9997 ± 0.0010	1.0012 ± 0.0007	0.3016	0.3039
33	PNL-3602 (4A.11)	Steel Reflector, 2.616 cm sepn.	4.306	0.9994 ± 0.0012	0.9974 ± 0.0007	0.2911	0.2927
34	PNL-3602 (4A.11)	Steel Reflector, 5.405 cm sepn.	4.306	0.9969 ± 0.0011	0.9951 ± 0.0007	0.2828	0.2860
35	PNL-3602 (4A.11)	Steel Reflector, Infinite sepn. ^{††}	4.306	0.9910 ± 0.0020	0.9947 ± 0.0007	0.2851	0.2864
36	PNL-3602 (4A.11)	Steel Reflector, with Boral Sheets	4.306	0.9941 ± 0.0011	0.9970 ± 0.0007	0.3135	0.3150
37	PNL-3926 (4A.12)	Lead Reflector, 0 cm sepn.	4.306	NC	1.0003 ± 0.0007	NC	0.3159
38	PNL-3926 (4A.12)	Lead Reflector, 0.55 cm sepn.	4.306	1.0025 ± 0.0011	0.9997 ± 0.0007	0.3030	0.3044
39	PNL-3926 (4A.12)	Lead Reflector, 1.956 cm sepn.	4.306	1.0000 ± 0.0012	0.9985 ± 0.0007	0.2883	0.2930

Table 4A.1

Summary of Criticality Benchmark Calculations

Reference	Identification	Enrich.	Calculated k_{eff}		EALF ¹ (eV)		
			MCNP4a	KENO5a	MCNP4a	KENO5a	
40	PNL-3926 (4A.12)	Lead Reflector, 5.405 cm sepn.	4.306	0.9971 ± 0.0012	0.9946 ± 0.0007	0.2831	0.2854
41	PNL-2615 (4A.13)	Experiment 004/032 - no absorber	4.306	0.9925 ± 0.0012	0.9950 ± 0.0007	0.1155	0.1159
42	PNL-2615 (4A.13)	Experiment 030 - Zr plates	4.306	NC	0.9971 ± 0.0007	NC	0.1154
43	PNL-2615 (4A.13)	Experiment 013 - Steel plates	4.306	NC	0.9965 ± 0.0007	NC	0.1164
44	PNL-2615 (4A.13)	Experiment 014 - Steel plates	4.306	NC	0.9972 ± 0.0007	NC	0.1164
45	PNL-2615 (4A.13)	Exp. 009 1.05% Boron-Steel plates	4.306	0.9982 ± 0.0010	0.9981 ± 0.0007	0.1172	0.1162
46	PNL-2615 (4A.13)	Exp. 012 1.62% Boron-Steel plates	4.306	0.9996 ± 0.0012	0.9982 ± 0.0007	0.1161	0.1173
47	PNL-2615 (4A.13)	Exp. 031 - Boral plates	4.306	0.9994 ± 0.0012	0.9969 ± 0.0007	0.1165	0.1171
48	PNL-7167 (4A.14)	Experiment 214R - with flux trap	4.306	0.9991 ± 0.0011	0.9956 ± 0.0007	0.3722	0.3812
49	PNL-7167 (4A.14)	Experiment 214V3 - with flux trap	4.306	0.9969 ± 0.0011	0.9963 ± 0.0007	0.3742	0.3826
50	PNL-4267 (4A.15)	Case 173 - 0 ppm B	4.306	0.9974 ± 0.0012	NC	0.2893	NC
51	PNL-4267 (4A.15)	Case 177 - 2550 ppm B	4.306	1.0057 ± 0.0010	NC	0.5509	NC
52	PNL-5803 (4A.16)	MOX Fuel - Type 3.2 Exp. 21	20% Pu	1.0041 ± 0.0011	1.0046 ± 0.0006	0.9171	0.8868

Table 4A.1

Summary of Criticality Benchmark Calculations

Reference	Identification	Enrich.	Calculated k_{eff}		EALF [†] (eV)		
			MCNP4a	KENO5a	MCNP4a	KENO5a	
53	PNL-5803 (4A.16)	MOX Fuel - Type 3.2 Exp. 43	20% Pu	1.0058 ± 0.0012	1.0036 ± 0.0006	0.2968	0.2944
54	PNL-5803 (4A.16)	MOX Fuel - Type 3.2 Exp. 13	20% Pu	1.0083 ± 0.0011	0.9989 ± 0.0006	0.1665	0.1706
55	PNL-5803 (4A.16)	MOX Fuel - Type 3.2 Exp. 32	20% Pu	1.0079 ± 0.0011	0.9966 ± 0.0006	0.1139	0.1165
56	WCAP-3385 (4A.17)	Saxton Case 52 PuO2 0.52" pitch	6.6% Pu	0.9996 ± 0.0011	1.0005 ± 0.0006	0.8665	0.8417
57	WCAP-3385 (4A.17)	Saxton Case 52 U 0.52" pitch	5.74	1.0000 ± 0.0010	0.9956 ± 0.0007	0.4476	0.4580
58	WCAP-3385 (4A.17)	Saxton Case 56 PuO2 0.56" pitch	6.6% Pu	1.0036 ± 0.0011	1.0047 ± 0.0006	0.5289	0.5197
59	WCAP-3385 (4A.17)	Saxton Case 56 borated PuO2	6.6% Pu	1.0008 ± 0.0010	NC	0.6389	NC
60	WCAP-3385 (4A.17)	Saxton Case 56 U 0.56" pitch	5.74	0.9994 ± 0.0011	0.9967 ± 0.0007	0.2923	0.2954
61	WCAP-3385 (4A.17)	Saxton Case 79 PuO2 0.79" pitch	6.6% Pu	1.0063 ± 0.0011	1.0133 ± 0.0006	0.1520	0.1555
62	WCAP-3385 (4A.17)	Saxton Case 79 U 0.79" pitch	5.74	1.0039 ± 0.0011	1.0008 ± 0.0006	0.1036	0.1047

Notes: NC stands for not calculated.

† EALF is the energy of the average lethargy causing fission.

†† These experimental results appear to be statistical outliers ($> 3\sigma$) suggesting the possibility of unusually large experimental error. Although they could justifiably be excluded, for conservatism, they were retained in determining the calculational basis.

Table 4A.2

COMPARISON OF MCNP4a AND KENO5a CALCULATED REACTIVITIES[†]
FOR VARIOUS ENRICHMENTS

Enrichment	Calculated $k_{eff} \pm 1\sigma$	
	MCNP4a	KENO5a
3.0	0.8465 \pm 0.0011	0.8478 \pm 0.0004
3.5	0.8820 \pm 0.0011	0.8841 \pm 0.0004
3.75	0.9019 \pm 0.0011	0.8987 \pm 0.0004
4.0	0.9132 \pm 0.0010	0.9140 \pm 0.0004
4.2	0.9276 \pm 0.0011	0.9237 \pm 0.0004
4.5	0.9400 \pm 0.0011	0.9388 \pm 0.0004

[†] Based on the GE 8x8R fuel assembly.

Table 4A.3

MCNP4a CALCULATED REACTIVITIES FOR
CRITICAL EXPERIMENTS WITH NEUTRON ABSORBERS

Ref.	Experiment		Δk Worth of Absorber	MCNP4a Calculated k_{eff}	EALF [†] (eV)
4A.13	PNL-2615	Boral Sheet	0.0139	0.9994±0.0012	0.1165
4A.7	B&W-1484	Core XX	0.0165	1.0008±0.0011	0.1724
4A.13	PNL-2615	1.62% Boron-steel	0.0165	0.9996±0.0012	0.1161
4A.7	B&W-1484	Core XIX	0.0202	0.9961±0.0012	0.2103
4A.7	B&W-1484	Core XXI	0.0243	0.9994±0.0010	0.1544
4A.7	B&W-1484	Core XVII	0.0519	0.9962±0.0012	0.2083
4A.11	PNL-3602	Boral Sheet	0.0708	0.9941±0.0011	0.3135
4A.7	B&W-1484	Core XV	0.0786	0.9910±0.0011	0.2092
4A.7	B&W-1484	Core XVI	0.0845	0.9935±0.0010	0.1757
4A.7	B&W-1484	Core XIV	0.1575	0.9953±0.0011	0.2022
4A.7	B&W-1484	Core XIII	0.1738	1.0020±0.0011	0.1988
4A.14	PNL-7167	Expt 214R flux trap	0.1931	0.9991±0.0011	0.3722

[†]EALF is the energy of the average lethargy causing fission.

Table 4A.4

COMPARISON OF MCNP4a AND KENO5a
CALCULATED REACTIVITIES[†] FOR VARIOUS ¹⁰B LOADINGS

¹⁰ B, g/cm ²	Calculated $k_{\text{eff}} \pm 1\sigma$	
	MCNP4a	KENO5a
0.005	1.0381 ± 0.0012	1.0340 ± 0.0004
0.010	0.9960 ± 0.0010	0.9941 ± 0.0004
0.015	0.9727 ± 0.0009	0.9713 ± 0.0004
0.020	0.9541 ± 0.0012	0.9560 ± 0.0004
0.025	0.9433 ± 0.0011	0.9428 ± 0.0004
0.03	0.9325 ± 0.0011	0.9338 ± 0.0004
0.035	0.9234 ± 0.0011	0.9251 ± 0.0004
0.04	0.9173 ± 0.0011	0.9179 ± 0.0004

[†] Based on a 4.5% enriched GE 8x8R fuel assembly.

Table 4A.5

**CALCULATIONS FOR CRITICAL EXPERIMENTS WITH
THICK LEAD AND STEEL REFLECTORS[†]**

Ref.	Case	E, wt%	Separation, cm	MCNP4a k_{eff}	KENO5a k_{eff}
4A.11	Steel Reflector	2.35	1.321	0.9980 ± 0.0009	0.9992 ± 0.0006
		2.35	2.616	0.9968 ± 0.0009	0.9964 ± 0.0006
		2.35	3.912	0.9974 ± 0.0010	0.9980 ± 0.0006
		2.35	∞	0.9962 ± 0.0008	0.9939 ± 0.0006
4A.11	Steel Reflector	4.306	1.321	0.9997 ± 0.0010	1.0012 ± 0.0007
		4.306	2.616	0.9994 ± 0.0012	0.9974 ± 0.0007
		4.306	3.405	0.9969 ± 0.0011	0.9951 ± 0.0007
		4.306	∞	0.9910 ± 0.0020	0.9947 ± 0.0007
4A.12	Lead Reflector	4.306	0.55	1.0025 ± 0.0011	0.9997 ± 0.0007
		4.306	1.956	1.0000 ± 0.0012	0.9985 ± 0.0007
		4.306	5.405	0.9971 ± 0.0012	0.9946 ± 0.0007

[†] Arranged in order of increasing reflector-fuel spacing.

Table 4A.6

CALCULATIONS FOR CRITICAL EXPERIMENTS WITH VARIOUS SOLUBLE BORON CONCENTRATIONS

Reference	Experiment	Boron Concentration, ppm	Calculated k_{eff}	
			MCNP4a	KENO5a
4A.15	PNL-4267	0	0.9974 ± 0.0012	-
4A.8	B&W-1645	886	0.9970 ± 0.0010	0.9924 ± 0.0006
4A.9	B&W-1810	1337	1.0023 ± 0.0010	-
4A.9	B&W-1810	1899	1.0060 ± 0.0009	-
4A.15	PNL-4267	2550	1.0057 ± 0.0010	-

Table 4A.7

CALCULATIONS FOR CRITICAL EXPERIMENTS WITH MOX FUEL

Reference	Case [†]	MCNP4a		KENO5a	
		k_{eff}	EALF ^{††}	k_{eff}	EALF ^{††}
PNL-5803 [4A.16]	MOX Fuel - Exp. No. 21	1.0041 ± 0.0011	0.9171	1.0046 ± 0.0006	0.8868
	MOX Fuel - Exp. No. 43	1.0058 ± 0.0012	0.2968	1.0036 ± 0.0006	0.2944
	MOX Fuel - Exp. No. 13	1.0083 ± 0.0011	0.1665	0.9989 ± 0.0006	0.1706
	MOX Fuel - Exp. No. 32	1.0079 ± 0.0011	0.1139	0.9966 ± 0.0006	0.1165
WCAP-3385-54 [4A.17]	Saxton @ 0.52" pitch	0.9996 ± 0.0011	0.8665	1.0005 ± 0.0006	0.8417
	Saxton @ 0.56" pitch	1.0036 ± 0.0011	0.5289	1.0047 ± 0.0006	0.5197
	Saxton @ 0.56" pitch borated	1.0008 ± 0.0010	0.6389	NC	NC
	Saxton @ 0.79" pitch	1.0063 ± 0.0011	0.1520	1.0133 ± 0.0006	0.1555

Note: NC stands for not calculated

[†] Arranged in order of increasing lattice spacing.

^{††} EALF is the energy of the average lethargy causing fission.

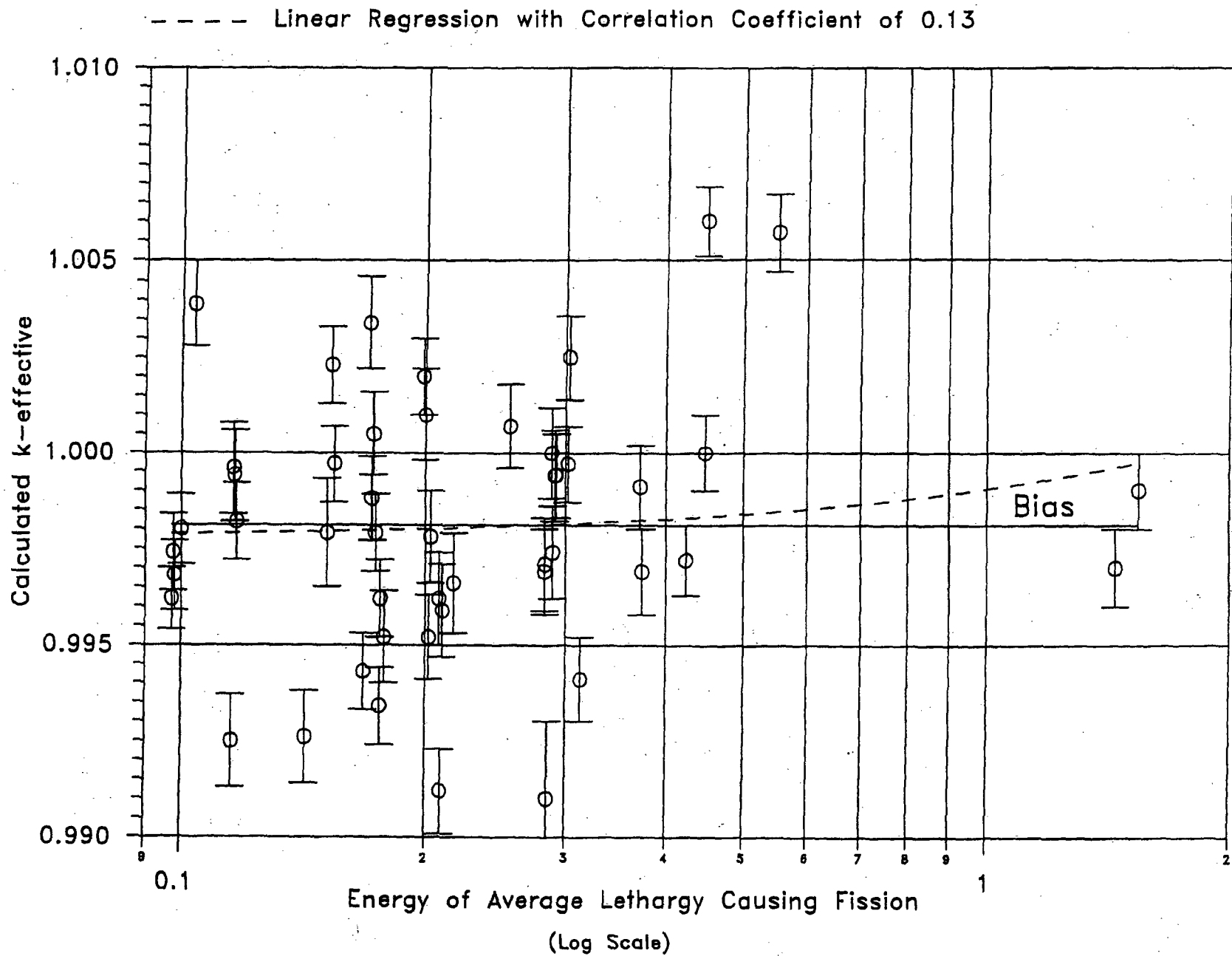


FIGURE 4A.1 MCNP CALCULATED k -eff VALUES for VARIOUS VALUES OF THE SPECTRAL INDEX

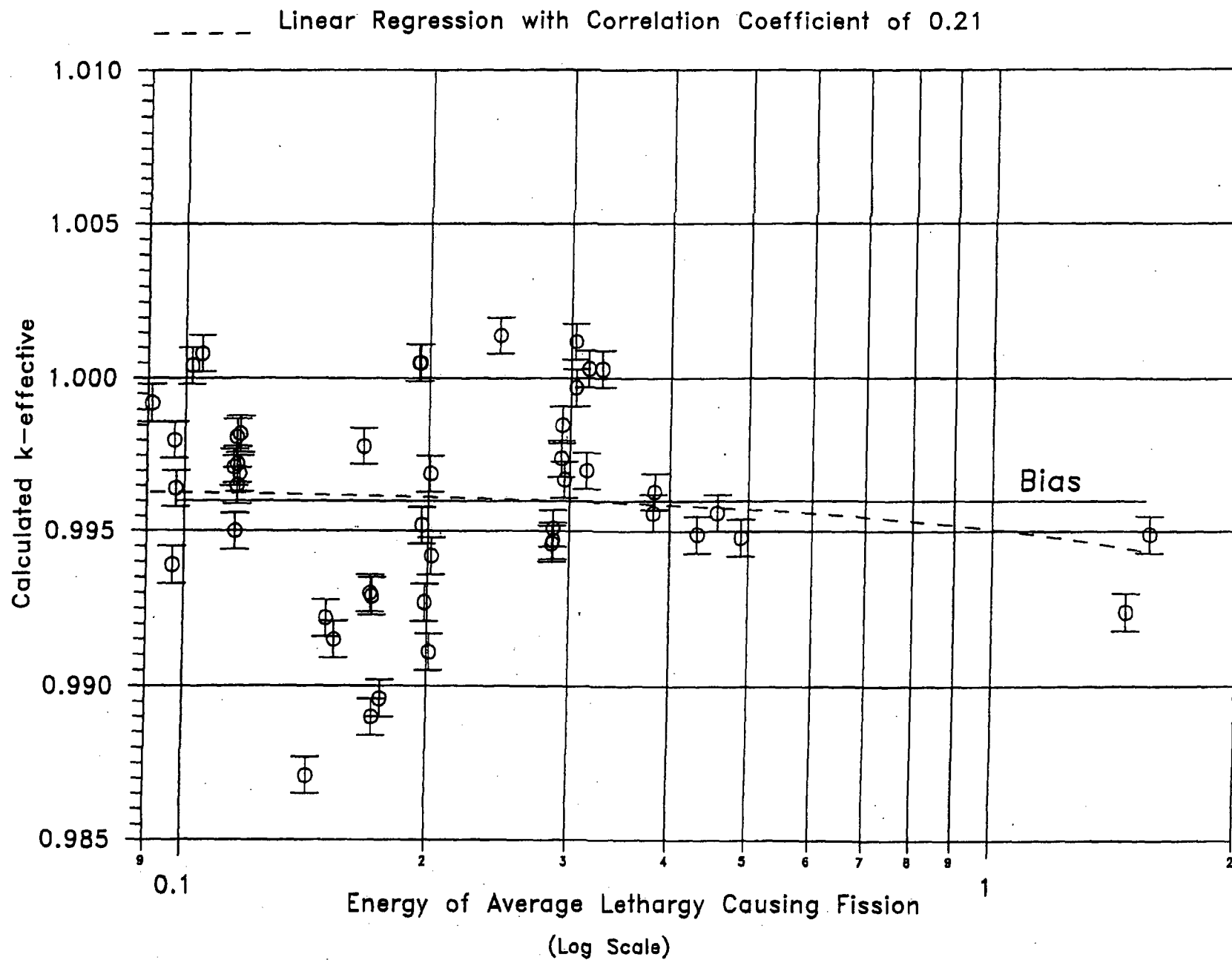


FIGURE 4A.2 KENO5a CALCULATED k -eff VALUES FOR VARIOUS VALUES OF THE SPECTRAL INDEX

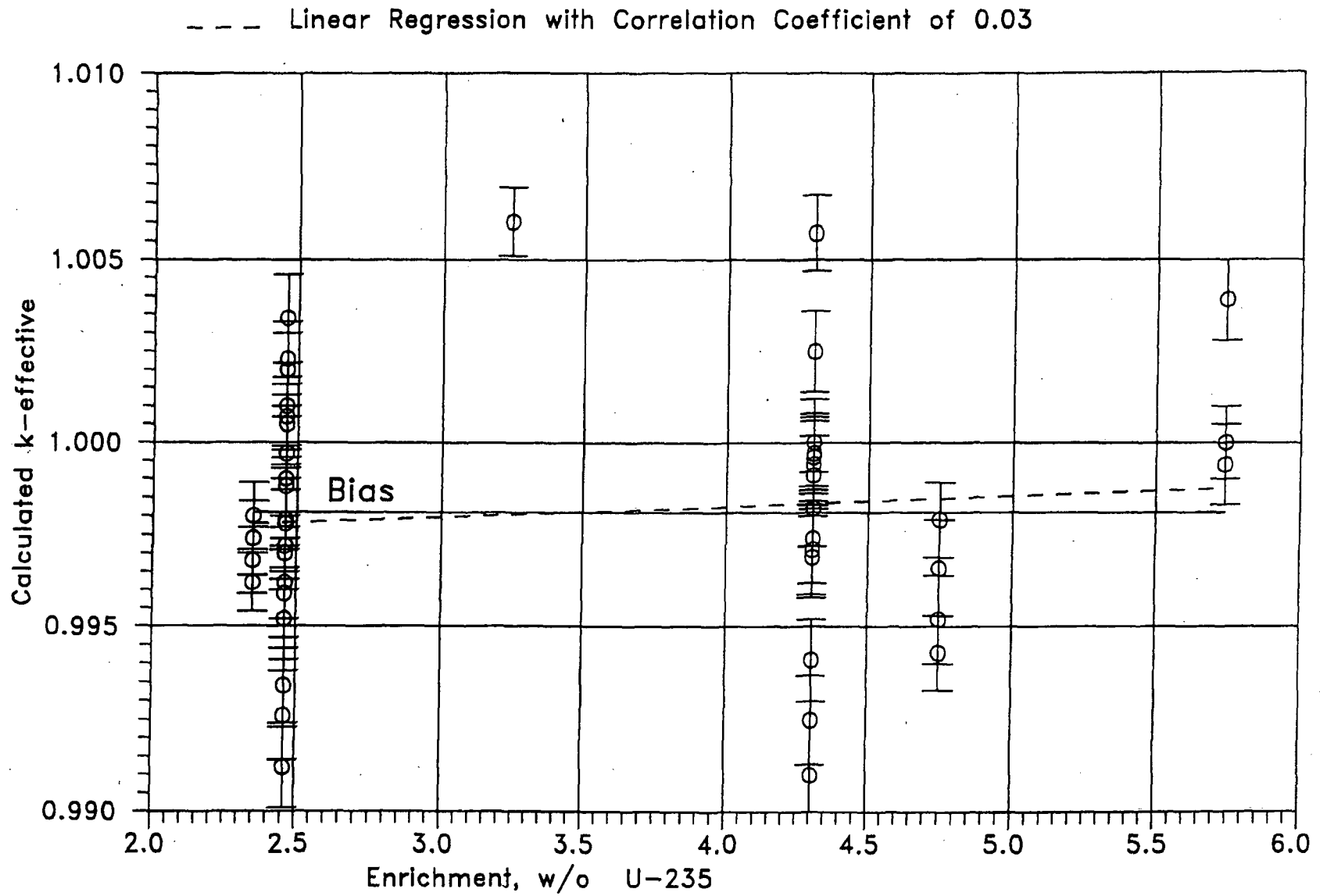


FIGURE 4A.3 MCNP CALCULATED k -eff VALUES AT VARIOUS U-235 ENRICHMENTS

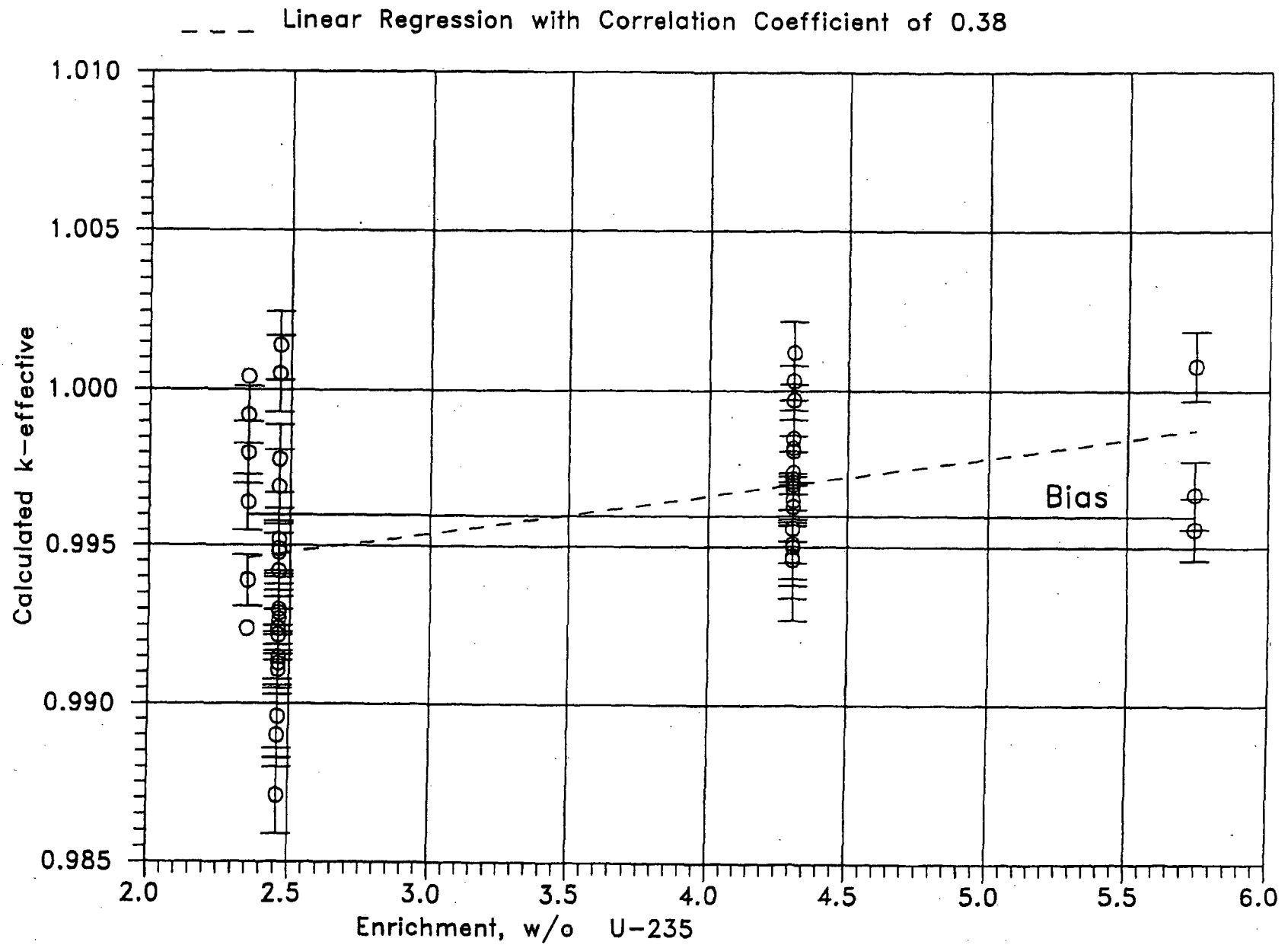


FIGURE 4A.4 KENO CALCULATED k-eff VALUES
AT VARIOUS U-235 ENRICHMENTS

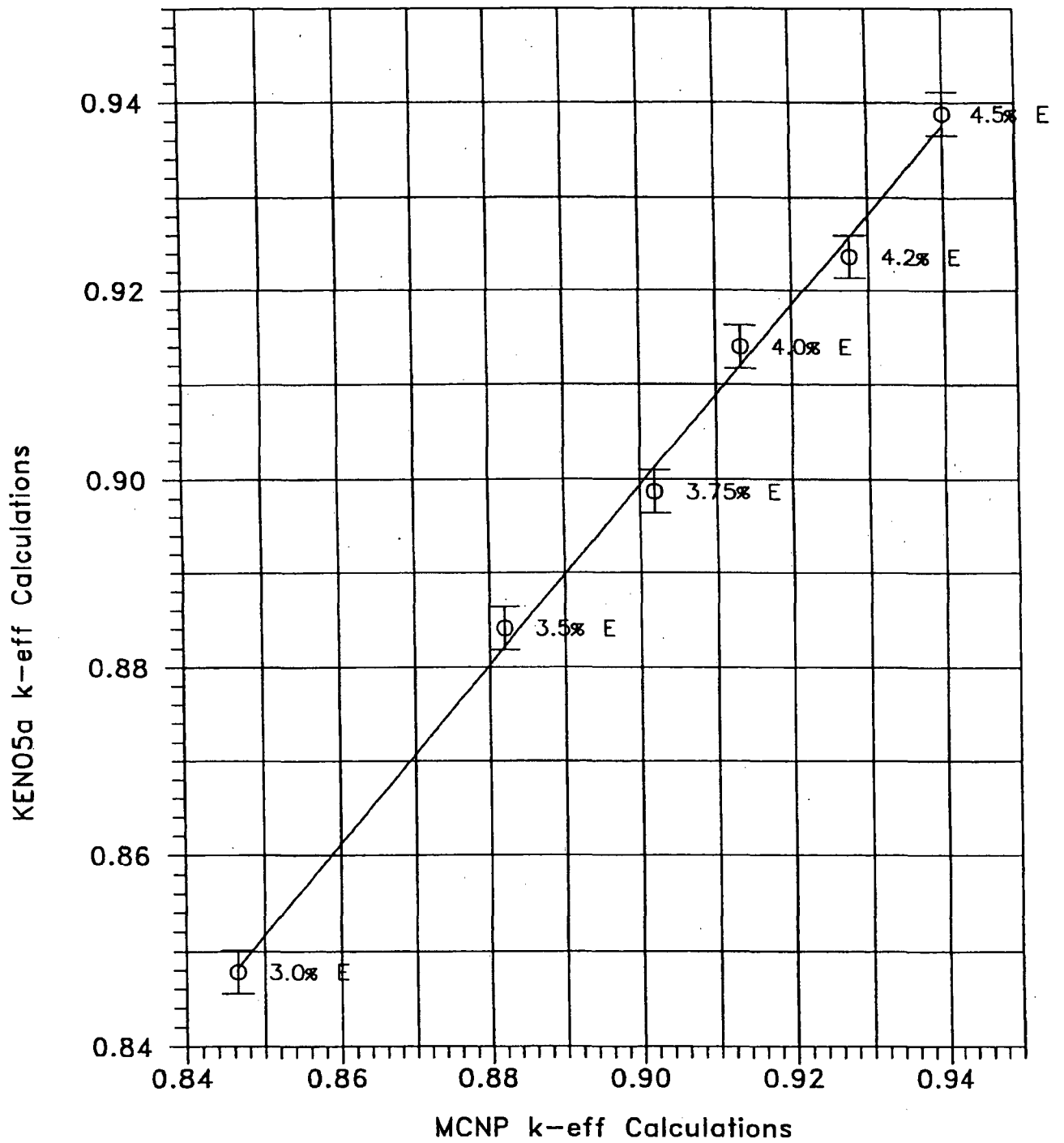


FIGURE 4A.5 COMPARISON OF MCNP AND KENO5A CALCULATIONS FOR VARIOUS FUEL ENRICHMENTS

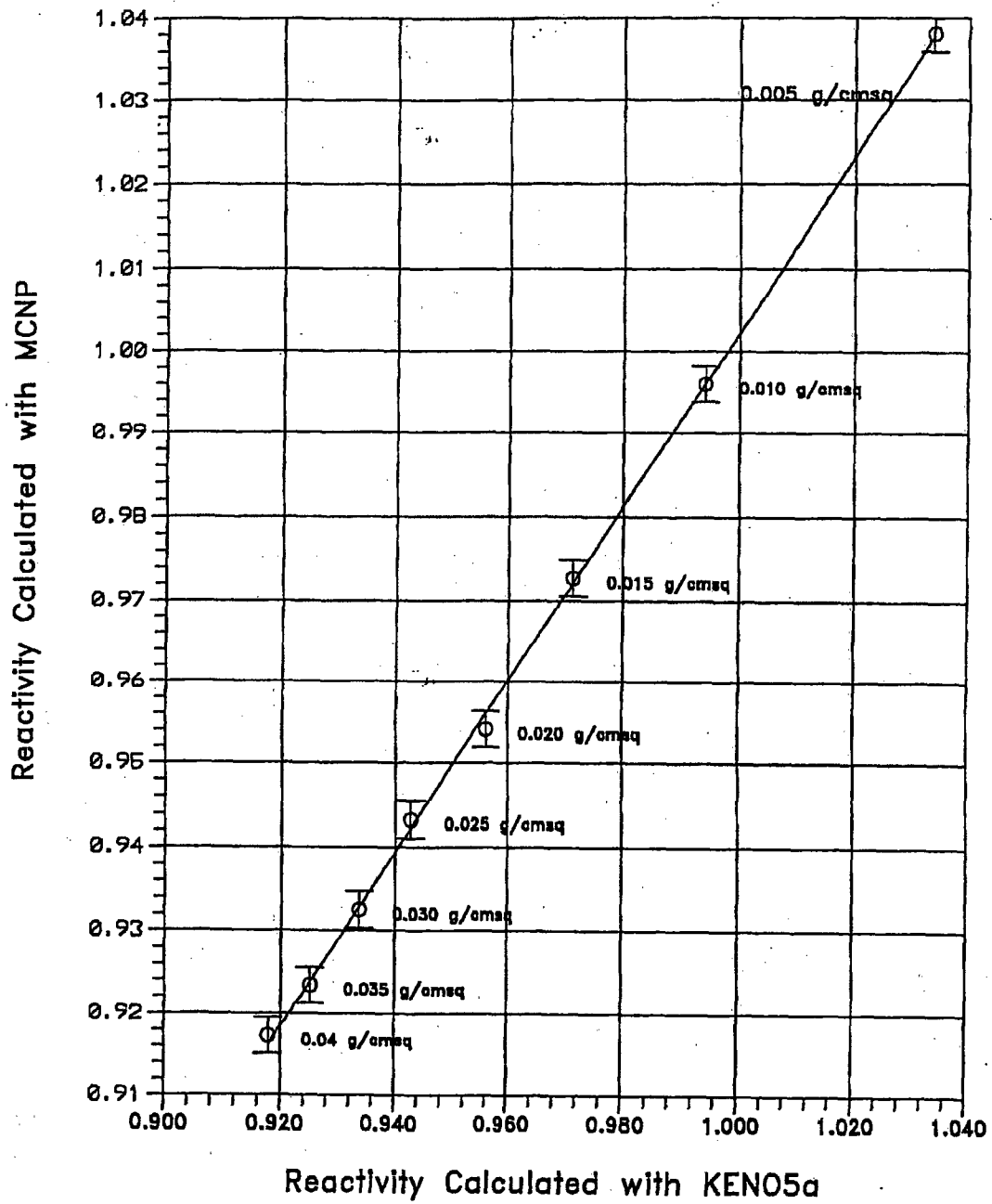


FIGURE 4A.6 COMPARISON OF MCNP AND KENO5a CALCULATIONS FOR VARIOUS BORON-10 AREAL DENSITIES

5.0 STRUCTURAL/SEISMIC CONSIDERATIONS

5.1 Introduction

This report provides information on the new spent fuel storage racks to support the license amendment process for the Beaver Valley Power Station (BVPS) Unit No. 2. This section, specifically, provides information on the required structural performance characteristics of the fuel storage racks.

5.2 Acceptance Criteria

To confirm the structural integrity of the racks, it is necessary to demonstrate compliance with the USNRC Standard Review Plan [5.1] and the OT Position Paper [5.2]. The rack structures are designed to meet the requirements of the ASME Code, Section III, Subsection NF for Class 3 linear-type supports. The relevant design criteria are discussed below, with additional details provided in the text associated with each analysis.

There are three principal design criteria, which must be satisfied by the rack modules:

a. Kinematic Criteria

According to Section 3.8.5 of Ref [5.1] and Ref [5.2], the minimum required safety margin against overturning under a Safe Shutdown Earthquake (SSE) event is 1.1. The margin of safety is defined here as the ratio of the rotation required to produce incipient tipping in either principal plane to the actual maximum rotation in that plane from the time history solution. The maximum rotations of the rack (about the two principal axes) are obtained from a post processing of the rack time history response output. All ratios from the SSE event should be greater than 1.1, to satisfy the regulatory acceptance criteria.

b. Stress Limit Criteria

The stress limits defined in ASME Code, Section III, Subsection NF must not be exceeded under the postulated load combinations. Load combinations are discussed in Section 5.3.

c. Fatigue Criteria

The cumulative damage factor, U, as defined in Section 5.6.9, must be shown to be less than or equal to 1.0.

5.3 Loads and Load Combinations

The applicable loads and their combinations that must be considered in the seismic analysis of rack modules are excerpted from Section 3.8.4 of Ref [5.1] and from Ref [5.2]. The load combinations considered are identified below.

Loading Combination	Service Level
D + L	Level A
D + L + T _o	
D + L + T _o + E	
D + L + T _a + E	Level B
D + L + T _o + P _f	
D + L + T _a + E'	Level D
D + L + T _o + F _d	The functional capability of the racks must be demonstrated

Abbreviations are those used in Ref [5.16]:

D = Dead weight induced loads (including fuel assembly weight)

L = Live load (not applicable for the fuel rack, since there are no moving objects in the rack load path). Note that it is accepted practice to consider the fuel weight as a dead weight.

- E = Operating Basis Earthquake (OBE)
- E' = Safety Shutdown Earthquake (SSE)
- T_o = Differential temperature induced loads, based on the most critical transient or steady state condition under normal operation or shutdown conditions.
- T_a = Differential temperature induced loads, based on the postulated abnormal design conditions.
- F_d = Force caused by the accidental drop of the heaviest load from maximum possible height. This load is considered to be an accident condition. The evaluation of this load condition is discussed in Section 7.
- F_r = Force on the racks caused by postulated stuck fuel assembly. This load is considered to be an accident condition. The evaluation of this load condition is discussed in Section 7.

The differential temperature induced loads namely T_a and T_o, defined above, produce local thermal stresses. The worst thermal stress field in a fuel rack is obtained when an isolated storage location has a fuel assembly generating heat at maximum postulated rate and surrounding storage locations contain no fuel. Heated water makes unobstructed contact with the inside of the storage walls, thereby producing maximum possible temperature difference between adjacent cells. Secondary stresses produced are limited to the body of the rack; that is, support pedestals do not experience secondary (thermal) stresses. Thermal stresses are considered in Subsection 5.6.10.2.

5.4 Analysis Methods

In this section we describe the analysis methods to be used in performing calculations to demonstrate that the structural performance requirements for the fuel storage racks are satisfied. Similar structural analyses have been used for previous fuel storage rack licensing at many nuclear plants worldwide (see Table 5.4.1 for a *partial* list).

5.4.1 Overview of Rack Structural Analysis Methodology

The response of a freestanding rack module to seismic inputs is highly nonlinear and involves a complex combination of motions (sliding, rocking, twisting, and turning), resulting in impacts and friction effects. Some of the unique attributes of the rack dynamic behavior include a large fraction of the total structural mass in a confined rattling motion, friction support of rack pedestals against lateral motion, and large fluid coupling effects due to deep submergence and independent motion of closely spaced adjacent structures.

Linear methods, such as modal analysis and response spectrum techniques, cannot accurately simulate the structural response of such a highly nonlinear structure to seismic excitation. An accurate simulation is obtained only by direct integration of the nonlinear equations of motion with the three pool slab acceleration time-histories applied as the forcing functions acting simultaneously.

Whole Pool Multi-Rack (WPMR) analysis is the vehicle required to simulate the dynamic behavior of the complex spent fuel storage rack configuration.

The following sections provide the basis for this section and discussion on the development of the methodology.

5.4.1.1 Background of Analysis Methodology

Reliable assessment of the stress field and kinematic behavior of the rack modules calls for a conservative dynamic model incorporating all *key attributes* of the actual structure. This means that the model must feature the ability to execute the concurrent motion forms compatible with the freestanding installation of the modules.

The model must possess the capability to affect momentum transfers which occur due to rattling of fuel assemblies inside storage cells and the capability to simulate lift-off and subsequent impact of support pedestals with the underlying bearing pads. The contribution of the water mass

in the interstitial spaces around the rack modules and within the storage cells must be modeled in an accurate manner, since erring in quantification of fluid coupling on either side of the actual value is no guarantee of conservatism.

The Coulomb friction coefficient at the pedestal-to-bearing pad interface may lie in a rather wide range and a conservative value of friction cannot be prescribed *a priori*. In fact, a perusal of results of rack dynamic analyses in numerous docket (Table 5.4.1) indicates that an upper bound value of the coefficient of friction often maximizes the computed rack displacements as well as the equivalent elastostatic stresses.

In short, there are a large number of parameters with potential influence on the rack kinematics. The comprehensive structural evaluation must deal with all of these without sacrificing conservatism.

The three-dimensional single rack dynamic model introduced by Holtec International in the Enrico Fermi Unit 2 rack project (ca. 1980) and used in some 50 rerack projects since that time (Table 5.4.1) addresses most of the above-mentioned array of parameters. The details of this methodology are also published in the permanent literature [5.3]. Despite the versatility of the 3-D seismic model, the accuracy of the single rack simulations has been suspect due to one key element; namely, hydrodynamic participation of water around the racks (not applicable to the dry new fuel storage racks). During dynamic rack motion, hydraulic energy is either drawn from or added to the moving rack, modifying its submerged motion in a significant manner. Therefore, the dynamics of one rack affects the motion of all others in the pool.

A dynamic simulation, which treats only one rack, or a small grouping of racks, is intrinsically inadequate to predict the motion of rack modules submerged in water with any quantifiable level of accuracy. Three-dimensional Whole Pool Multi-Rack analyses carried out for many previous plants demonstrate that single rack simulations under predict rack displacement during seismic responses in a water environment [5.4].

Briefly, the 3-D rack model dynamic simulation, involving one or more spent fuel racks, handles the array of variables as follows:

Interface Coefficient of Friction: Parametric runs are made with upper bound and lower bound values of the coefficient of friction. The limiting values are based on experimental data, which have been found to be bounded by the values 0.2 and 0.8. Simulations are also performed with the array of pedestals having randomly chosen coefficients of friction in a Gaussian distribution with a mean of 0.5 and lower and upper limits of 0.2 and 0.8, respectively. In the fuel rack simulations, the Coulomb friction interface between rack support pedestal and bearing pad is simulated by piecewise linear (friction) elements. These elements function only when the pedestal is physically in contact with the bearing pad.

Rack Beam Behavior: Rack elasticity, relative to the rack base, is included in the model by introducing linear springs to represent the elastic bending action, twisting, and extensions.

Impact Phenomena: Compression-only gap elements are used to provide for opening and closing of interfaces such as the pedestal-to-bearing pad interface, and the fuel assembly-to-cell wall interface. These interface gaps are modeled using nonlinear spring elements. The term "nonlinear spring" is a generic term used to denote the mathematical representation of the condition where a restoring force is not linearly proportional to displacement.

Fluid Coupling: Holtec International extended Fritz's classical two-body fluid coupling model to multiple bodies and utilized it to perform the first two-dimensional multi-rack analysis (Diablo Canyon, ca. 1987). Subsequently, laboratory experiments were conducted to validate the multi-rack fluid coupling theory. This technology was incorporated in the Holtec-proprietary computer program DYNARACK [5.6], which handles simultaneous simulation of all racks in the pool as a Whole Pool Multi-Rack 3-D analysis. This development was first utilized in Chinshan, Oyster Creek, and Shearon Harris plants [5.3, 5.5] and, subsequently, in numerous other rack projects. The WPMR analyses have corroborated the accuracy of the single rack 3-D solutions in predicting the maximum structural stresses, and also serve to improve predictions of rack kinematics.

For closely spaced racks, demonstration of kinematic compliance is verified by including all modules in one comprehensive simulation using a WPMR model. In WPMR analysis, all rack modules are modeled simultaneously and the coupling effect due to this multi-body motion is included in the analysis. Due to the superiority of this technique in predicting the dynamic behavior of closely spaced submerged storage racks, the Whole Pool Multi-Rack analysis methodology is used to analyze the spent fuel storage rack configurations.

5.4.2 WPMR Methodology

Recognizing that the analysis work effort must deal both with stress and displacement criteria, the sequence of model development and analysis steps that must be undertaken are summarized in the following:

- a. Prepare 3-D dynamic models suitable for a time-history analysis of the fuel storage racks. These models include the assemblage of all rack modules in the spent fuel pool. Include all fluid coupling interactions and mechanical coupling appropriate to performing an accurate non-linear simulation. This 3-D simulation is referred to as a Whole Pool Multi-Rack model.
- b. Perform 3-D dynamic analyses on various physical conditions (such as coefficient of friction and extent of cells containing fuel assemblies). Archive appropriate displacement and load outputs from the dynamic model for post-processing.
- c. Perform stress analysis of high stress areas for the limiting case of all the rack dynamic analyses. Demonstrate compliance with ASME Code Section III, Subsection NF limits on stress and displacement.

5.4.2.1 Model Details for Racks

The dynamic modeling of the rack structure must be prepared with special consideration of all nonlinearities and parametric variations. Particulars of modeling details and assumptions for the WPMR analysis of racks are given in the following:

- a. The fuel rack structure motion is captured by modeling the rack as a 12 degree-of-freedom structure. Movement of the rack cross-section at any height is described by six degrees-of-freedom of the rack base and six degrees-of-freedom at the rack top. In this manner, the response of the module, relative to the baseplate, is captured in the dynamic analyses once suitable springs are introduced to couple the rack degrees-of-freedom and simulate rack stiffness.
- b. Rattling fuel assemblies within the rack are modeled by five lumped masses located at H , $0.75H$, $0.5H$, $0.25H$, and at the rack base (H is the rack height measured above the baseplate). Each lumped fuel mass has two horizontal degrees-of-freedom. Vertical motion of the fuel assembly mass is assumed equal to rack vertical motion at the baseplate level. The centroid of each fuel assembly mass can be located off-center, relative to the rack structure centroid at that level, to simulate a partially loaded rack.
- c. Seismic motion of a fuel rack is characterized by random rattling of fuel assemblies in their individual storage locations. The out of phase motion of the individual fuel assemblies has been appropriately considered by modifying the mass of the individual lumped masses discussed above.
- d. Fluid coupling between the rack and fuel assemblies, and between the rack and wall, is simulated by appropriate inertial coupling in the system kinetic energy. Inclusion of these effects uses the methods of [5.9, 5.10] for rack-to-fuel coupling and for rack-to-rack coupling.
- e. Fluid damping and form drag are conservatively neglected.
- g. Potential impacts between the cell walls of the racks and the contained fuel assemblies are accounted for by appropriate compression-only gap elements between masses involved. The possible incidence of rack-to-wall or rack-to-rack impact is simulated by gap elements at the top and bottom of the rack in two horizontal directions. Bottom gap elements are located at the baseplate elevation. The initial gaps reflect the presence of baseplate extensions, and the rack stiffnesses are chosen to simulate local structural detail.
- h. The model for the rack is considered supported, at the base level, on four or five pedestals. Pedestals are modeled by non-linear compression gap elements in the vertical direction and as "rigid links" for transferring horizontal stress. Each pedestal support is linked to the bearing pad by two piecewise linear friction spring elements. These elements are properly located with respect to the centerline of the rack beam, and allow for arbitrary rocking and sliding motions. The spring rate for the friction springs includes any lateral elasticity of the stub pedestals. Local pedestal vertical spring stiffness accounts for floor elasticity and for local rack elasticity just above the pedestal.

- i. Rattling of fuel assemblies inside the storage locations causes the gap between fuel assemblies and cell wall to change from a maximum of twice the nominal gap to a theoretical zero gap. Fluid coupling coefficients are based on the nominal gap in order to provide a conservative measure of fluid resistance to gap closure.

5.4.2.2 Element Details

Figure 5.1 shows a schematic of the dynamic model of a single rack. The schematic depicts many of the characteristics of the model including all of the degrees-of-freedom and most of the spring restraint elements.

Table 5.4.2 provides a complete listing of each of the 22 degrees-of-freedom for a rack model. Six translational and six rotational degrees-of-freedom (three of each type at top and bottom of rack) describe the motion of the rack structure. Rattling fuel mass motions (shown at nodes 1*, 2*, 3*, 4*, and 5* in Figure 5.1) are described by ten horizontal translational degrees-of-freedom (two at each of the five fuel masses). The vertical fuel mass motion is assumed (and modeled) to be the same as that of the rack baseplate.

Figure 5.2 depicts the fuel to rack impact springs (used to develop potential impact loads between the fuel assembly mass and rack cell inner walls) in a schematic isometric. Only one of the five fuel masses is shown in this figure. Four compression-only springs, acting in the horizontal direction, are provided at each fuel mass.

Figure 5.3 provides a 2-D schematic elevation of the storage rack model, discussed in more detail in Section 5.4.2.4. This view shows the vertical location of the five storage masses and some of the support pedestal spring members.

Figure 5.4 shows the modeling technique and degrees-of-freedom associated with rack elasticity. In each bending plane a shear and bending spring simulate elastic effects [5.11]. Linear elastic springs coupling rack vertical and torsional degrees-of-freedom are also included in the model.

Figure 5.5 depicts the inter-rack impact springs (used to develop potential impact loads between racks or between rack and wall).

5.4.2.3 Multi-Body Fluid Coupling Phenomena

During the seismic event, all racks in the pool are subject to the input excitation simultaneously. The motion of each freestanding module would be autonomous and independent of others as long as they did not impact each other and no water were present in the pool. While the scenario of inter-rack impact is not a common occurrence and depends on rack spacing, the effect of water (the so-called fluid coupling effect) is a universal factor. As noted in Refs [5.10, 5.12], the fluid forces can reach rather large values in closely spaced rack geometries. It is, therefore, essential that the contribution of the fluid forces be included in a comprehensive manner for the spent fuel pool analyses. This is possible only if all racks in the pool are *allowed* to execute 3-D motion in the mathematical model. For this reason, single rack or even multi-rack models involving only a portion of the racks in the pool, are inherently inaccurate. The Whole Pool Multi-Rack model removes this intrinsic limitation of the rack dynamic models by simulating the 3-D motion of all modules simultaneously. The fluid coupling effect, therefore, encompasses interaction between *every* set of racks in the pool (i.e., the motion of one rack produces fluid forces on all other racks and on the pool walls). Stated more formally, both near-field and far-field fluid coupling effects are included in the analysis.

The derivation of the fluid coupling matrix [5.12] relies on the classical inviscid fluid mechanics principles, namely the principle of continuity and Kelvin's recirculation theorem. While the derivation of the fluid coupling matrix is based on no artificial construct, it has been nevertheless verified by an extensive set of shake table experiments [5.12].

In its simplest form, the so-called "fluid coupling effect" [5.9, 5.10] can be explained by considering the proximate motion of two bodies under water. If one body (mass m_1) vibrates adjacent to a second body (mass m_2), and both bodies are submerged in frictionless fluid, then Newton's equations of motion for the two bodies are:

$$\begin{aligned}(m_1 + M_{11}) A_1 + M_{12} A_2 &= \text{applied forces on mass } m_1 + O(X_1^2) \\ M_{21} A_1 + (m_2 + M_{22}) A_2 &= \text{applied forces on mass } m_2 + O(X_2^2)\end{aligned}$$

A_1 , A_2 denote absolute accelerations of masses m_1 and m_2 , respectively, and the notation $O(X^2)$ denotes nonlinear terms.

M_{11} , M_{12} , M_{21} , and M_{22} are fluid coupling coefficients which depend on body shape, relative disposition, etc. Fritz [5.10] gives data for M_{ij} for various body shapes and arrangements. The fluid adds mass to the body (M_{11} to mass m_1), and an inertial force proportional to acceleration of the adjacent body (mass m_2). Thus, acceleration of one body affects the force field on another. This force field is a function of inter-body gap, reaching large values for small gaps. Lateral motion of a fuel assembly inside a storage location encounters this effect. For example, fluid coupling behavior will be experienced between nodes 2 and 2* in Figure 5.1. The rack analysis also contains inertial fluid coupling terms, which model the effect of fluid in the gaps between adjacent racks.

Rack-to-rack gap elements have initial gaps set to 100% of the physical gap between the racks or between outermost racks and the adjacent pool walls.

5.4.2.4 Stiffness Element Details

Three element types are used in the rack models. Type 1 elements represent the linear elastic beam-like behavior of the integrated rack cell matrix. Type 2 elements are the piecewise linear friction springs used to develop the appropriate horizontal forces between the rack pedestals and the supporting bearing pads. Type 3 elements are non-linear gap elements, which model gap closures and subsequent impact loadings (i.e., between fuel assemblies and the storage cell inner walls, rack outer periphery spaces and the vertical forces between the rack pedestals and the supporting bearing pads).

If the simulation model is restricted to two dimensions (one horizontal motion plus one vertical motion, for example), for the purposes of model clarification only, then Figure 5.3 describes the configuration. This simpler model is used to elaborate on the various stiffness modeling elements.

Type 3 gap elements modeling impacts between fuel assemblies and racks have local stiffness K_i in Figure 5.3. Support pedestal spring rates K_S are modeled by type 3 gap elements. Local compliance of the concrete floor is included in K_S . The type 2 friction elements are shown in Figure 5.3 as K_f . The spring elements depicted in Figure 5.4 represent type 1 elements.

Friction at the support/bearing pad interface is modeled by the piecewise linear friction springs with suitably large stiffness K_f up to the limiting lateral load μN , where N is the current compression load at the interface between support and liner. At every time-step during transient analysis, the current value of N (either zero if the pedestal has lifted off the liner, or a compressive finite value) is computed.

The gap element K_S , modeling the effective compression stiffness of the structure in the vicinity of the support, includes stiffness of the pedestal, local stiffness of the underlying pool slab, and local stiffness of the rack cellular structure above the pedestal.

The previous discussion is limited to a 2-D model solely for simplicity. Actual analyses incorporate 3-D motions.

5.4.2.5 Coefficients of Friction

To eliminate the last significant element of uncertainty in rack dynamic analyses, multiple simulations must be performed to adjust the friction coefficient ascribed to the support pedestal/pool bearing pad interface. These friction coefficients are chosen consistent with the two bounding extremes from Rabinowicz's data [5.8]. Simulations are also performed by imposing intermediate value friction coefficients developed by a random number generator with Gaussian normal distribution characteristics. The assigned values are then held constant during the entire simulation in order to obtain reproducible results.[†] Thus, in this manner, the WPMR analysis results are brought closer to the realistic structural conditions.

The coefficient of friction (μ) between the pedestal supports and the pool floor is indeterminate. According to Rabinowicz [5.8], results of 199 tests performed on austenitic stainless steel plates submerged in water show a mean value of μ to be 0.503 with standard deviation of 0.125. Upper and lower bounds (based on twice standard deviation) are 0.753 and 0.253, respectively. Analyses are therefore performed for coefficient of friction values of 0.2 (lower limit) and for 0.8 (upper limit), and for random friction values clustered about a mean of 0.5. The bounding values of $\mu = 0.2$ and 0.8 have been found to envelope the upper limit of module response in previous rerack projects.

[†] It is noted that DYNARACK has the capability to change the coefficient of friction at any pedestal at each instant of contact based on a random reading of the computer clock cycle. However, exercising this option would yield results that could not be reproduced. Therefore, the random choice of coefficients is made only once per run.

5.4.2.6 Governing Equations of Motion

Using the structural model discussed in the foregoing, equations of motion corresponding to each degree-of-freedom are obtained using Lagrange's Formulation [5.11]. The system kinetic energy includes contributions from solid structures and from trapped and surrounding fluid. The final system of equations obtained has the matrix form:

$$[M] \left[\frac{d^2 q}{dt^2} \right] = [Q] + [G]$$

where:

[M] is the total mass matrix (including structural and fluid mass contributions). The size of this matrix will be $22n \times 22n$ for a WPMR analysis (n = number of racks in the model).

q is the nodal displacement vector relative to the pool slab displacement (the term with q indicates the second derivative with respect to time, i.e., acceleration)

[G] is a vector dependent on the given ground acceleration

[Q] is a vector dependent on the spring forces (linear and nonlinear) and the coupling between degrees-of-freedom

The above column vectors have length $22n$. The equations can be rewritten as follows:

$$\left[\frac{d^2 q}{dt^2} \right] = [M]^{-1} [Q] + [M]^{-1} [G]$$

This equation set is mass uncoupled, displacement coupled at each instant in time. The numerical solution uses a central difference scheme built into the Holtec-proprietary computer program DYNARACK [5.6].

5.5 Structural Evaluation of Racks

To provide a demonstration that the proposed rack layouts and rack designs (see Sections 1 and 2) will appropriately satisfy the requirements discussed in the preceding sections of this section, a series of structural evaluations have been performed and are described in the remaining sections.

5.5.1 Description of Rack Layout

The various components for each of the rack styles are described in detail in Section 2.6. The models prepared for the DYNARACK simulations account for all of the pertinent features and characteristics of each rack. Rack material is defined in Table 5.4.3.

The cartesian coordinate system utilized within the dynamic models has the following orientation:

- x = Horizontal axis along plant North (in a north-south direction)
- y = Horizontal axis along plant East (in an east-west direction)
- z = Vertical axis upward from the rack base

For the dynamic rack simulations, the dry fuel weight is conservatively taken to be 1,616 lbs to account for the maximum fuel weight at every location.

5.5.2 Synthetic Time-Histories

Synthetic time-histories in three orthogonal directions (N-S, E-W, and vertical) were generated in accordance with the provisions of Section 3.7.1 of the SRP [5.1]. In order to prepare an acceptable set of acceleration time-histories, the Holtec-proprietary code GENEQ [5.7] was utilized. As required by the recent issue of the SRP [5.1], the code GENEQ was used to develop five sets of acceleration time histories for the design basis response spectra.

The following criteria required by SRP Section 3.7.1 have been satisfied:

1. Each time history set (2 horizontal and 1 vertical) must be statistically independent. This is demonstrated by calculating the cross correlation coefficient for each time history with each of the other two events. The absolute value of each of the three correlation coefficients must be less than 0.15.
2. For each of the time histories:
 - The time history shall have a sufficiently small time increment and sufficiently long duration. Records shall have a Nyquist frequency of at least 50 Hz, (e.g., a time increment of at most 0.010 seconds) and a total duration of at least 20 seconds.
 - Spectral acceleration at 5% damping shall be computed at a minimum of 100 points per frequency decade, uniformly spaced over the log frequency scale from 0.1 Hz to 50 Hz or the Nyquist frequency. The comparison of the response spectrum obtained from the artificial ground motion time history with the target response spectrum shall be made at each frequency computed in the frequency range of interest.
3. For each of the *average* response spectra:
 - The computed 5% damped response spectrum of the accelerogram shall not fall more than 10% below the target response spectrum at any one frequency.
 - The computed 5% damped response spectrum of the artificial ground motion time history shall not exceed the target response spectrum at any frequency by more than 30% (a factor of 1.3) in the frequency range of interest. If the response spectrum for the accelerogram exceeds the target response spectrum by more than 30% at any frequency range, the power spectrum density of the accelerogram needs to be computed and shown to not have significant gaps in energy at any frequency over this frequency range.

5.5.3 Stress Limit Evaluations

The stress limits presented below apply to the rack structure and are derived from the ASME Code, Section III, Subsection NF [5.13]. Parameters and terminology are in accordance with the ASME Code. Material properties are obtained from the ASME Code Section II, Part D [5.16], and are listed in Table 5.4.3.

(i) Normal and Upset Conditions (Level A or Level B)

- a. Allowable stress in tension on a net section is:

$$F_t = 0.6 S_y$$

where, S_y = yield stress at temperature, and F_t is equivalent to primary membrane stress.

- b. Allowable stress in shear on a net section is:

$$F_v = .4 S_y$$

- c. Allowable stress in compression on a net section is:

$$F_a = S_y \left(.47 - \frac{k \ell}{444 r} \right)$$

where $k\ell/r$ for the main rack body is based on the full height and cross section of the honeycomb region and does not exceed 120 for all sections.

- l = unsupported length of component
- k = length coefficient which gives influence of boundary conditions. The following values are appropriate for the described end conditions:
- 1 (simple support both ends)
 - 2 (cantilever beam)
 - ½ (clamped at both ends)
- r = radius of gyration of component

- d. Maximum allowable bending stress at the outermost fiber of a net section, due to flexure about one plane of symmetry is:
- $$F_b = 0.60 S_y \quad (\text{equivalent to primary bending})$$

- e. Combined bending and compression on a net section satisfies:

$$\frac{f_a}{F_a} + \frac{C_{mx} f_{bx}}{D_x F_{bx}} + \frac{C_{my} f_{by}}{D_y F_{by}} < 1$$

where:

- f_a = Direct compressive stress in the section
- f_{bx} = Maximum bending stress along x-axis
- f_{by} = Maximum bending stress along y-axis
- C_{mx} = 0.85
- C_{my} = 0.85
- D_x = $1 - (f_a/F'_{ex})$
- D_y = $1 - (f_a/F'_{ey})$
- $F'_{ex,ey}$ = $(\pi^2 E)/(2.15 (kl/r)_{x,y}^2)$
- E = Young's Modulus

and subscripts x,y reflect the particular bending plane.

- f. Combined flexure and compression (or tension) on a net section:

$$\frac{f_a}{0.6 S_y} + \frac{f_{bx}}{F_{bx}} + \frac{f_{by}}{F_{by}} < 1.0$$

The above requirements are to be met for both direct tension or compression.

g. Welds

Allowable maximum shear stress on the net section of a weld is given by:

$$F_w = 0.3 S_u$$

where S_u is the weld material ultimate strength at temperature. For fillet weld legs in contact with base metal, the shear stress on the gross section is limited to $0.4S_y$, where S_y is the base material yield strength at temperature.

(ii) Level D Service Limits

Section F-1334 (ASME Section III, Appendix F) [5.14], states that the limits for the Level D condition are the minimum of 2 or $1.167 S_u/S_y$ times the corresponding limits for the Level A condition if $S_u > 1.2S_y$, or 1.4 if $S_u \leq 1.2S_y$ except for requirements specifically listed below. S_u and S_y are the ultimate strength and yield strength at the specified rack design temperature. Examination of material properties for 304 and 304L stainless demonstrates that the $S_u > 1.2S_y$ condition above is met.

Exceptions to the above general multiplier are the following:

- a) Stresses in shear shall not exceed the lesser of $0.72S_y$ or $0.42S_u$. In the case of the Austenitic Stainless material used here, $0.72S_y$ governs.
- b) Axial Compression Loads shall be limited to $2/3$ of the calculated buckling load.
- c) Combined Axial Compression and Bending - The equations for Level A conditions shall apply except that:
 $F_a = 0.667 \times \text{Buckling Load} / \text{Gross Section Area}$,
and the terms F'_{ex} and F'_{ey} may be increased by the factor 1.65.

d) For welds, the Level D allowable maximum weld stress is not specified in Appendix F of the ASME Code. An appropriate limit for weld throat stress is conservatively set here as:

$$F_w = (0.3 S_u) \times \text{factor}$$

where:

$$\begin{aligned} \text{factor} &= (\text{Level D shear stress limit})/(\text{Level A shear stress limit}) \\ &= 0.72 \times S_y / 0.4 \times S_y = 1.8 \end{aligned}$$

5.5.3.1 Dimensionless Stress Factors

For convenience, the stress results are presented in dimensionless form. Dimensionless stress factors are defined as the ratio of the actual developed stress to the specified limiting value. The limiting value of each stress factor is 1.0.

Stress factors reported are:

- R₁ = Ratio of direct tensile or compressive stress on a net section to its allowable value (note pedestals only resist compression)
- R₂ = Ratio of gross shear on a net section in the x-direction to its allowable value
- R₃ = Ratio of maximum x-axis bending stress to its allowable value for the section
- R₄ = Ratio of maximum y-axis bending stress to its allowable value for the section
- R₅ = Combined flexure and compressive factor (as defined in the foregoing)
- R₆ = Combined flexure and tension (or compression) factor (as defined in the foregoing)
- R₇ = Ratio of gross shear on a net section in the y-direction to its allowable value.

5.5.4 Parametric Simulations

Comprehensive 3-D acceleration-time history analyses were performed for the SSE and OBE design basis event. The following rack configurations (cases) have been analyzed for Spent Fuel Racks:

- 1) Whole Pool Multi Rack Configuration: This configuration is used for the spent fuel racks in the spent fuel pool. All the racks in the spent fuel pool are included in the seismic analysis with appropriate surrounding gaps.

- 2) Single Rack Configuration: In order to evaluate the structural integrity of the cask pit platform, additional dynamic analysis is performed. The cask pit platform is a beam like structure which temporarily supports a single loaded rack during the SFR loading campaign. Since only one rack is supported, a separate single rack analysis is performed. The single rack analysis method, and the analysis code used to perform the calculations, is identical to the WPMR analysis method except that the model includes a single rack as opposed to all racks in the pool. In fact, the “building block” for the WPMR analysis is a 3-D multi-degree of freedom model of each rack in the pool. Since a random COF is shown to bound the WPMR analysis, the random COF is used in the single rack analysis.

The following presents a complete listing of the simulations discussed herein. Consideration of the parameters described in Section 5.4.2 resulted in the following runs.

LIST OF SPENT FUEL RACK SIMULATIONS				
<u>Run</u>	<u>Model</u>	<u>Load Case</u>	<u>COF</u>	<u>Event</u>
1	WPMR	All Racks Fully Loaded	0.2	SSE, Set 4
2	WPMR	All Racks Fully Loaded	Random	SSE, Set 4
3	WPMR	All Racks Fully Loaded	0.8	SSE, Set 4
4	WPMR	All Racks Fully Loaded	0.2	OBE, Set 4
5	WPMR	All Racks Fully Loaded	Random	OBE, Set 4
6	WPMR	All Racks Fully Loaded	0.8	OBE, Set 4
7♦	Single Rack	Fully Loaded rack	Random	SSE, Set 4

where Random = Gaussian distribution with a mean of 0.5 coefficient of friction and upper and lower limits of 0.8 and 0.2.

5.6 Mechanical Evaluation of Racks

This section discusses the results of the structural analysis of the racks and the mechanical evaluation performed to show that the acceptance criteria, discussed in Section 5.2, are met. The evaluation of the racks to address their ability to withstand the postulated mechanical accidents is discussed in Section 7.

The results from the DYNARACK runs are provided in this section by extracting the worst case values from the parameters of interest; namely displacements, support pedestal forces, impact loads, and stress factors. This section also summarizes other analyses performed to develop and evaluate structural member stresses, which are not determined by the DYNARACK postprocessor.

-
- ♦ Since Set 4 seismic event (i.e. run 2) produces the largest stresses in the rack modules, the single rack analysis is run with Set 4 seismic event as well for conservatism.

5.6.1 Rack Displacements

The largest top of rack displacement for the spent fuel rack configurations considered is 2.79". Other simulations have smaller, but comparable, displacements in both x and y directions.

By comparison of the maximum displacement with the minimum width of the rack, which is approx. 81" per Table 2.1.1, it is obvious that rack overturning is of no concern and the required safety factor against the overturning of 1.1 will be easily exceeded.

5.6.2 Pedestal Vertical Forces

The highest vertical pedestal load from all spent fuel racks is 326,000 lbs, which bounds all simulations.

5.6.3 Pedestal Friction Forces

The maximum friction load for the spent fuel racks in either x or y direction is 122,000 lbs. This load has been used to evaluate the female pedestal-to-baseplate weld, as discussed in Section 5.6.7 (part b).

5.6.4 Rack Impact Loads

A freestanding rack, by definition, is a structure subject to potential impacts during a seismic event. Impacts arise from rattling of the fuel assemblies in the storage rack locations and, in some instances, from localized impacts between the racks, or between a peripheral rack and the pool wall. The following sections discuss the bounding values of these impact loads.

5.6.4.1 Rack Impacts

In order to protect the rack cell structure from impact during a seismic event and maintain the proper rack spacing, the rack baseplates extend beyond the perimeter envelope of the cell region. The racks are then installed in the pool with a very small separation between adjacent rack baseplates. Therefore, by design the racks are predisposed to impact each other at the baseplate level during a seismic event, rather than at the top of rack elevation. As a result, the 3/4 inch thick rack baseplates have been designed to accommodate the in-plane contact forces.

The impact loads at the rack base are experienced on the perimeter edges of the baseplates and are insignificant compared to the plate capacity in compression. Local deformations will result in the impact load being spread across a substantial width of the entire baseplate. Rack to rack impacts do occur at the top of rack elevation between adjacent spent fuel racks at several locations in the spent fuel pool. The maximum rack to rack impact load at rack top is 108,430 lb observed between two racks. A buckling failure analysis of the impacted racks has been performed, and the safety factor against buckling collapse of the storage cells has been determined to be greater than 1.5.

No rack-to-wall impacts occur in any of the dynamic simulations. Thus, the freestanding racks do not transmit any forces to the SFP walls.

5.6.4.2 Fuel to Cell Wall Impact Loads

Even though limits on secondary stresses are not prescribed in the ASME Code for Class 3 NF structures, evaluations must be made to ensure that the localized impacts do not lead to plastic deformations in the storage cells which affect the sub-criticality of the stored fuel array. Local cell wall integrity is conservatively estimated from peak impact loads. Plastic analysis is used to obtain the limiting impact load, which would lead to gross permanent deformation.

A review of all simulations performed allows determination of the maximum instantaneous impact load between fuel assembly and fuel cell wall at any modeled impact site. For the spent

fuel racks with a wall thickness of 0.075", the limiting side load is 3,204 lbs. The maximum fuel assembly impact load is 610.2 lbs. Therefore, the cell walls are structurally adequate.

5.6.5 Rack Stress Factors

The time history results from the DYNARACK solver provide the pedestal normal and lateral interface forces, which may be converted to the limiting bending moment and shear force at the bottom baseplate-pedestal interface. In particular, maximum values for the previously defined stress factors are determined for every pedestal in the array of racks. The net section maximum (in time) bending moments and shear forces can also be determined at the bottom baseplate-rack cellular structure interface for each spent fuel rack in the pool. Using these forces and moments, the maximum stress in the limiting rack cell (box) can be evaluated.

The stress factor results for male and female pedestals, and for the entire spent fuel rack cellular cross section just above the baseplate have been determined. These factors are reported for every rack in each simulation, and for each pedestal in every rack. These locations are the most heavily loaded net sections in the structure so that satisfaction of the stress factor criteria at these locations ensures that the overall structural criteria set forth in Section 5.5.3 are met.

For the spent fuel racks, the maximum stress factor for the DYNARACK simulations is 0.888, which occurs in the cellular region of the rack and conservatively accounts for the effective width of the cell wall based on its slenderness ratio. This calculated value of stress factor is less than the allowable of 1.0. The maximum stress factor computed for the rack supports is less than computed for the cellular region and obviously less than the allowable of 1.0.

The stress factors, as defined in Subsection 5.5.3.1, for all of the simulations performed, leads to the conclusion that all stress factors are less than the mandated limit. Therefore, the requirements of Section 5.2 are satisfied for the load levels considered for every limiting location in the racks.

5.6.6 Pedestal Thread Shear Stress

For the Spent Fuel Racks the maximum average shear stress in the engagement region is 8,684 psi and 11,555 psi for OBE and SSE, respectively. These stresses are bounding for both the male and female pedestal threads. The allowable shear stress for Level A conditions is $0.4 S_y = 10,000$ psi (based on S_y for SA240-304 at 200°F). The allowable shear stress for Level D conditions is the lesser of: $0.72 S_y = 18,000$ psi or $0.42 S_u = 29,400$ psi (based on S_y and S_u for SA240-304 at 200°F).

5.6.7 Weld Stresses

Weld locations subjected to significant seismic loading are located at the bottom of the rack at the baseplate-to-cell connection, at the top of the pedestal support at the baseplate connection, and at cell-to-cell connections. Bounding values of resultant loads are used to qualify the connections.

a. Baseplate-to-Rack Cell Welds

Reference [5.13] (ASME Code Section III, Subsection NF) permits, for Level A or B conditions, an allowable weld stress $\tau = .3 * (66,200) = 19,860$ psi. As stated in Subsection 5.5.3 (part ii) the allowable for Level D is $0.54 S_u$, giving an allowable of 35,748 psi.

Weld stresses are determined through the use of a simple conversion factor (based on area ratios) applied to the corresponding stress factor in the adjacent rack material. The conversion factor is developed from the differences in base material thickness and length versus weld throat dimension and length as follows:

$$\frac{0.075 * (8.8 + 0.075)}{0.0625 * 0.7071 * 6.0} = 2.51$$

where

0.075 is the cell wall thickness

8.8+0.075	is the mean box dimension
0.0625*0.7071	is the box-baseplate fillet weld throat size
6.0	is the length of the weld

The highest predicted cell to baseplate weld stress is calculated based on the highest R2, R6, and R7 values for the rack cell region (refer to Subsection 5.5.3.1 for definition of R2, R6, and R7 factors). These cell wall stress factors are converted into weld stress values as follows:

For SSE Simulation

$$\begin{aligned} & \{[R6 * (1.2)]^2 + [R2 * (0.72)]^2 + [R7 * (0.72)]^2\}^{1/2} * S_y * \text{Ratio} \\ & = \{[0.367 * (1.2)]^2 + [0.059 * (0.72)]^2 + [0.052 * (0.72)]^2\}^{1/2} * (21,300) * 2.51 \\ & = 23,731 \text{ psi} \end{aligned}$$

For OBE Simulation

$$\begin{aligned} & \{[R6 * (0.6)]^2 + [R2 * (0.4)]^2 + [R7 * (0.4)]^2\}^{1/2} * S_y * \text{Ratio} \\ & = \{[0.563 * (0.6)]^2 + [0.102 * (0.4)]^2 + [0.094 * (0.4)]^2\}^{1/2} * (21,300) * 2.51 \\ & = 18,301 \text{ psi} \end{aligned}$$

Since the calculated stress values are less than the corresponding allowable weld stresses, all welds between the baseplate and cell wall base are acceptable.

b. Baseplate-to-Pedestal Welds

The weld between baseplate and support pedestal is checked using finite element analysis to determine that the maximum stress is 15,860 psi for a ¼" fillet weld under a Level D event. This calculated stress value is conservatively compared with the Level A allowable of 19,860 psi.

c. Cell-to-Cell Welds

Cell-to-cell connections are by a series of connecting welds along the cell height. Stresses in storage cell to cell welds develop due to fuel assembly impacts with the cell wall. These weld stresses are conservatively considered by assuming that fuel assemblies in adjacent cells are moving out of phase with one another so that impact loads in two adjacent cells are in opposite directions and are applied simultaneously. This load application tends to separate the two cells from each other at the weld. In addition the cell-to-cell welds experience flexural shear loads due to bending of the rack cell structure. An evaluation of the SSE loads shows that the computed weld stress of 6,756 psi is less than the Level A allowable weld shear stress value of 19,860 psi. It is therefore concluded that the cell-to-cell welds and the adjacent materials are acceptable under all cases considered.

5.6.8 Level A Evaluation

The dead weight per pedestal for the heaviest loaded rack is 61,910 lbs, which is very low compared to an SSE load of 326,000 lbs. Since the Level A loads are approximately 20% of the Level D loads, while the Level A limits are approximately 50% of the Level D limits, the SSE load condition bounds the dead load condition and no further evaluation is performed for dead load only.

5.6.9 Assessment of Rack Fatigue Margin

Alternating stresses in metals produce metal fatigue if the amplitude of the stress cycles is sufficiently large. In high-density racks designed for sites with moderate to high postulated seismic action, the stress intensity amplitudes frequently reach values above the material endurance limit, leading to expenditure of the fatigue "usage" reserve in the material.

Because the locations of maximum stress (viz., the pedestal/rack baseplate junction) and the close placement of racks, a post-earthquake inspection of the high stressed regions in the racks is not feasible. Therefore, the racks must be engineered to withstand multiple earthquakes without reliance of nondestructive inspections for post-earthquake integrity assessment. ASME subsection NF does not require a fatigue evaluation for Class 3 linear-type supports, which is the applicable code for rack design. However, for conservatism, a fatigue life evaluation has been performed for the racks. The time-history method of analysis, deployed in this report, provides the means to obtain a complete cycle history of the stress intensities in the highly stressed regions of the rack. Having determined the amplitude of the stress intensity cycles and their number, the cumulative damage factor, U , can be determined using the classical Miner's rule:

$$U = \sum \frac{n_i}{N_i}$$

where n_i is the number of stress intensity cycles of amplitude σ_i , and N_i is the permissible number of cycles corresponding to σ_i from the ASME fatigue curve for the material of construction. U must be less than or equal to 1.0.

The cumulative damage factor is determined as 0.615, which is well below the ASME Code limit of 1.0.

5.6.10 Local Stress Considerations

This section presents the results of evaluations for the possibility of cell wall buckling and the secondary stresses produced by temperature effects.

5.6.10.1 Cell Wall Buckling

The allowable local buckling stresses in the fuel cell walls is obtained by using classical plate buckling analysis as taken from Section 9.2 of Reference [5.15]. The resulting local buckling stress limit of 15,928 psi is not violated anywhere in the body of the rack modules, since the maximum compressive stress in the outermost cell is

$$\mathbf{SSE:} \quad \sigma = (1.2)(21,300) * R6 \text{ (which is } 0.367) = 9,380.5 \text{ psi}$$

$$\mathbf{OBE:} \quad \sigma = (0.6)(21,300) * R6 \text{ (which is } 0.563) = 7,195.2 \text{ psi}$$

5.6.10.2 Analysis of Welded Joints in Rack

Cell-to cell welded joints are examined in this subsection under the loading conditions arising from thermal effects due to an isolated hot cell. This secondary stress condition is evaluated alone and not combined with primary stresses from other load conditions.

A thermal gradient between cells will develop when an isolated storage location contains a fuel assembly emitting maximum postulated heat, while the surrounding locations are empty. A conservative estimate of weld stresses along the length of an isolated hot cell can be obtained by considering a beam strip uniformly heated by 50°F, which is restrained from growth along one long edge. This thermal gradient is based on the results of the thermal-hydraulic analysis, which

shows that the difference between the local cell maximum temperature and the bulk pool temperature is less than this value (actual temperature difference is less than 40°F per Section 6 results).

Using shear beam theory and subjecting the strip to a uniform temperature rise $\Delta T = 50^\circ\text{F}$, one can calculate an estimate of the maximum value of the average shear stress in the strip. The strip is subjected to the following boundary conditions.

- a. Displacement $U_x(x,y) = 0$ at $x = 0$, at $y = H/2$, for all x .
- b. Average force $N_x(x) = 0$ at $x = L$

The final result for wall shear stress, maximum at $x = L$, is found to be given as

$$\tau_{\max} = \frac{E \alpha \Delta T}{0.931}$$

where $E = 27.6 \times 10^6$ psi, $\alpha = 9.5 \times 10^{-6}$ in/in $^\circ\text{F}$ and $\Delta T = 50^\circ\text{F}$.

Therefore, the maximum weld shear stress in an isolated hot cell, due to thermal gradient, is

$$\tau_{\max} = 14,082 \text{ psi}$$

Since this is a secondary thermal stress, which does not have a specified limit in the ASME Code for Level D conditions, the allowable shear stress criteria for faulted conditions ($0.42 * S_u = 27,804$ psi) is used as a guide to indicate that this maximum shear is acceptable. Therefore, the safety factor against cell wall shear failure due to secondary thermal stresses from cell wall growth under the worst case hot cell conditions is larger than 1.

5.7 Cask Pit Rack Platform Analysis

A Cask Pit Platform has been designed to provide a stable support for a loaded spent fuel storage rack in the cask pit at BVPS Unit No. 2. The Platform is designed to rest on the pool floor and to support the rack from below. The Platform consists of four tubular members, one beneath each rack support pedestal, with intervening cross-braces to prevent the Platform from “rocking”.

As stated in Section 5.5.4, a single rack analysis is performed in order to evaluate the seismic loads induced by a single rack on the supporting Cask Pit Rack Platform. These loads were used to evaluate the structural integrity of the Platform using the ASME Section III, Subsection NF code allowables. The platform was conservatively assumed to be fixed to the pit floor and a finite element structural analysis was performed. The coefficient of friction at the interface between the rack support pedestals and the platform is based on a Gaussian distribution with a mean value of 0.5 and upper and lower bound values of 0.8 and 0.2, respectively. A fine element model of the platform was developed using the ANSYS computer code. The pedestal loads calculated from the single rack analysis described in section 5.5.4 were then applied to the platform to evaluate stresses in the platform. All safety factors were determined to be greater than 1.0. The minimum safety factor was calculated to be 1.12.

The maximum rack support pedestal displacement from the single rack run described in Section 5.5.4 is 0.70”. The platform supports on which the rack support pedestals rest on are about 12” x 12”. The rack support pedestals are 4.5” in diameter. The displacement of 0.70” is insignificant to cause the rack to slide off the platform and cause the tip over of the rack.

5.8 Bearing Pad Analysis

Bearing pads are placed between rack pedestals and the SFP floor to reduce the otherwise high stresses in the SFP concrete slab by spreading the concentrated load of each pedestal over a larger concrete contact area. This evaluation demonstrates that under maximum vertical forces in seismic events, the average compressive stress in the underlying concrete (calculated only over

the interface contact area) remains below the allowable value permitted by the American Concrete Institute, ACI-349 [5.17].

There are three types of bearing pads, Type 1, Type 2 and Type 3. Type 1 bearing pad is an assembly made of two plates staked together to support a single pedestal. Each plate is approximately 11.5" x 16" wide, and 2.25" minimum thick. Type 2 bearing pad is a 12" x 12" wide, and 2" minimum thick and also supports a single pedestal. Type 3 bearing pad is a 11" x 11" and 1 ½" minimum thick plate. Type 1 bearing pads are specially designed to be placed underneath the pedestals that are situated above leak chases in the concrete floor slab. Due to the clearance issue, Type 1 pads are designed to fit in the available space and also provide sufficient support for pedestals. Type 2 bearing pads are typical pads placed between the pedestals and the solid concrete without leak chases in vicinity. Type 3 bearing pads, and three of the Type 2 bearing pads, are placed on the supporting steel blocks of the existing beam structures at the pool bottom instead of directly on the SFP liner. The BVPS Unit No. 2 SFP contains a series of beam structures supported by the pool floor. The existing racks are bolted to these beam structures. These beam structures are designed to carry the load of the existing racks and the stored fuel assemblies. The existing beam structures will not be removed from the SFP floor during this rerack. The new racks are designed such that the majority of the support pedestals are primarily supported by the bearing pads placed directly on the underlying pool floor slab, except for a few racks which are designed to be supported by the existing beam structures using Type 2 and Type 3 bearing pads.

The bearing pads adequately diffuses the peak pedestal load so that the compressive stress in the concrete slab is below the limit set by the governing concrete code. Also, for Type 2 and Type 3 bearing pads, the existing beam structure has been analyzed to determine that it can support the rack pedestal loads.

5.9 Interface Loads on Spent Fuel Pool Structure

The SFP at BVPS Unit No. 2 is a Safety Related, Seismic Category 1, reinforced concrete structure. From the BVPS drawings it is noted that the BVPS Unit No. 2 SFP is the mirror reflection of the BVPS Unit No. 1 in terms of the storage locations (viz. the spent fuel storage area, the cask area and the fuel transfer canal) and the elevation of the slab and the confining walls.

Since a comprehensive evaluation of the pool structure was performed previously for the BVPS Unit No. 1 SFP in support of rerack license amendment application under NRC Docket No. 50-334, (Amendment No. 178 issued on November 1, 1993), the applicable loads (i.e. all Level A and Level D loads) and the capacities of both the BVPS Unit No. 1 and BVPS Unit No. 2 SFPs have been compared, and the key results for the BVPS Unit No. 2 SFP have been calculated using linear interpolation methodology.

A comparison of the bounding load cases is performed between the BVPS Unit No. 1 and BVPS Unit No. 2 SFPs by comparing the moment capacities and based on that comparison between the BVPS Unit No. 1 and BVPS Unit No. 2 SFP and the corresponding linear interpolation of the BVPS Unit No. 1 SFP safety factors.

The safety factor for the BVPS Unit No. 2 pool structure is determined by mixed interpolation, based on the increase (or decrease) in the load and the corresponding increase (or decrease) in the moment capacities for individual entities (walls and slab) of the pool structure, with the safety factor for the corresponding entity from BVPS Unit No. 1 SFP.

The safety factors obtained for the BVPS Unit No. 2 SFP are shown in table below.

BVPS Unit No. 2 SFP Component (Wall / Slab)	Minimum Safety Factor
Slab	1.41
North Wall	1.63
East Wall	1.64
East-South Wall	1.17
South-East Wall	1.04
South Wall	1.59
West Wall	1.27

The safety factor is defined as the ratio of the moment capacity to the induced moment in the structure. All calculated safety factors must be shown to be above one to demonstrate the structural adequacy of the pool structure of the BVPS Unit No. 2 SFP. As shown in Table above, all safety factors exceed the required minimum value of one. Therefore, it is concluded that the BVPS Unit No. 2 SFP structure is structurally adequate.

5.10 References

- [5.1] USNRC NUREG-0800, Standard Review Plan, March 2007, (SRP 3.8.4 Rev. 2) and (SRP 3.7.1. Rev 3).
- [5.2] (USNRC Office of Technology) "OT Position for Review and Acceptance of Spent Fuel Storage and Handling Applications", dated April 14, 1978, and January 18, 1979 amendment thereto.
- [5.3] Soler, A.I. and Singh, K.P., "Seismic Responses of Free Standing Fuel Rack Constructions to 3-D Motions", Nuclear Engineering and Design, Vol. 80, pp. 315-329 (1984).
- [5.4] Soler, A.I. and Singh, K.P., "Some Results from Simultaneous Seismic Simulations of All Racks in a Fuel Pool", INNM Spent Fuel Management Seminar X, January, 1993.
- [5.5] Singh, K.P. and Soler, A.I., "Seismic Qualification of Free Standing Nuclear Fuel Storage Racks - the Chin Shan Experience, Nuclear Engineering International, UK (March 1991).
- [5.6] Holtec Computer Code MR216 (multi-rack transient analysis code, a.k.a. DYNARACK), Holtec Proprietary Report HI-961465 - WPMR Analysis User Manual for Pre&Post Processors & Solver, August 1997.
- [5.7] Holtec Proprietary Report HI-89364 - Verification and User's Manual for Computer Code GENEQ, January 1990.
- [5.8] Rabinowicz, E., "Friction Coefficients of Water Lubricated Stainless Steels for a Spent Fuel Rack Facility," MIT, a report for Boston Edison Company, 1976.
- [5.9] Singh, K.P. and Soler, A.I., "Dynamic Coupling in a Closely Spaced Two-Body System Vibrating in Liquid Medium: The Case of Fuel Racks," 3rd International Conference on Nuclear Power Safety, Keswick, England, May 1982.
- [5.10] Fritz, R.J., "The Effects of Liquids on the Dynamic Motions of Immersed Solids," Journal of Engineering for Industry, Trans. of the ASME, February 1972, pp 167-172.
- [5.11] Levy, S. and Wilkinson, J.P.D., "The Component Element Method in Dynamics with Application to Earthquake and Vehicle Engineering," McGraw Hill, 1976.

- [5.12] Paul, B., "Fluid Coupling in Fuel Racks: Correlation of Theory and Experiment", (Proprietary), NUSCO/Holtec Report HI-88243.
- [5.13] ASME Boiler & Pressure Vessel Code, Section III, Subsection NF, 1998 Edition.
- [5.14] ASME Boiler & Pressure Vessel Code, Section III, Appendices, 1998 Edition.
- [5.15] Theory of Elastic Stability, Timoshenko and Gere, 2nd Edition, 1961, McGraw Hill.)
- [5.16] ASME Boiler & Pressure Vessel Code, Section II, Part D, 1998 Edition.
- [5.17] ACI 349-85, Code Requirements for Nuclear Safety Related Concrete Structures, American Concrete Institute, Detroit, Michigan.
- [5.18] ACI 318-89, Building Code requirements for Structural Concrete," American Concrete Institute, Detroit, Michigan.
- [5.19] "Nuclear Reactors and Earthquakes, U.S. Department of Commerce, National Bureau of Standards, National Technical Information Service, Springfield, Virginia (TID 7024).

Table 5.4.1 PARTIAL LISTING OF FUEL RACK APPLICATIONS USING DYNARACK		
PLANT	DOCKET NUMBER(s)	YEAR
Enrico Fermi Unit 2	USNRC 50-341	1980
Quad Cities 1 & 2	USNRC 50-254, 50-265	1981
Rancho Seco	USNRC 50-312	1982
Grand Gulf Unit 1	USNRC 50-416	1984
Oyster Creek	USNRC 50-219	1984
Pilgrim	USNRC 50-293	1985
V.C. Summer	USNRC 50-395	1984
Diablo Canyon Units 1 & 2	USNRC 50-275, 50-323	1986
Byron Units 1 & 2	USNRC 50-454, 50-455	1987
Braidwood Units 1 & 2	USNRC 50-456, 50-457	1987
Vogtle Unit 2	USNRC 50-425	1988
St. Lucie Unit 1	USNRC 50-335	1987
Millstone Point Unit 1	USNRC 50-245	1989
Chinshan	Taiwan Power	1988
D.C. Cook Units 1 & 2	USNRC 50-315, 50-316	1992
Indian Point Unit 2	USNRC 50-247	1990
Three Mile Island Unit 1	USNRC 50-289	1991
James A. FitzPatrick	USNRC 50-333	1990
Shearon Harris Unit 2	USNRC 50-401	1991
Hope Creek	USNRC 50-354	1990
Kuosheng Units 1 & 2	Taiwan Power Company	1990
Ulchin Unit 2	Korea Electric Power Co.	1990
Laguna Verde Units 1 & 2	Comision Federal de Electricidad	1991
Zion Station Units 1 & 2	USNRC 50-295, 50-304	1992
Sequoyah	USNRC 50-327, 50-328	1992
LaSalle Unit 1	USNRC 50-373	1992
Duane Arnold Energy Center	USNRC 50-331	1992
Fort Calhoun	USNRC 50-285	1992
Nine Mile Point Unit 1	USNRC 50-220	1993

Table 5.4.1 (continued)		
PARTIAL LISTING OF FUEL RACK APPLICATIONS USING DYNARACK		
PLANT	DOCKET NUMBER(s)	YEAR
BVPS Unit No. 1	USNRC 50-334	1992
Salem Units 1 & 2	USNRC 50-272, 50-311	1993
Limerick	USNRC 50-352, 50-353	1994
Ulchin Unit 1	KINS	1995
Yonggwang Units 1 & 2	KINS	1996
Kori-4	KINS	1996
Connecticut Yankee	USNRC 50-213	1996
Angra Unit 1	Brazil	1996
Sizewell B	United Kingdom	1996
Waterford 3	USNRC 50-382	1997
J.A. Fitzpatrick	USNRC 50-333	1998
Callaway	USNRC 50-483	1998
Nine Mile Unit 1	USNRC 50-220	1998
Chin Shan	Taiwan Power Company	1998
Vermont Yankee	USNRC 50-271	1998
Millstone 3	USNRC 50-423	1998
Byron/Braidwood	USNRC 50-454, 50-455, 50-567, 50-457	1999
Wolf Creek	USNRC 50-482	1999
Plant Hatch Units 1 & 2	USNRC 50-321, 50-366	1999
Harris Pools C and D	USNRC 50-401	1999
Davis-Besse	USNRC 50-346	1999
Enrico Fermi Unit 2	USNRC 50-341	2000
Kewaunee	USNRC 50-305	2001
V.C. Summer	USNRC 50-395	2001
St. Lucie	USNRC 50-335, 50-389	2002
Turkey Point	USNRC 50-250, 251	2002
Clinton	USNRC 50-461	2003
Diablo Canyon Unit 1 & 2	USNRC 50-275, 50-323	2004
Cooper	USNRC 50-298	2006

Table 5.4.1 (continued)		
PARTIAL LISTING OF FUEL RACK APPLICATIONS USING DYNARACK		
PLANT	DOCKET NUMBER(s)	YEAR
ANO Unit 2	USNRC 50-368	2007

Table 5.4.2

DEGREES-OF-FREEDOM

<u>LOCATION (Node)</u>	<u>DISPLACEMENT</u>			<u>ROTATION</u>		
	U_x	U_y	U_z	θ_x	θ_y	θ_z
1	p_1	p_2	p_3	q_4	q_5	q_6
2	p_7	p_8	p_9	q_{10}	q_{11}	q_{12}
Node 1 is attached to the rack at the bottom most point. Node 2 is attached to the rack at the top most point. Refer to Figure 5.1 for node identification.						
2*	D_{13}	D_{14}				
3*	D_{15}	D_{16}				
4*	D_{17}	D_{18}				
5*	D_{19}	D_{20}				
1*	D_{21}	D_{22}				
	D_{21}	D_{22}				
where the relative displacement variables q_i are defined as: $p_i = q_i(t) + U_x(t) \quad i = 1,7,13,15,17,19,21$ $= q_i(t) + U_y(t) \quad i = 2,8,14,16,18,20,22$ $= q_i(t) + U_z(t) \quad i = 3,9$ $= q_i(t) \quad i = 4,5,6,10,11,12$ p_i denotes absolute displacement (or rotation) with respect to inertial space q_i denotes relative displacement (or rotation) with respect to the floor slab * denotes fuel mass nodes $U(t)$ are the three known earthquake displacements						

Table 5.4.3 RACK MATERIAL DATA (200°F) (ASME - Section II, Part D)			
Material	Young's Modulus E (psi)	Yield Strength S _y (psi)	Ultimate Strength S _u (psi)
SA240; 304L S.S.	27.6 x 10 ⁶	21,300	66,200
SUPPORT MATERIAL DATA (200°F)			
SA240, Type 304 (upper part of support feet)	27.6 x 10 ⁶	25,000	71,000
SA-564-630 (lower part of support feet; age hardened at 1100°F)	28.5 x 10 ⁶	106,300	140,000

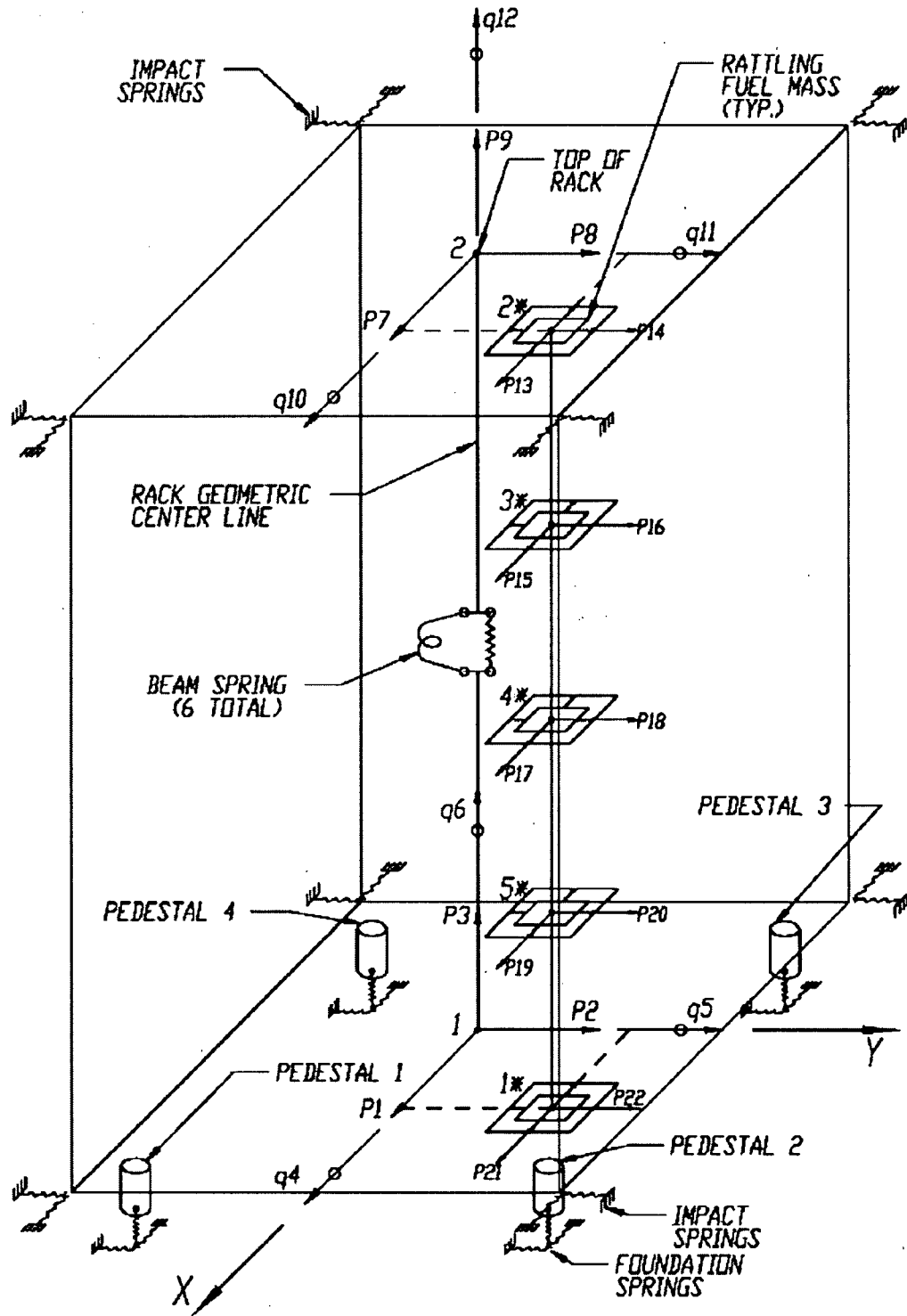


Figure 5.1: Single Rack Dynamic Model

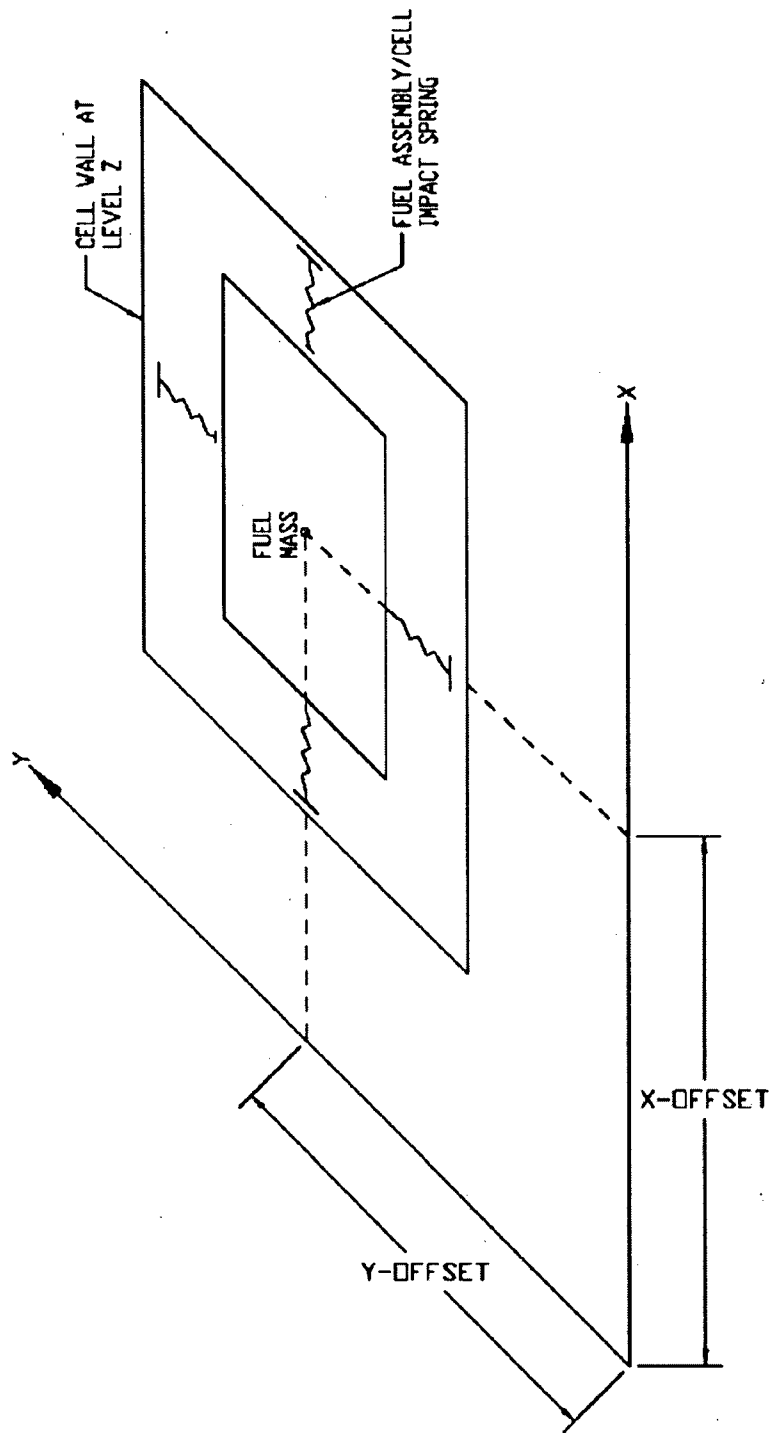


Figure 5.2: Fuel-to-Rack Impact Springs

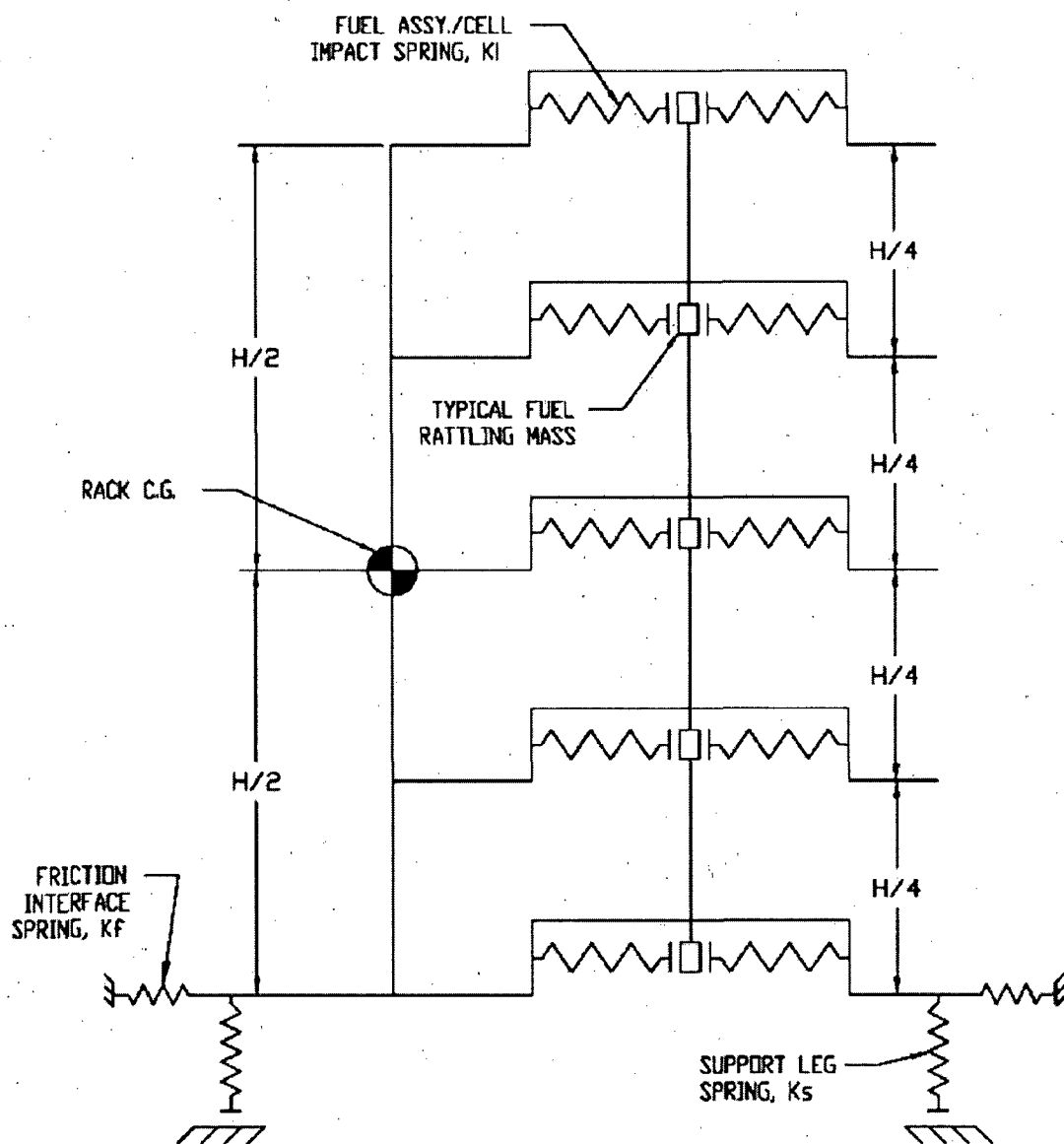
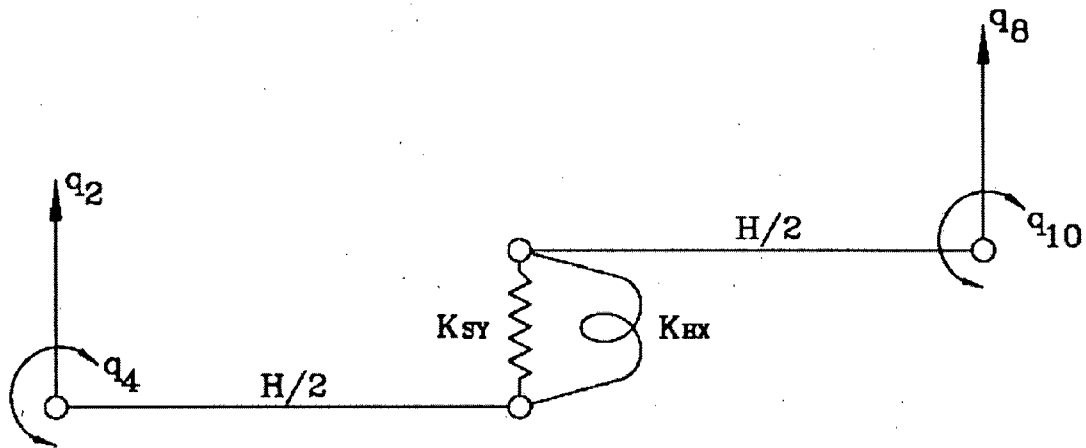


Figure 5.3: 2-D Schematic Elevation of the Storage Rack Model



RACK DEGREES-OF-FREEDOM FOR Y-Z PLANE BENDING
WITH SHEAR AND BENDING SPRING

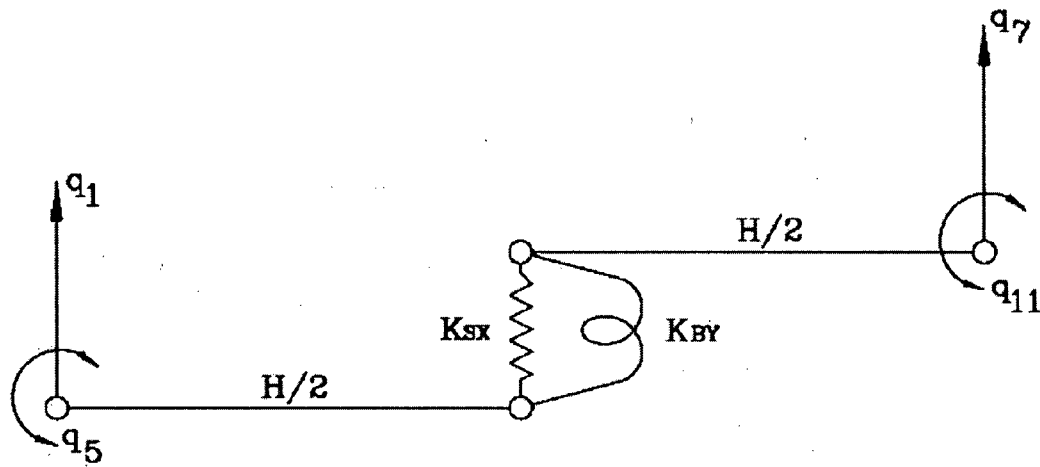


Figure 5.4: Rack Degrees of Freedom and Modeling Technique

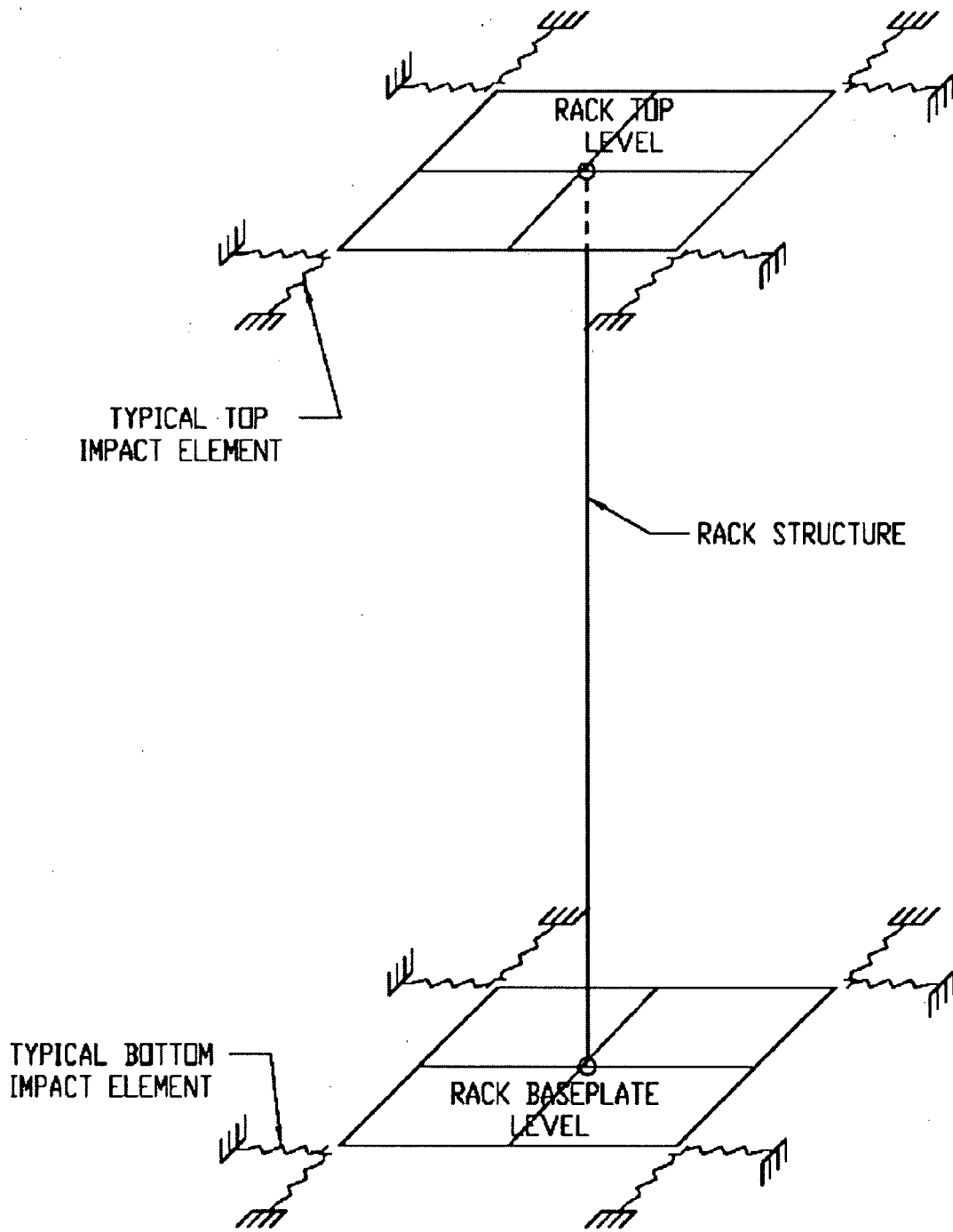


Figure 5.5: 2-D Inter-Rack Impact Springs

6.0 THERMAL-HYDRAULIC EVALUATION

6.1 Introduction

Beaver Valley Power Station (BVPS) Unit No. 2 is a Pressurized Water Reactor (PWR) nuclear power plant owned and operated by FirstEnergy Nuclear Operating Company (FENOC). The plant contains a Spent Fuel Pool (SFP) for holding offloaded spent fuel assemblies, with an attendant SFP cooling system (SFPCS). The SFP is currently equipped with spent fuel storage racks containing the neutron absorber Boraflex, which must be replaced. To maximize storage capacity, FENOC proposes to replace all of the existing racks with maximum density, non-flux-trap storage racks. In the reracked configuration, 15 new fuel racks are added to replace the removed racks. The total number of storage locations in the SFP will increase from 1088 to 1690.

This section provides a summary of the methods, models, analyses and numerical results to demonstrate that the BVPS Unit No. 2 spent fuel pool meets the thermal-hydraulic requirements for safe storage of spent fuel set forth in Section 6.2 herein. Similar thermal-hydraulic analyses have been used in spent fuel pool licensing at many nuclear plants worldwide (see Table 6.1.1 for a partial list).

The following specific thermal-hydraulic analyses for the BVPS Unit No. 2 SFP are performed:

1. Calculation of the spent fuel decay heat. The decay heat contributions from both previously stored (i.e., at least one cycle decay time) fuel assemblies and recently discharged fuel assemblies are considered.
2. Determination of the SFP bulk thermal response versus time in accordance with each discharge scenario.
3. Calculation of the time-to-boil during a postulated loss of forced cooling event for each discharge scenario.
4. A rigorous Computational Fluid Dynamics (CFD) based study to conservatively quantify the peak local water temperature in the SFP.
5. Determination of a bounding maximum fuel cladding temperature.

These analyses are described in detail in Sections 6.4 through 6.7. The following discharge scenarios are postulated and analyzed:

- Normal Full Core Offload [Case I]:

A full core (157 fuel assemblies) is transferred to the SFP at the end of a normal operating cycle starting after 100 hours of decay time at the rate of 6 assemblies per hour. The heat load from this recently discharged batch and the background heat load from previous discharges (a total of 1698 assemblies from 24 operating cycles) are removed by one SFPCS pump (the second pump is assumed a single active failure) and both SFPCS heat exchangers.

- Abnormal Full Core Offload [Case II]:

A full core (157 fuel assemblies) is transferred to the SFP starting after 100 hours of decay time at the rate of 6 assemblies per hour. A normal refueling is assumed to have occurred 36 days prior to the start of an abnormal shutdown. The heat load from this recent discharge and the background heat load from previous discharges (a total of 1698 assemblies from 24 operating cycles) are removed by both SFPCS pumps and both SFPCS heat exchangers.

- Loss of Cooling Scenario [Case III]:

Following each full core discharge, a loss of SFP cooling occurs. The spent fuel pool water surface is allowed to reach 212°F.

In the sections that follow, analysis methods are described, results are presented and discharge scenarios evaluated.

6.2 Acceptance Criteria

Applicable codes, standards and regulations include the following:

- a. NUREG-0800, Standard Review Plan, Section 9.1.3.
- b. USNRC OT Position Paper for Review and Acceptance of Spent Fuel Storage and Handling Application, 4/78 [6.2.1].

The design of the rack modules must ensure that fuel assemblies are adequately cooled by natural circulation of water for the bounding discharge conditions. The BVPS Unit No. 2 SFP storage is evaluated to the following criteria:

1. Under a normal full core offload with a single active SFPCS failure (Case I, refer to Section 6.1), the bulk pool temperature shall be limited to 170°F. Local temperatures in the rack cells shall be demonstrated to be below the local saturation temperature.
2. Under an abnormal full core offload without any SFPCS failures (Case II, refer to Section 6.1), the bulk pool temperature shall be limited to 173°F. Local temperatures in the rack cells shall be demonstrated to be below the local saturation temperature.
3. Under a loss of cooling scenario and a full core offload (Case III, refer to Section 6.1), the pool surface is allowed to reach 212°F. For a loss of cooling scenario, sufficient time must be available to restore cooling water flow to the SFP.

6.3 Assumptions and Design Data

6.3.1 Assumptions

The following assumptions are applied to render a conservative portrayal of thermal-hydraulic conditions in the BVPS Unit No. 2 SFP.

6.3.1.1 Maximum Bulk SFP Temperature and Minimum Time-To-Boil Calculation

1. On the basis of maximum storage capacity (1690 cells), a total of 1698 fuel assemblies from 24 operating cycles are assumed. This conservatively overstates the number of fuel assemblies in the pool under all analyzed scenarios (Case I through Case III).
2. Heat loss by conduction through the pool walls and by radiation cooling from the pool water surface is conservatively neglected.
3. The thermal capacity of the SFP is based on the net water volume only, completely neglecting the thermal capacity of the fuel assemblies, racks, liner and concrete SFP structure. The water in the cask area, which although separate can be in communication with the SFP, is also neglected. Since this assumption understates the SFP thermal capacity, it results in faster computed heat-up rates and shorter times-to-boil.

4. The decay heat load contribution of previously discharged (i.e., with at least one cycle decay time) fuel assemblies is assumed constant during all discharge scenarios. This assumption is conservative because it neglects the exponential decay of the heat generation from these old fuel assemblies.
5. All postulated (i.e., future) refueling batches are assumed to have a bounding exposure (62 GWD/MTU). This conservatively maximizes the decay heat load associated with these fuel assemblies.
6. The postulated full core offloads are assumed to have two regions. The first region, equivalent in size to a maximum refueling batch (e.g., 72 assemblies), is assumed to have a bounding exposure (62 GWD/MTU). The second region, comprising the remainder of the assemblies in the full core, has an exposure that bounds the average of once and twice burned assemblies (42.6 GWD/MTU). This conservatively maximizes the decay heat load associated with these fuel assemblies.
7. The loss of forced cooling of the SFP is assumed to occur when the maximum bulk SFP temperature for each discharge scenario occurs. This conservatively minimizes the time-to-boil.
8. The normal maximum fuel building temperature is assumed and is held constant for evaporative heat loss calculations. This conservatively minimizes credit for evaporative cooling of the spent fuel.
9. No credit is taken for evaporative heat losses in time-to-boil calculations. This conservatively maximizes the net SFP heat load.

6.3.1.2 Maximum Local Water and Fuel Clad Temperature Calculation

1. All passive losses (i.e., conduction through walls and slab or losses from the surface) are completely neglected. This conservatively maximizes the net heat load, maximizing both global and local temperatures.
2. All calculations are performed with the hydraulic resistance of the most resistive spent fuel assembly type in the most resistive storage rack type assigned to every rack storage location. This conservatively maximizes the overall hydraulic resistance of the rack.
3. No downcomer flow is assumed to exist between the rack modules.

4. The large flow holes in the rack base plate are not credited, and all rack cells are assumed to have the side flow hole geometry of the pedestal cells. This conservatively reduces the water flow area into the storage cells, thereby increasing the hydraulic resistance.
5. The hydraulic resistance of every rack cell in each spent fuel storage rack includes the inertial resistance that would result from a dropped fuel assembly lying across the top of the rack. This conservatively increases the total rack cell hydraulic resistance and bounds the thermal-hydraulic effects of a fuel assembly dropped anywhere in the spent fuel storage area.
6. The hottest fuel assemblies are assumed to be located together at the center of the spent fuel pool, conservatively maximizing the local decay heat generation rates.
7. Instead of explicitly modeling the pipes that supply and remove water from the SFP (and direct it into the SFP cooling system), the inlets and outlets are modeled as 4" high slots along the length of north and south SFP walls just below the water surface. As the mixing of relatively warmer and cooler water within the SFP is dominated by buoyancy effects, this geometric simplification should have no significant effect on the calculated results.
8. An additional heat transfer resistance of $0.0005 \text{ (hr}\times\text{ft}^2\times\text{°F)/Btu}$ is conservatively imposed on the outside of the fuel rods, to account for any crud layer, thereby increasing the calculated fuel clad superheat.
9. The maximum local water temperature (at the fuel rack cell exit) and peak heat flux (typically near the mid-height of the active fuel region) are considered to occur coincidentally. The superposition of these two maximum values ensures that the calculated peak fuel cladding temperature bounds the fuel cladding temperature anywhere along the length of the fuel assembly.

6.3.2 Design Data

6.3.2.1 Background Decay Heat Calculation

The decay heat calculations for both old and recently discharged fuel assemblies are performed using the ORIGEN2 computer program from Oak Ridge National Laboratory [6.2.2]. The cumulative background decay heat load from 1541 assemblies total from 23 operating cycles is conservatively assumed, at which time the ability to accommodate a full core discharge will be lost. To maximize decay heat, a bounding exposure is assumed for all fuel assemblies.

6.3.2.2 Maximum Bulk SFP Temperatures Calculation

The principal input data employed to determine the maximum SFP bulk temperature of the BVPS Unit No. 2 SFP is summarized in Table 6.3.1.

6.3.2.3 Maximum Local Water and Fuel Clad Temperature

In addition to the input data listed in Table 6.3.1, the principal input data employed for the local thermal-hydraulic analyses are presented in Table 6.3.2.

6.4 Fuel Rod Cladding Temperatures

The peak fuel rod cladding temperature is computed by following a series of calculation steps as outlined below:

Step 1: Compute the maximum local water temperature in the SFP for the stipulated discharge scenarios. This procedure is described in Section 6.7.

Step 2: Compute the maximum cladding to local water temperature difference (ΔT_c).

Step 3: Compute the peak fuel rod cladding temperature by adding ΔT_c to the maximum local water temperature.

The final results are discussed in Section 6.7. The procedure to perform Step 2 is presented next.

The maximum specific decay power of a single fuel assembly among the recently discharged batch of assemblies is denoted by Q_A . A fuel rod can produce f_z times the average heat emission rate over a small length, where f_z is the axial peaking factor. The axial heat distribution in a fuel rod is maximum in the central region, and tapers off at its two extremities. Thus, peak cladding heat flux per unit heat transfer area of fuel assembly is given by the equation:

$$q_{peak} = \frac{Q_A \times f_z}{A_{rod}}$$

where:

A_{rod} is the total external heat transfer area of the cladding in the active fuel region of a single fuel assembly, ft²

Within each fuel assembly sub-channel, water is continuously heated by the cladding as it moves axially upwards from bottom to top under laminar flow conditions. Rohsenow and Hartnett [6.4.1] report a Nusselt number, Nu, for heat transfer in a laminar flow situation through a heated channel. Nu is defined as follows:

$$Nu = \frac{h_c}{k_{water}} \times D_h = 4.364$$

$$h_c = 4.364 \times \frac{k_{water}}{D_h}$$

where:

k_{water} is the water thermal conductivity, Btu/(hr-ft-°F)

h_c is the laminar flow convective heat transfer coefficient, Btu/(hr-ft²-°F)

D_h is the sub-channel hydraulic diameter, ft

In order to introduce some additional conservatism in the analysis, we assume that the fuel cladding has a crud deposit thermal resistance, R_{crud} , that covers the entire surface. Therefore, the overall heat transfer coefficient U, considering a crud deposit resistance R_{crud} , can be defined by the following:

$$U = \frac{1}{\left(\frac{1}{h_c} + R_{crud} \right)}$$

The temperature drop, ΔT_c , between the outer surface of the fuel cladding and the water flowing up through the assembly at the peak cladding flux location is computed by the following:

$$\Delta T_c = \frac{q_{peak}}{U}$$

Finally, the maximum fuel rod temperature is defined by the following:

$$T_{rod} = T_{local} + \Delta T_c$$

where:

T_{rod} is the maximum fuel clad temperature
 T_{local} is the maximum local water temperature in the hottest cell calculated by the local temperature analysis (Section 6.7)

6.5 Description of Spent Fuel Pool Cooling System

The BVPS Unit No. 2 SFPCS is designed to remove the decay heat produced by spent fuel assemblies stored in the pool following a unit refueling and accumulated fuel from previous discharges. The system incorporates two 100% capacity cooling trains designed to maintain the SFP at or below 140°F with a component cooling water supply at 100°F under non-refueling conditions.

Each cooling train of the SFPCS incorporates a heat exchanger, pump, associated piping, valves, and instrumentation. Each cooling train is designed to service the SFP for the design-basis heat loads and to maintain the bulk temperature of the pool water below 140°F during non-refueling operation. The SFPCS transfers decay heat from stored fuel via the fuel pool heat exchanger to the component cooling water system.

The SFPCS heat exchangers are shell-and-tube construction. Spent fuel water circulates through the tubes while component-cooling water is circulated on the shell side. The use of two 100% capacity heat exchangers provides redundancy so that normal condition safety functions are unaffected by a single active failure. The design flow rates and inlet temperatures are provided in Table 6.3.1.

6.6 Heat Loads and Bulk Pool Temperatures

6.6.1 Background Decay Heat Load Calculation

An analysis is performed to calculate the accumulated decay heat of all previously discharged fuel assemblies (i.e., assemblies with at least one complete cycle of decay time) stored in the SFP

prior to recently discharged fuel assemblies. The decay heat is calculated using Oak Ridge National Laboratory's ORIGEN2 program [6.2.2]. The cumulative decay heat from previous discharges (P_{cons}) irradiated to a bounding exposure is computed as approximately 5.6 million Btu/hr for a normal full core offload and 6.0 million Btu/hr for an abnormal full core offload. The decay heat, P_{cons} , is included in the bulk pool temperature calculations as a constant background heat input as described next.

6.6.2 Maximum Bulk SFP Temperature Calculation

This analysis is performed to determine the transient SFP bulk temperature and decay heat profiles for the postulated discharge of fuel assemblies into the SFP.

The mathematical formulation for this analysis can be explained with reference to the simplified heat exchanger alignment shown in Figure 6.6.1. The governing differential equation for bulk pool temperature can be written by utilizing conservation of energy as:

$$C \times \frac{dT}{d\tau} = P_{cons} + Q(\tau) - Q_{HX}(T) - Q_{EV}(T, T_A)$$

where:

C	is the thermal capacity of water in the pool, Btu/°F
P_{cons}	is the heat generation rate from "old" fuel, Btu/hr
$Q(\tau)$	is the heat generation rate from recently discharged fuel vs. time, Btu/hr
$Q_{HX}(T)$	is the SFP cooling system heat rejection, Btu/hr
$Q_{EV}(T, T_A)$	is the evaporative and passive sensible heat losses, Btu/hr
T	is the bulk pool temperature, °F
T_A	is the fuel building ambient temperature, °F

The SFPCS heat rejection, $Q_{HX}(T)$ is defined by the following governing equation.

$$Q_{HX}(T) = W_C \times c_p \times p \times (T - T_C)$$

where:

W_C	is the coolant flow rate, lb/hr
c_p	is the coolant specific heat, Btu/(lb-°F)
p	is the temperature effectiveness of heat exchanger
T	is the bulk pool temperature, °F
T_C	is the coolant inlet water temperature, °F

The equation used to determine the temperature effectiveness, p of the SFPCS heat exchanger is as follows:

$$p = \frac{T_{Co} - T_C}{T_{Pi} - T_C}$$

where:

T_C is the cooling water inlet temperature, °F
 T_{Co} is the cooling water outlet temperature, °F
 T_{Pi} is the pool water inlet temperature, °F

A computer program used in the nuclear industry for heat exchanger thermal performance rating is used to calculate the temperature values for this equation. In performing thermal performance prediction evaluations, the inlet temperatures of each flow stream are inputs to the program. Thus, the only calculated value that is input to this equation is the coolant water outlet temperature (T_{Co}).

The SFP decay heat contribution from all previously stored fuel assemblies is held constant during the entire analysis because its decrease with decay time after shutdown can be conservatively neglected. The decay heat generation, $Q(\tau)$, of the recently discharged fuel will decay exponentially with elapsed time after reactor shutdown. The decay heat generation $Q(\tau)$ is a function of the elapsed time after reactor shutdown, number of fuel assemblies discharged, and in-core exposure time. For all discharge scenarios, the SFP decay heat contribution from the recently discharged fuel equals $Q(\tau)$.

The evaporative and passive sensible heat losses, $Q_{EV}(T, T_A)$, are a nonlinear function of pool temperature (T) and ambient temperature (T_A), and include cooling by evaporation and natural convection heat transfer from the pool surface. The evaporation and passive sensible heat loss can be expressed as [6.6.1]:

$$Q_{EV}(T, T_A) = hA_S(T - T_A) + \varepsilon\sigma A_S(T^4 - T_A^4) + \alpha A_S(P_w - P_a)$$

where:

T is the temperature of the pool water, °R
 h is the natural convection heat transfer coefficient, Btu/(hr-ft²-°R)

A_S is the water surface area, ft²
 T_A is the fuel building ambient temperature, °R
 ϵ is the emissivity of water
 σ is the Stefan-Boltzman constant, Btu/(hr-ft²-°R⁴)
 α is the evaporation rate constant, Btu/(hr-ft²-psi)
 P_w is the vapor pressure of water at the bulk temperature, psi
 P_a is the vapor pressure of water at the building temperature, psi

The results of the maximum bulk pool temperature analyses for the discharge scenarios are summarized in Table 6.6.1. The results demonstrate that bulk pool water temperatures remain below the prescribed limits during fuel discharges. These results comply with the acceptance criteria set forth in Section 6.2.

The decay heat load profiles and the bulk pool temperatures in the spent fuel pool as functions of time (after reactor shutdown) are shown in Figures 6.6.2 and 6.6.3 for the normal and abnormal full-core discharge scenarios, respectively. The maximum pool decay heat is reached upon completion of fuel transfer. The thermal inertia of the pool water delays the bulk pool temperature maximum, the lag being a direct result of the system thermal capacitance. The coincident time to the maximum temperature is the summation of in-core hold time, fuel transfer time and the lag time.

6.6.3 Minimum Time-To-Boil Calculation

This analysis is to determine the time that it takes for the pool water to boil, in case all forced cooling becomes unavailable. Clearly, the most critical instant of loss-of-cooling is when the pool water temperature has reached its maximum value. Although the probability of a loss-of-cooling event occurring when the pool water is hottest is low, the calculations are performed based on the hottest possible initial temperature. The following differential equation governs the thermal response of the water in the spent fuel pool without including the heat rejection terms.

$$C(\tau) \times \frac{dT}{d\tau} = P_{cons} + Q(\tau)$$

where:

$C(\tau)$ is the time-varying thermal capacity of the pool, Btu/°F

P_{cons} is the heat generation rate from “old” fuel, Btu/hr
 $Q(\tau)$ is the heat generation rate from recently discharged fuel vs. time, Btu/hr
 T is the bulk pool temperature, °F

The time-to-boil calculations are conservatively performed assuming no makeup water is available. The time-to-boil results are summarized in Table 6.6.2. The results show that a minimum of nearly 2 hours is required for the pool water to start boiling (reach 212°F). For a scenario of loss of all spent fuel pool cooling, sufficient time would be available for necessary repairs or to implement alternate cooling or makeup water.

6.7 Local Water and Fuel Cladding Temperatures

The objective of the local temperature analysis is to demonstrate that the principal thermal-hydraulic criteria of ensuring local subcooled conditions in the pool are met for all scenarios. Adequate cooling of recently discharged fuel in the fuel pool is demonstrated by performing a rigorous evaluation of the velocity and temperature fields in the pool created by the interaction of buoyancy driven flows and water injection/egress. A 3-Dimensional Computational Fluid Dynamics (CFD) analysis for this demonstration is implemented.

There are several significant geometric and thermal-hydraulic features of the BVPS Unit No. 2 SFP that need to be considered for a rigorous CFD analysis. From a fluid flow-modeling standpoint, there are two regions to be considered. One region is the bulk pool region where the classical Navier-Stokes equations are solved with turbulence effects included. The other region is the heat-generating zone of spent fuel storage racks loaded with fuel assemblies, located near the SFP bottom. In this region, water flow is directed vertically upwards by the buoyancy forces through relatively small flow channels formed by the fuel assembly rod arrays in each rack cell. This situation is modeled as a porous medium region in which Darcy’s Law [6.7.1] governs fluid flow.

The distributed heat sources in the spent fuel pool racks are modeled by identifying distinct heat generation zones considering full-core discharge, peaking effects, and presence of background decay heat from old discharges. Three heat generating zones were modeled. The first consists of

background fuel assemblies from previous discharges, while the remaining two zones are for fuel assemblies recently discharged from the reactor. This is a conservative model, since all recently discharged fuel assemblies with higher than average decay heats are postulated to be placed in a contiguous area.

The CFD analysis is performed using the FLUENT [6.7.2] fluid flow and heat transfer modeling program. The FLUENT code enables buoyancy flow and turbulence effects to be included in the CFD analysis. Turbulence effects are modeled by relating time-varying “Reynolds’ Stresses” to the mean bulk flow quantities by the standard k - ϵ turbulence model.

A single local temperature scenario that bounds both the normal and abnormal full core offload conditions defined in Section 6.2 is considered. A solution of the CFD model is performed to obtain the SFP flow and temperature fields. Temperature contours in a vertical plane through the hottest fuel assemblies are shown in Figure 6.7.1. The plot confirms that hot fuel is safely and reliably cooled by natural convection action. Local hot spots induced by water circulation in the racks are rapidly dissipated in the pool water resulting in a nearly uniform temperature distribution away from the hot racks. The bounding local water temperature in the SFP racks and the fuel clad superheat for the bounding scenario are summarized in Table 6.7.1. At the top of the active fuel, the local saturation temperature is approximately 240°F. From the local water and fuel cladding temperature results, it is concluded that local water and fuel cladding temperatures remain below saturation.

During installation of the new racks in the SFP, one new rack will temporarily be placed in the cask pit to provide additional fuel storage space. This is needed to provide enough fuel storage space to permit emptying existing racks for removal. Only fuel assemblies with significant cooling time may be placed in the rack in the cask pit. As part of the new rack installation sequence, all fuel in the rack in the cask pit will be shuffled into the SFP and the rack moved to its final position in the SFP. An additional CFD model of the rack in the cask pit was constructed and analyzed, and demonstrated that the rack in cask pit condition is bounded by the normal condition with all racks in the SFP.

6.8 References

- [6.2.1] "OT Position Paper for Review and Acceptance of Spent Fuel Storage and Handling Applications," April 14, 1978.
- [6.2.2] A. G. Croff, "ORIGEN 2 – A Revised and Updated Version of the Oak Ridge Isotope Generation and Depletion Code," ORNL-5621, Oak Ridge National Laboratory, 1980.
- [6.4.1] Rohsenow, W.M. and J.P. Hartnett, "Handbook of Heat Transfer," McGraw Hill Book Company, NY, 1973.
- [6.6.1] Holtec Report HI-971664, "An Improved Correlation for Evaporation from Spent Fuel Pools", Revision 0.
- [6.7.1] "Flow of Fluids Through Valves, Fittings, and Pipe," Crane Technical Paper No. 410, Crane Valve Company, Twenty-Second Printing, 1985.
- [6.7.2] FLUENT Computational Fluid Dynamics Software, Fluent Inc., Centerra Resource Park, 10 Cavendish Court, Lebanon, NH 03766.

Table 6.1.1 PARTIAL LISTING OF RERACK APPLICATIONS USING SIMILAR METHODS OF THERMAL-HYDRAULIC ANALYSIS	
PLANT	DOCKET NO.
Enrico Fermi Unit 2	USNRC 50-341
Quad Cities 1 and 2	USNRC 50-254, 50-265
Rancho Seco	USNRC 50-312
Grand Gulf Unit 1	USNRC 50-416
Oyster Creek	USNRC 50-219
Pilgrim	USNRC 50-293
V.C. Summer	USNRC 50-395
Diablo Canyon Units 1 and 2	USNRC 50-275, 50-455
Byron Units 1 and 2	USNRC 50-454, 50-455
Braidwood Units 1 and 2	USNRC 50-456, 50-457
Vogtle Unit 2	USNRC 50-425
St. Lucie Unit 1	USNRC 50-425
Millstone Point Unit 1	USNRC 50-245
D.C. Cook Units 1 and 2	USNRC 50-315, 50-316
Indian Point Unit 2	USNRC 50-247
Three Mile Island Unit 1	USNRC 50-289
J.A. FitzPatrick	USNRC 50-333
Shearon Harris Unit 2	USNRC 50-401
Hope Creek	USNRC 50-354
Kuosheng Units 1 and 2	Taiwan Power Company
Ulchin Unit 2	Korea Electric Power Corp.
Laguna Verde Units 1 and 2	Comision Federal de Electricidad
Zion Station Units 1 and 2	USNRC 50-295, 50-304
Sequoyah	USNRC 50-327, 50-328
La Salle Unit One	USNRC 50-373

Table 6.1.1 (continued)	
PARTIAL LISTING OF RERACK APPLICATIONS USING SIMILAR METHODS OF THERMAL-HYDRAULIC ANALYSIS	
PLANT	DOCKET NO.
Duane Arnold	USNRC 50-331
Chin Shan Units 1 and 2	Taiwan Power Company
Fort Calhoun	USNRC 50-285
Nine Mile Point Unit One	USNRC 50-220
BVPS Unit No. 1	USNRC 50-334
Limerick Unit 2	USNRC 50-353
Ulchin Unit 1	Korea Electric Power Corp.
J.A. Fitzpatrick	USNRC 50-333
Callaway	USNRC 50-483
Byron/Braidwood	USNRC 50-454, 50-455, 50-567, 50-457
Wolf Creek	USNRC 50-482
Hatch Units 1 & 2	USNRC 50-321, 50-366
Harris Pools C and D	USNRC 50-401
Waterford 3	USNRC 50-382

Table 6.3.1 SUMMARY OF INPUTS FOR BULK TEMPERATURE ANALYSIS	
INPUT DATA	VALUE
SFP Exchanger Coolant Flow Rate (total for two exchangers)	1,094,020 lb/hr
SFP Exchanger Inlet Temperatures	100°F (Coolant) 140°F (SFP Water)
Pool Nominal Dimensions	North Wall: 471 in South Wall: 304 in East Wall: 260 in West Wall: 351 in
Minimum Water Depth of SFP	38.5 ft
Nominal Height of Spent Fuel Racks	180 3/4 in
Reactor Thermal Power (including uncertainty)	2918 MW
Reactor Core Size	157 assemblies
Fuel Building Temperature	96°F (Maximum Normal)
In-Core Hold Time	100 hr
Fuel Transfer Rate	6 per hour
Maximum Refueling Batch Size	72 assemblies
Cycle Length	18 months
Number of Fuel Storage Cells	1690

Table 6.3.2

SUMMARY OF INPUTS FOR LOCAL TEMPERATURE ANALYSIS

INPUT DATA	VALUE
Rack-to-Wall Gaps North Wall South Wall East Wall West Wall	4 in 9 in 2 in 4 in
Rack Bottom Plenum Height	11 3/8"
Rack Baseplate + Cell Height	169 3/8"
Active Fuel Length	144 in
Fuel Assembly Array Size	17x17
Rack Cell Pitch	9.03 in
Minimum Rack Cell Nominal ID	8.8 in
Number of Side Holes per Cell	4
Pedestal Cell Side Hole Diameter	1 1/2"
Assembly Axial Peaking Factor	1.55

Table 6.6.1 SUMMARY OF BULK POOL TEMPERATURE RESULTS			
Discharge Scenario	Maximum SFP Bulk Temperature (°F)	Coincident Time After Shutdown (hrs)	Coincident Net SFP Heat Load (Btu/hr)
Normal Full Core (Case I)	169.0	135	36.13×10^6
Abnormal Full Core (Case II)	169.8	134	42.83×10^6

Table 6.6.2
SUMMARY OF TIME-TO-BOIL RESULTS

Discharge Scenario	Time-to-Boil (hrs)	Time-to-10' Above Racks (hrs)	Max. Water Loss (gpm)
Normal Full Core (Case I)	2.35	25.4	77.1
Abnormal Full Core (Case II)	1.94	21.2	91.6

Table 6.7.1

SUMMARY OF LOCAL TEMPERATURE RESULTS

Parameter	Calculated Value
Maximum Water Temperature (°F)	202.8
Cladding Superheat (°F)	24.9
Peak Cladding Temperature (°F)	227.7

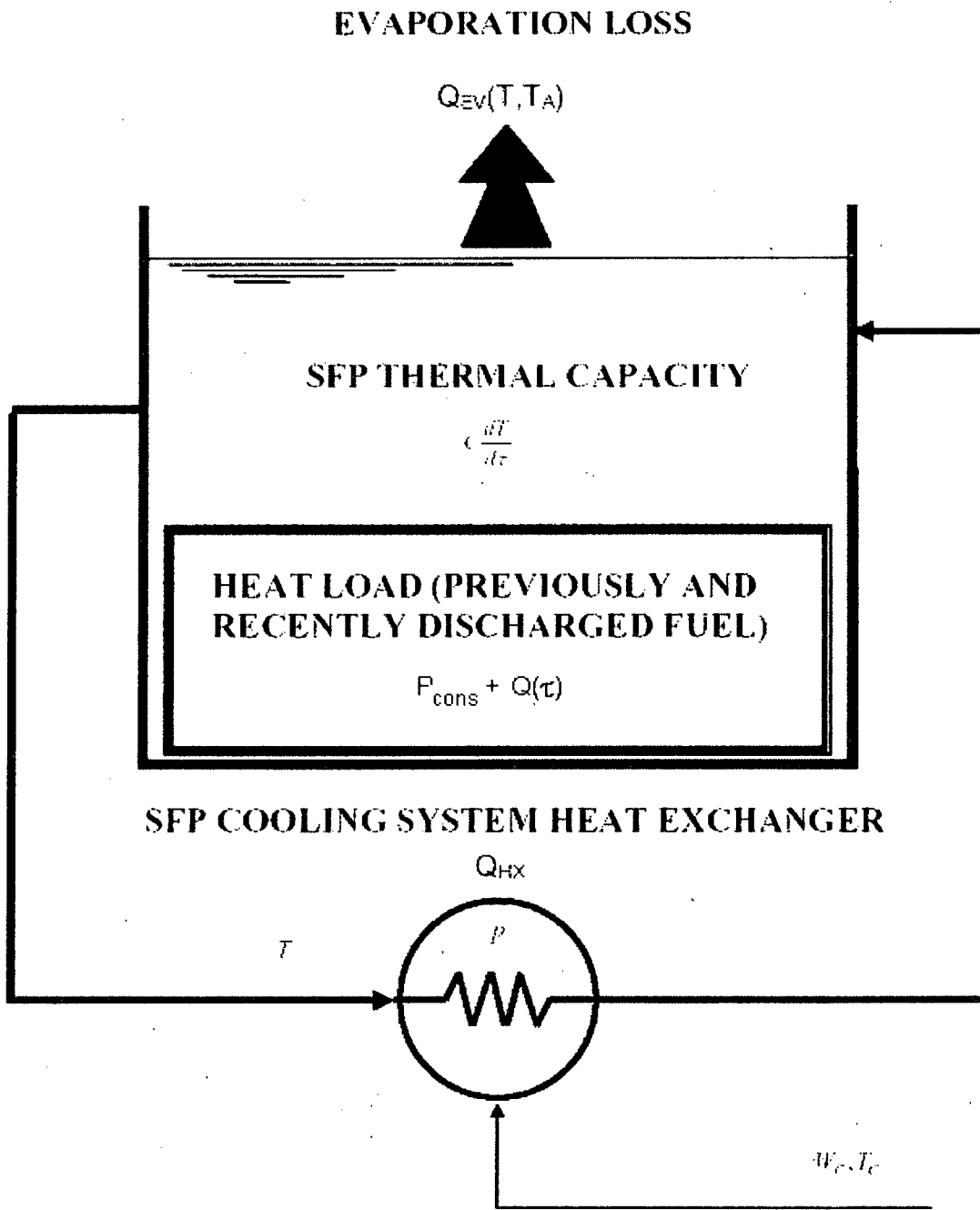


Figure 6.6.1: Simplified Heat Exchanger Alignment

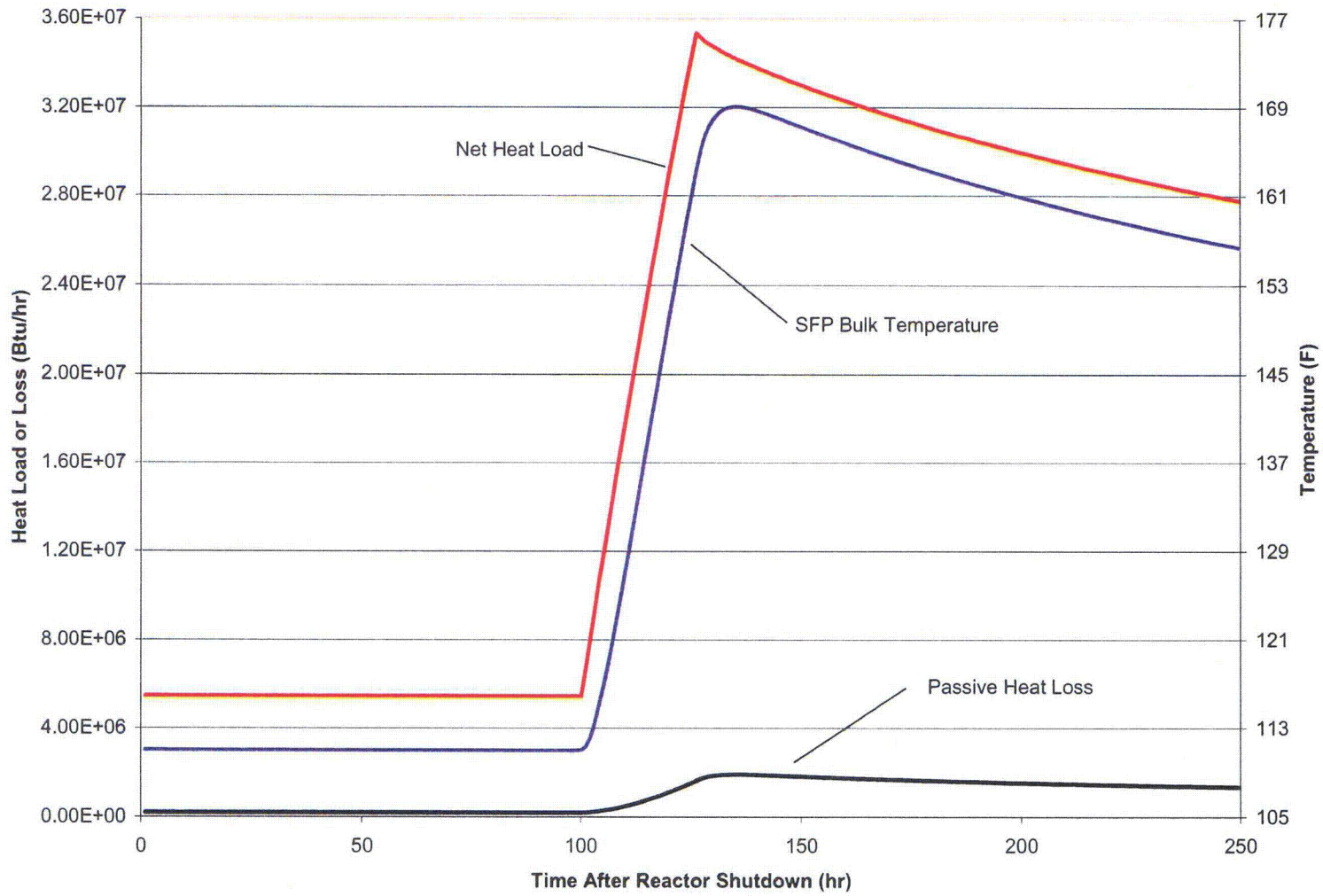


Figure 6.6.2: SFP Bulk Temperature, Net SFP Heat and Passive Heat Loss Profiles – Normal Full Core

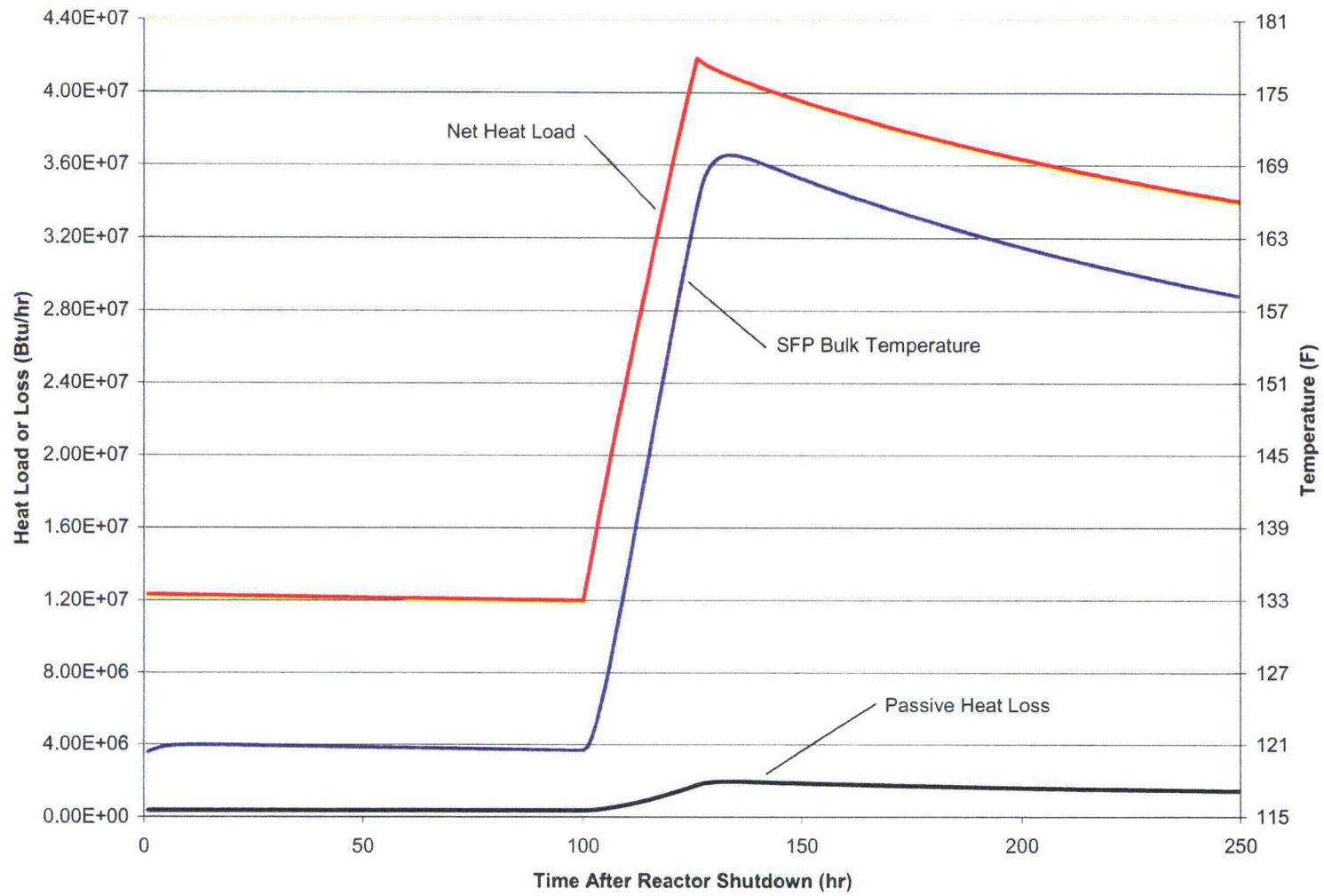
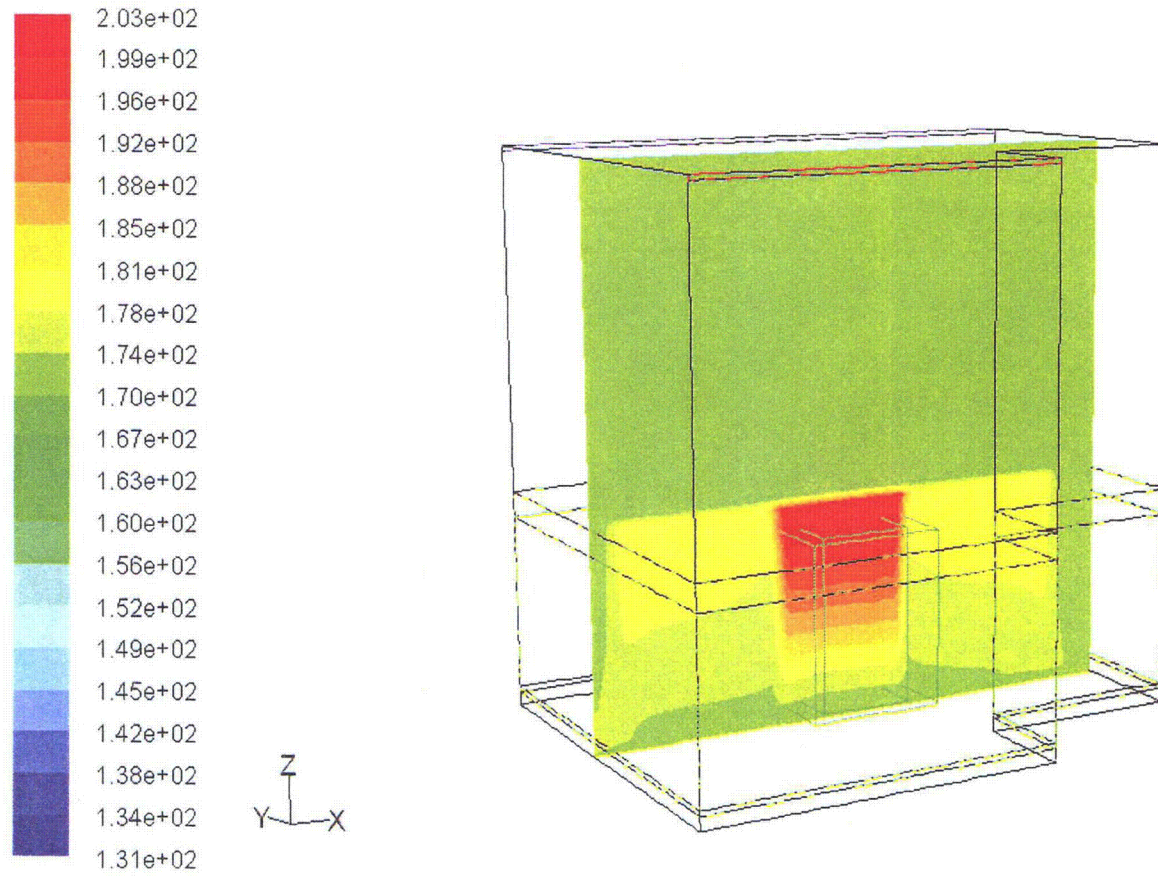


Figure 6.6.3: SFP Bulk Temperature, Net SFP Heat and Passive Heat Loss Profiles – Abnormal Full Core



Contours of Static Temperature (f)

Mar 09, 2009
 FLUENT 6.3 (3d, dp, pbns, ske)

Figure 6.7.1: Contours of Static Temperature in a Vertical Plane through the Center of the SFP

7.0 MECHANICAL ACCIDENTS CONSIDERATIONS

7.1 Introduction

The USNRC OT position paper [7.1.1] specifies that the design of the rack must ensure the functional integrity of the spent fuel racks under all credible fuel assembly drop events.

This section contains synopses of the analyses carried out to demonstrate the regulatory compliance of the proposed racks under postulated accidental drop events [7.1.2] germane to the fuel pools; namely, that of a fuel assembly, a fuel rack and a gate. Detailed analyses are documented in Ref. [7.1.3].

7.2 Description of Mechanical Accidents

Several categories of accidental drop events are considered. Fuel drop evaluations are performed to evaluate the racks subsequent to a fuel assembly impact. The pool structure is evaluated for the drop of a fuel rack during installation. A pool gate drop is also evaluated to assess damage to the rack. Additionally, damage to the fuel assembly as a result of dropping of a fuel assembly on top of a stored fuel assembly in the rack is also considered and evaluated. Additional evaluations were also performed to consider the ability of the rack to withstand the uplift force from a stuck fuel assembly.

In the so-called "shallow" drop event, a fuel assembly, along with the portion of handling tool, which is severable in the case of a single element failure, is assumed to drop vertically and hit the top of the rack. Additionally, a dropping of the pool gate is also postulated wherein the gate is assumed to be dropped over a rack to determine the extent of damage to the rack. Inasmuch as the new racks are of honeycomb construction, the deformation produced by the impact is expected to be confined to the region of collision. However, the "depth" of damage to the affected cell walls must be demonstrated to remain limited to the portion of the cell above the top of the "active fuel region", which is essentially the elevation of the top of the neutron absorber.

Stated in qualitative terms, this criterion implies that the plastic deformation of the rack cell walls should not extend more than 19.75 inches nom. (downwards) from the top. In order to utilize an upper bound of kinetic energy at impact, the impactor (fuel assembly including the handling tools) is conservatively assumed to weigh 2,450 lbs and the free-fall height is assumed to be 24 inches. Similarly, the pool gate weighing 4,020 lbs is assumed to free fall from the height of 24”.

It is readily apparent from the description of the rack modules in Section 3 that the impact resistance of a rack at its periphery is considerably less than its interior. Accordingly, the limiting shallow drop scenario, which would produce maximum cell wall deformation, is the case where the fuel assembly impacts the peripheral cell wall, as shown in Figure 7.2.1.

The second class of fuel drop event postulates that the impactor falls through an empty storage cell impacting the fuel assembly support surface (i.e., rack baseplate). This so-called “deep” drop event threatens the structural integrity of the baseplate. If the baseplate is pierced and the fuel assembly impacts the pool liner, then an abnormal condition may develop where the enriched zone of fuel assembly is outside the “poisoned” space of the fuel rack. To preclude damage to the pool liner and to avoid the potential of an abnormal fuel storage configuration in the aftermath of a deep drop event, it is required that the baseplate remain unpierced and that the maximum lowering of the baseplate is considered in the criticality evaluations.

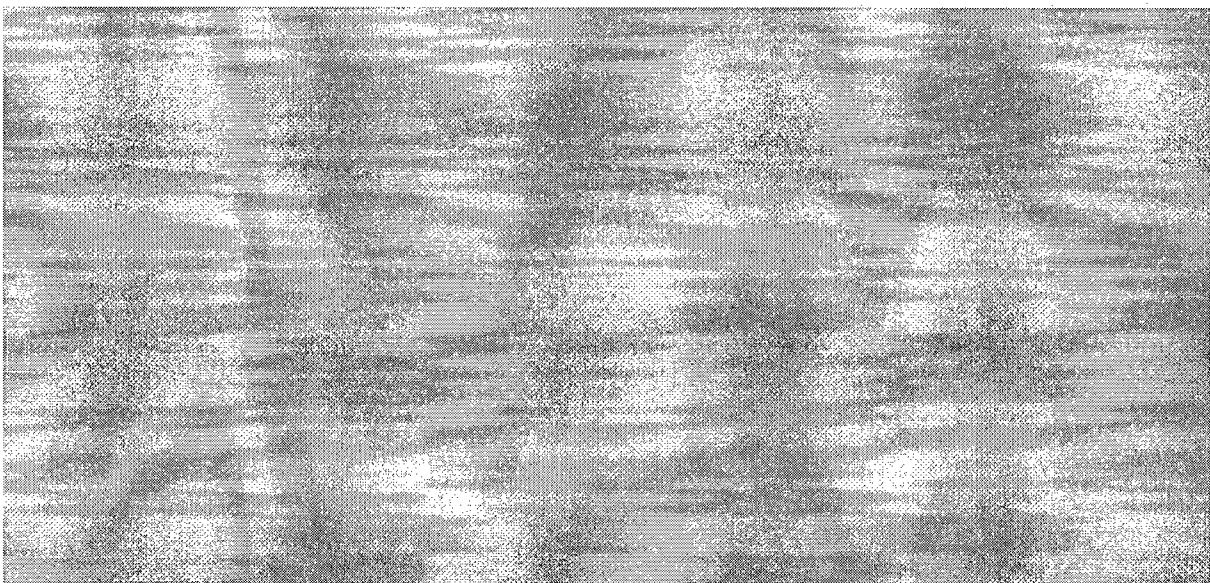
The deep drop event can be classified into two scenarios, namely, drop in an interior cell away from the support pedestal (Scenario 1), as shown in Figure 7.2.2, and drop through cell located above a support leg (Scenario 2), as shown in Figure 7.2.3. In deep drop scenario 1, the fuel assembly impacts the baseplate away from the support pedestal, where it is more flexible. Severing or large deflection of the baseplate leading to a secondary impact with the pool liner are unacceptable results. In deep drop scenario 2, the baseplate is buttressed by the support pedestal and presents a hardened impact surface, resulting in a high impact load. The principal design objective is to ensure that this accident does not compromise the structural integrity of the SFP floor liner leading to uncontrollable water leakage.

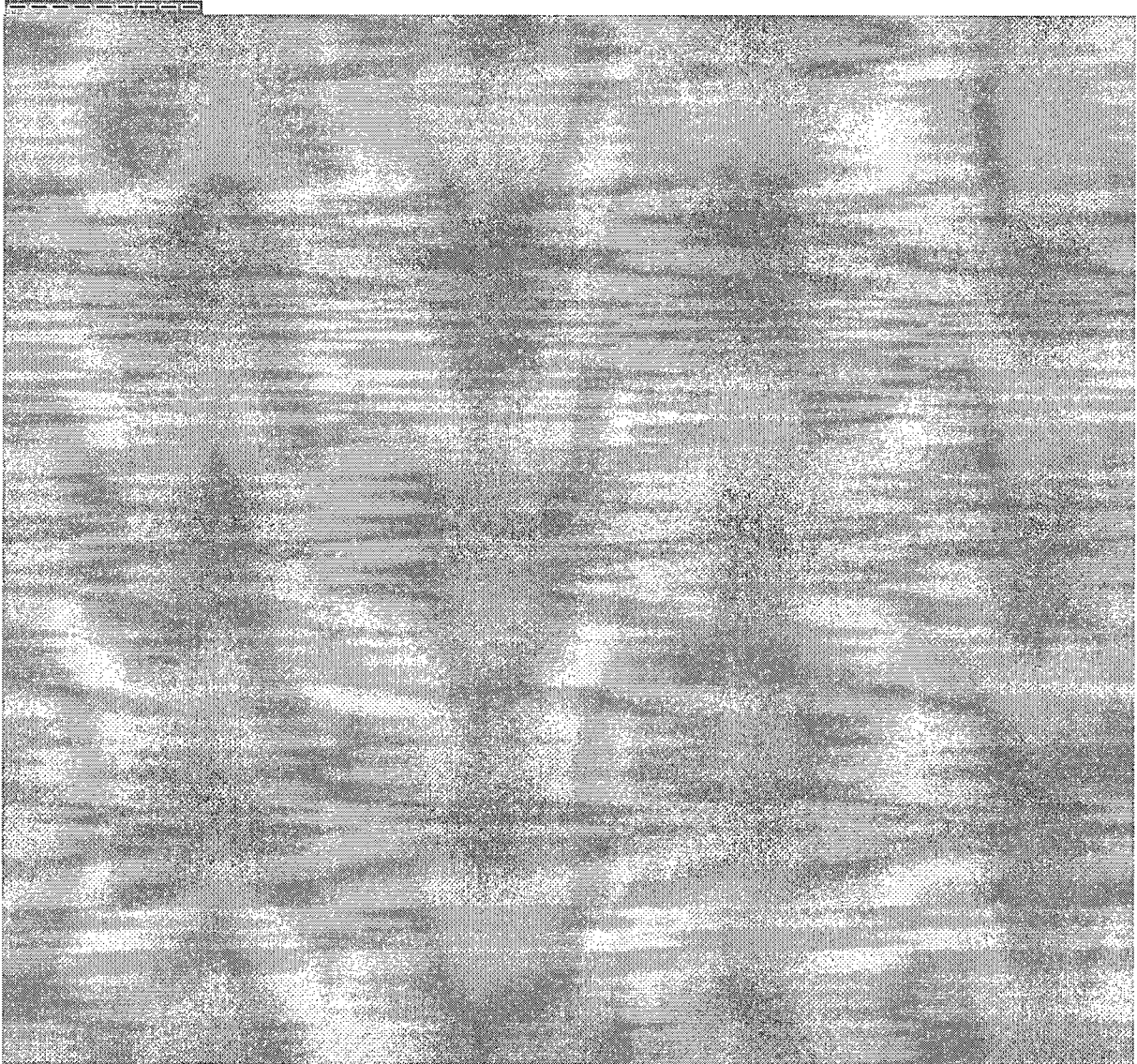
In the third type of drop event, a rack is assumed to drop from the top water level in the pool and hits the pool floor, as shown in Figure 7.2.4. A representative model of the heaviest rack in the pool is used for the rack drop analysis. The structural integrity of the concrete floor must be demonstrated to be maintained in the rack drop event, and the effect on the liner plate is also evaluated. The acceptance criterion is that catastrophic pool structure damage, such that there is rapid loss of pool water inventory, is not allowed. In addition to the fuel and rack drops, the consequences of a potential gate drop onto the rack is also considered.

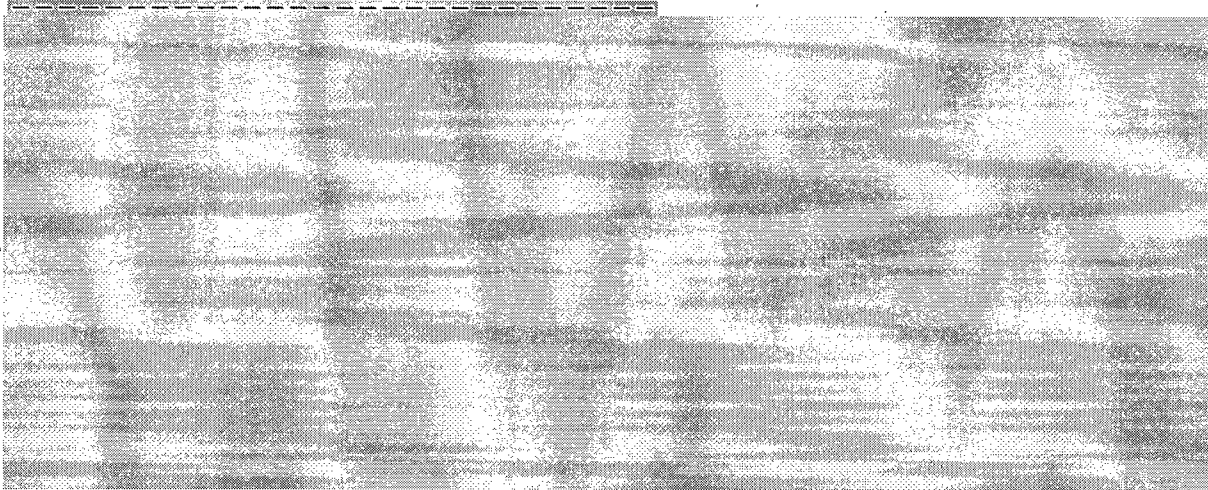
The last type of drop event is the postulated drop of a fuel assembly on top of a stored fuel assembly in the rack. The principal design objective is to ensure that this accident does not cause catastrophic damage (i.e. failure of all rods) to the fuel assembly.

In addition to the above drop events, the structural integrity of rack cell walls under the uplift load caused by a postulated stuck fuel assembly is also evaluated. The rack cell wall must be able to withstand this load without deforming the rack cell such that it does not adversely affect the integrity of the neutron absorber and thus affects the subcriticality of stored fuel array.

7.3 Incident Impact Velocity







7.4 Mathematical Model

In the first step of the solution process, the velocity of the dropped object (impactor) is computed for the condition of underwater free fall in the manner of the formulation presented in the above section. Table 7.4.1 contains the computed velocities for the various drop events.

In the second step of the solution, an elasto-plastic finite element model for each drop event is prepared with the Holtec QA validated computer Code LS-DYNA. The model simulates the transient collision event with full consideration of plastic, large deformation, wave propagation, and elastic/plastic buckling modes.

In the “shallow” and the “deep” drop events, the fuel assembly is modeled by an equivalent elasto-plastic rod with a concentrated mass (representing the handling tool) and a properly modeled rigid end-fitting at its two extremities. The structurally weakest impact region is considered in performing the “shallow” and the “deep” drop analysis. Shell elements are used to model the thin cell walls and weld connections. The rack baseplate is modeled with thick shell elements. Moreover, the rack support female block and pedestal are modeled with solid elements. Other structural components, such as the liner and concrete slab, are also properly modeled with elasto-plastic shell and solid elements in all drop events. For the fuel-to-fuel impact drop event (for fuel damage evaluation), the fuel assembly’s fuel rods and guide tubes are explicitly modeled using beam elements, and the rack is represented by a single storage cell (with its bottom end nodes fully constrained), which provides lateral supports to the deformed

fuel rods. The physical properties of material types undergoing deformation in the postulated impact events are summarized in Table 7.4.2.

7.5 Results

7.5.1 Shallow Drop Event

For the shallow drop event, the dynamic analysis shows that the top of the impacted region undergoes localized plastic deformation. Figure 7.5.1 shows an isometric view of the post-impact geometry of the rack. The maximum depth of plastic deformation is limited to less than 18 inches, which is below the design limit of 19.75 inches as shown in Figure 7.5.1.

The vertical gate drop accident will involve at least three rack cells because of the dimensions of the gate; a gate drop accident hitting only a periphery cell wall would lead to immediate gate rotation because the gate width is more than three times the size of the rack cell. However, the impact energy of the gate is only about 1.4 times that of the fuel assembly in the shallow drop event. Therefore, it can be concluded that the gate drop accident is bounded by the shallow drop event in terms of the depth of permanent deformation measured from the top of the rack.

7.5.2 Deep Drop Events

The deep drop through an exterior cell does produce some deformation of the baseplate and localized severing of the baseplate/cell wall welds. Figure 7.5.2 shows the deformed baseplate configuration. However, the fuel assembly support surface is lowered by less than 2 inches, which is much less than the distance of the baseplate to the liner. Therefore, the pool liner will not be contacted by the deformed baseplate. The lowering of the baseplate has been considered in the criticality evaluation and is specifically addressed in Section 4 of this report.

7.5.3 Rack Drop Event

The maximum plastic strain of the SFP floor liner caused by the rack drop is calculated to be 0.0524, as shown in Figure 7.5.3, which is well below the failure strain of 0.4 for the liner

stainless steel material, indicating that there is no rupture of the liner and hence, no loss of water after the rack drop event. The SFP floor slab does, however, experience limited localized damage as shown in Figure 7.5.4 due to excessive compressive stress resulting from the impact load at the pedestal/liner interface. However, the localized damage does not represent any structural threat to the SFP slab. In addition, the dropped rack also experiences local plastic deformation in the cells adjacent to the pedestal as expected.

7.5.4 Uplift Force Evaluation

The uplift force evaluation shows that the rack is able to withstand the vertical uplift force of 5,000 pounds. Results of the analysis show that the maximum stress in the rack cell as a result of trying to pull the stuck fuel assembly out is only 6,500 psi which is well below the material yield strength. Therefore, the fuel racks are adequate to withstand a 5,000 lbf uplift load due to a stuck fuel assembly.

7.5.5 Fuel to Fuel Drop Event

The total number of damaged fuel rods damaged resulting from an impact of a stored fuel assembly in the rack by a dropped fuel assembly is calculated to be ten fuel rods for a drop height of 24" above the top of the rack. Figure 7.5.5 shows the deformed shape of the damaged fuel rods. The fuel damage in this Fuel to- Fuel Drop Event is bounded by the existing Fuel Handling Accident Analysis provided for Beaver Valley Unit 2 License Amendment No. 121.

7.6 Conclusion

The drop accident events postulated for the Beaver Valley Power Station (BVPS) Unit No. 2 fuel pool were analyzed and found to produce localized damage well within the design limits for the racks. The shallow drop event is found to produce some localized plastic deformation in the top of the storage cell, but the region of permanent strain is limited to the portion of the rack structure situated above the top of the active fuel region. The analysis of the deep drop event at cell locations selected to maximize baseplate deformation indicates that the downward displacement of the baseplate is limited to less than 2 inches, which ensures that a secondary impact of the fuel assembly with the pool liner would not occur. Rack drop analysis shows that the concrete slab can maintain its structural integrity under the postulated impact of the heaviest rack in the pool. Only local concrete crushing is observed. The rack uplift force evaluation shows that configuration of the fuel and poison (Metamic) is not compromised from the configurations analyzed in the criticality evaluations discussed in Section 4.0. Additionally, it is demonstrated that the damage to the fuel assembly rods from the fuel-to-fuel impact drop is not severe.

It is therefore concluded that the new Holtec high-density spent fuel racks for the BVPS Unit No. 2 fuel pool possess acceptable margins of safety under the postulated mechanical accidents.

7.7 References for Section 7

- [7.1.1] "OT Position for Review and Acceptance of Spent Fuel Storage and Handling Applications," dated April 14, 1978, and addendum dated 1979.
- [7.1.2] "Specification for Spent Fuel Storage Racks Replacement – Beaver Valley Unit 2", Design Specification No. 10080-DMS-0505, Rev. 1 (Holtec Report No. HI-2073792, Rev. 2).
- [7.1.3] "Mechanical Drop Accident Analyses Supporting Beaver Valley Unit 2 Reracking Project," Holtec Report HI-2084010, Rev. 1.
- [7.1.4] "Summary and Evaluation of Low-Velocity Impact Tests of Solid Steel Billets onto Concrete Pads," Lawrence Livermore National Laboratory, UCRL-ID-129211, February 1998. Prepared for the NRC and also appears as NUREG /CR-6608.

Table 7.4.1

IMPACT EVENT DATA

Case	Impactor Weight (lb)	Impactor Type	Drop Height (in)	Impact Velocity (in/sec)
1. Shallow drop event	2,450	Fuel assembly	24 inches above the top of rack	129.2
2. Deep drop event scenario 1 (away from pedestal)	2,450	Fuel assembly	„	275.6
3. Deep drop event scenario 2 (above pedestal)	2,450	Fuel assembly	„	105.8
4. Rack drop event	24,700	Rack	From top of water level in the pool	222.0
5. Gate drop event	4,020	Gate	24 inches above the top of rack	119.1
6. Fuel assembly on Fuel assembly drop scenario 2 (above rack)	2,450	Fuel Assembly	24 inches above the top of rack	129.2

Table 7.4.2

MATERIAL DEFINITION

Material Name	Material Type	Density (pcf)	Elastic Modulus (psi)	Stress		Strain	
				First Yield (psi)	Failure (psi)	Elastic	Failure
Stainless Steel Rack Walls, Rack Female Pedestal and Spent Fuel Pool Liner	SA240-304L	490	2.799e+07	2.270e+04	6.805e+04	8.110e-04	4.000e-01
Zircaloy Fuel Cladding	--	404	1.040e+07	8.05e+04	9.20e+04	7.740e-03	2.000e-02
Stainless Steel Male Pedestal	SA564-630	490	2.823e+07	1.092e+05	1.400e+05	3.868e-02	1.400e-01
Concrete†	$f_c=4,000$ psi	150	3.605e+06	--	--	--	--

† The concrete is modeled as recommended in NUREG /CR-6608 [7.1.4].

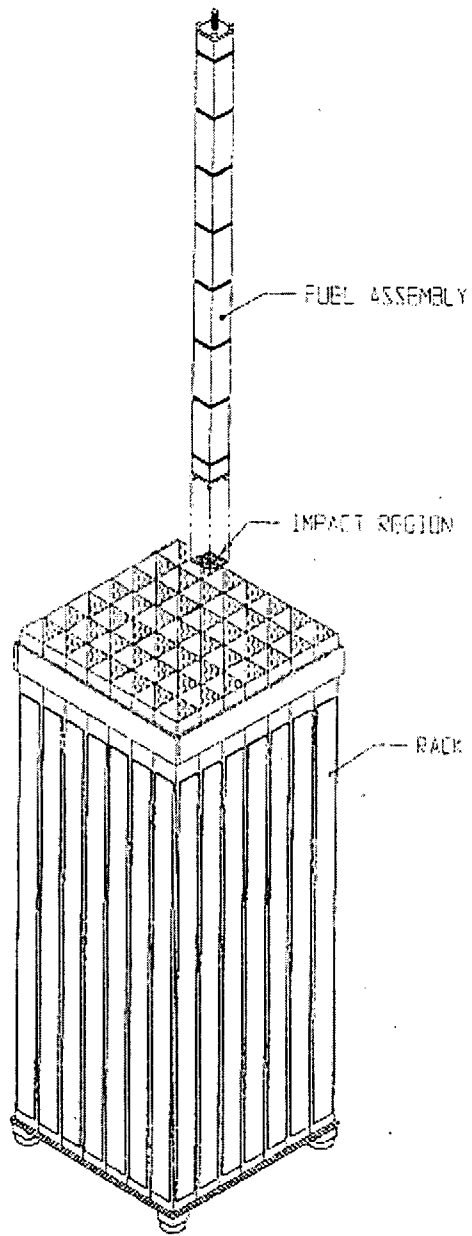


Fig. 7.2.1 Schematics of the Straight Shallow Drop on a Rack Cell

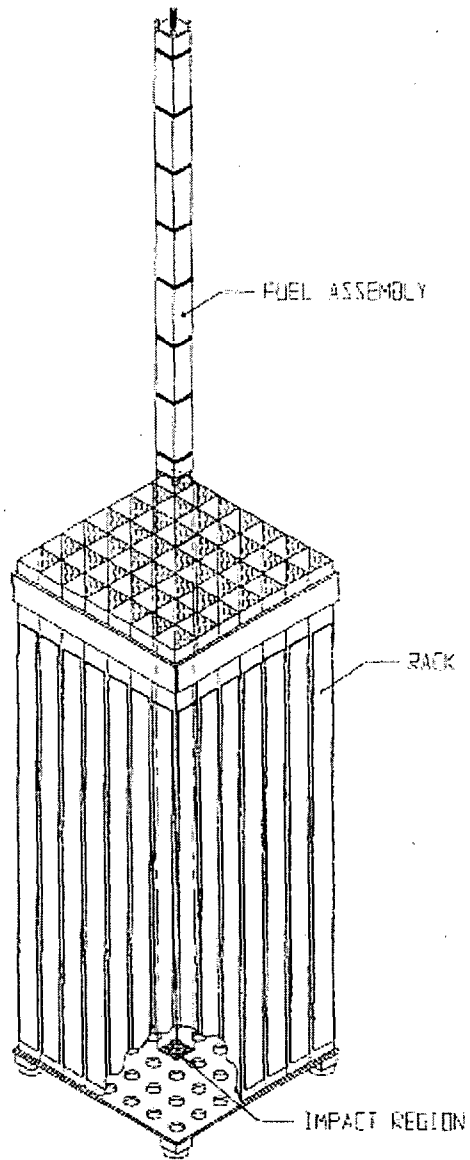


Fig. 7.2.2 Schematics of the "Deep" Drop (Scenario 1) on a Center Cell Location

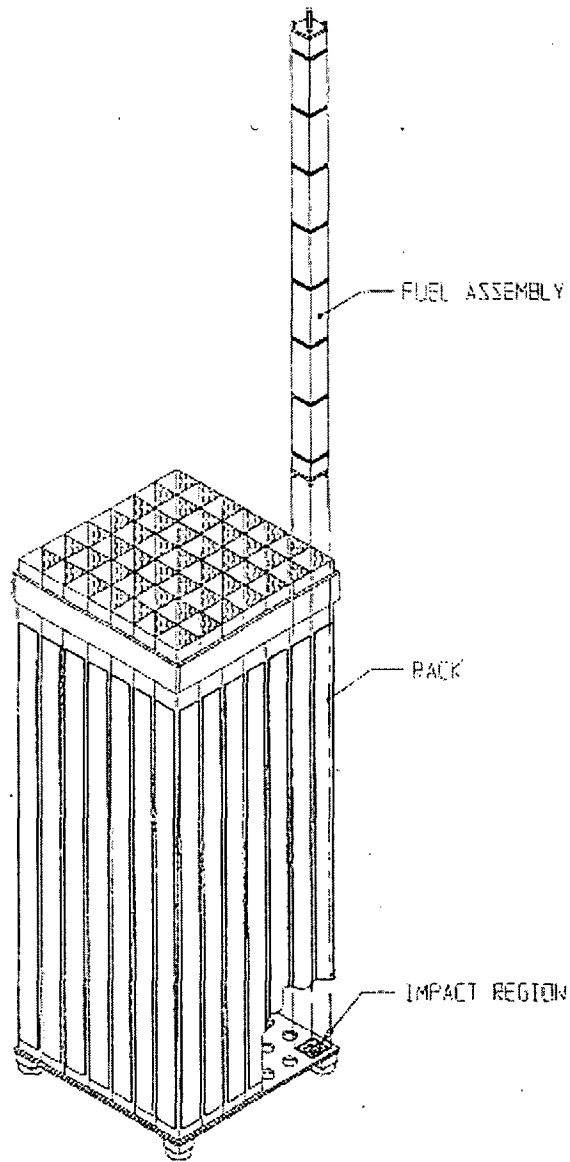


Fig. 7.2.3 Schematics of the "Deep" Drop (Scenario 2) on a Support Leg Location

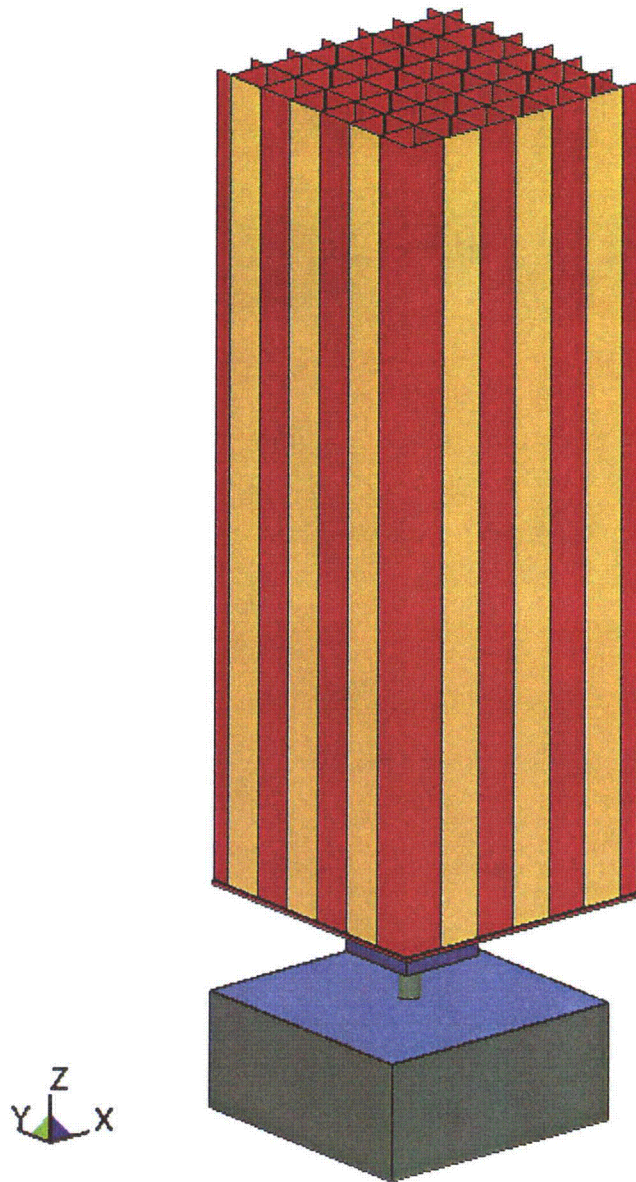


FIGURE 7.2.4: Schematic of Rack Drop Scenario

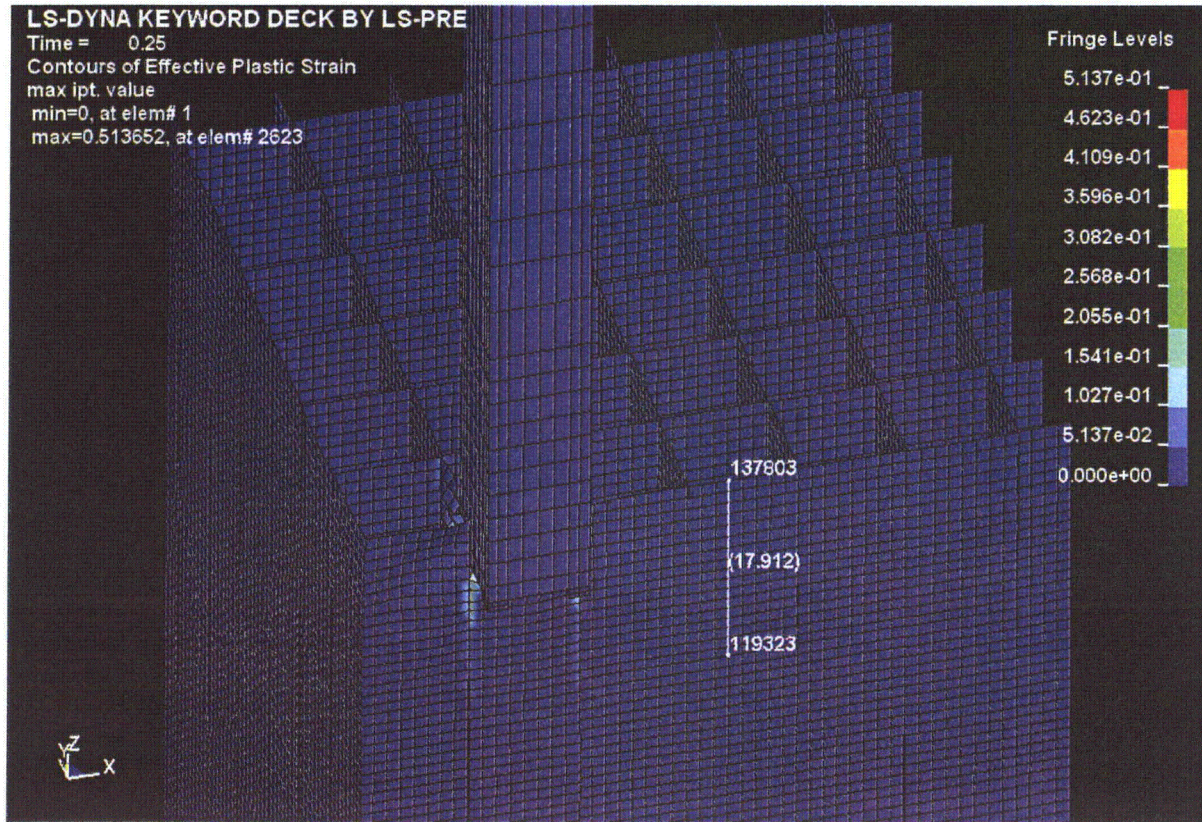


FIGURE 7.5.1: Shallow Drop- Rack cell deformation

LS-DYNA KEYWORD DECK BY LS-PRE

Contours of Z-displacement
min=-1.83682, at node# 132586
max=0.0183667, at node# 132874

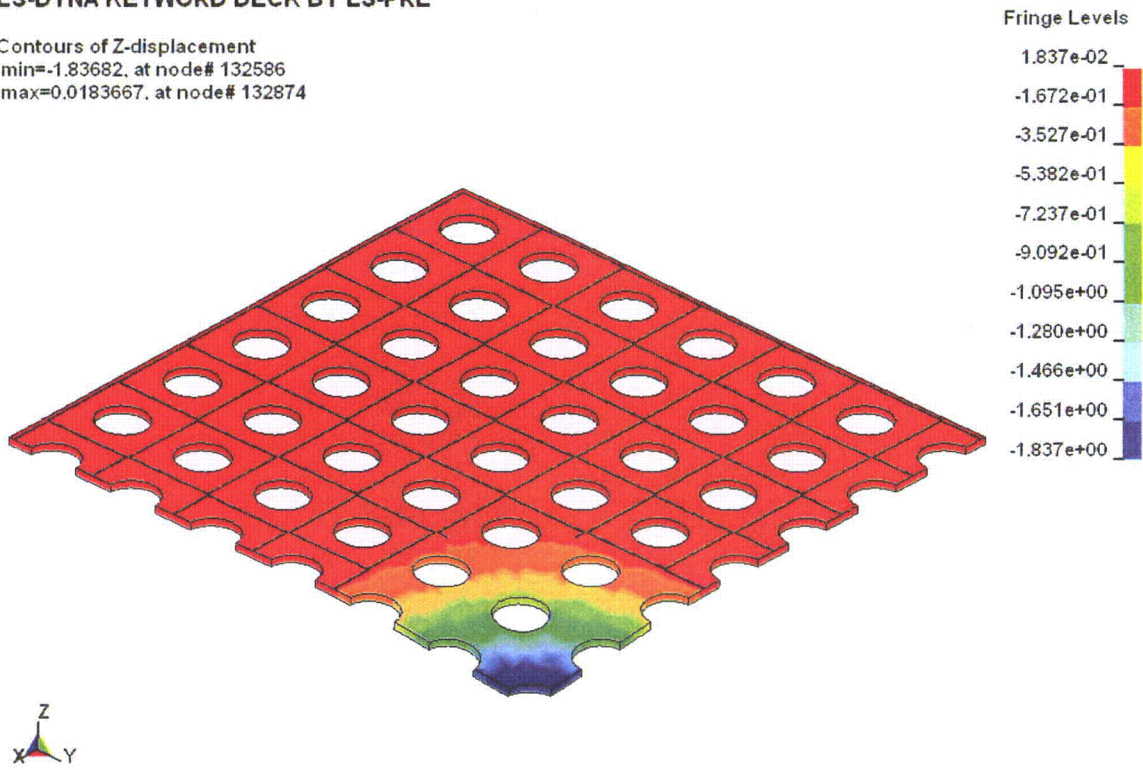


Figure 7.5.2: Peak Baseplate Vertical Deflection – Deep Drop Scenario 1

LS-DYNA KEYWORD DECK BY LS-PRE

Contours of Effective Plastic Strain
max ipt. value
min=0, at elem# 150001
max=0.0523984, at elem# 150049

Fringe Levels

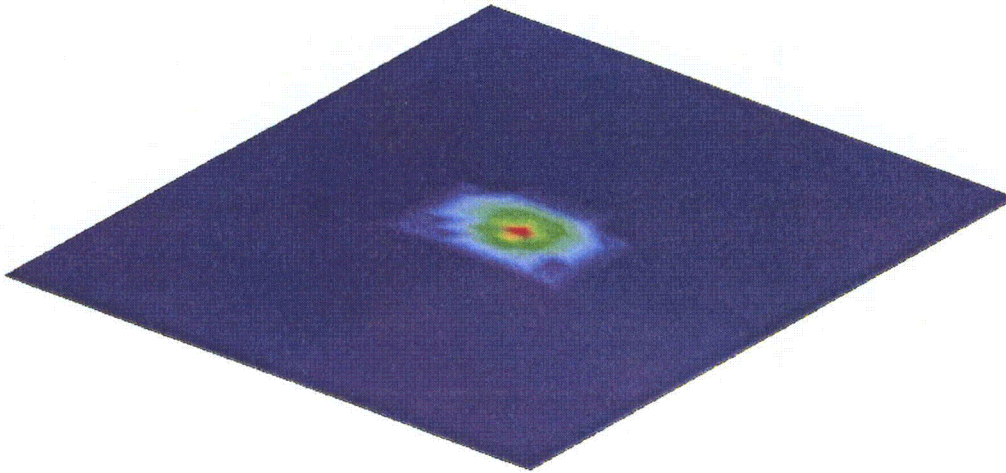
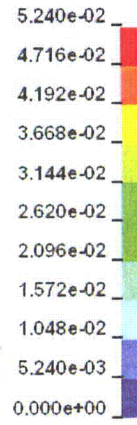


Figure 7.5.3: SFP Floor Liner Maximum Plastic Strain – Rack Drop

LS-DYNA KEYWORD DECK BY LS-PRE
Time = 0.0089999
Contours of Minimum Principal Stress
max ipt. value
min=-13245.1, at elem# 150773
max=280.032, at elem# 150749

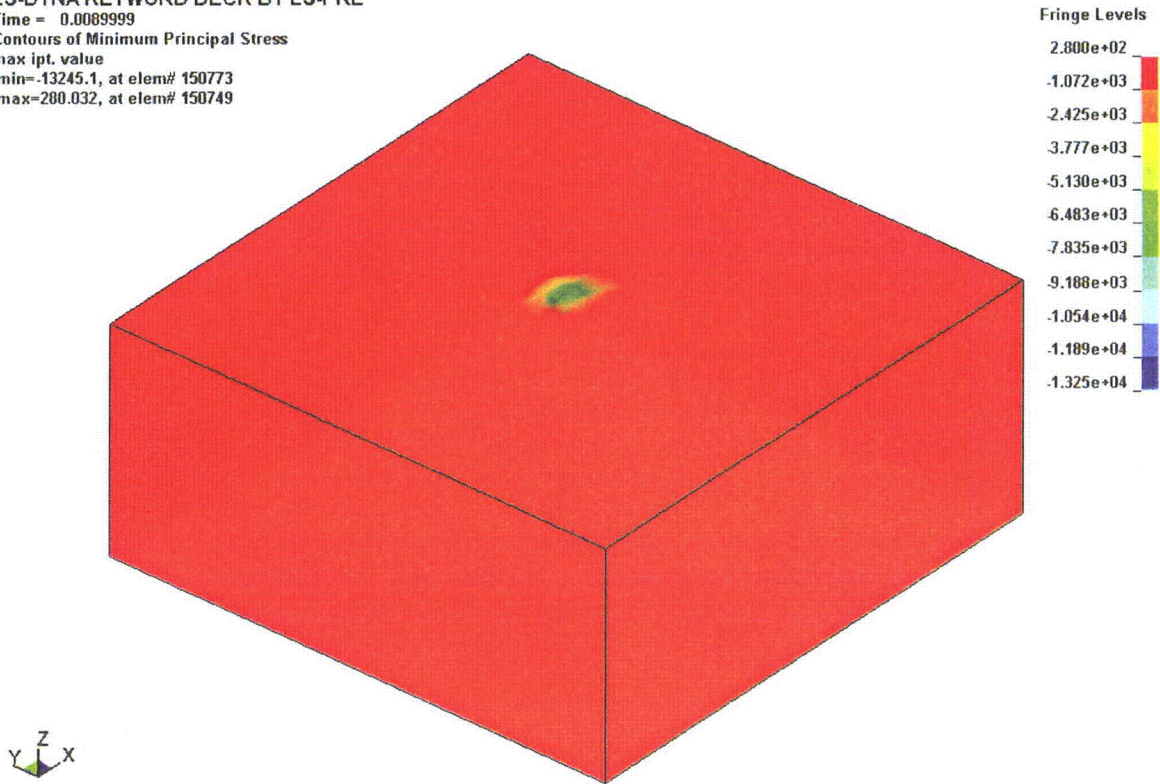


Figure 7.5.4: SFP Floor Concrete Slab Maximum Compressive Stress – Rack Drop

FUEL-TO-FUEL IMPACT
Time = 0.000001

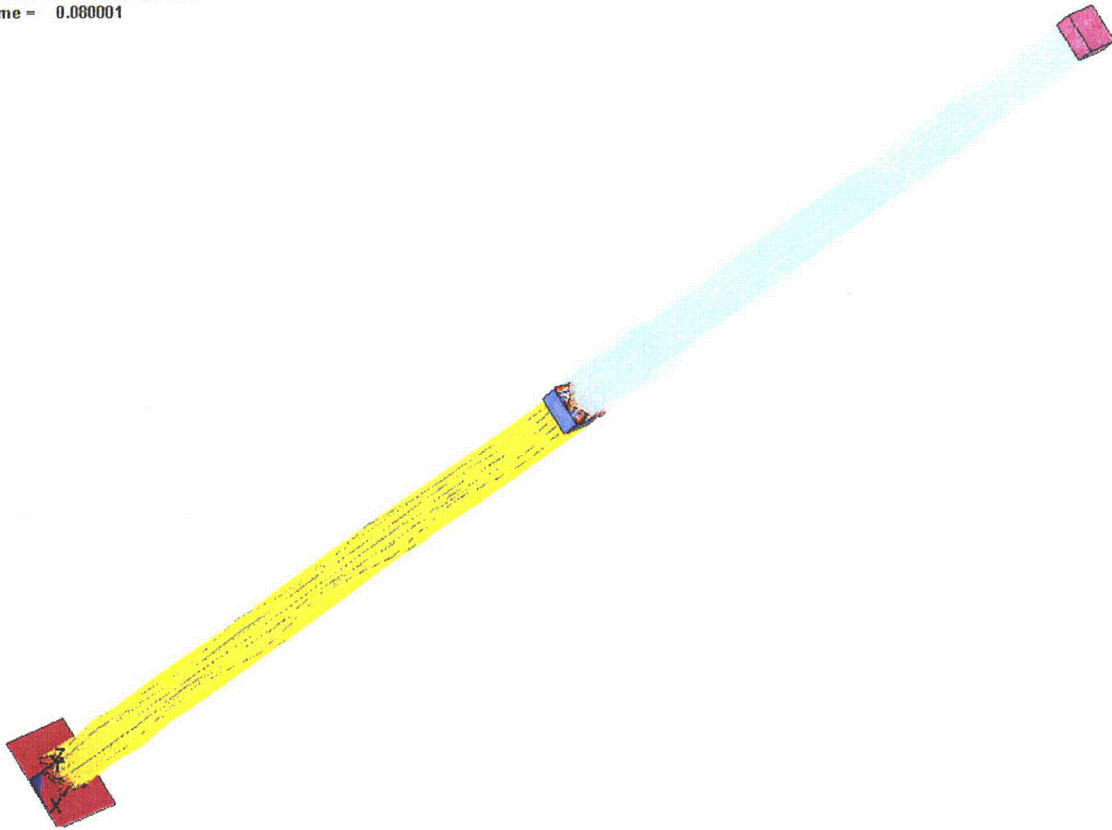


Figure 7.5.5: Deformed Shape of Fuel Rods (rack cell not shown) – Fuel-to-Fuel Impact

8.0 RADIOLOGICAL EVALUATION

8.1 Introduction

The new maximum-density fuel storage racks for the plant are capable of storing a greater number of spent fuel assemblies than the racks that are to be replaced. Consequently, an evaluation of the radiological effect of the increased number of fuel assemblies on the gamma dose rate at the surface of the fuel pool water is prudent. In addition, the radiological consequences of a fuel-handling accident must be addressed. Finally, the person-rem exposure resulting from the removal of the old racks and the installation of the new ones must be considered.

This section provides a summary of the radiological evaluations undertaken in support of the use of the new maximum-density storage racks.

8.2 Acceptance Criteria

The radiation dose incurred in the removal of the old racks and their preparation for shipment, as well as the installation of the new racks, must be consistent with operations carried out in full observance of ALARA principles.

8.3 Assumptions

Certain basic parameter values, all of which are consistent with values specified in the licensing basis for the station, or are anticipated for the future, were assumed to apply to the radiological evaluation. The basic parameter values assumed to apply to the radiological evaluations are given in Table 8.3.1.

8.4 Dose Rate at the Surface of the Pool

The calculated gamma dose rate at the surface of the fuel pool is the sum of the dose rate from radionuclides in the pool water, the dose rate from a fuel assembly in transit, and the dose rate from the fuel stored in the racks. These surface dose rates are not significantly affected by the increase in spent fuel storage capability, since the relative contribution from the fuel stored in the racks to the total surface dose rate is small.

8.4.1 Dose Due to Radionuclides in the Water

Normally, the sources of radionuclides in the spent fuel pool water are crud and some fission products plated on the fuel surfaces, and small amounts of primary system water carried over in the spent fuel pool during refueling operations. This is currently estimated to be 23.5 mrem/hr. These sources result in an increase in the contamination level of the pool during refueling and are soon reduced to normal levels after refueling is completed. Since quantities of radionuclides transferred from the core during future refuelings will be similar to that now experienced, there will be no significant change after rack installation is completed. Therefore, the existing pool cleanup system will continue to be adequate to maintain the radionuclide concentrations in the pool water similar to what is now being experienced. New rack installation will not increase the burden to the pool cleanup system, except perhaps for some crud temporarily stirred up during installation of the new racks.

8.4.2 Dose Due to Spent Fuel

The dose rate at the pool surface (and consequent radiation dose rate to personnel) is not significantly increased with an increased number of spent fuel assemblies stored in the pool. The estimated dose rate at the SFP surface from stored spent fuel is $\ll 1$ mrem/hr. The pool surface dose rate is determined by the fuel being unloaded from the core in refueling and this is the same as that experienced before installation of the racks. The dose at the spent fuel pool surface from an assembly in transit from the core during refueling is dependant upon the operating specific power in the core, fuel burnup, and the time after shutdown when the spent fuel is moved, and

the depth of the water above the spent fuel. The estimated dose rate at the surface from a freshly discharged fuel assembly is approximately 4.0 mrem/hr. Fuel assemblies that are in the spent fuel racks are shielded such that their contribution to the pool surface dose rate is negligible compared to the assembly in transit. Therefore, the spent fuel in storage does not contribute significantly to the radiation dose above the pool.

8.5 Fuel Handling Accident

For Beaver Valley Power Station (BVPS) Unit No. 2, the doses from the fuel-handling accident were calculated for the currently installed racks. The factors affecting the calculation, such as depth of the pool, the exposure of the fuel assembly considered when the accident occurs, the maximum number of rods ruptured in a fuel handling accident, and the cooling time of the assembly, have not changed. Consequently, the doses from the fuel-handling accident remain the values determined in the earlier calculations.

8.6 Person-Rem Exposure

The person-rem exposure from re-racking one plant is shown in Table 8.6.1. The values are estimates of exposures associated with different aspects of the job, and they are based upon practical experience with re-racking projects at many nuclear plants in the U.S. and overseas.

8.7 Conclusions

The total refueling outage dose rate at the surface of the pool water following installation of the new racks is below 50 mrem/hr and should not require changes in the radiation zoning of the plant.

The overall personnel (person-rem) dose from the operations necessary for the removal of the old racks and the installation of the new ones is low and should be acceptable as part of the annual dose incurred at the plant.

Table 8.3.1. Parameter Values Utilized in the Radiological Evaluations

<u>PARAMETER</u>	<u>VALUE</u>
Core power	2918 MWt
Initial fuel enrichment	5.0 wt % ²³⁵ U
Fuel exposure	62,000 MWd/MtU
Fuel cooling time	100 hours

Table 8.6.1. Person-rem Exposure from Re-racking One Plant

Activity	Number of Personnel	Total Man-Hours	Dose Rate	Estimated Person-Rem Exposure
Remove & Package 17 Empty Racks	8	N/A	100 mrem/rack	1.7
Clean and Vacuum Pool	4	300	2 mrem/hr	0.6
Install 15 New Rack Modules	8	500 (in SFP area)	2 mrem/hr	1.0
Move Fuel to New Racks	3	450	4 mrem/hr	1.8
Total Exposure, Person-Rem				5.1

9.0 INSTALLATION

9.1 Introduction

The reracking at Beaver Valley Power Station (BVPS) Unit No. 2 involves the removal of all 17 existing spent fuel racks and the installation of 15 new maximum density spent fuel racks in the spent fuel pool (SFP). All installation work at the plant will be performed in compliance with NUREG-0612, "Control of Heavy Loads at Nuclear Power Plants," and applicable Holtec and plant procedures.

Crane operators will be trained in the operation of overhead cranes per the requirements of ANSI/ASME B30.2 and the plant's specific training program. Consistent with past practices, a videotape-aided training session will be presented to the installation team, all of whom will be required to successfully complete a written examination prior to the commencement of work.

To move the old and new fuel racks out and into the spent fuel pool, a temporary crane will be assembled on site and will share the same rails with the existing movable platform. The existing movable platform and its electric hoists will be used for all of the fuel shuffling involved in the reracking, and will also be the motive power for the new temporary crane used solely to carry the fuel racks. The temporary crane will be qualified to meet a 10:1 lift ratio for the "new" and "old" racks. Allowing two tons for any lift rig, the temporary crane will be designed to support a total vertical load of 150 tons without suffering plastic collapse. A hoist system with an ultimate load rating of at least 150 tons will be used to effect the load movements.

The lifting device designed for removal of the existing racks engages the racks near the bottom of the rack cells. The lifting device designed for installation of the new racks engages the rack baseplate. Both of these lifting devices are engaged to and disengaged from the racks utilizing a long handled tool. The lifting devices comply with the provisions of ANSI N14.6-1992 and NUREG-0612, including compliance with the design stress criteria, load testing at a multiplier of maximum working load, and nondestructive examination of critical welds.

A surveillance and inspection program will be maintained throughout the installation phase of the project. A set of inspection points, which have been proven to eliminate any incidence of rework or erroneous installation in previous rack projects, will be implemented by the installer.

The Holtec procedures cover the scope of activities for the rack removal and installation effort. Similar procedures have been utilized and successfully implemented on many previous rack installation projects. These procedures are written to include ALARA practices and provide requirements to assure equipment, personnel, and plant safety. These procedures will be reviewed and approved in accordance with the plant administrative procedures prior to use on site. The following is a list of the procedures, which will be used to implement the installation phase of the project.

A. Removal and Handling/Installation Procedure:

This procedure provides overall direction for the handling and removal of the existing rack modules and the handling and installation of the new storage rack modules. This procedure delineates the steps necessary to receive the new racks on site, the proper method for unloading and uprighting the new racks, staging the new racks prior to installation, removal of the existing racks, and installation of the new racks. The procedure also provides for the installation of new rack bearing pads, adjustment of the new rack pedestals and verification of the as-built field configuration to ensure compliance with design documents. With regard to the removal of the existing racks, this procedure also delineates steps necessary to their handling after removal from the spent fuel pool.

B. Receipt Inspection Procedure:

This procedure delineates the steps necessary to perform a thorough receipt inspection of a new rack module after its arrival on site. The receipt inspection includes dimensional measurements, cleanliness inspection, visual weld examination, and verticality measurements.

C. Cleaning Procedure:

This procedure provides for the cleaning of a new rack module if required. The modules are to meet the requirements of ANSI N45.2.1, Level B prior to placement in the pool. Methods and limitations on materials to be utilized are provided.

D. Pre- and Post-Installation Drag Test Procedures:

These two procedures stipulate the requirements for performing a functional test on a new rack module prior to and following installation into the pool. The procedures provide direction for inserting and withdrawing an inspection gage into designated cell locations, and establish an acceptance criterion in terms of maximum drag force.

E. ALARA Procedure:

The plant ALARA Program and associated procedures provide guidance to minimize the total man-rem received during the rack installation project, by accounting for time, distance, and shielding.

F. Liner Inspection Procedure:

In the event that a visual inspection of any submerged portion of the spent fuel pool liner is deemed necessary, this procedure describes the method to perform such an inspection using an underwater camera and describes the requirements for documenting any observations.

G. Leak Detection Procedure:

This procedure describes the method to test the pool liner for potential leakage using a vacuum box. This procedure will be applied to any suspect area of the pool liner.

H. Liner Repair and Underwater Welding Procedure:

In the event of a positive leak test result, underwater welding procedures will be implemented which will provide for a weld repair or placement of a stainless steel repair patch over the area in question. The procedures contain appropriate qualification records documenting relevant variables, parameters, and limiting conditions. The weld procedure is qualified in accordance with AWS D3.6-93, Specification for Underwater Welding.

9.2 Rack Arrangement

The existing rack arrangement contains 17 racks bolted to an array of subbase beams on the spent fuel pool floor providing a total of 1088 storage locations. All of the existing racks are of a flux-trap design. Upon completion of the reracking project, the plant SFP will have enough storage spaces for a total capacity of 1690 assemblies in 15 freestanding racks (the subbase beams will remain, but the racks will not be bolted to them). A schematic plan view depicting the new rack arrangement can be seen in Figure 1.1.

9.3 Installation Sequence

Installation of new racks involves the following activities. Necessary fuel movements will be performed prior to rack removal and installation activities. Fuel movement operations will be conducted in accordance with plant procedures. Fuel movements will happen several times over the project duration in order to support the planned sequence of existing rack removal and new rack installation.

Existing rack modules, after they have been emptied of spent fuel and surveyed by Health Physics, will be removed from the SFP using a temporary crane and a remotely engaged lift rig. The rack will be cleaned using a pressure washer and then removed from the SFP following a safe load path. The rack will then be downended into a horizontal orientation and be ready for packaging and transport to a processing location.

The new racks will be delivered in the horizontal position. A new rack module will be removed from the shipping trailer using a suitably rated crane and a spreader beam, while maintaining the horizontal configuration. The rack will be placed on an upender frame and secured. Using two independent overhead hooks, or a single overhead hook and a spreader beam, the module will be up-righted into a vertical position.

The new rack lifting device will be engaged in the lift points at the bottom of the rack. The rack will then be transported to a pre-leveled surface where, after leveling the rack, the appropriate quality control receipt inspection will be performed.

To address ALARA considerations, fuel in the SFP will be moved in preparation for rack installation. Additionally, the pool floor will be inspected and any debris that might inhibit the installation of bearing pads will be removed.

After pool floor preparation, new rack bearing pads will be positioned on the floor before the module is lowered into the SFP. The new rack module, the heaviest of which weighs less than eleven tons, will be lifted with a temporary crane installed specifically for this purpose and transported along the pre-established safe load path. The rack modules will be cautiously lowered into the pool and onto the bearing pads.

Elevation readings will be taken to confirm that the module is level. In addition, rack-to-rack and rack-to-wall offset distances will be measured. Adjustments will be made as necessary to ensure compliance with design documents. The lifting device will then be disengaged and removed from the pool under Health Physics direction. Post-installation free path verification will be performed using an inspection gage in order to ensure that no cell location poses excessive resistance to the insertion or withdrawal of a fuel assembly. This test confirms final acceptability of the installed rack module.

Enclosure D

Holtec Affidavit Pursuant to 10 CFR 2.390



Holtec Center, 555 Lincoln Drive West, Marlton, NJ 08053

Telephone (856) 797-0900

Fax (856) 797-0909

U.S. Nuclear Regulatory Commission
ATTN: Document Control Desk

AFFIDAVIT PURSUANT TO 10 CFR 2.390

I, Evan Rosenbaum, state as follows:

- (1) I am the Holtec International Adjunct Project Manager for the Beaver Valley Unit 2 Fuel Storage Racks Project and have reviewed the information described in paragraph (2) which is sought to be withheld, and am authorized to apply for its withholding.
- (2) The information sought to be withheld is Revision 3 of Holtec Licensing Report HI-2084175, which contains Holtec Proprietary information and is appropriately marked as such.
- (3) In making this application for withholding of proprietary information of which it is the owner, Holtec International relies upon the exemption from disclosure set forth in the Freedom of Information Act ("FOIA"), 5 USC Sec. 552(b)(4) and the Trade Secrets Act, 18 USC Sec. 1905, and NRC regulations 10CFR Part 9.17(a)(4), 2.390(a)(4), and 2.390(b)(1) for "trade secrets and commercial or financial information obtained from a person and privileged or confidential" (Exemption 4). The material for which exemption from disclosure is here sought is all "confidential commercial information", and some portions also qualify under the narrower definition of "trade secret", within the meanings assigned to those terms for purposes of FOIA Exemption 4 in, respectively, Critical Mass Energy Project v. Nuclear Regulatory Commission, 975F2d871 (DC Cir. 1992), and Public Citizen Health Research Group v. FDA, 704F2d1280 (DC Cir. 1983).



Holtec Center, 555 Lincoln Drive West, Marlton, NJ 08053

Telephone (856) 797-0900

Fax (856) 797-0909

U.S. Nuclear Regulatory Commission
ATTN: Document Control Desk

AFFIDAVIT PURSUANT TO 10 CFR 2.390

- (4) Some examples of categories of information which fit into the definition of proprietary information are:
- a. Information that discloses a process, method, or apparatus, including supporting data and analyses, where prevention of its use by Holtec's competitors without license from Holtec International constitutes a competitive economic advantage over other companies;
 - b. Information which, if used by a competitor, would reduce his expenditure of resources or improve his competitive position in the design, manufacture, shipment, installation, assurance of quality, or licensing of a similar product.
 - c. Information which reveals cost or price information, production, capacities, budget levels, or commercial strategies of Holtec International, its customers, or its suppliers;
 - d. Information which reveals aspects of past, present, or future Holtec International customer-funded development plans and programs of potential commercial value to Holtec International;
 - e. Information which discloses patentable subject matter for which it may be desirable to obtain patent protection.

The information sought to be withheld is considered to be proprietary for the reason set forth in paragraph 4.a and 4.b, above.

- (5) The information sought to be withheld is being submitted to the NRC in confidence. The information (including that compiled from many sources) is of



Holtec Center, 555 Lincoln Drive West, Marlton, NJ 08053

Telephone (856) 797-0900

Fax (856) 797-0909

U.S. Nuclear Regulatory Commission
ATTN: Document Control Desk

AFFIDAVIT PURSUANT TO 10 CFR 2.390

a sort customarily held in confidence by Holtec International, and is in fact so held. The information sought to be withheld has, to the best of my knowledge and belief, consistently been held in confidence by Holtec International. No public disclosure has been made, and it is not available in public sources. All disclosures to third parties, including any required transmittals to the NRC, have been made, or must be made, pursuant to regulatory provisions or proprietary agreements which provide for maintenance of the information in confidence. Its initial designation as proprietary information, and the subsequent steps taken to prevent its unauthorized disclosure, are as set forth in paragraphs (6) and (7) following.

- (6) Initial approval of proprietary treatment of a document is made by the manager of the originating component, the person most likely to be acquainted with the value and sensitivity of the information in relation to industry knowledge. Access to such documents within Holtec International is limited on a "need to know" basis.
- (7) The procedure for approval of external release of such a document typically requires review by the staff manager, project manager, principal scientist or other equivalent authority, by the manager of the cognizant marketing function (or his designee), and by the Legal Operation, for technical content, competitive effect, and determination of the accuracy of the proprietary designation. Disclosures outside Holtec International are limited to regulatory bodies, customers, and potential customers, and their agents, suppliers, and licensees, and others with a legitimate need for the information, and then only in accordance with appropriate regulatory provisions or proprietary agreements.
- (8) The information classified as proprietary was developed and compiled by Holtec International at a significant cost to Holtec International. This information is classified as proprietary because it contains detailed descriptions of analytical



Holtec Center, 555 Lincoln Drive West, Marlton, NJ 08053

Telephone (856) 797-0900

Fax (856) 797-0909

U.S. Nuclear Regulatory Commission
ATTN: Document Control Desk

AFFIDAVIT PURSUANT TO 10 CFR 2.390

approaches and methodologies not available elsewhere. This information would provide other parties, including competitors, with information from Holtec International's technical database and the results of evaluations performed by Holtec International. A substantial effort has been expended by Holtec International to develop this information. Release of this information would improve a competitor's position because it would enable Holtec's competitor to copy our technology and offer it for sale in competition with our company, causing us financial injury.

- (9) Public disclosure of the information sought to be withheld is likely to cause substantial harm to Holtec International's competitive position and foreclose or reduce the availability of profit-making opportunities. The information is part of Holtec International's comprehensive spent fuel storage technology base, and its commercial value extends beyond the original development cost. The value of the technology base goes beyond the extensive physical database and analytical methodology, and includes development of the expertise to determine and apply the appropriate evaluation process.

The research, development, engineering, and analytical costs comprise a substantial investment of time and money by Holtec International.

The precise value of the expertise to devise an evaluation process and apply the correct analytical methodology is difficult to quantify, but it clearly is substantial.

Holtec International's competitive advantage will be lost if its competitors are able to use the results of the Holtec International experience to normalize or verify their own process or if they are able to claim an equivalent understanding by demonstrating that they can arrive at the same or similar conclusions.



Holtec Center, 555 Lincoln Drive West, Marlton, NJ 08053

Telephone (856) 797-0900

Fax (856) 797-0909

U.S. Nuclear Regulatory Commission
ATTN: Document Control Desk

AFFIDAVIT PURSUANT TO 10 CFR 2.390

The value of this information to Holtec International would be lost if the information were disclosed to the public. Making such information available to competitors without their having been required to undertake a similar expenditure of resources would unfairly provide competitors with a windfall, and deprive Holtec International of the opportunity to exercise its competitive advantage to seek an adequate return on its large investment in developing these very valuable analytical tools.

Executed at Marlton, New Jersey, this 7th day of April, 2009.

Evan Rosenbaum
Holtec International



Holtec Center, 555 Lincoln Drive West, Marlton, NJ 08053

Telephone (856) 797-0900

Fax (856) 797-0909

U.S. Nuclear Regulatory Commission
ATTN: Document Control Desk

AFFIDAVIT PURSUANT TO 10 CFR 2.390

I, Evan Rosenbaum, state as follows:

- (1) I am the Holtec International Adjunct Project Manager for the Beaver Valley Unit 2 Fuel Storage Racks Project and have reviewed the information described in paragraph (2) which is sought to be withheld, and am authorized to apply for its withholding.
- (2) The information sought to be withheld is Revision 3 of Holtec Licensing Report HI-2084175, which contains Holtec Proprietary information and is appropriately marked as such.
- (3) In making this application for withholding of proprietary information of which it is the owner, Holtec International relies upon the exemption from disclosure set forth in the Freedom of Information Act ("FOIA"), 5 USC Sec. 552(b)(4) and the Trade Secrets Act, 18 USC Sec. 1905, and NRC regulations 10CFR Part 9.17(a)(4), 2.390(a)(4), and 2.390(b)(1) for "trade secrets and commercial or financial information obtained from a person and privileged or confidential" (Exemption 4). The material for which exemption from disclosure is here sought is all "confidential commercial information", and some portions also qualify under the narrower definition of "trade secret", within the meanings assigned to those terms for purposes of FOIA Exemption 4 in, respectively, Critical Mass Energy Project v. Nuclear Regulatory Commission, 975F2d871 (DC Cir. 1992), and Public Citizen Health Research Group v. FDA, 704F2d1280 (DC Cir. 1983).



Holtec Center, 555 Lincoln Drive West, Marlton, NJ 08053

Telephone (856) 797-0900

Fax (856) 797-0909

U.S. Nuclear Regulatory Commission
ATTN: Document Control Desk

AFFIDAVIT PURSUANT TO 10 CFR 2.390

- (4) Some examples of categories of information which fit into the definition of proprietary information are:
- a. Information that discloses a process, method, or apparatus, including supporting data and analyses, where prevention of its use by Holtec's competitors without license from Holtec International constitutes a competitive economic advantage over other companies;
 - b. Information which, if used by a competitor, would reduce his expenditure of resources or improve his competitive position in the design, manufacture, shipment, installation, assurance of quality, or licensing of a similar product.
 - c. Information which reveals cost or price information, production, capacities, budget levels, or commercial strategies of Holtec International, its customers, or its suppliers;
 - d. Information which reveals aspects of past, present, or future Holtec International customer-funded development plans and programs of potential commercial value to Holtec International;
 - e. Information which discloses patentable subject matter for which it may be desirable to obtain patent protection.

The information sought to be withheld is considered to be proprietary for the reason set forth in paragraph 4.a and 4.b, above.

- (5) The information sought to be withheld is being submitted to the NRC in confidence. The information (including that compiled from many sources) is of



Holtec Center, 555 Lincoln Drive West, Marlton, NJ 08053

Telephone (856) 797-0900

Fax (856) 797-0909

U.S. Nuclear Regulatory Commission
ATTN: Document Control Desk

AFFIDAVIT PURSUANT TO 10 CFR 2.390

a sort customarily held in confidence by Holtec International, and is in fact so held. The information sought to be withheld has, to the best of my knowledge and belief, consistently been held in confidence by Holtec International. No public disclosure has been made, and it is not available in public sources. All disclosures to third parties, including any required transmittals to the NRC, have been made, or must be made, pursuant to regulatory provisions or proprietary agreements which provide for maintenance of the information in confidence. Its initial designation as proprietary information, and the subsequent steps taken to prevent its unauthorized disclosure, are as set forth in paragraphs (6) and (7) following.

- (6) Initial approval of proprietary treatment of a document is made by the manager of the originating component, the person most likely to be acquainted with the value and sensitivity of the information in relation to industry knowledge. Access to such documents within Holtec International is limited on a "need to know" basis.
- (7) The procedure for approval of external release of such a document typically requires review by the staff manager, project manager, principal scientist or other equivalent authority, by the manager of the cognizant marketing function (or his designee), and by the Legal Operation, for technical content, competitive effect, and determination of the accuracy of the proprietary designation. Disclosures outside Holtec International are limited to regulatory bodies, customers, and potential customers, and their agents, suppliers, and licensees, and others with a legitimate need for the information, and then only in accordance with appropriate regulatory provisions or proprietary agreements.
- (8) The information classified as proprietary was developed and compiled by Holtec International at a significant cost to Holtec International. This information is classified as proprietary because it contains detailed descriptions of analytical



Holtec Center, 555 Lincoln Drive West, Marlton, NJ 08053

Telephone (856) 797-0900

Fax (856) 797-0909

U.S. Nuclear Regulatory Commission
ATTN: Document Control Desk

AFFIDAVIT PURSUANT TO 10 CFR 2.390

approaches and methodologies not available elsewhere. This information would provide other parties, including competitors, with information from Holtec International's technical database and the results of evaluations performed by Holtec International. A substantial effort has been expended by Holtec International to develop this information. Release of this information would improve a competitor's position because it would enable Holtec's competitor to copy our technology and offer it for sale in competition with our company, causing us financial injury.

- (9) Public disclosure of the information sought to be withheld is likely to cause substantial harm to Holtec International's competitive position and foreclose or reduce the availability of profit-making opportunities. The information is part of Holtec International's comprehensive spent fuel storage technology base, and its commercial value extends beyond the original development cost. The value of the technology base goes beyond the extensive physical database and analytical methodology, and includes development of the expertise to determine and apply the appropriate evaluation process.

The research, development, engineering, and analytical costs comprise a substantial investment of time and money by Holtec International.

The precise value of the expertise to devise an evaluation process and apply the correct analytical methodology is difficult to quantify, but it clearly is substantial.

Holtec International's competitive advantage will be lost if its competitors are able to use the results of the Holtec International experience to normalize or verify their own process or if they are able to claim an equivalent understanding by demonstrating that they can arrive at the same or similar conclusions.



Holtec Center, 555 Lincoln Drive West, Marlton, NJ 08053

Telephone (856) 797-0900

Fax (856) 797-0909

U.S. Nuclear Regulatory Commission
ATTN: Document Control Desk

AFFIDAVIT PURSUANT TO 10 CFR 2.390

The value of this information to Holtec International would be lost if the information were disclosed to the public. Making such information available to competitors without their having been required to undertake a similar expenditure of resources would unfairly provide competitors with a windfall, and deprive Holtec International of the opportunity to exercise its competitive advantage to seek an adequate return on its large investment in developing these very valuable analytical tools.

Executed at Marlton, New Jersey, this 7th day of April, 2009.

A handwritten signature in cursive script, appearing to read "Evan Rosenbaum".

Evan Rosenbaum
Holtec International